UC San Diego

UC San Diego Electronic Theses and Dissertations

Title

Synthesis of Caged Garcinia Xanthones and Rational Design of Fluorescent Sensors for Amyloid Detection /

Permalink

https://escholarship.org/uc/item/4gz3c8mp

Author

Elbel, Kristyna M.

Publication Date

2013

Peer reviewed|Thesis/dissertation

eScholarship.org Powered by the California Digital Library
University of California

UNIVERSITY OF CALIFORNIA, SAN DIEGO

Synthesis of Caged *Garcinia* Xanthones and Rational Design of Fluorescent Sensors for Amyloid Detection

A thesis submitted in partial satisfaction of the
requirements for the degree
Master of Science

in

Chemistry

by

Kristyna M. Elbel

Committee in charge:

Professor Emmanuel A. Theodorakis, Chair
Professor Christina J. Sigurdson
Professor Jerry Yang

2013

Copyright
Kristyna M. Elbel, 2013
All rights reserved.

The thesis of Kristyna M. Elbel is approved, and it is acceptable in quality and form for publication on microfilm and electronically:

_____

_____

_____

Chair

University of California, San Diego

2013

TABLE OF CONTENTS

LIST OF FIGURES

LIST OF SCHEMES

LIST OF SPECTRA

ACKNOWLEDGEMENTS

First, I want to thank Professor Emmanuel Theodorakis for allowing me to work in his lab. His guidance these past two years has been invaluable to me and has allowed me to become a better chemist. The projects that I have worked on have let me develop new ideas and follow them through until the end. I have truly enjoyed my time working in Emmanuel's lab and without his advice and training, none of this would be possible.

Next, I would like to thank Kevin Cao of the Yang Lab, whom I have worked closely with on the rotors project. His countless hours of work, support, and guidance have been vital to my success.

I would also like to thank all the members of the Theodorakis Lab for their support, guidance, and making my time in lab that much more enjoyable: Ed Caro, Michelle Lacoske, Jing Xu, Alec Saitman, Steven Sullivan, Marianna Dakanali, Celso Rezende, Thai Do, Joey Hung, Henry Korman, and Oraphin Chantarasriwong.

I would also like to thank Jerry Yang and his lab members for their support, time, and guidance.

I owe a great deal of gratitude to Professor Haim Weizman for his support throughout my time at UCSD, both undergrad and graduate. He has taught me how to not only be a better chemist, but also a teacher. The lessons I have learned from him I will carry for the rest of my career.

I would also like to thank the UCSD Chemistry and Biochemistry Department and the many students in it that I have gotten to know and respect during my time here.

My love of science truly began back in high school and I would like to thank two teachers who went above and beyond to nurture my excitement: Mr. Colarusso and Mr. Raley.

I would like to thank Dmitriy Uchenik for standing by me throughout this journey.

Lastly, I would like to thank my family for encouraging me to pursue my passion even from a young age.

Chapter 1, in full, is a reprint of the material as it appears in Organic and Biomolecular Chemistry **2013**. Elbel, K. M., Guizzunti, G., Theodoraki, M. A., Xu, J., Batova, A., Dakanali, M., Theodorakis, E. A. "A-ring oxygenation modulates the

chemistry and bioactivity of caged *Garcinia* xanthones" *Org. Biomol. Chem.* **2013**, *11*, 3341-3348.

ABSTRACT OF THE THESIS

Synthesis of Caged *Garcinia* Xanthones and Rational Design of Fluorescent Sensors for Amyloid Detection

by

Kristyna M. Elbel

Master of Science in Chemistry

University of California, San Diego, 2013

Professor Emmanuel A. Theodorakis, Chair

The family of caged *Garcinia* xanthones (CGX) possess a unique chemical structure along with promising antitumor and anti-inflammatory pharmacological profiles. We report the synthesis and biological evaluation of A-ring oxygenated structures related to the natural product, which reveal pharmacophoric insights into the SAR profile of CGXs. This synthesis is achieved utilizing a Pd(0)-catalyzed reverse prenylation and a unique tandem Claisen/Diels-Alder reaction.

Fluorescent molecular rotors possess a unique structure which give them an intrinsic ability to detect various properties of their environment through both an increase of quantum yield and a hypsochromic shift. Our lab has synthesized a family of fluorescent molecular rotors, which have the ability to selectively bind to beta-amyloid protein

($A\beta$), seen in Alzheimer's disease (AD). These compounds were tested for their stability, binding ability, and fluorescence profile in order to further develop a rational design of novel fluorescent molecular rotors.

Chapter 1

A-ring Oxygenation Modulates the Chemistry and Bioactivity of Caged *Garcinia* Xanthones

1.1 Abstract

Natural products of the caged *Garcinia* xanthones (CGX) family are characterized by a unique chemical structure, potent bioactivities and promising pharmacological profiles. We have developed a Claisen/Diels-Alder reaction cascade that, in combination with a Pd(0)-catalyzed reverse prenylation, provide rapid and efficient access to the CGX pharmacophore, represented by the structure of cluvenone. To further explore this pharmacophore, we have synthesized various A-ring oxygenated analogues of cluvenone and have evaluated their bioactivities in terms of growth inhibition, mitochondrial fragmentation, induction of mitochondrial-dependent cell death and Hsp90 client inhibition. We found that installation of an oxygen functionality at various positions of the A-ring influences significantly both the site-selectivity of the Claisen/Diels-Alder reaction and the bioactivity of these compounds, due to remote electronic effects.

1.2 Introduction

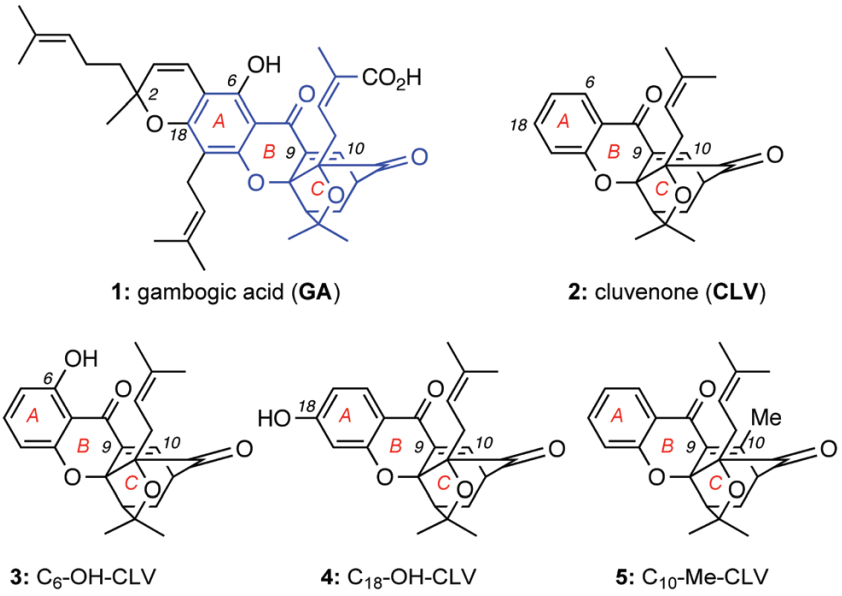

Figure 1.1: Structures of selected caged *Garcinia* xanthones (CGXs).

Tropical plants of the genus *Garcinia* have led to the identification of an intriguing family of xanthone-derived natural products that have interesting bioactivities and

a documented value in traditional Eastern medicine.[1] Collectively referred to as caged *Garcinia* xanthones (CGXs),[2] these compounds are structurally defined by an unusual architecture in which a 4-oxa-tricyclo[4.3.1.$0^{3,7}$] dec-8-en-2-one scaffold has been built onto the C-ring of a xanthone backbone. This motif is further decorated via substitutions at the A-ring and peripheral oxidations to produce a variety of related subfamilies. Gambogic acid (**1**, GA),[3] the archetype of this family, has been studied as a potent antitumor and anti-inflammatory agent and has entered phase I clinical trials in China.[4] Various biological studies have suggested that **1** can induce cell apoptosis by activating the mitochondrial pathway via mechanisms that are partly dependent on the Bcl-2 family of proteins.[5] Although the primary direct molecular target of **1** is still under investigation, recent studies have suggested that it can bind with low micromolar k_d to the heat shock protein Hsp90,[6] thereby reducing the expression levels of Hsp90-dependent clients that are involved in cell growth, apoptosis, angiogenesis and metastasis.[7] Intrigued by the unusual chemical motif and therapeutic promise of CGXs, we sought to design a general synthetic strategy that would allow us to further explore and optimize its biological properties.[8,9] These studies led to the identification of cluvenone (**2**, CLV), a structurally simplified CGX that retains the biological activities of **1**.[10] Along these lines, we have shown that CLV parallels the activity of GA in inducing cell stress and apoptosis in various cancer lines at low micromolar concentration. Fluorescent labeling studies have indicated that both **1** and **2** localize in mitochondria and induce significant changes in the morphology and structure of this organelle, thereby leading to cell apoptosis.[11] It has been proposed that the C_9-C_{10} enone functionality of these compounds contributes to their bioactivity, presumably by acting as a conjugate electrophile.[9a–b] To further explore and optimize the CGX pharmacophore, we synthesized A-ring oxygenated xanthones **3** and **4** and compared their activities to those of **1**, **2** and **5**.[10] Here we show that that installation of an oxygen group at C_6 or C_{18} positions of the CGX motif (gambogic acid numbering) affects significantly both the synthesis and the bioactivity of these compounds (Fig. 1.1).

1.3 Results and Discussion

1.3.1 Synthesis of A-ring hydroxylated caged *Garcinia* xanthones

The synthesis of caged *Garcinia* xanthones containing a protected phenolic group at the C_6 and C_{18} positions of the A ring is highlighted. Acyl chloride **7a**, prepared via oxalyl chloride/DMF-mediated chlorination of commercially available 2,6-dimethoxybenzoic acid (**6a**), was subjected to an $AlCl_3$-catalyzed Friedel-Crafts acylation with pyrogallol trimethyl ether (**8**) (Scheme 1.1). The resulting benzophenone intermediate was treated with NaOH to produce xanthone **9a** in 90% combined yield. Demethylation of **9a** with 48% HBr in AcOH gave rise to hydroxylated xanthone **10a** (95% yield). Protection of the C-ring catechol of **9a** as the corresponding diphenylketal, followed by alkylation of the C_6 phenol with MOMCl/NaH and deprotection of the ketal functionality yielded xanthone **11a** (3 steps, 56% overall yield).[9d] Pd(0)-catalyzed reverse prenylation of **11a** with carbonate **12** produced diallyl ether **13a** in 63% yield.[10] In a similar manner, **13b** was produced from 2,4-dimethoxybenzoic acid (**6b**) in 7 steps and 17% overall yield.

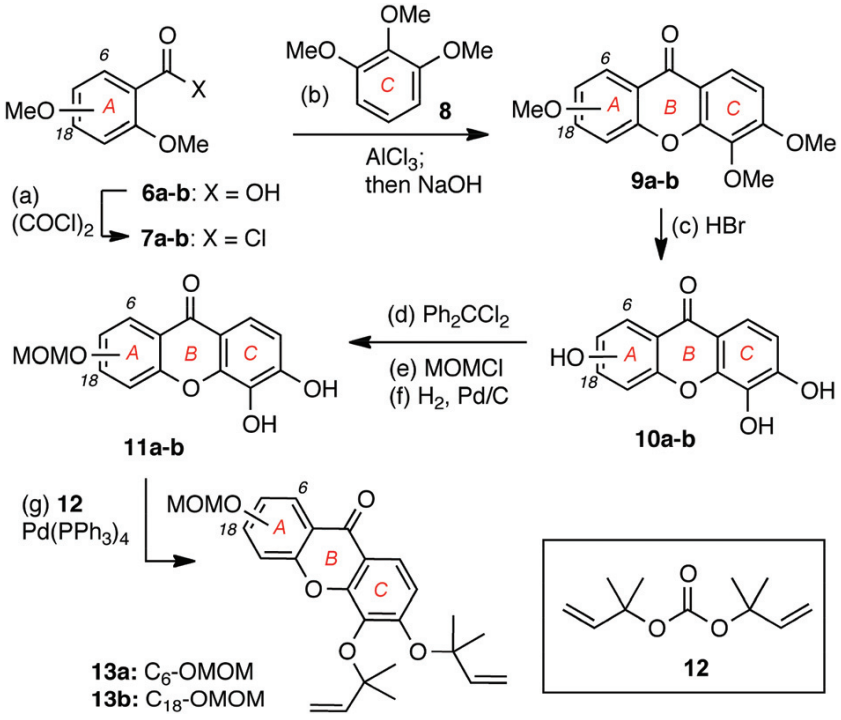

Scheme 1.1: Synthesis of **13a** and **13b**.

Conversion of **13a** and **13b** to the corresponding caged structures was achieved via the tandem Claisen/Diels-Alder reaction cascade (Scheme 1.2).[12] To this end, heating of **13a** (DMF, 120 °C, 2 h) produced two isomeric caged xanthones: the "regular" caged structure **15** (80% yield) that is formed upon initial Claisen migration of the C_{12} allyl ether at the C_{13} position, and the "neo" caged structure **16** (20% yield) that is formed upon initial Claisen migration of the C_{13} allyl ether at the C_{12} position (gambogic acid numbering). On the other hand, $ZnCl_2$-induced cleavage of the MOM group (40 °C, 2 h) of **13a** formed **14** (93% yield) that, upon heating, underwent the Claisen/Diels-Alder reaction to form regular caged xanthone **3** (92% yield) together with the neo caged compound **17** (8% yield). In a similar manner, heating of **13b** (DMF, 2 h, 120 °C) produced the regular caged structure **19** (80% yield) together with the neo structure **20** (20% yield). To our surprise, removal of the MOM group from **13b** under $ZnCl_2$ conditions proved to be problematic and led to partial or full loss of the dimethylallyl ethers. Thus, this deprotection was accomplished after conversion of **13b** to the corresponding caged compounds **19** and **20**. To this end, treatment of **19** and **20** with $ZnCl_2$ (40 °C, 24 h) afforded caged xanthones **4** and **21** respectively in ca 75% yield.[13]

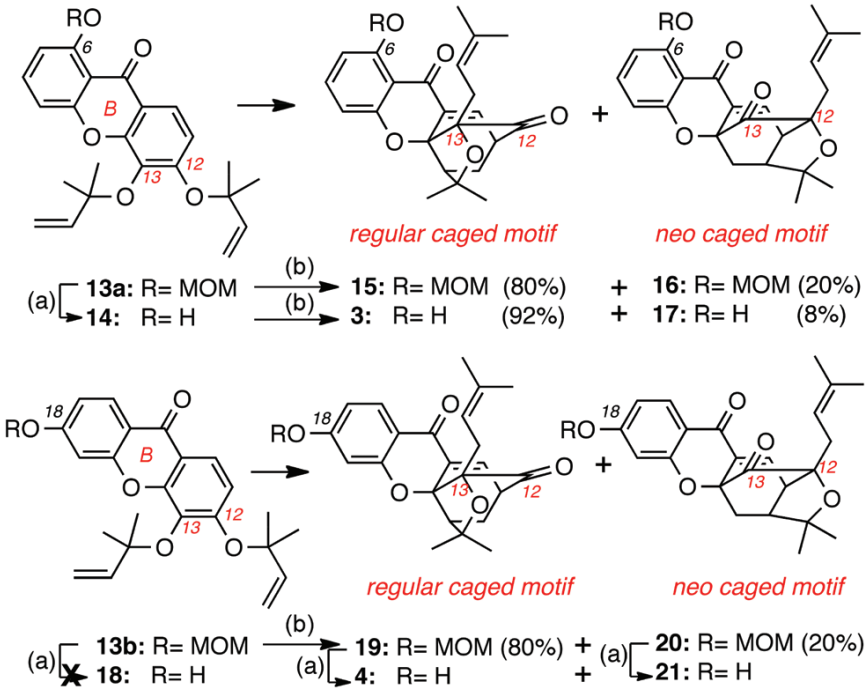

Scheme 1.2: Claisen/ Diels-Alder Cascade.

The products distribution of the Claisen/Diels-Alder reaction deserves some comments. We have previously postulated that the site selectivity of this reaction can be rationalized by considering the electronic deficiency of the B-ring carbonyl group, that, being para to the C_{12} allyl ether, facilitates its rupture during the inaugural Claisen rearrangement.[13] In turn, Claisen migration of this group at the C_{13} position leads to a site selective Diels-Alder reaction ultimately forming the regular caged motif as the major product. In contrast, the competing Claisen migration of the C_{13} dimethylallyl ether at the C_{12} position is not electronically favored. Thus, the corresponding neo caged motif is formed only as the minor product.[14,15] The results of our study with compounds **13a**, **13b** and **14** further support this proposal. Specifically, the Claisen/Diels-Alder reaction of **14** produces the regular and the neo caged compounds **3** and **17** in a 92:8 ratio. This enhanced site selectivity can be explained by considering that the C6 hydroxyl group increases the electron deficiency of the B-ring carbonyl group via hydrogen bonding and thus facilitates the rupture of the C_{12} allyl ether, leading predominantly to the regular caged motif of **3**. In contrast, the presence of a MOM ether at C_6 or C_{18} (i.e. **13a** or **13b**) donates electron density at the B-ring carbonyl group thus attenuating the site selectivity of the Claisen/Diels-Alder reaction (regular/neo motifs: 80/20).

1.3.2 Cell proliferation studies of A-ring hydroxylated caged *Garcinia* xanthones

The ability of the synthesized CGXs to inhibit cancer cell growth was evaluated in the T-cell acute lymphoblastic leukemia cell line (CEM). Based on our previous studies, this cell line was found to be one of the most sensitive.[8] The inhibitory concentrations at 50% inhibition (IC_{50}) of the active CGXs ranged from 0.12-1.0 μM. Compound **5**[10] was found to be relatively inactive with an IC_{50} greater than 5μM (Figure 1.2). It is interesting to relate the activities of these CGXs to their structure, in particular as they relate to the reactivity of the C_9-C_{10} enone as a conjugate electrophile (Figure 1.2). Comparison of **3** with **15** suggests that the presence of a free phenolic group at the C_6 position of the A ring (*i.e.* compound **3**) increases the potency of this compound, while its protection as a MOM ether (*i.e.* compound **15**) decreases its potency. This modulation of potency parallels the effect of the C_6 oxygen on the activation of the C_9-C_{10}

Compound	IC50 (μM)
1	0.12
2	0.18
3	0.3
4	1
5	5.1
15	0.5
19	0.5

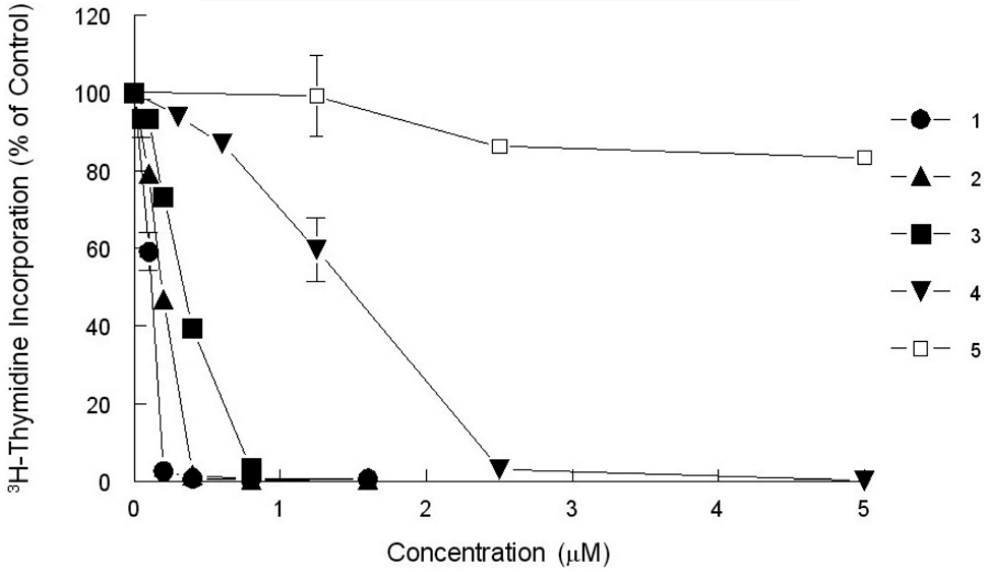

Figure 1.2: Inhibition of cell proliferation by CGXs in CEM cells.

enone. Specifically, in compound **3**, the C_6 free phenolic functionality can create a hydrogen bond with the adjacent carbonyl group, thereby enhancing the electrophilicity of the C_{10} center. In contrast, the MOM ether functionality at C_6 of **15** enriches the electron density of the B-ring carbonyl group (vinylogous carbonyl system), thereby reducing the electrophilicity of the C_{10} center. In a similar manner, compound **19** (containing a MOM ether at C_{18}) is twice as potent as **4** (that contains a free phenolic group at C_{18}). This is consistent with the prediction that a free phenolic group para to the B ring carbonyl would act as a strong electron donor, thereby reducing the electrophilicity of the C_{10} center. Along these lines, compound **5** (containing a methyl group at C_{10}) is about twenty times less potent than **2** in which the C_{10} center is not substituted and thus more accessible for a conjugate addition reaction with a bionucleophile. Overall, these comparative studies support the notion that increasing the electrophilicity of the

C_{10} enone enhances the potency of the CGX motif.

1.3.3 Effect of GA and CLV on mitochondria

We have previously reported that CLV (**2**) and GA (**1**) localize in mitochondria, and induce mitochondrial fragmentation leading to activation of caspase-3 (C3) ultimately resulting in cell apoptosis.[11] Despite having similar phenotypes, the cellular effects of **1** and **2** have not been compared. To this end, we began by analyzing the timing of induction of the apoptotic pathway, by western blot (WB) analysis of active caspase-9, a known initiator caspase,[16] and caspase-3, the known downstream executioner of apoptosis.[17] Caspase-9 (C9) was examined due to its well established connection to the mitochondrial apoptotic pathway and its subsequent activation of C3. HeLa cells were treated with 2μM GA (Figure 1.3a) or CLV (Figure 1.3b) from 0 min (control cells, incubated with equal volume of DMSO) to 180 min. Both compounds induced similar activation of C9 and C3 after about 120 min of incubation. In fact, C9 appears to be activated right before C3 since it is visible after about 90 min of incubation. We then evaluated the status of the mitochondrial network by immunofluorescence (IF). As shown in Figure 1.3 (g and h), both GA and CLV induced a similar degree of mitochondrial disruption. Both compounds were found to induce a first degree of fragmentation after 30 min incubation, at which time the mitochondrial network appeared fragmented in larger discrete elements (Fig. 1.3d for GA and 1.3g for CLV). At longer incubation times (1h treatment for both compounds) the mitochondria appeared collapsed in the perinuclear area and the mitochondrial network was no longer visible (Fig. 1.3e and 1.3h).

Comparison of the IF results with the WB analysis supports the notion that mitochondrial fragmentation (visible after 30 min incubation) appears before the activation of the initiatory C9 (visible after 90 min incubation). This observation confirms that both GA and CLV induce cell death via the intrinsic pathway, in which mitochondrial damage leads initially to C9 activation that subsequently activates C3. These results also suggest that GA and CLV act with a similar timing to activate the mitochondrial-dependent (intrinsic) apoptotic pathway.

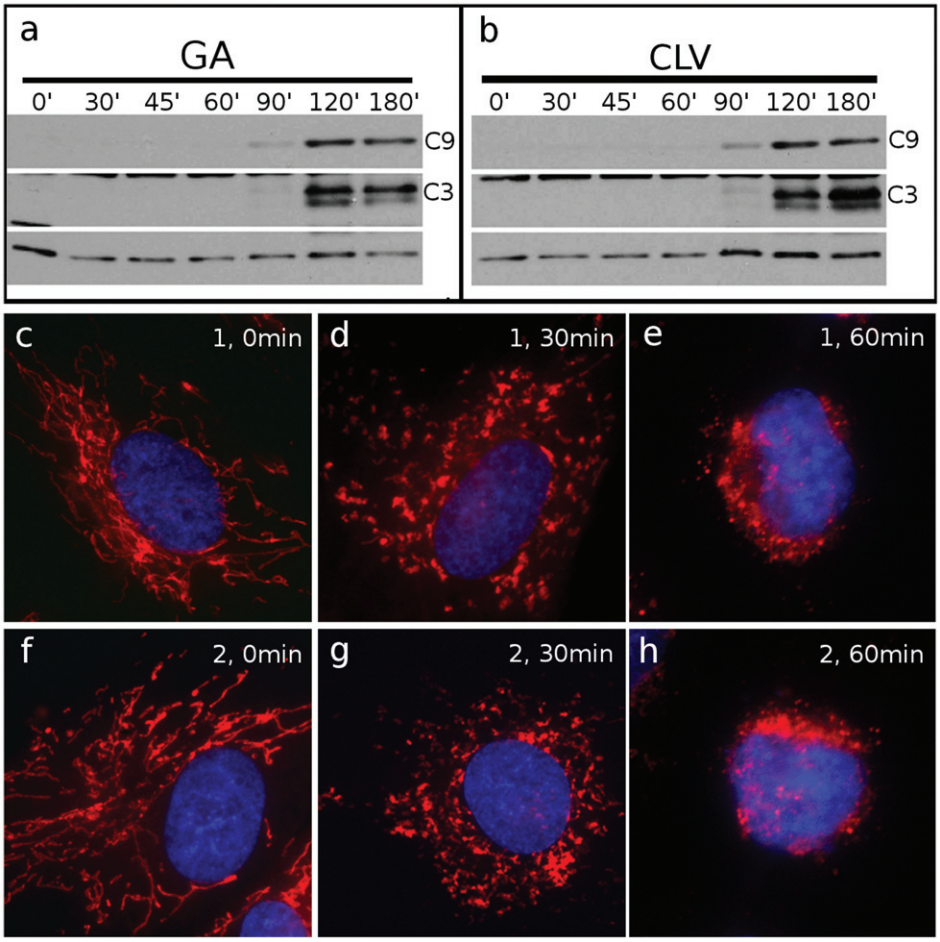

Figure 1.3: Comparison between GA and CLV with respect to mitochondrial fragmentation and induction of apoptosis.

1.3.4 Effect of A-ring hydroxylated caged *Garcinia* xanthones on apoptosis and mitochondria

We then evaluated the ability of compounds **3**, **4** and **5** to induce mitochondrial fragmentation and cell death in HeLa cells. Cells incubated for 60 to 180 min with CLV and derivatives **3**, **4** and **5** were analyzed to assess induction of apoptosis by WB analysis of active caspase-3 (C3). As shown in Figure 1.4, **2** and **3** were able to induce apoptosis after 90 min incubation (compare lanes 3 and 7). On the other hand, compound **4**, which carried the phenolic group at C_{18} was less effective, inducing C3 activation only after 120 min treatment (lane 12). Moreover, compound **5** proved to be inactive at the concentrations tested (2 μM). Even at much higher concentrations (up to 80 μM), **5**

proved to be the least effective of the compounds, requiring 180 min to induce comparable levels of apoptosis. The results parallel the potency profile of these compounds and provide additional arguments in favor of the role of A ring hydroxylation in modulating the reactivity of the C_9-C_{10} enone as an electrophile. We also tested compounds **3**, **4**

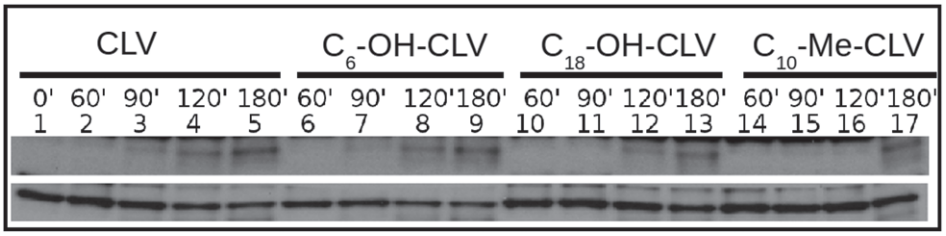

Figure 1.4: Effect of selected CGXs on apoptosis.

and **5** for their ability to induce mitochondrial fragmentation. Control untreated cells are shown in Figure 1.5a. Compound **3** induced mitochondrial disruption after 30 min of incubation (Fig. 1.5b), while extensive levels of fragmentation were reached after 60 minutes of incubation (Fig. 1.5c). The action of compound **3** was therefore similar to that of CLV at identical time points. To achieve similar levels of fragmentation, compound **4** had to be incubated for 60 min (Fig. 1.5e) and 90 min (Fig. 1.5f). Moreover, compound **5** showed the lowest levels of fragmentation, being able to induce partial mitochondrial disruption only after 120 min incubation at 80 μM concentration (Fig. 1.5i). Overall, the findings suggest that the extent of mitochondrial fragmentation parallels the activation of the C_9-C_{10} enone as an electrophile.

1.3.5 The caged *Garcinia* xanthones induce irreversible mitochondrial fragmentation

Inspired by the above findings we sought to evaluate if the effect of CGXs on mitochondria can be reversed upon removal of these compounds from the incubation media. We begun by treating HeLa cells with 2μM of GA or CLV for 0 min, 15 min and 30 min. The cells were then allowed to recover for 90 min in fresh medium and subsequently were fixed and processed for IF. As shown in Figure 1.6, 30 min incubation with GA (Fig. 1.6c) and CLV (Fig. 1.6f) were necessary and sufficient to induce a permanent mitochondrial fragmentation, while shorter time point (15 min) proved to be not

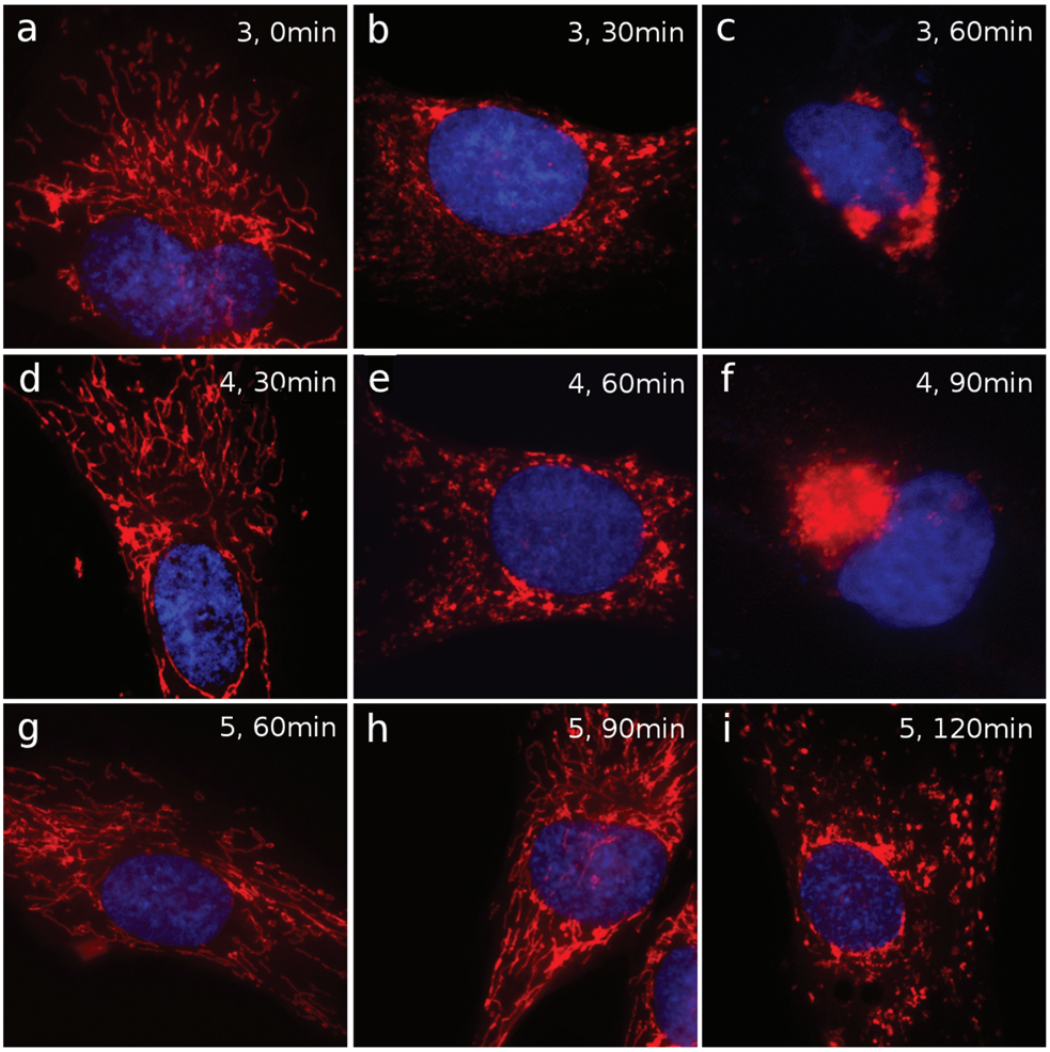

Figure 1.5: Effect of **3**, **4**, and **5** on mitochondria.

effective and mitochondrial integrity was recovered (Fig. 1.6b for GA and Fig. 1.6e for CLV). To assess whether the phenotype of the irreversible mitochondrial fragmentation corresponded to an irreversible effect on apoptosis we incubated cells with GA and CLV for 0 min, 30 min, 45 min, 60 min and 90 min, and then allowed them to recover for 90 min in fresh medium. The cells were then analyzed by western blot in order to visualize caspase-3 activation. As shown in Figure 1.6 (g, h), no signs of apoptosis (measured by caspase-3 activation) were visible prior to 90 min incubation with either GA (Fig. 1.6g, lanes 1-5) or CLV (Fig. 1.4h, lanes 10-13). However, when cells were treated for 45 min and then allowed to recover for 90 min (Fig. 1.6g lane 7 and Fig. 1.6h lane 15),

caspase-3 was active, indicating that, during 45 min of incubation, both GA and CLV were inducing irreversible morphological changes to mitochondrial structure leading to the irreversible activation of the apoptotic pathway. We then tested the irreversibility of mitochondrial fragmentation upon exposure to compounds **3**, **4** and **5** (Fig. 1.7). The cells were treated as in Figure 1.6; after the incubation with CGXs for different amounts of time, the cells were subjected to 90 min recovery in fresh medium and were then processed for IF and WB analysis to detect mitochondria fragmentation and caspase-3 activation. All the compounds were incubated at 2 μM (with the exception of 5 that was

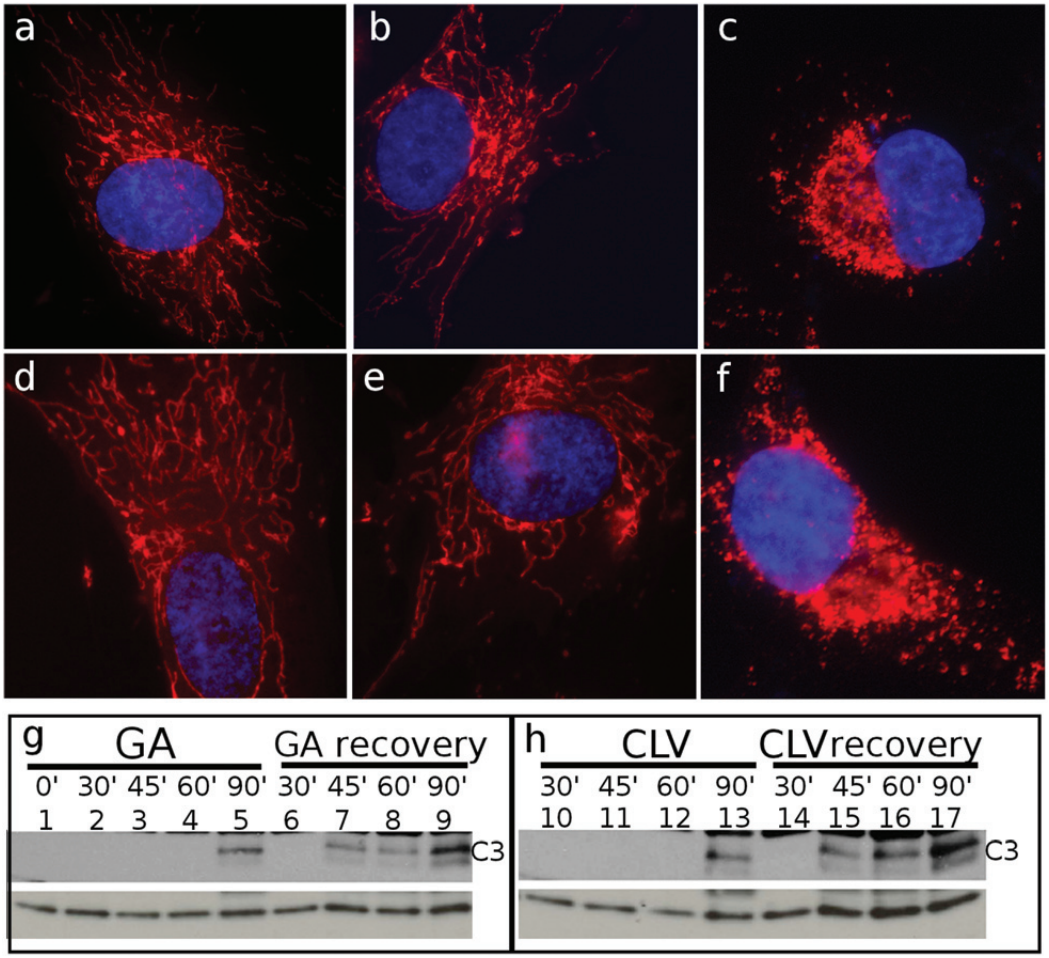

Figure 1.6: Irreversibility of mitochondrial fragmentation by GA and CLV.

used at 80 μM) for times ranging from 0 min to the minimum time necessary to induce caspase-3 activation, at 15 min intervals. This time varies from each compound, being equal to 90 min for **3**, 120 min for **4** and 180 min for **5**. After washing of the com-

pounds, the cells were allowed to recover for 90 min and processed for IF. Figure 1.7 shows the results for compounds **3** and **4**. Compound **5** proved to have a reversible effect at the times and concentrations tested (data not shown). Compound **3** behaved similarly to CLV, since 30 min incubation were sufficient to induce an irreversible mitochondrial fragmentation (Fig. 1.7c). On the other hand, compound **4** proved to be less effective, requiring 45 min (Fig. 1.7f) to induce the same level of mitochondrial disruption. We then performed WB analysis to confirm that the irreversible mitochondria fragmentation corresponded to the activation of caspase-3. As shown in Figure 1.7g, compound **3** induced caspase activation after 45 min of incubation, reproducing the results obtained for both CLV and GA. Analogue **4** was once again less effective, inducing caspase-3 activation following 45 min of treatment. Compound **5** was ineffective for up to 120 min of incubation.

1.3.6 Effect of A-ring hydroxylated caged *Garcinia* xanthones on the modulation of Hsp90

Hsp90 is a nodal protein that plays critical role in protein folding and is essential to cell proliferation.[7] In cancer cells this protein is overexpressed and also exists in a high-affinity conformation that facilitates malignant progression.[18] As such, it represents an important target for the development of anticancer agents.[19] Treatment of different cancer cell lines with known Hsp90 inhibitors is known to induce degradation of kinases, transcription factors and other protein clients of Hsp90.[20] Encouraged by recent studies suggesting that Hsp90 is a major target of GA,[6] we evaluated the effect of CLV and its A-ring hydroxylated derivatives **3** and **4** on this protein in SKBR3 cells, a breast cancer cell line. The cells were treated with different concentrations of GA, CLV, **3** and **4** or just the solvent (DMSO) for 24 hours and analyzed for several different client kinases, as well as Hsp70 and Hsp90. As seen on Figure 1.8, the active form of the survival kinase Akt, pAkt (anti-phospho Ser473) disappears faster than the total Akt (tAkt). The kinase Raf-1 that functions in the MAPK/ERK signaling pathway controlling cell growth degrades in a concentration dependent manner for all compounds tested. Also, Her2 kinase, a well established therapeutic target for breast cancer, proves to be extremely sensitive to treatment with GA, CLV and **3** (starts degrading at the lowest

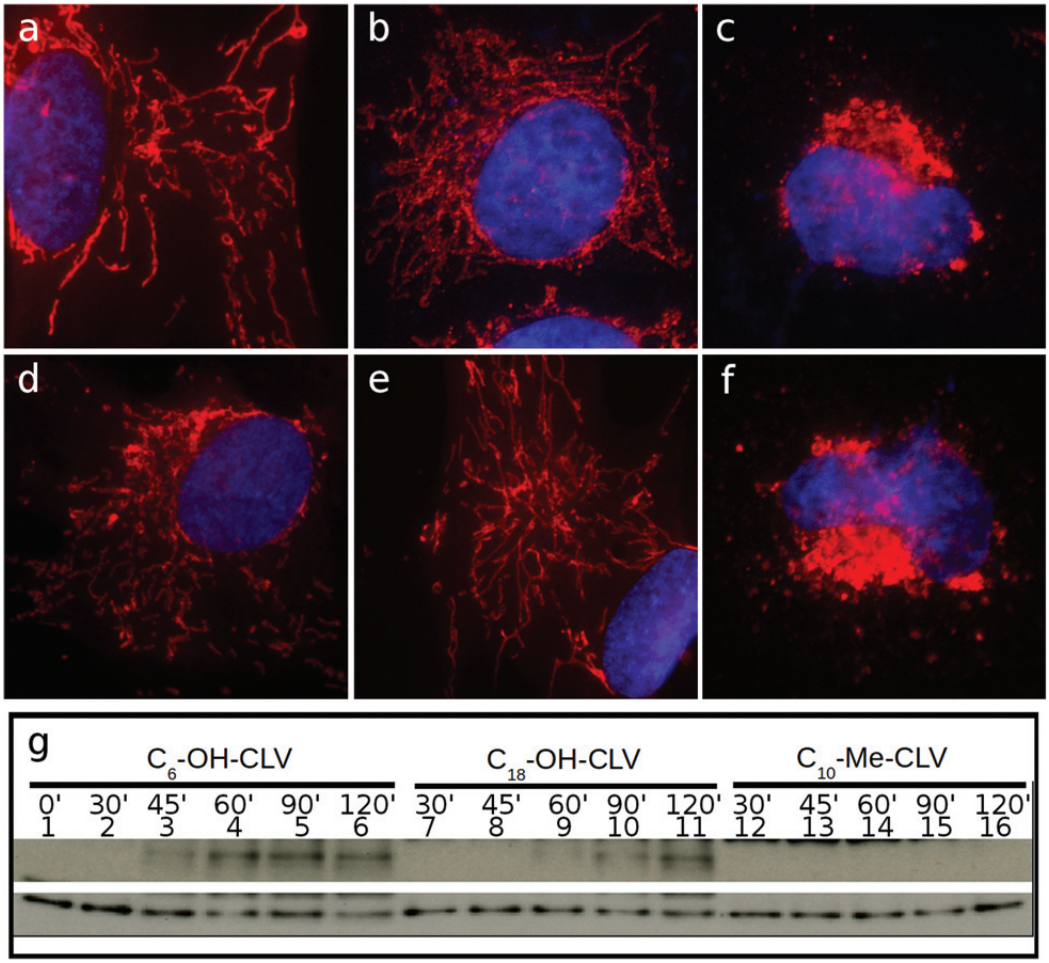

Figure 1.7: Irreversibility of mitochondrial fragmentation by **3**, **4**, and **5**.

dose tested) and less sensitive to compound **4** (degradation happens only at the higher concentration used). Additionally, the mass induction of Hsp70 and the less prominent induction of Hsp90, are indicators of Hsp90 inhibition, upon which the heat shock factor (HSF1) becomes activated and leads to transcriptional induction of the heat shock genes (e.g. Hsp70). Comparisons of the amounts of client degradation and induction of Hsp70 using the different compounds, suggests that both CLV and **3** behave similarly and they resemble the client degradation rates and Hsp70 induction observed with GA. In order to test the SKBR3 cells for induction of apoptosis, after treating the cells with the same concentrations of GA, CLV, **3** and **4** that lead to degradation of Hsp90 clients, we analyzed the cell lysates for cleavage of PARP, a DNA polymerase involved in DNA repair and cell death (Fig. 1.9). Again, 24 hours post treatment, even at the low concentration

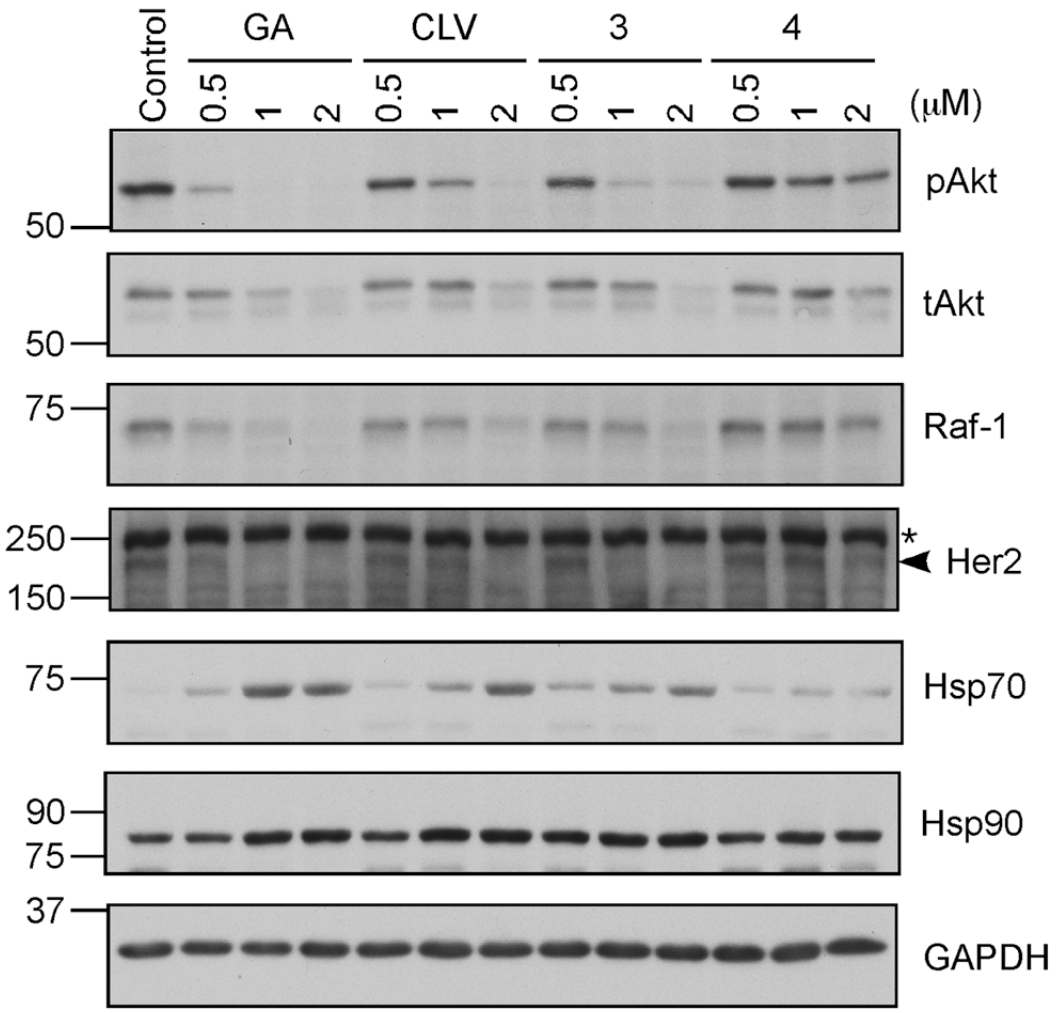

Figure 1.8: Gambogic acid (GA), CLV, **3** and **4** induce degredation of Hsp90 client proteins.

of 0.5 μM both GA and CLV induce cleavage of PARP (MW 89-lower band) which clearly indicates that the cells are already undergoing apoptosis. Comparison between CLV and **3**, shows that both compounds are able to induce apoptosis at similar rates (compare CLV and **3** at 2 μM). As expected, compound **4** did not induce significant apoptosis at the concentrations used.

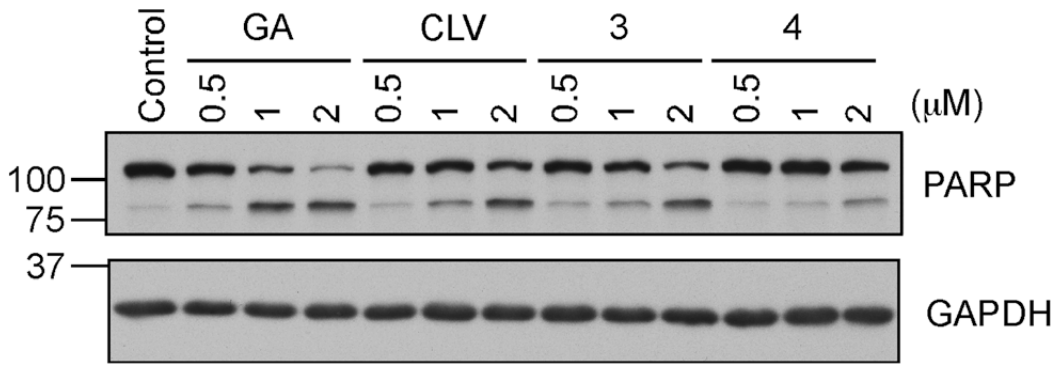

Figure 1.9: GA, CLV, **3** and **4** induce apoptosis in a concentration dependent manner in SKBR3 cells.

1.4 Conclusions

Inspired by the biological potential of cluvenone (CLV) and related caged *Garcinia* xanthones (CGXs), we synthesized selected A-ring hydroxylated analogues and evaluated their effect on cell growth, mitochondrial fragmentation, mitochondriotoxicity and Hsp90 client protein degradation. We found that both the C_6 and C_{18} hydroxylated cluvenones inhibit growth of CEM cells at low micromolar concentrations and induce cell death via the mitochondrial pathway. In addition, gambogic acid, CLV and the hydroxylated cluvenones induce Hsp90-dependent protein client degradation at low micromolar concentrations. Interestingly, the site of A ring hydroxylation significantly influences the site selectivity of the Claisen/Diels-Alder cascade. For instance, introduction of a MOM ether group at C_6 or C_{18} (*e.g.* compound **4**) increases via resonance the electron density of the B ring carbonyl group leading to formation of both regular and neo caged motifs (4:1 ratio in favor of the regular caged structure). In contrast, the presence of a free phenolic group at C_6 (*i.e.* compound **3**) decreases the electron density of the B ring carbonyl, thus favoring formation of the regular motif (produced in 11.5:1 ratio over the neo caged motif). Importantly, the site of A ring hydroxylation also affects the bioactivity of the CGX motif. Specifically, **3** is approximately 3 times more active than **4** in inhibiting cell growth of CEM cells. A similar trend is observed in the mitochondrial fragmentation, the caspase activation and the Hsp90 client inhibition assays. We postulate that this trend stems from tuning the reactivity of the C_9-C_{10} enone as a conjugate electrophile. In support of this postulate, methylation at C10 (*i.e.* com-

pound **5**) significantly limits the reactivity of this enone thereby decreasing the overall bioactivity of the CGX motif. Overall, our studies indicate that the A-ring of the caged Garcinia xanthones is amenable to functionalization in a manner that modulates not only the site selectivity of the Claisen/Diels-Alder reaction cascade but also their biological potency.

Chapter 1, in full, is a reprint of the material as it appears in Organic and Biomolecular Chemistry **2013**. Elbel, K. M., Guizzunti, G., Theodoraki, M. A., Xu, J., Batova, A., Dakanali, M., Theodorakis, E. A. "A-ring oxygenation modulates the chemistry and bioactivity of caged *Garcinia* xanthones" *Org. Biomol. Chem.* **2013**, *11*, 3341-3348.

1.4.1 Acknowledgements

Financial support from the National Institutes of Health (CA 133002) is gratefully acknowledged. We thank the National Science Foundation for instrumentation grants CHE9709183 and CHE0741968. We also thank Dr Anthony Mrse (UCSD NMR Facility) and Dr Yongxuan Su (UCSD MS Facility).

1.5 Experimental Section

1.5.1 General Techniques

Unless indicated, all commercially available reagents and anhydrous solvents were purchased at the highest commercial quality and were used as received without further purification. All non-aqueous reactions were carried out under argon atmosphere using dry glassware that had been flame-dried under a stream of argon unless otherwise noted. Anhydrous tetrahydrofuran (THF) and dichloromethane (CH_2Cl_2) were obtained by passing commercially available pre-dried, oxygen-free formulations through activated alumina columns. Flash column chromatography was performed on silica gel (Merck Kieselgel 60, 230-400 mesh) using Hexanes-EtOAc or CH_2Cl_2 / MeOH mixtures of increasing polarity. The progress of all the reactions was monitored by thin-layer chromatography (TLC) using glass plates precoated with silica gel-60 F254 to a thickness of 0.5 mm (Merck), and compounds were visualized by irradiation with UV light and/or by treatment with a solution of CAM stain or Seebach's stain followed by heating. ^{13}C NMR and ^{1}H NMR spectra were recorded on either 400 MHz or 500 MHz Varian instrument or 500 MHz JEOL instrument. $CDCl_3$ was treated with anhydrous K_2CO_3, chemical shifts (δ) are quoted in parts per million (ppm) referenced to the appropriate residual solvent peak reference ($CDCl_3$ or CD_3OD), with the abbreviations s, br s, d, t, q, m, td, dt and qd denoting singlet, broad singlet, doublet, triplet, quartet, multiplet, quartet of doublets, triplet of doublets, doublet of triplets and quartet of doublets respectively. J = coupling constants given in Hertz (Hz). High-resolution Mass spectra (HRMS) were recorded on a trisector WG AutoSpecQ spectrometer. Compound **5** was prepared as reported in reference 10.

1.5.2 Experimental Procedures and Data

1,5,6-trimethoxy-9H-xanthen-9-one (9a). To a suspension of 2,6-dimethoxybenzoic acid **6a** (5 g, 27.1 mmol) in dry CH_2Cl_2 (120 mL), oxalyl chloride (11.6 mL, 136 mmol), and DMF (0.2 mL, 2.7 mmol) were added. The mixture was left stirring for 16 h, concentrated under reduced pressure, and dried under high vacuum for 2 h to afford 2,6-dimethoxybenzoyl chloride **7a**. To a solution of the above synthesized **7a** and 1,2,3-trimethoxy benzene **8** (5.1 g, 30.2 mmol) in dry ether (40 mL), aluminum trichloride (11 g, 82.4 mmol) was added at 0 ° C and the solution was left stirring for 12 h at room temperature under inert atmosphere. A mixture of 15% hydrochloric acid and ethyl acetate (200 mL, 1:1) was then added. The ethyl acetate layer was collected, washed with brine, dried over magnesium sulfate, and concentrated under reduced pressure. The residue was suspended in a solution containing methanol (47 mL), water (31 mL), and NaOH (8.3 g, 208.6 mmol) at 0 °C and the solution was acidified with dilute HCl until pH = 2-3. The precipitate was filtered, washed with cold water, and dried to yield **9a** as yellow solid (7.0 g, 90% yield). ^{1}H NMR (400 MHz, $CDCl_3$) δ 7.76 (d, J = 12.0 Hz, 1H), 7.64 (d, J = 8.0 Hz, 1H), 7.11 (d, J = 4.0 Hz, 1H), 7.10 (s, 1H), 6.92 (d, J = 8.0 Hz, 1H), 3.91 (s, 3H), 3.87 (s, 3H), 3.86 (s, 3H); ^{13}C NMR (100 MHz, $CDCl_3$) δ 174.7, 160.8, 158.0, 157.4, 149.3, 136.1, 135.9, 122.0, 117.8, 111.9, 110.3, 109.9, 107.1, 61.6, 57.0, 56.8; HRMS (ESI) m/e 309.0732 [M + Na^+] calcd for $C_{16}H_{14}O_5Na^+$: 309.0733.

3,4,6-trimethoxy-9H-xanthen-9-one (9b). Same procedure as for **9a** was used to yield **9b** as a brown solid (4.5 g, 58% yield). ^{1}H NMR (400 MHz, $CDCl_3$) δ 8.13 (d, J = 8.0 Hz, 1H), 7.95 (d, J = 8.0 Hz, 1H), 7.20 (d, J = 4.0 Hz, 1H), 7.10 (s, 1H), 7.01 (dd, J = 8.0 Hz, 4.0 Hz, 1H), 4.03 (s, 3H), 4.00 (s, 3H), 3.97 (s, 3H); ^{13}C NMR^{13}C (100 MHz, $CDCl_3$) δ 174.2, 164.6, 157.4, 157.0, 149.8, 135.8, 127.3, 121.3, 115.5, 113.5, 109.4, 100.5, 60.9, 56.3, 56.1; HRMS (ESI) m/e 287.0912 [M + H^+] calcd for $C_{16}H_{15}O_5{}^+$: 287.0914.

1,5,6-trihydroxy-9H-xanthen-9-one (10a). To a solution of 48% hydrobromic acid (34 mL) and acetic acid (65 mL), **9a** (1.0 g, 3.49 mmol) was added and the mixture was stirred for 18 h at 120 °C. Upon completion, the solution was cooled to 0 °C and 10% NaOH solution was added until pH = 3-4. The precipitate was filtered, washed

with cold water, and dried to yield **10a** as a yellow solid (807 mg, 95% yield). ^{1}H NMR (400 MHz, DMSO-*d6*) δ 7.73 (t, J = 9.0 Hz, 1H), 7.59 (d, J = 12.0 Hz, 1H), 7.07 (d, J = 9.0 Hz, 1H), 6.99 (d, J = 12.0 Hz, 1H), 6.80 (d, J = 9.0 Hz, 1H); ^{13}C NMR (100 MHz, DMSO-*d6*) δ 181.3, 161.2, 155.8, 152.6, 146.5, 136.8, 132.6, 116.3, 113.2, 109.9, 107.6, 107.1; HRMS (ESI) m/e 243.0298 $[M-H]^-$ calcd for $C_{13}H_7O_5^-$: 243.0299.

3,4,6-trihydroxy-9H-xanthen-9-one (10b). Same procedure as for **10a** was used with **9b** (1 g, 3.49 mmol) to yield **10b** as a brown solid (692 mg, 81% yield). ^{1}H NMR (400 MHz, DMSO-*d6*) δ 10.80 (s br, 1H), 10.31 (s br, 1H), 9.32 (s br, 1H), 7.97 (d, J = 8.0 Hz, 1H), 7.49 (d, J = 8.0 Hz, 1H), 6.85 (m, 2H); ^{13}C NMR (100 MHz, DMSO-*d6*) δ 175.11, 164.0, 158.1, 151.6, 146.9, 133.2, 128.5, 117.0, 115.4, 114.4, 114.3, 113.4, 102.8; HRMS (ESI) m/e 245.0446 $[M + H]^+$ calcd for $C_{13}H_9O_5^+$: 245.0444.

5,6-dihydroxy-1-(methoxymethoxy)-9H-xanthen-9-one (11a). To a solution of 10a (770 mg, 3.15 mmol) in diphenyl ether (28 mL), α,α-dichlorodiphenyl methane (0.97 mL, 5.04 mmol) was added and the mixture was stirred for 4 h at 175 °C. Upon completion, the reaction mixture was cooled to 60 °C and was poured into petroleum ether (200 mL). The precipitate was filtered, washed with petroleum ether, and dried under vacuum to yield the diphenyl protected diol as a brown solid (1.2 g, 94% yield). ^{1}H NMR (500 MHz, $CDCl_3$) δ 7.90 (d, J = 8.0 Hz, 1H), 7.64 (m, 3H), 7.57 (t, J = 8.0 Hz, 1H), 7.42 (m, 5H), 7.32 (t, J = 8.0 Hz, 1H), 7.00 (m, 3H), 6.79 (d, J = 8.0 Hz, 1H); ^{13}C NMR (125 MHz, $CDCl_3$) δ 181.5, 162.3, 156.1, 153.4, 141.1, 139.2, 136.8, 134.0, 129.9, 129.8, 128.6, 126.5, 123.4, 121.3, 119.0, 116.9, 111.1, 108.6, 107.1, 106.5; HRMS (ESI) m/e 409.1069 $[M + H]^+$ calcd for $C_{26}H_{17}O_5^+$: 409.1071. To a solution of the above intermediate (500 mg, 1.22 mmol) in acetone (10 mL), sodium hydride (73 mg, 3.06 mmol) was added and the mixture was stirred for 30 min at 0 °C. To this mixture, MOMCl (0.19 mL, 2.45 mmol) was added dropwise and the reaction left stirring at room temperature for 12 h. Upon completion, the mixture was poured into ice water and the precipitate was filtered, washed with brine, and dried under high vacuum to yield the fully protected xanthone as a yellow powder (546 mg, 99% yield). ^{1}H NMR (400 MHz, $CDCl_3$) δ 7.89 (d, J = 8.5 Hz, 1H), 7.65 (m, 4H), 7.56 (t, J = 8.5 Hz, 1H), 7.41 (m, 6 H), 7.18 (d, J = 8.0 Hz, 1H), 7.05 (d, J = 8.5 Hz, 1H), 6.95 (d, J = 8.5

Hz, 1H), 5.37 (s, 2H), 3.57 (s, 3H); ^{13}C NMR (100 MHz, $CDCl_3$) δ 175.9, 158.7, 158.0, 152.7, 140.5, 139.9, 135.1, 130.2, 128.9, 127.0, 122.2, 119.9, 111.9, 111.3, 106.5, 96.0, 57.2, 30.2; HRMS (ESI) m/e 475.1151 $[M + Na]^+$ calcd for $C_{28}H_{20}O_6Na^+$: 475.1152. To a solution of the above intermediate (276 mg, 0.61 mmol) in methanol: THF (6 mL), $NaHCO_3$ (3.05 eq, 256 mg) and 10% Pd/C (27 mg) were added and the mixture was stirred under hydrogen atmosphere for 18 h at room temperature. Upon completion, the mixture was filtered through a plug of celite and was concentrated under reduced pressure. The residue was washed with hexanes and dried under vacuum to yield **11a** as a light brown solid (105 mg, 60% yield). ^{1}H NMR (400 MHz, DMSO-*d6*) δ 7.56 (t, J = 8.0 Hz, 1H), 7.33 (d, J = 8.5 Hz, 1H), 7.10 (d, J = 8.0 Hz, 1H), 6.93 (d, J = 8.0 Hz, 1H), 6.59 (d, J = 8.5 Hz, 1H), 5.25 (s, 2H), 3.44 (s, 3H); ^{13}C NMR (100 MHz, DMSO-*d6*) δ 174.4, 157.1, 151.1, 145.1, 134.3, 132.2, 128.7, 128.3, 125.9, 116.3, 112.8, 111.0, 110.5, 95.1, 55.9; HRMS (ESI) m/e 311.0524 $[M+Na]^+$ calcd for $C_{15}H_{12}O_6Na^+$: 311.0526.

3,4-dihydroxy-6-(methoxymethoxy)-9H-xanthen-9-one (11b). Same procedure as for **11a** was used. **10b** (209 mg, 0.86 mmol) yielded diphenyl protected xanthone as a brown solid (290 mg, 83% yield. Diphenyl protected xanthone (217 mg, 0.531 mmol) yielded fully protected xanthone as a yellow powder (230 mg, 95% yield). Fully protected xanthone (350 mg, 0.77 mmol) yielded free diol **11b** as a green powder (121 mg, 54% yield). The di-phenyl protected intermediate: ^{1}H NMR (300 MHz, acetone-d6) δ 8.10 (d, J = 9.6 Hz, 1H), 7.86 (d, J = 8.5 Hz, 1H), 7.67 (m, 4H), 7.48 (m, 6H), 7.12 (d, J = 8.5 Hz, 1H), 6.96 (m, 2H); ^{13}C NMR (75 MHz, acetone-*d6*) δ 174.0, 163.7, 157.8, 152.3, 145.0, 142.0, 134.5, 139.6, 129.9, 128.8, 128.6, 126.4, 121.4, 119.6, 118.4, 114.8, 113.9, 106.1, 102.5; HRMS (ESI) m/e 409.1072 $[M+H]^+$ calcd for $C_{26}H_{17}O_5^+$: 409.1071.

The di-phenyl and MOM protected intermediate: ^{1}H NMR (400 MHz, DMSO-*d6*) δ 8.09 (d, J = 9.0 Hz, 1H), 7.80 (d, J = 8.5 Hz, 1H), 7.61 (m, 4H), 7.49 (m, 6H), 7.28 (s, 1H), 7.24 (d, J = 8.5 Hz, 1H), 7.11 (d, J = 8.0 Hz, 1H), 5.40 (s, 2H), 3.43 (s, 3H); ^{13}C NMR (100 MHz, DMSO-*d6*) δ 173.8, 162.1, 156.7, 151.6, 140.4, 138.7, 133.1, 129.9, 128.8, 127.9, 125.9, 125.7, 121.2, 119.4, 117.7, 115.4, 114.5, 106.5, 103.1, 94.1, 93.9, 56.1; HRMS (ESI) m/e 453.1329 $[M+H]^+$ calcd for $C_{28}H_{21}O_6^+$: 453.1333.

11b: ^{1}H NMR (400 MHz, acetone-*d6*) δ 8.14 (d, J = 8.0 Hz, 1H), 7.65 (d, J

= 8.0 Hz, 1H), 7.14 (s, 1H), 7.06 (d, *J* = 8.0 Hz, 1H), 6.96 (d, *J* = 8.0 Hz, 1H), 5.37 (s, 2H), 3.49 (s, 3H); ^{13}C NMR (100 MHz, acetone-*d6*) δ 174.7, 162.4, 157.7, 150.7, 146.5, 132.6, 128.0, 117.2, 116.2, 115.7, 114.2, 112.9, 102.9, 94.5, 55.8; HRMS (ESI) m/e 289.0704 $[M+H]^+$ calcd for $C_{15}H_{13}O_6^+$: 289.0707.

1-(methoxymethoxy)-5,6-bis((2-methylbut-3-en-2-yl)oxy)-9H-xanthen-9-one (13a). To a 50 mL round bottom flask was added **11a** (70 mg, 0.24 mmol) followed by dry THF (1.3 mL). The flask was degassed by argon and was placed in an ice water bath. To the homogenous solution was added carbonate **12** (482 mg, 2.43 mmol), via syringe, followed by $Pd(PPh_3)_4$ (28 mg, 0.0243 mmol). The reaction vessel was stirred under argon at 5 ° C for 2 hours. Upon completion, the solvent was removed by rotary evaporation and the crude material was purified through flash chromatography (5-15% EtOAc-hexanes) to yield **13a** as a white solid (64 mg, 63% yield). ^{1}H NMR (400 MHz, $CDCl_3$) δ 7.87 (d, *J* = 8.0 Hz, 1H), 7.55 (t, *J* = 8.0 Hz, 1H), 7.14 (d, *J* = 8.0 Hz, 1H), 7.08 (d, *J* = 8.0 Hz, 1H), 7.04 (d, *J* = 8.0 Hz, 1H), 6.31-6.15 (m, 2H), 5.38 (s, 2H), 5.22-5.16 (m, 3H), 5.02 (d, *J* = 8.0 Hz, 1H), 3.57 (s, 3H), 1.57 (s, 6H), 1.56 (s, 6H); ^{13}C NMR (100 MHz, $CDCl_3$) δ 176.4, 158.1, 158.0, 156.6, 151.6, 143.9, 143.7, 135.6, 134.5, 121.3, 117.1, 114.3, 113.3, 113.3, 111.7, 110.6, 95.6, 83.7, 82.3, 56.8, 29.9, 27.4, 27.2; HRMS (ESI) m/e 447.1779 $[M+Na]^+$ calcd for $C_{25}H_{28}O_6Na^+$: 447.1778.

6-(methoxymethoxy)-3,4-bis((2-methylbut-3-en-2-yl)oxy)-9H-xanthen-9-one (13b). Same procedure for **13a** was used. **11b** (80 mg, 0.28 mmol) yielded **13b** as a white solid (100 mg, 84% yield). ^{1}H NMR (400 MHz, $CDCl_3$) δ 8.22 (d, *J* = 8.0 Hz, 1H), 7.90 (d, *J* = 8.0 Hz, 1H), 7.11-7.02 (m, 3H), 6.31-6.15 (m, 2H), 5.28 (s, 2H), 5.22-5.16 (m, 3H), 5.02 (d, *J* = 8.0 Hz, 1H), 3.52 (s, 3H), 1.58 (s, 6H), 1.56 (s, 6H); ^{13}C NMR (100 MHz, $CDCl_3$) δ 176.0, 162.2, 157.4, 156.5, 152.5, 143.6, 143.5, 135.8, 128.2, 120.9, 117.2, 116.9, 116.3, 114.0, 113.6, 113.0, 103.3, 94.3, 83.5, 82.1, 56.4, 27.1, 26.9; HRMS (ESI) m/e 447.1776 $[M+Na]^+$ calcd for $C_{25}H_{28}O_6Na^+$: 447.1778.

1-hydroxy-5,6-bis((2-methylbut-3-en-2-yl)oxy)-9H-xanthen-9-one (14). To a solution of **13a** (130 mg, 0.31 mmol) in THF (1 mL), ZnCl2 (1M in ether, 0.31 mL, 0.31 mmol) was added and the mixture was left stirring at 40 °C for 2 hours. The solvent was then removed by rotary evaporation and the crude material was purified through flash

column chromatography (5% EtOAc-hexane) to yield **14** (110 mg, 93%). ^{1}H NMR (500 MHz, $CDCl_3$) δ 7.84 (d, J = 8.0 Hz, 1H), 7.54 (t, J = 8.0 Hz, 1H), 7.13 (d, J = 8.0 Hz, 1H), 6.92 (d, J = 8.0 Hz, 1H), 6.76 (d, J = 8.0 Hz, 1H), 6.27-6.14 (m, 2H), 5.23-5.16 (m, 3H), 5.02 (d, J = 8.0 Hz, 1H), 1.57 (s, 6H), 1.56 (s, 6H); ^{13}C NMR (100 MHz, $CDCl_3$) δ 182.0, 162.0, 157.8, 156.2, 152.6, 143.6, 143.4, 136.4, 135.6, 120.5, 116.7, 115.7, 114.4, 113.3, 110.4, 108.6, 107.0, 83.8, 82.5, 27.3, 27.0; HRMS (ESI) m/e 381.1699 $[M+H]^+$ calcd for $C_{23}H_{25}O_5^+$: 381.1697.

8-hydroxy-2,2-dimethyl-3a-(3-methylbut-2-en-1-yl)-1,2-dihydro-1,5-methanofuro[2,3-d]xanthene-4,7(3aH,5H)-dione (3). A solution of **14** (13 mg, 34 mmol) in DMF (340 mL) was left stirring at 120 °C for 1 hour. The mixture was then cooled to room temperature and the solvent was removed by rotary evaporation. The crude material was then purified by preparative TLC (5% EtOAc-hexanes) to yield the regular caged xanthone **3** (12 mg, 92%) along with the neo isomer (1 mg, 8%). **3:** ^{1}H NMR (400 MHz, $CDCl_3$) δ 12.08 (s, 1H), 7.47 (d, J = 8.0 Hz, 1H), 7.38 (t, J = 8.0 Hz, 1H), 6.51 (m, 2H), 4.38 (m, 1H), 3.51 (m, 1H), 2.62-2.32 (m, 4H), 1.69 (s, 3H), 1.35 (s, 3H), 1.29 (s, 3H), 0.99 (s, 3H); ^{13}C NMR (100 MHz, $CDCl_3$) δ 203.0, 181.5, 163.0, 159.8, 139.0, 135.5, 135.1, 134.0, 118.9, 109.5, 107.6, 106.3, 90.2, 84.7, 83.8, 49.0, 47.2, 30.5, 29.4, 29.3, 25.7, 25.1, 16.9; HRMS (ESI) m/e 381.1696 $[M+H]^+$ calcd for $C_{23}H_{25}O_5^+$: 381.1697.

neo isomer: ^{1}H NMR (400 MHz, $CDCl_3$) δ 12.01 (s, 1H), 7.42 (t, J = 8.6 Hz, 1H), 7.30 (d, J = 6.9 Hz, 1H), 6.64 (d, J = 7.5 Hz, 1H), 6.53 (d, J = 7.5 Hz, 1H), 4.99 (m, 1H), 3.78 (m, 1H), 2.54 (d, J = 13.2 Hz, 1H), 2.50 (m, 1H), 2.16 (m, 2H), 1.85 (dd, J = 13.8 Hz, 10.3 Hz, 1H), 1.72 (s, 3H), 1.60 (s, 3H), 1.38 (s, 3H), 1.35 (s, 3H); ^{13}C NMR (100 MHz, $CDCl_3$) δ 199.6, 180.0, 163.0, 160.1, 139.4, 136.6, 136.4, 134.6, 117.4, 109.8, 107.9, 106.6, 84.0, 83.9, 79.2, 45.1, 42.2, 33.1, 30.4, 29.7, 26.8, 26.0, 18.3; HRMS (ESI) m/e 381.1698 $[M+H]^+$ calcd for $C_{23}H_2O_5^+$: 381.1697.

8-(methoxymethoxy)-2,2-dimethyl-3a-(3-methylbut-2-en-1-yl)-1,2-dihydro--1,5-methanofuro[2,3-d]xanthene-4,7(3aH,5H)-dione (15). A solution of **13a** (10 mg, 23.6 mmol) in DMF (240 mL) was left stirring at 120 °C for 1 hour. The mixture was then cooled to room temperature and the solvent was removed by rotary evaporation. The crude material was then purified by preparative TLC (5% EtOAc-hexanes) to yield

the regular caged xanthone **15** (8 mg, 80%) along with the neo isomer **16** (2 mg, 20%). **15:** ^{1}H NMR (500 MHz, $CDCl_3$) δ 7.38 (t, J = 8.0 Hz, 1H), 7.28 (d, J = 6.8 Hz, 1H), 6.78 (d, J = 8.4 Hz, 1H), 6.71 (d, J = 8.4 Hz, 1H), 5.29 (s, 2H), 4.46 (m, 1H), 3.51 (s, 3H), 3.44 (m, 1H), 2.60 (m, 2H), 2.39 (d, J = 9.3 Hz,1H), 2.29 (dd, J = 13.2 Hz, 4.4 Hz, 1H), 1.68 (s, 3H), 1.37 (s, 3H), 1.27 (s, 3H), 1.25 (m, 1H), 1.07 (s, 3H); ^{13}C NMR (125 MHz, $CDCl_3$) δ 203.4, 175.8, 161.1, 158.4, 136.5, 136.1, 134.9, 132.6, 118.7, 111.7, 108.7, 94.9, 89.9, 84.5, 83.5, 56.6, 48.6, 46.8, 30.4, 29.1, 25.7, 25.6, 17.1; HRMS (ESI) m/e 447.1777 $[M+Na]^+$ calcd for $C_{25}H_{28}O_6Na^+$: 447.1778.

neo isomer: ^{1}H NMR (500 MHz, $CDCl_3$) δ 7.41 (t, J = 8.6 Hz, 1H), 7.10 (d, J = 6.9 Hz, 1H), 6.86 (d, J = 7.5 Hz, 1H), 6.78 (d, J = 7.5 Hz, 1H), 5.27 (s, 2H), 5.06 (m, 1H), 3.72 (m, 1H), 3.51 (s, 3H), 2.49 (m, 2H), 2.17 (m, 1H), 2.01 (m, 1H), 1.84 (m, 1H), 1.71 (s, 3H), 1.58 (s, 3H), 1.37 (s, 3H), 1.33 (s, 3H); ^{13}C NMR (125 MHz, $CDCl_3$) δ 200.6, 175.2, 161.9, 158.3, 137.8, 136.6, 136.2, 133.5, 117.5, 112.0, 111.5, 108.8, 95.0, 83.8, 78.9, 56.6, 44.5, 42.5, 32.7, 30.0, 29.7, 26.8, 26.0, 18.3; HRMS (ESI) m/e 447.1780 $[M+Na]^+$ calcd for $C_{25}H_{28}O_6Na^+$: 447.1778.

10-(methoxymethoxy)-2,2-dimethyl-3a-(3-methylbut-2-en-1-yl)-1,2-dihydro-1,5-methanofuro[2,3-d]xanthene-4,7(3aH,5H)-dione (19). A solution of **13b** (15 mg, 39 mmol) in DMF (340 mL) was left stirring at 120 °C for 1 hour. The mixture was then cooled to room temperature and the solvent was removed by rotary evaporation. The crude material was then purified by preparative TLC (5% EtOAc-hexanes) to yield the regular caged xanthone **19** (12 mg, 80%) along with the neo isomer **20** (3 mg, 20%). **19:** ^{1}H NMR (500 MHz, $CDCl_3$) δ 7.89 (d, J = 10.7 Hz, 1H), 7.40 (d, J = 8.2 Hz, 1H), 6.74 (dd, J = 8.4 Hz, 2.5 Hz, 1H), 6.65 (d, J = 2.5 Hz, 1H), 5.23 (s, 2H), 4.44 (m, 1H), 3.48 (s, 3H), 3.48 (m, 1H), 2.61 (m, 2H), 2.44 (d, J = 11.9 Hz,1H), 2.32 (dd, J = 16.9 Hz, 5.7 Hz, 1H), 1.71 (s, 3H), 1.33 (s, 3H), 1.30 (s, 3H), 1.00 (s, 3H); ^{13}C NMR (125 MHz, $CDCl_3$) δ 203.4, 175.5, 163.9, 161.5, 134.9, 134.8, 133.3, 128.9, 118.7, 113.9, 111.6, 103.5, 94.1, 90.8, 84.6, 83.6, 60.5, 56.5, 48.9, 46.8, 30.5, 29.2, 29.1, 25.5, 25.3, 21.2, 16.9, 14.3; HRMS (ESI) m/e 447.1775 $[M+Na]^+$ calcd for $C_{25}H_{28}O_6Na^+$: 447.1778.

neo isomer **20:** ^{1}H NMR (500 MHz, $CDCl_3$) δ 7.87 (d, J = 8.6 Hz, 1H), 7.21 (d, J = 6.9 Hz, 1H), 6.81 (d, J = 2.3 Hz, 1H), 6.70 (dd, J = 7.5 Hz, 2.3 Hz, 1H), 5.25 (d, J = 6.9 Hz, 1H), 5.18 (d, J = 6.9 Hz, 1H), 5.03 (m, 1H), 3.75 (m, 1H), 3.48 (s, 3H),

2.49 (m, 2H), 2.13 (m, 1H), 2.06 (m, 1H), 1.86 (m, 1H), 1.72 (s, 3H), 1.59 (s, 3H), 1.37 (s, 3H), 1.34 (s, 3H); ^{13}C NMR (125 MHz, $CDCl_3$) δ 200.2, 174.4, 164.3, 162.3, 136.3, 136.0, 134.3, 129.0, 117.5, 112.1, 103.8, 94.2, 84.6, 83.9, 79.1, 56.6, 44.7, 42.1, 33.1, 30.2, 29.7, 26.8. 26.0, 18.3, 14.3; HRMS (ESI) m/e 447.1781 $[M+Na]^+$ calcd for $C_{25}H_{28}O_6Na^+$: 447.1778.

10-hydroxy-2,2-dimethyl-3a-(3-methylbut-2-en-1-yl)-1,2-dihydro-1,5-methanofuro[2,3-d]xanthene-4,7(3aH,5H)-dione (4). To a solution of **19** (1.5 mg, 3.5 mmol) or neo-isomer **20** (1.5 mg, 3.5 mmol) in THF (20 mL), $ZnCl_2$ (10 eq, 1 M in ether) was added and the mixture was left stirring at 40 °C for 24 hours. The solvent was then removed by rotary evaporation and the crude material was purified through preparative TLC (20% EtOAc-hexane) to yield **4** (1 mg, 75%) or neo-isomer **21** (1 mg, 75%). **4:** ^{1}H NMR (500 MHz, CD_3OD) δ 7.74 (d, J = 8.6 Hz, 1H), 7.33 (d, J = 6.9 Hz, 1H), 6.54 (dd, J = 8.6 Hz, 2.3 Hz, 1H), 6.39 (d, J = 2.3 Hz, 1H), 4.37 (m, 1H), 3.44 (m, 1H), 2.59-2.32 (m, 4H), 1.68 (s, 3H), 1.31 (s, 3H), 1.25 (s, 3H), 1.00 (s, 3H); ^{13}C NMR (125 MHz, CD_3OD) δ 203.4, 175.8, 166.0, 162.1, 134.9, 134.2, 133.4, 128.7, 118.6, 112.0, 111.3, 102.4, 90.6, 84.4, 83.6, 60.2, 29.3, 28.7, 28.0, 24.7, 24.4, 15.7, 13.1; HRMS (ESI) m/e 381.1696 $[M+H]^+$ calcd for $C_{23}H_{25}O_5^+$: 381.1697.

neo isomer **21:** ^{1}H NMR (500 MHz, CD_3OD) δ 7.72 (d, J = 8.6 Hz, 1H), 7.19 (d, J = 7.5 Hz, 1H), 6.53 (d, J = 10.9 Hz, 1H), 6.48 (s, 1H), 4.94 (m, 1H), 3.83 (m, 1H), 2.47 (d, J = 13.2 Hz, 1H), 2.38 (m, 1H), 2.24 (m, 2H), 2.18 (m, 1H), 1.88 (m, 1H), 1.67 (s, 3H), 1.59 (s, 3H), 1.32 (s, 3H), 1.27 (s, 3H); ^{13}C NMR (125 MHz, CD_3OD) δ 200.6, 180.1, 166.2, 162.8, 135.9, 135.3, 134.7, 128.7, 117.4, 111.5, 102.6, 101.7, 84.4, 84.0, 79.2, 44.8, 41.6, 32.4, 30.0, 28.5, 25.4, 24.7, 16.7; HRMS (ESI) m/e 381.1699 $[M+H]^+$ calcd for $C_{23}H_2O_5^+$: 381.1697.

Experimental Procedures: Biological Assays

3H-thymidine incorporation assay: CEM cells were plated in a 96-well plate at 20,000 cells/well in RPMI supplemented with 10% fetal bovine serum, 2 mM glutamine, 100 units/ml of penicillin/streptomycin (complete medium). The caged Garcinia xanthones were added to the cells at increasing concentrations and 0.1% DMSO was added to control cells. Cells were incubated for 48 h and then pulsed with 3H-thymidine for 7 h. Incorporation of 3H-thymidine was determined in a scintillation counter (Beckman Coulter Inc., Fullerton, CA) after cells were washed and deposited onto glass microfiber filters using a cell harvester M-24 (Brandel, Gaithersburg, MD).

Cells, antibodies and reagents: HeLa cells were grown in DMEM supplemented with 10% FBS. For immunofluorescence and western blot the following antibodies were used: mouse anti-Tom20 (BD Transduction Laboratories, #612278); rabbit anti-cleaved Caspase-9 (Cell Signaling, D315 human spasific); rabbit anti-cleaved Caspase-3 (Cell Signaling, #96645); rabbit anti-beta Tubulin (Abcam, ab6046).

Immunofluorescence analysis: HeLa cells plated on 12mm glass coverslips were fixed with 4% formaldehyde, permeabilized with 0.1% TritonX100 in PBS for 5 min, then incubated in blocking buffer (PBS containing 5% fetal goat serum) for 30 min at room temperature. The cells were then incubated for 1 h at room temperature in primary antibody diluted in blocking buffer. The cells were then washed three times with PBS and incubated with secondary antibody, diluted in blocking buffer, for 1 h at room temperature. Alexa Fluor 594 goat anti mouse (1:500) from Molecular Probes was used. Cells were washed three times with PBS containing Hoechst (1:100,000) (H33342, Molecular Probes) to stain DNA. Coverslips were then mounted onto glass slides and visualized using a Zeiss Observer Z1 156 inverted microscope with 63? objective controlled by 157 AxioVision software (Zeiss, Thornwood, NY).

Immunoblot blot analysis: Cells were lysed with PAGE loading buffer (60 mM Tris, pH 6.8, 5% 2-mercaptoethanol, 2% SDS, 0.01% Bromophenol blue, and 10% glycerol). Proteins in the lysate were separated by SDSÐPAGE using a 12% running gel. Proteins were transferred on a nitrocellulose membrane (Western Blot) (60 min, 350 mA) that was then kept in blocking buffer (50 mN, Tris, pH 7.5, 150 mM NaCl, 0.05% Tween 20, and 3% BSA) for 1 h. The membrane was incubated for overnight at

4 °C with the primary antibodies diluted in blocking buffer. After washing 3 times with TBS-T buffer, the membranes were incubated for 1 h at room temperature in secondary antibody (anti rabbit IgG HRP-linked, GE Healthcare #NA934V) diluted in blocking buffer. After 3 more washing steps in TBS-T, the reagent for ECL was added (Perkin-Elmer). Kodak Biomax films were used for exposure.

Hsp90 client assay: SKBR3 cells were seeded at 250,000 cells per well in a 6-well plate and were left to grow in DMEM/F12 supplemented with 10% fetal bovine serum for 48 hours. Different concentrations of GA and CLV were prepared in DMSO and used to treat the SKBR3 cells for 24 hours, upon which the cells were trypsinized and lysed in a Nonidet P-40 lysis buffer (1% NP-40, 20 mM HEPES [pH 7.5], 0.12 M NaCl, 1 mM EDTA, 2.5 mM glycerophosphate, 10 mM NaF, 1 mM sodium vanadate, 1 mM phenylmethylsulfonyl fluoride and protease inhibitors). The lysates were cleared at 4 °C for 10 min and the concentration of protein quantified by the Bradford assay. Samples of 20 μg were analyzed in appropriate percentages of SDS-polyacrylamide gels, transferred to PVDF membranes (Immobilon-P, Millipore, Bedford, MA) and blocked for 1 h at room temperature with 5% nonfat dry milk in TBS buffer (20 mM Tris-HCl [pH 7.5], 0.5 M NaCl). Incubation with the primary antibodies was done overnight at 4 °C, while the appropriate secondary antibody (horseradish peroxidase-conjugated goat anti-mouse or anti-rabbit IgG) was done for 2 h at room temperature. The blots were treated with the enhanced chemiluminescence reagent (Pierce) and exposed to x-ray film (Kodak) for detection. Antibodies used were: Akt, pAkt(S473), Her2 (Cell Signaling, Beverly, MA), Raf-1, Hsp90 (SPA-830) and Hsp70 (SPA-822) (Stressgen, Victoria, Canada).

1.5.3 ^{1}H and ^{13}C NMR Spectra

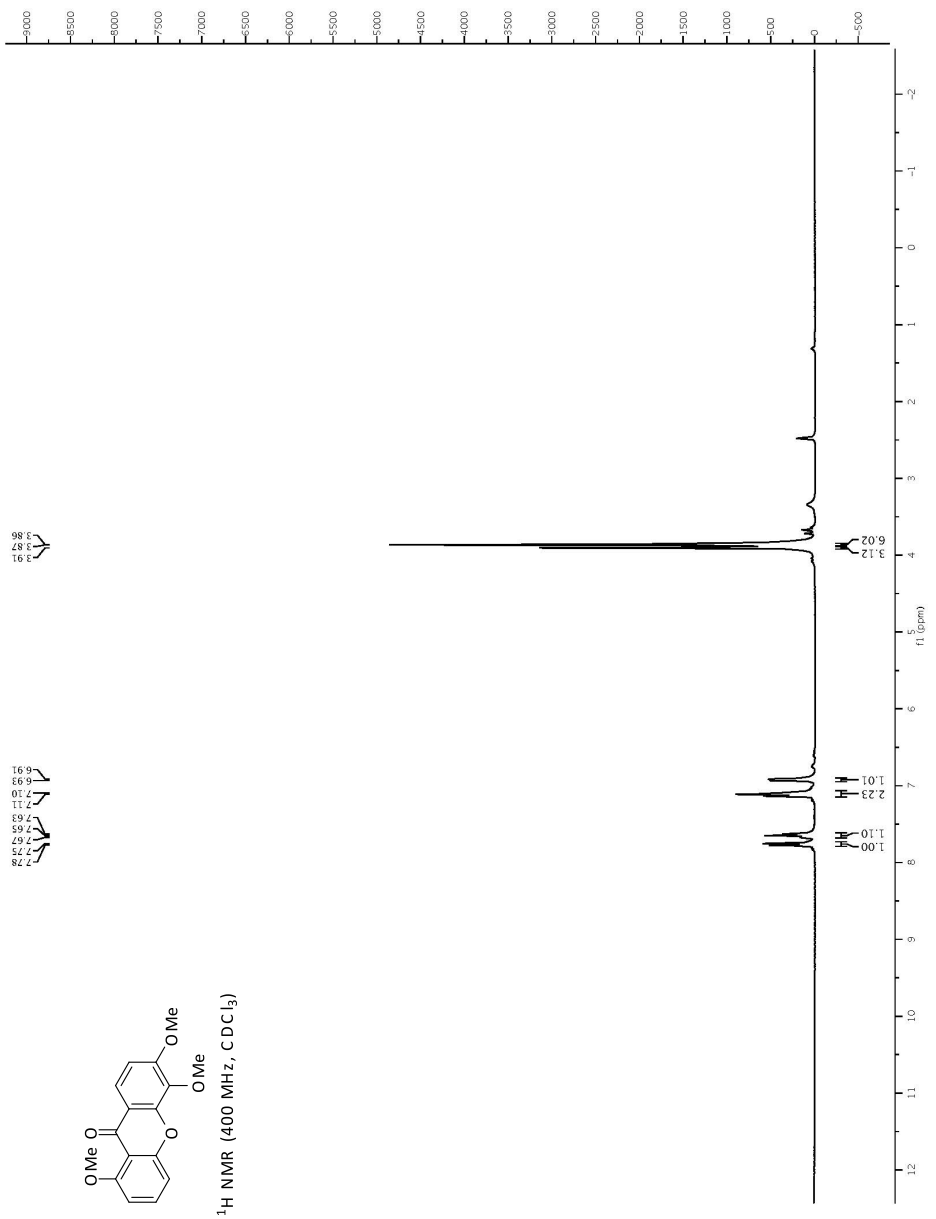

Spectrum 1.1: Compound 9a: ^{1}H NMR

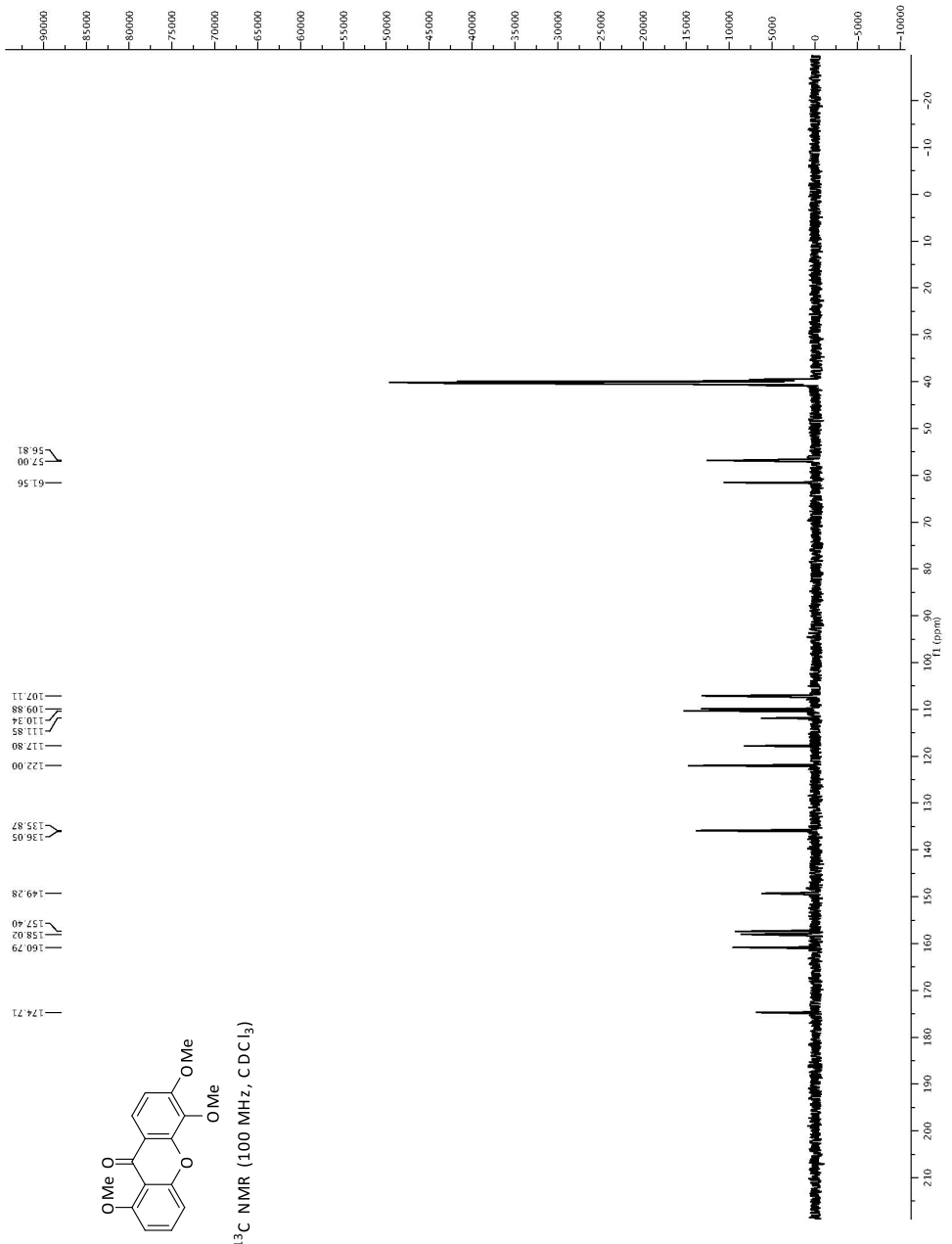

Spectrum 1.2: Compound 9a: ^{13}C NMR

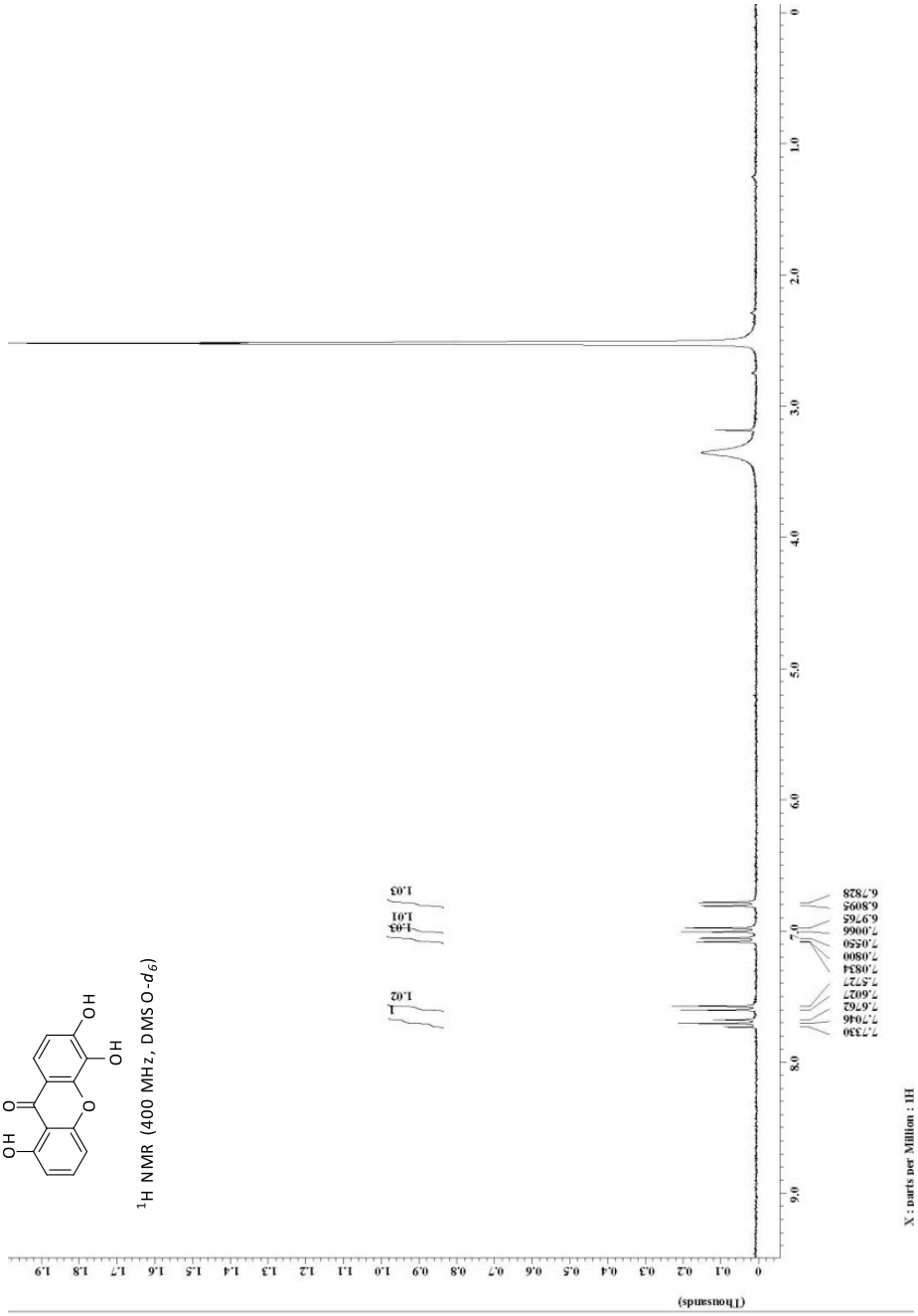

Spectrum 1.3: Compound 10a: ^{1}H NMR

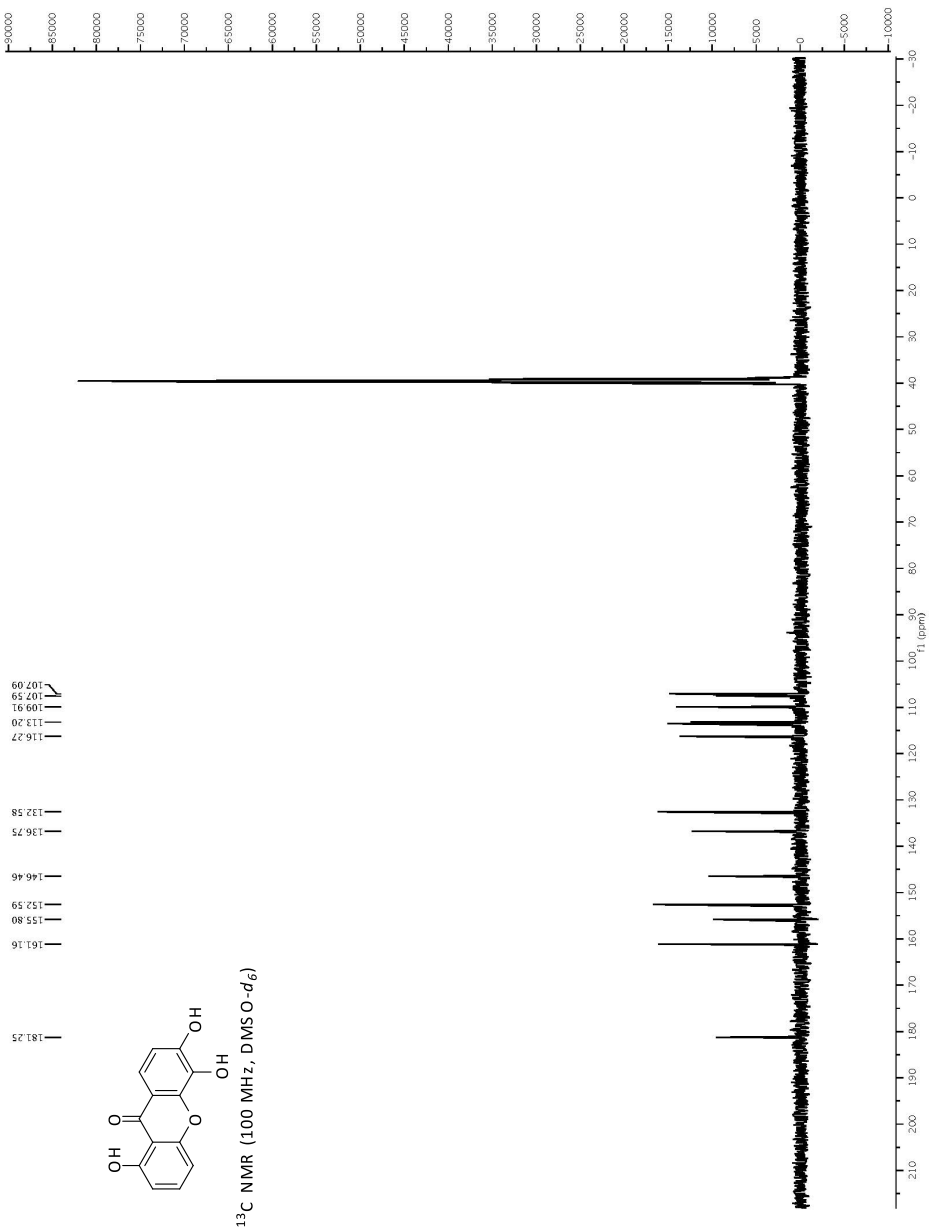

Spectrum 1.4: Compound 10a: ^{13}C NMR

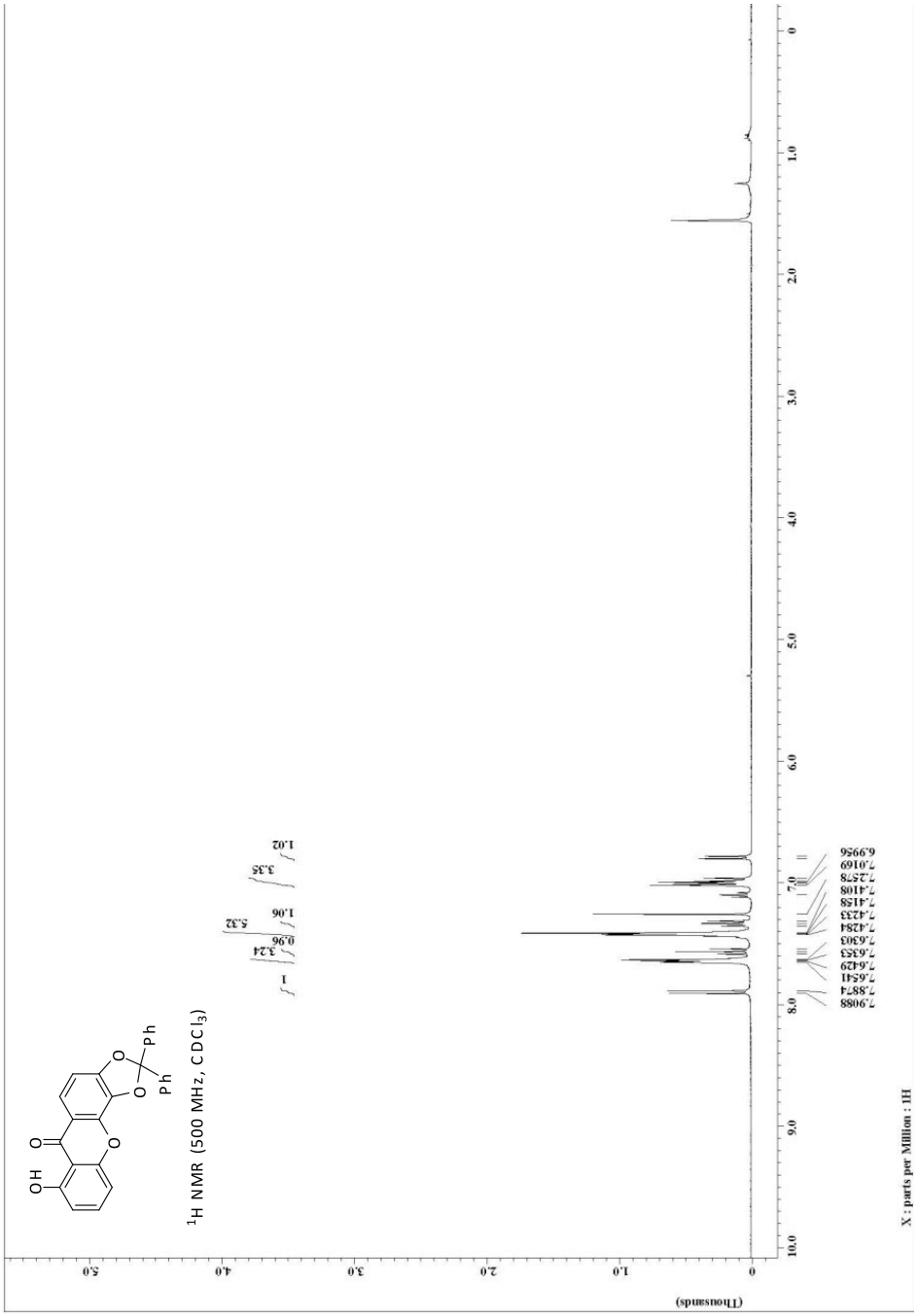

Spectrum 1.5: Compound 10a-i: ^{1}H NMR

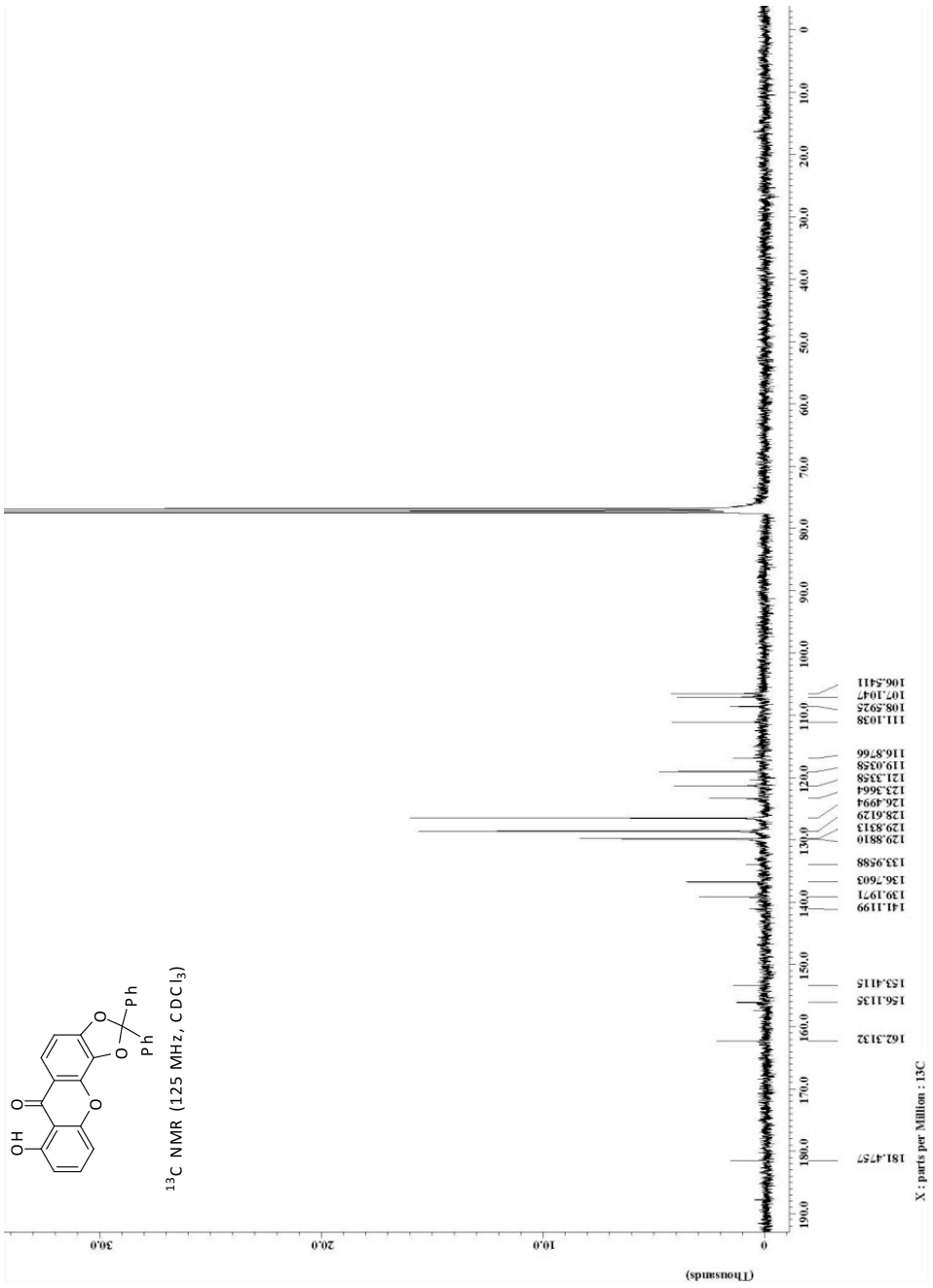

Spectrum 1.6: Compound 10a-i: ^{13}C NMR

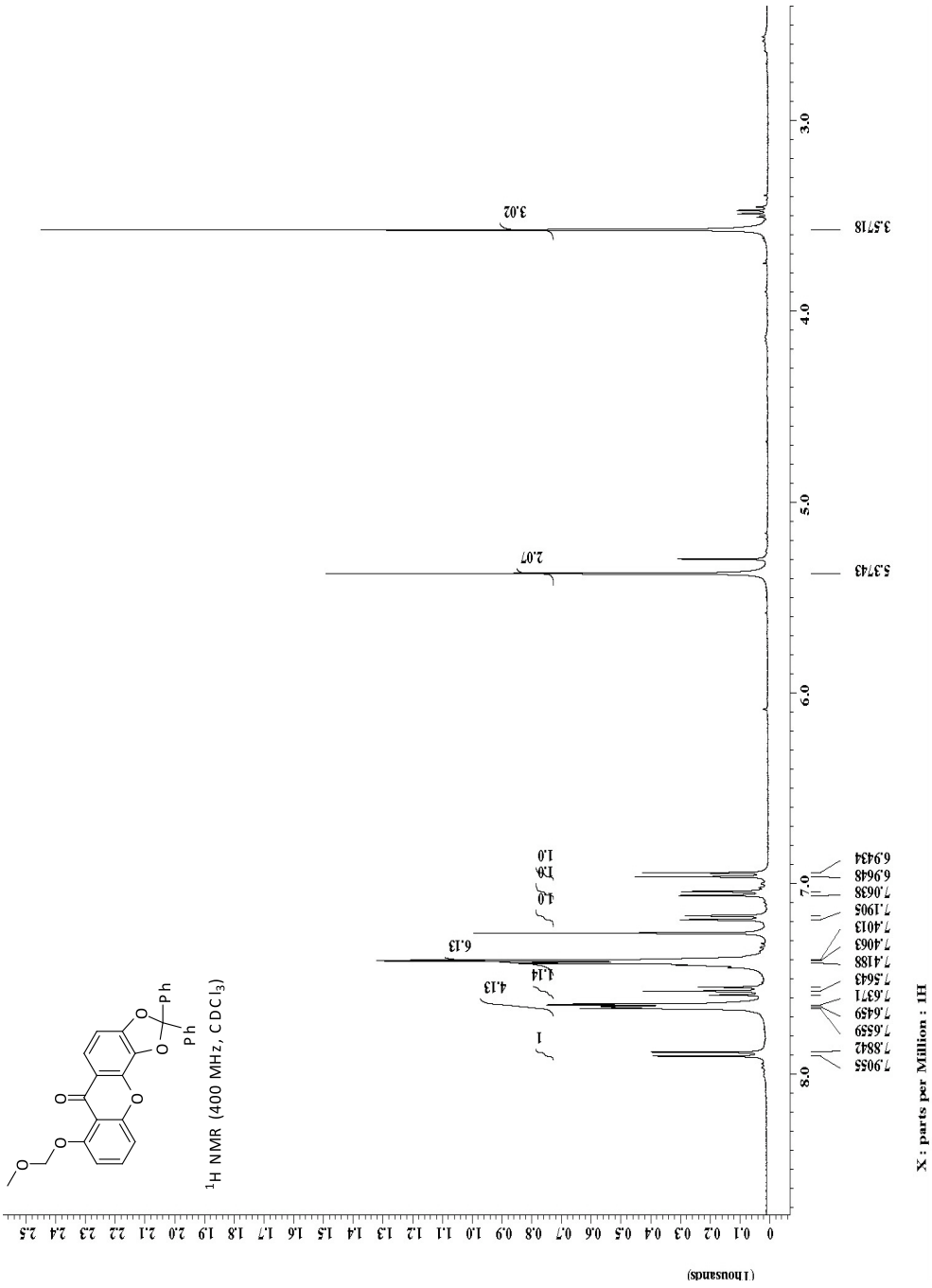

Spectrum 1.7: Compound 10a-ii: ^{1}H NMR

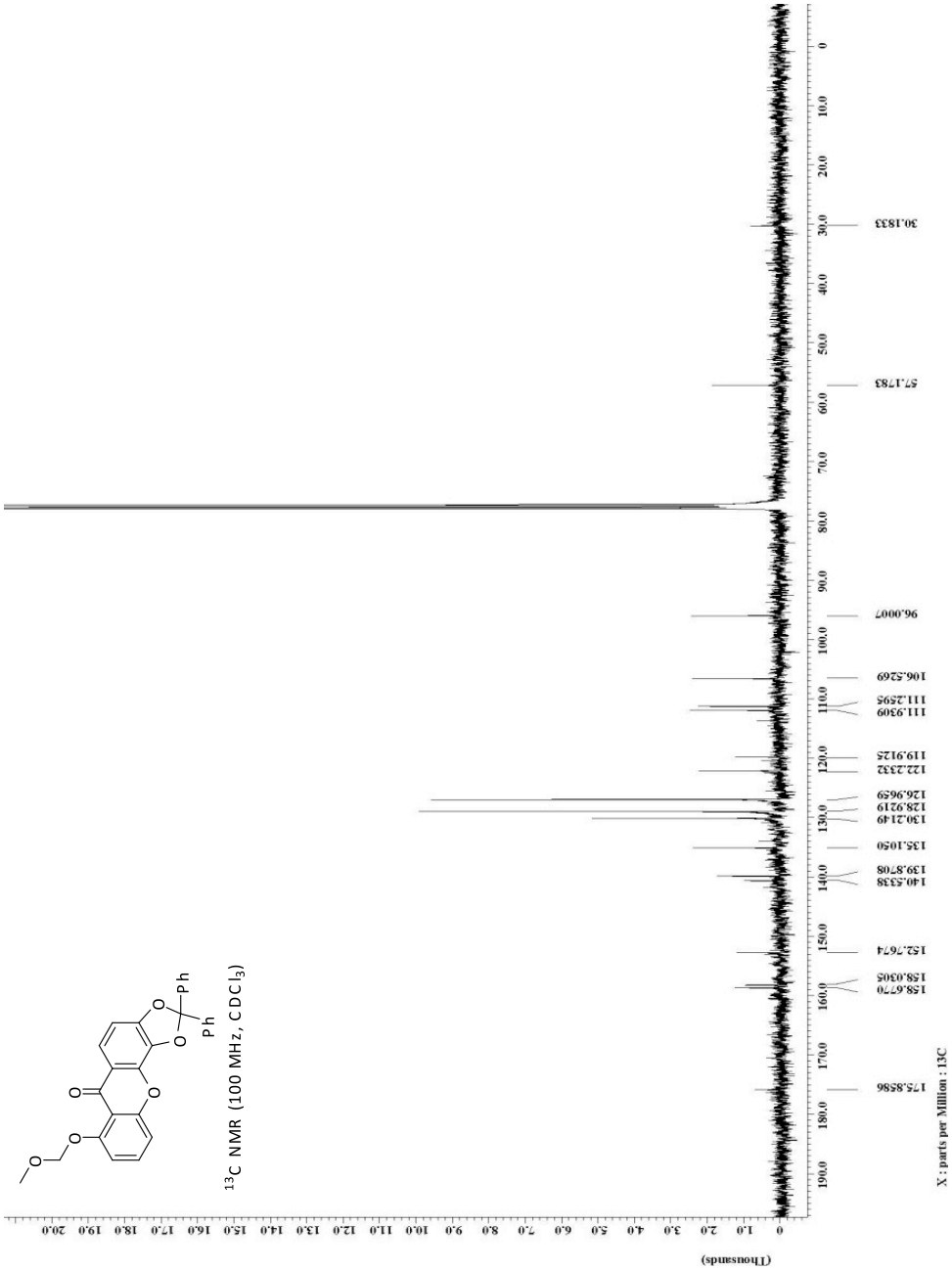

Spectrum 1.8: Compound 10a-ii: ^{13}C NMR

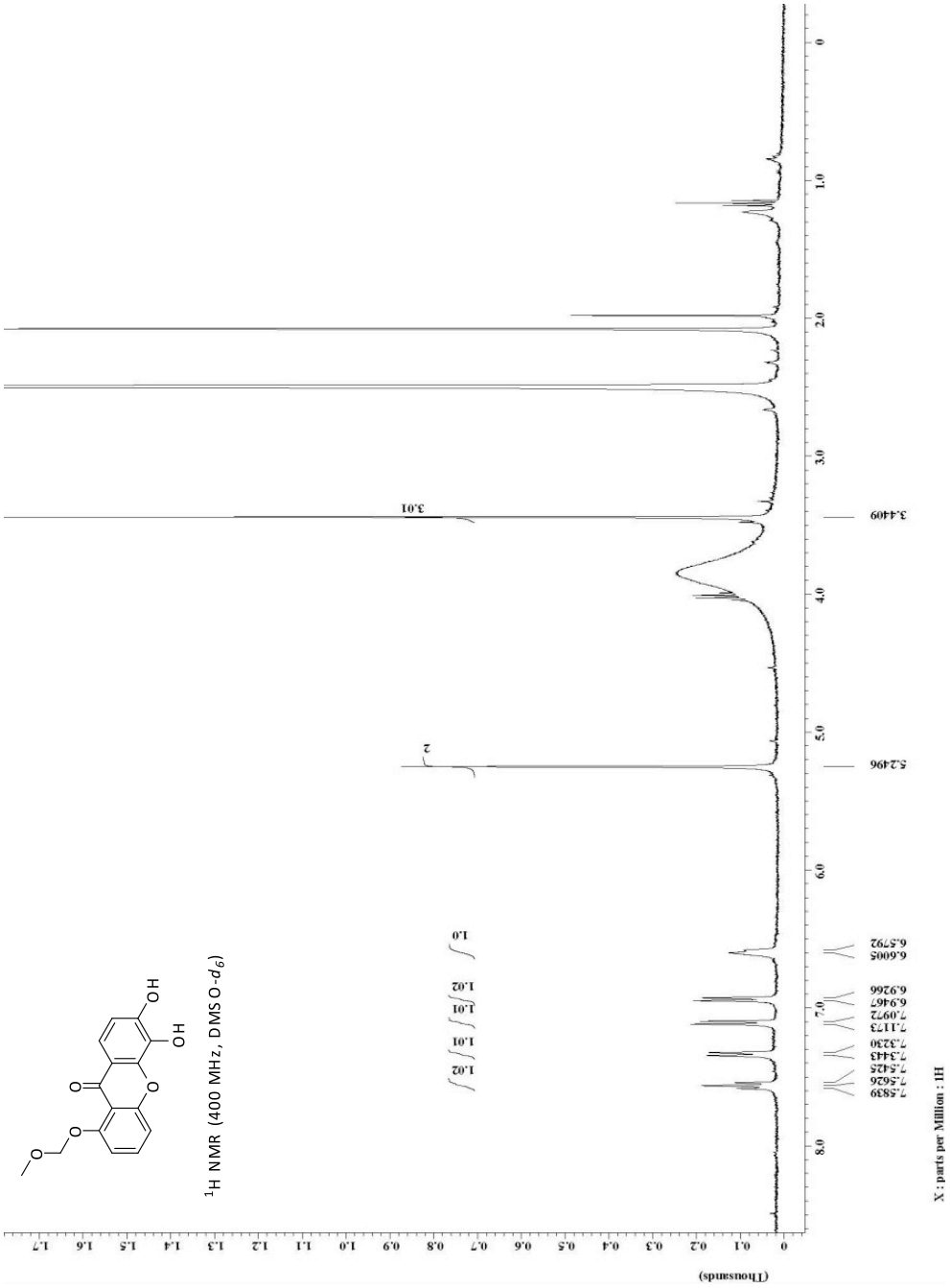

Spectrum 1.9: Compound 11a: ^{1}H NMR

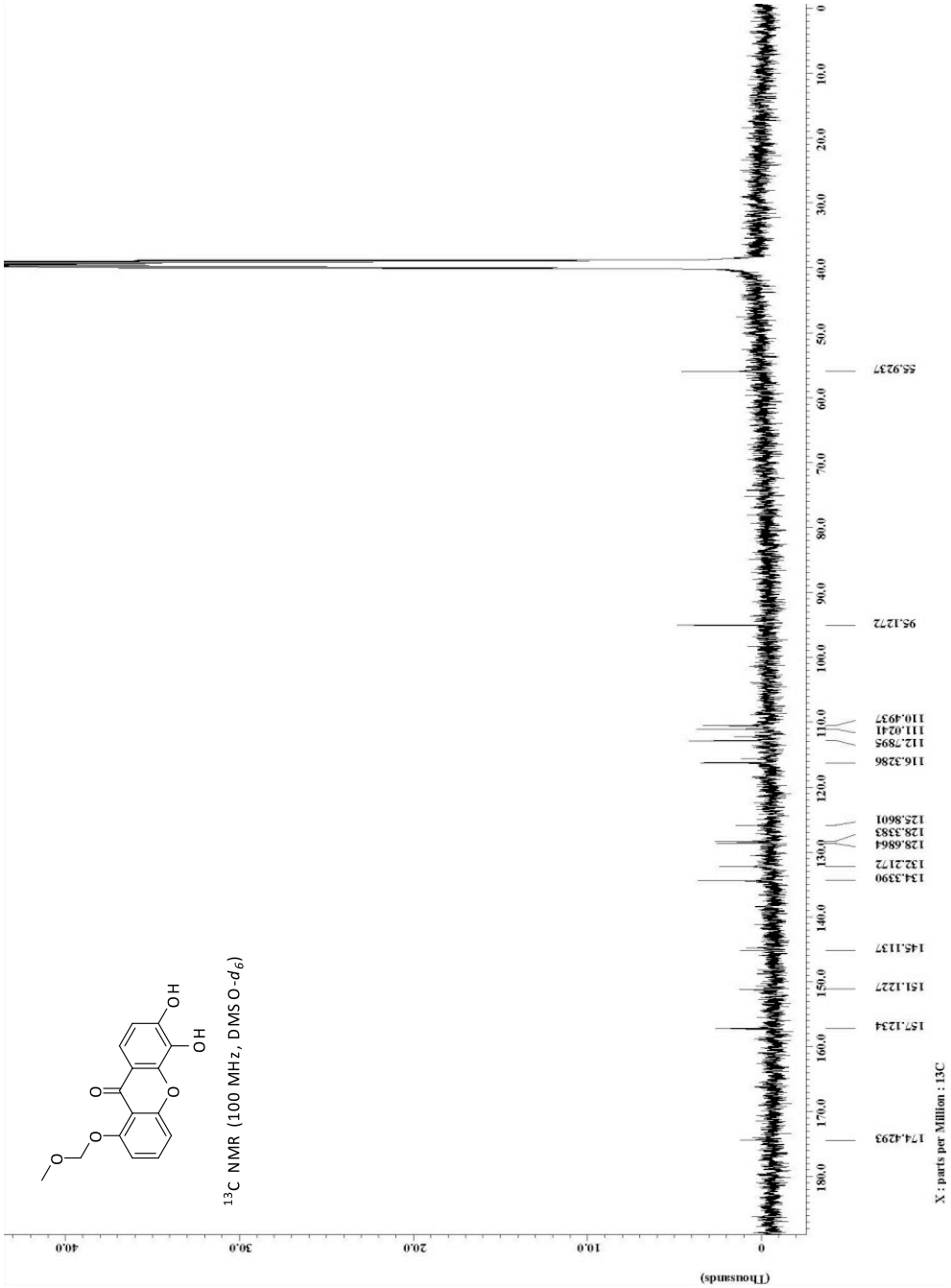

Spectrum 1.10: Compound 11a: ^{13}C NMR

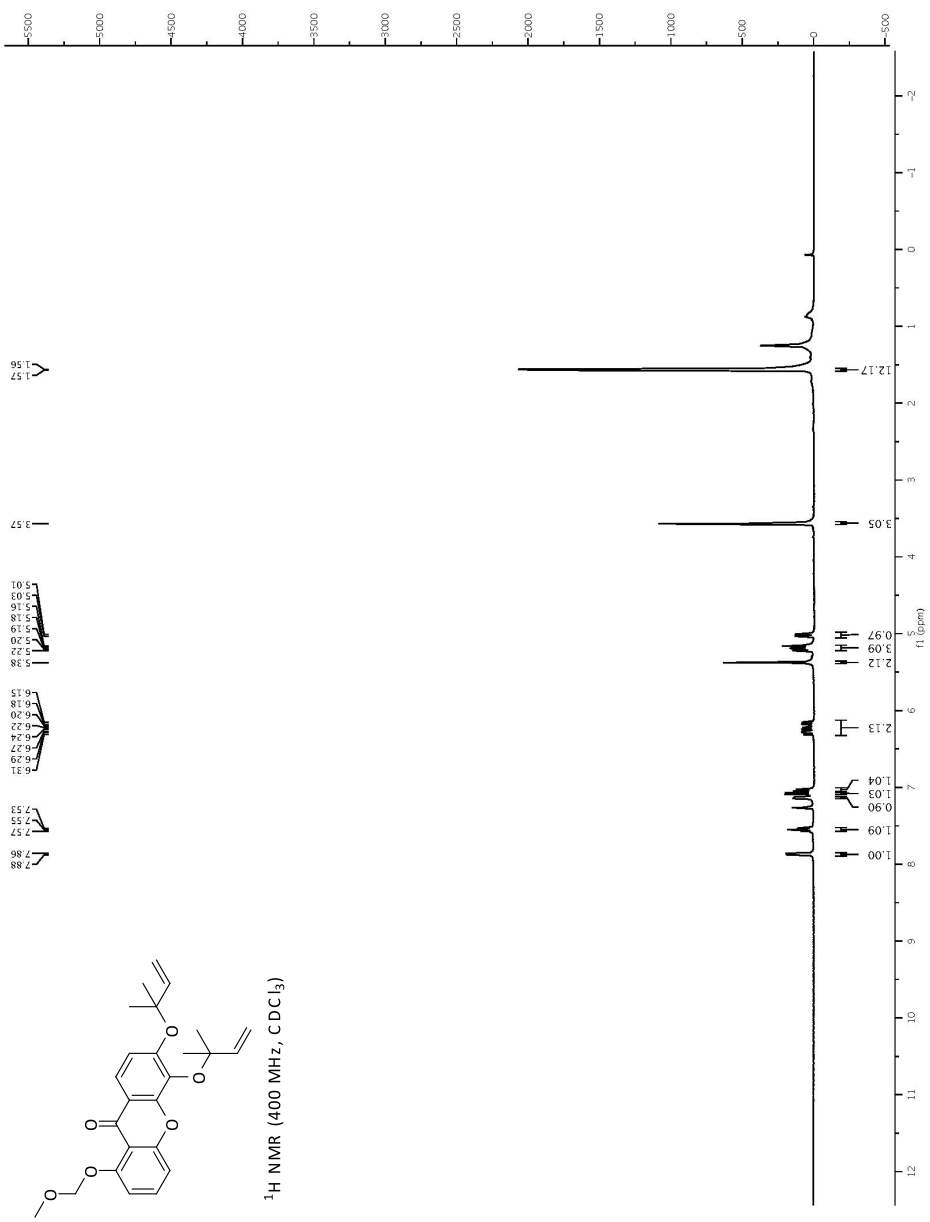

Spectrum 1.11: Compound 13a: ^{1}H NMR

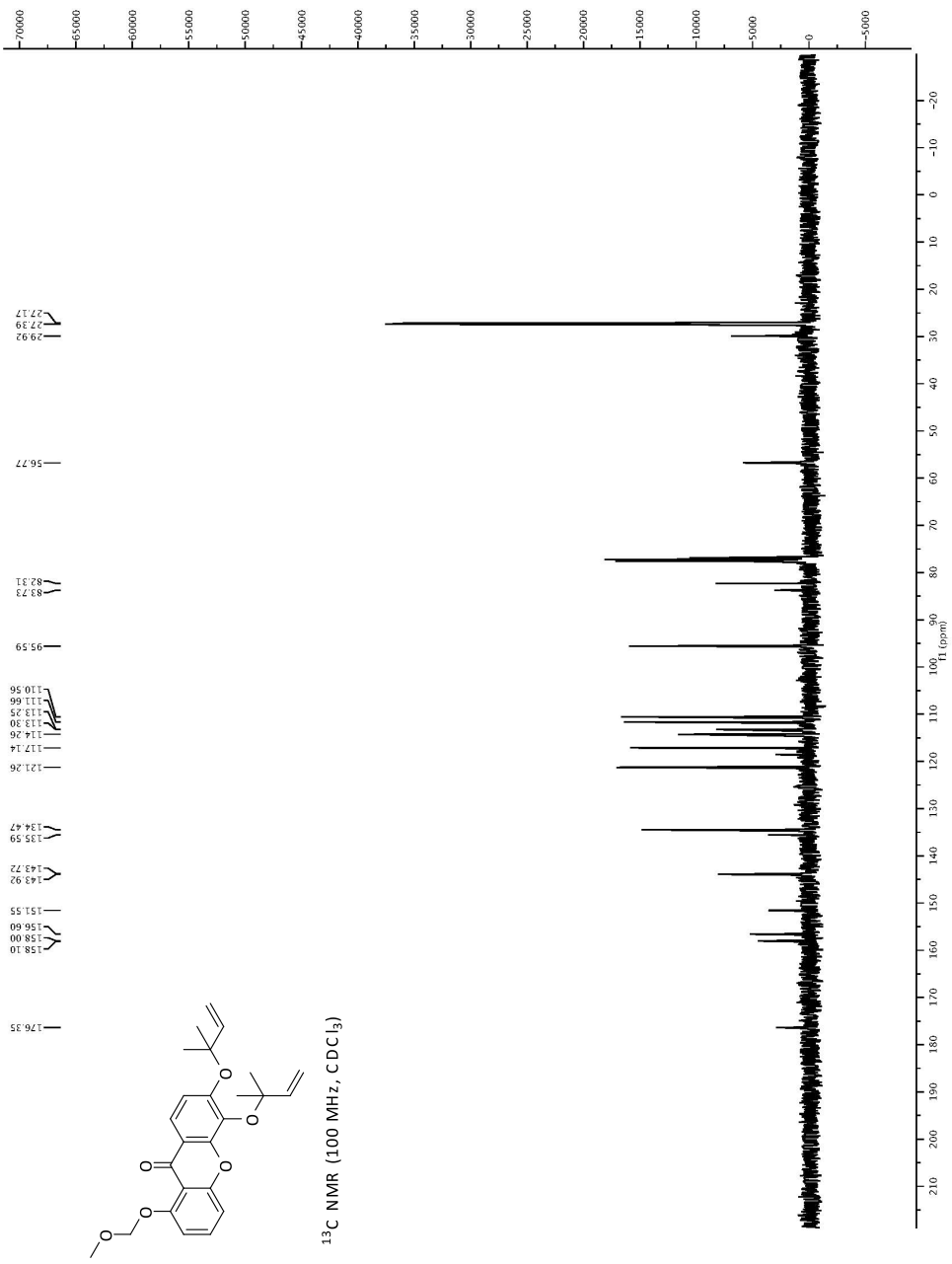

Spectrum 1.12: Compound 13a: ^{13}C NMR

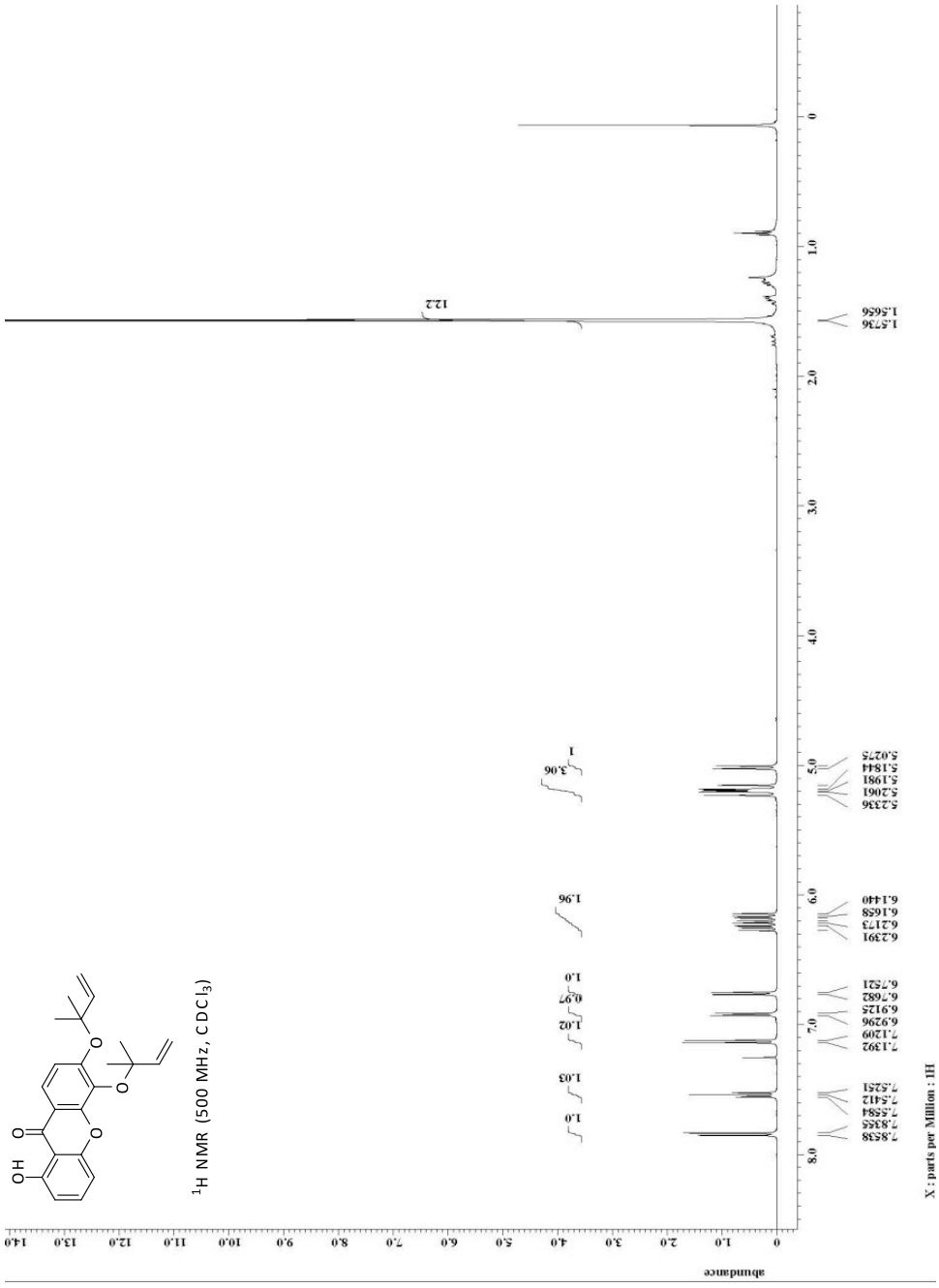

Spectrum 1.13: Compound 14: ^{1}H NMR

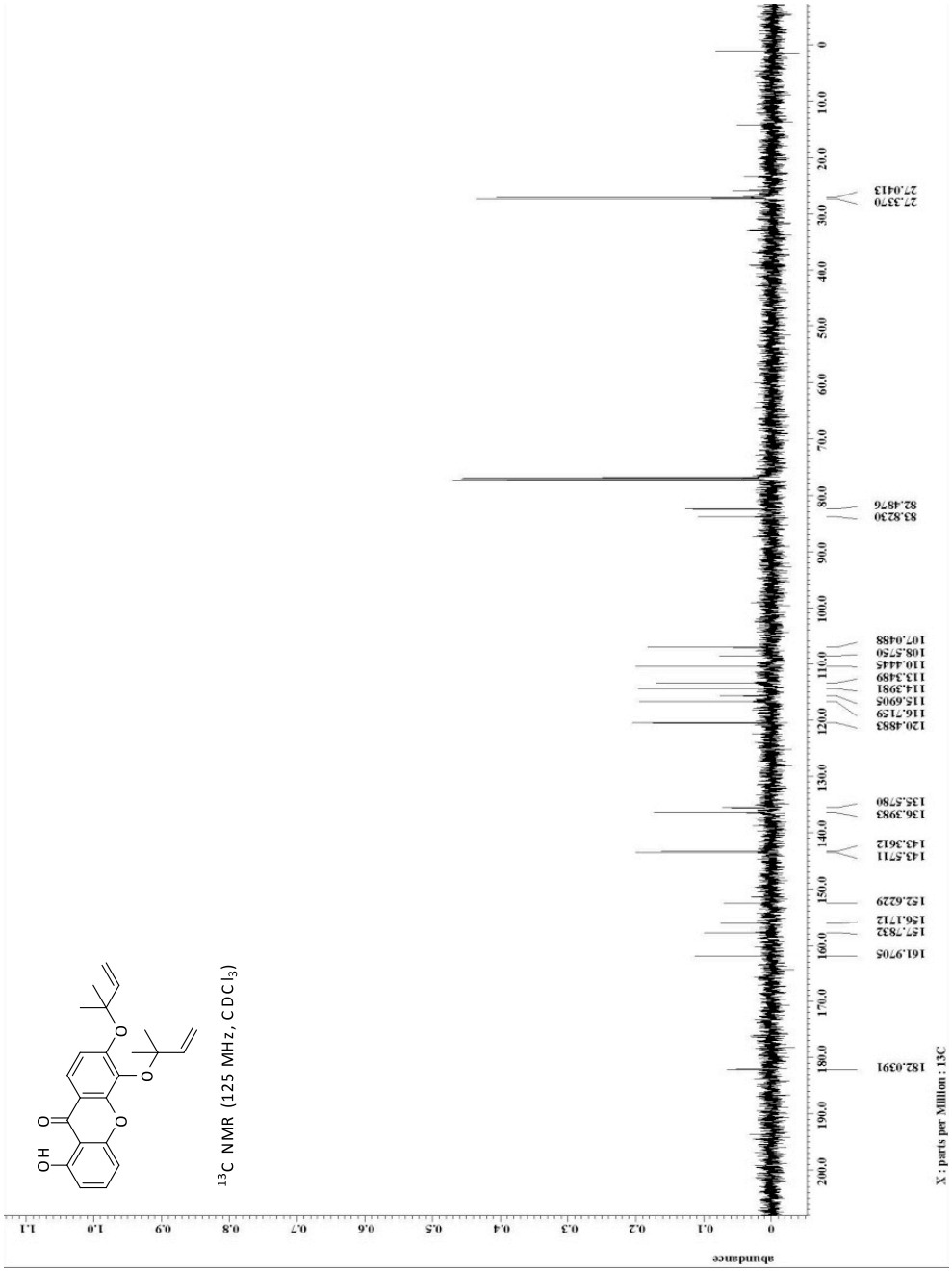

Spectrum 1.14: Compound 14: ^{13}C NMR

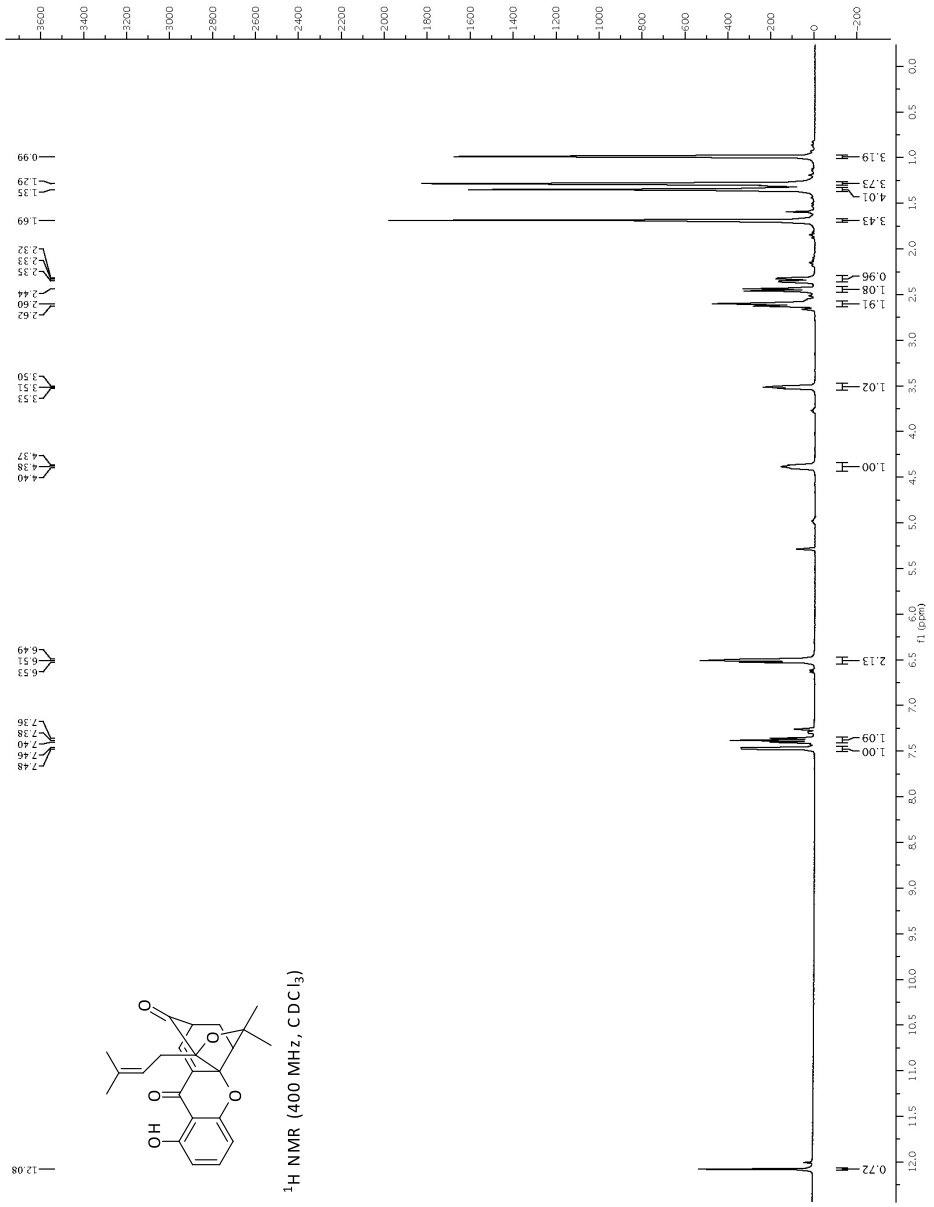

Spectrum 1.15: Compound 3: ^{1}H NMR

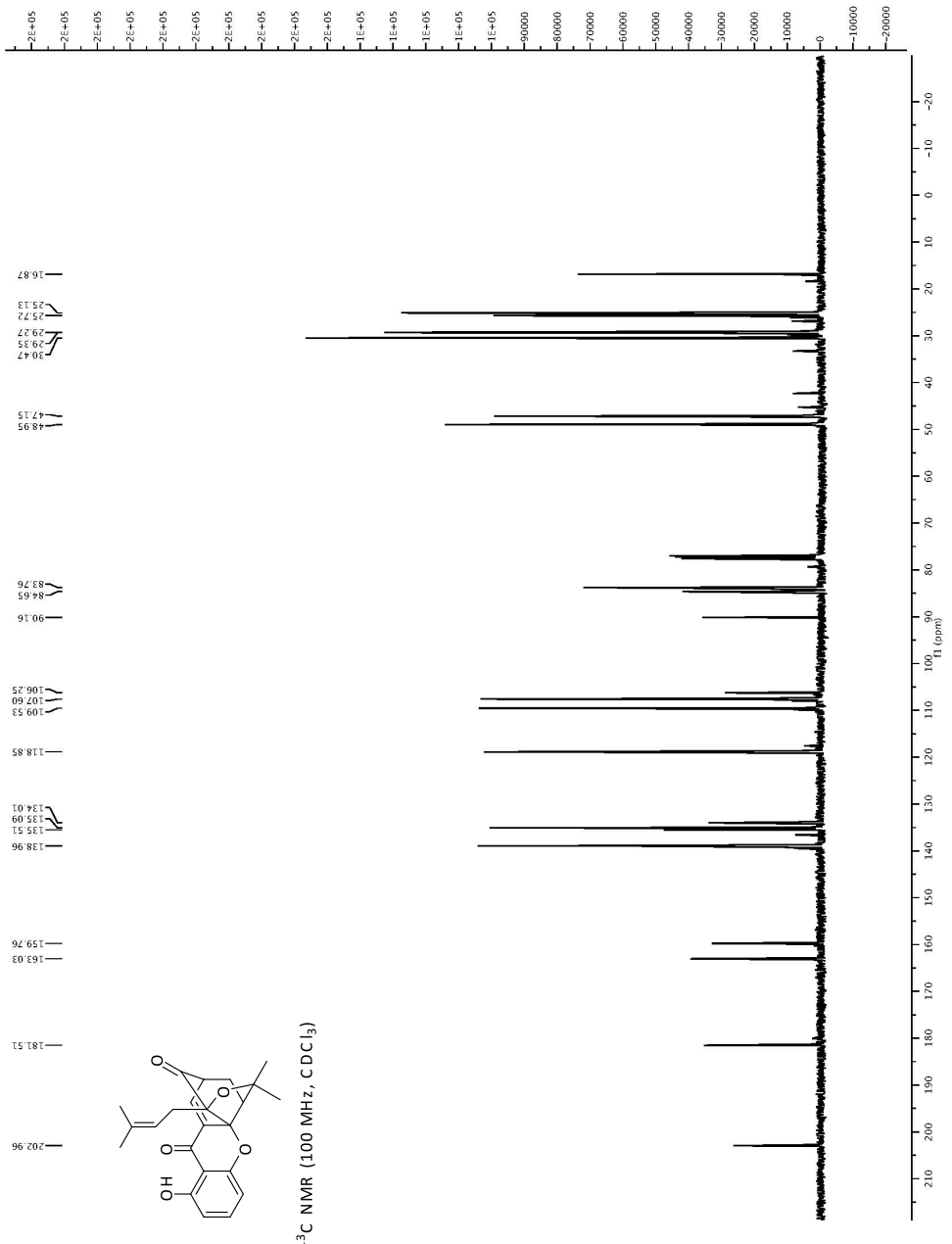

Spectrum 1.16: Compound 3: ^{13}C NMR

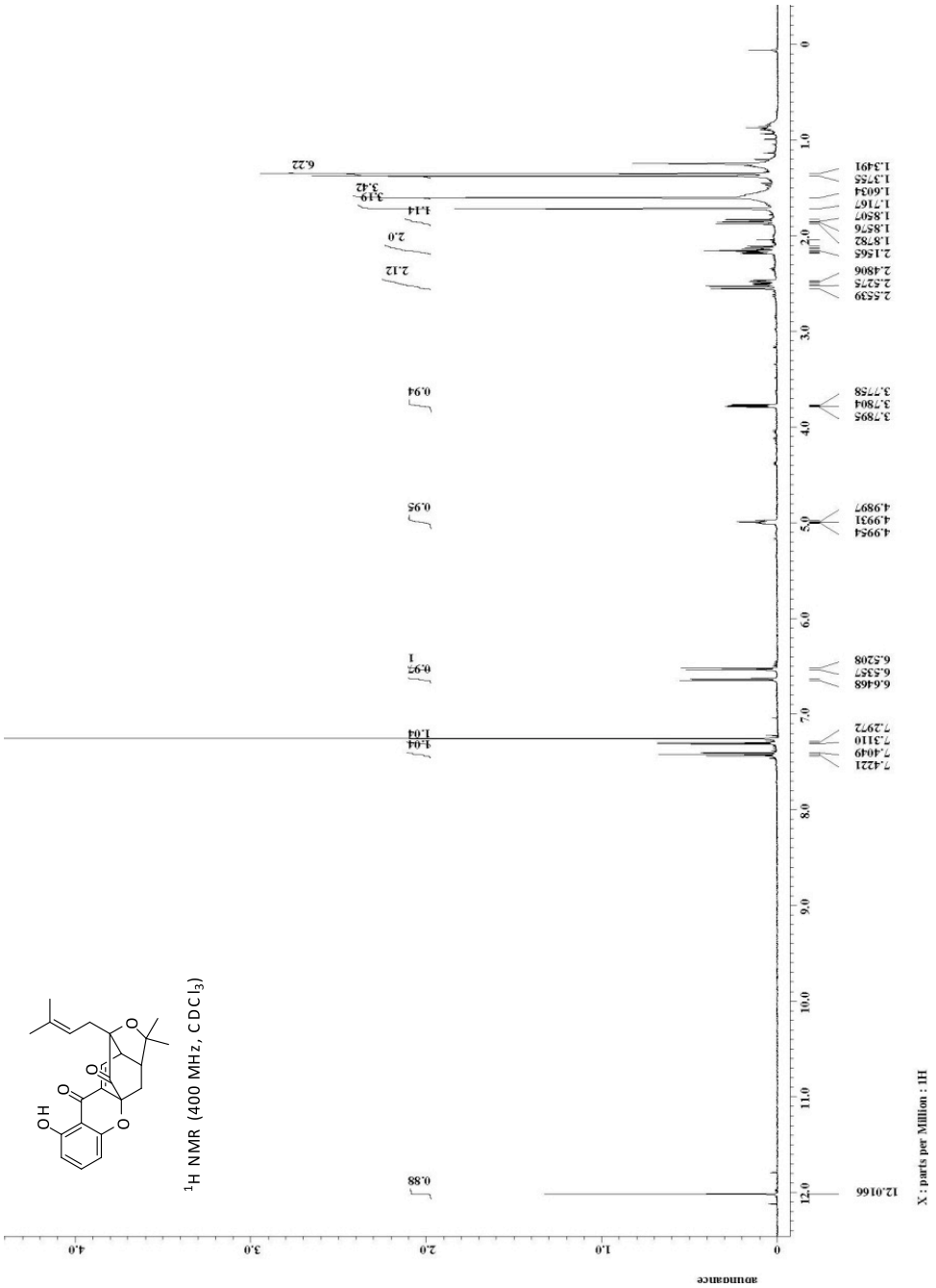

Spectrum 1.17: Compound 17 : ^{1}H NMR

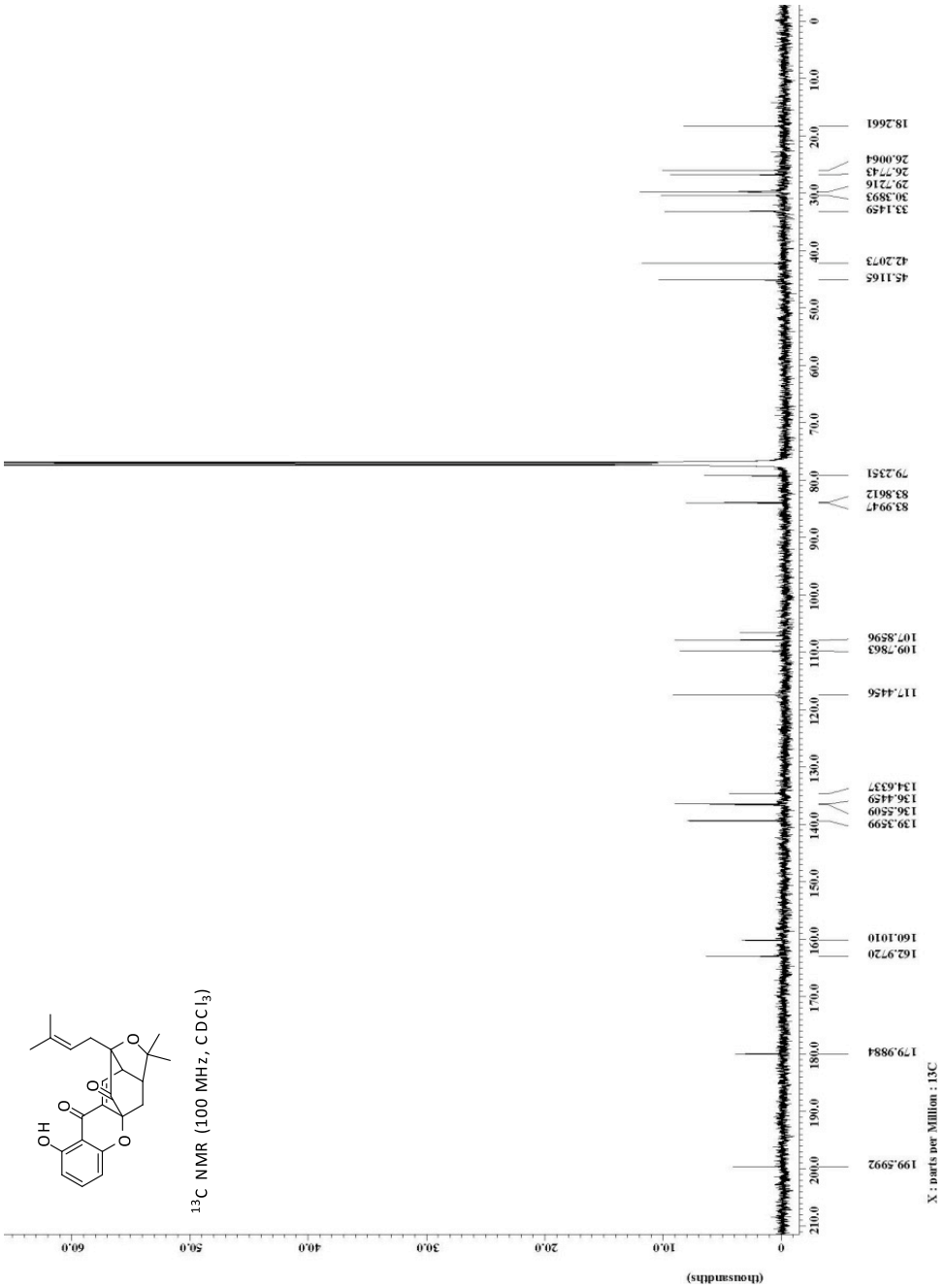

Spectrum 1.18: Compound 17: ^{13}C NMR

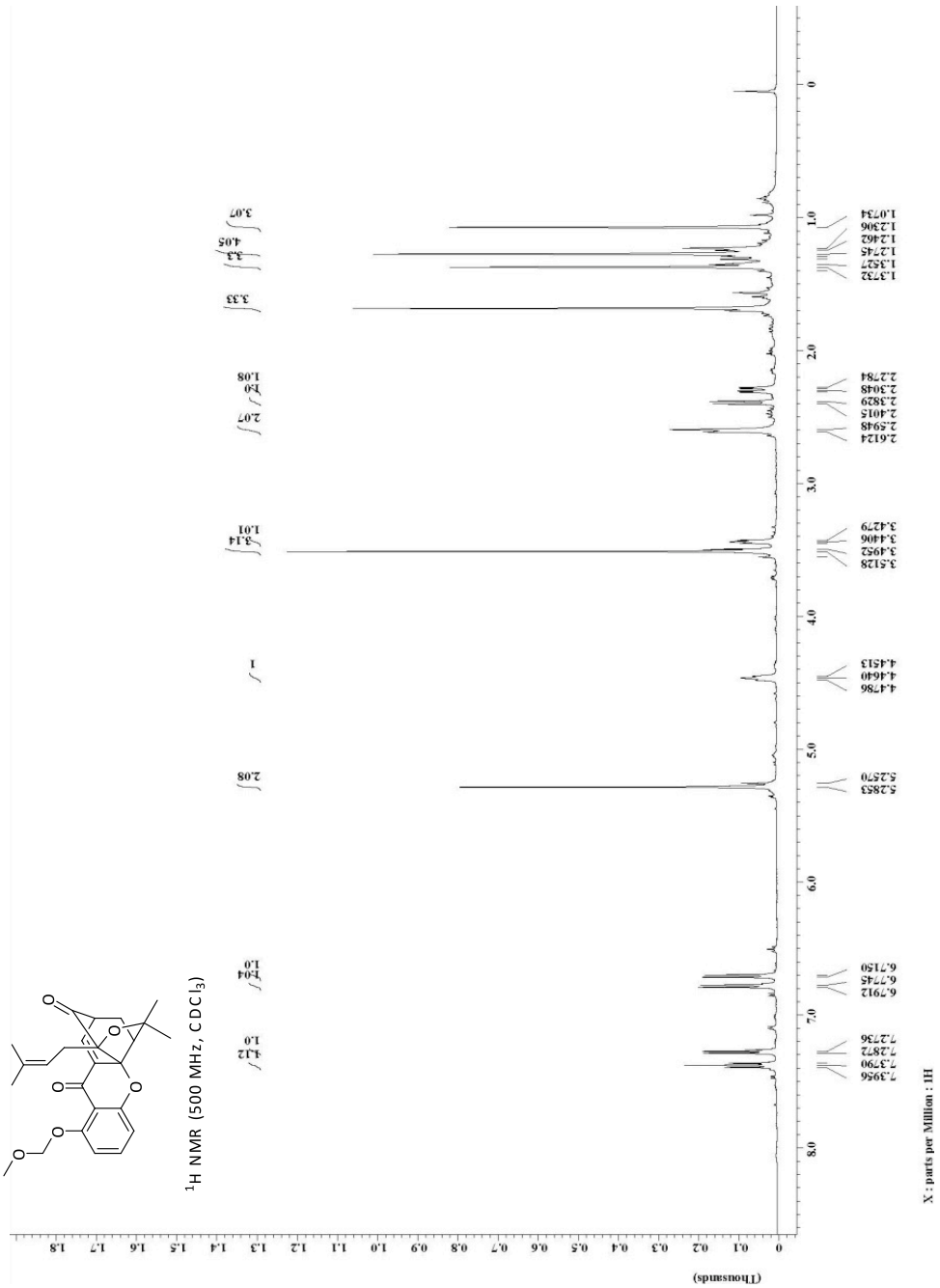

Spectrum 1.19: Compound 15: ^{1}H NMR

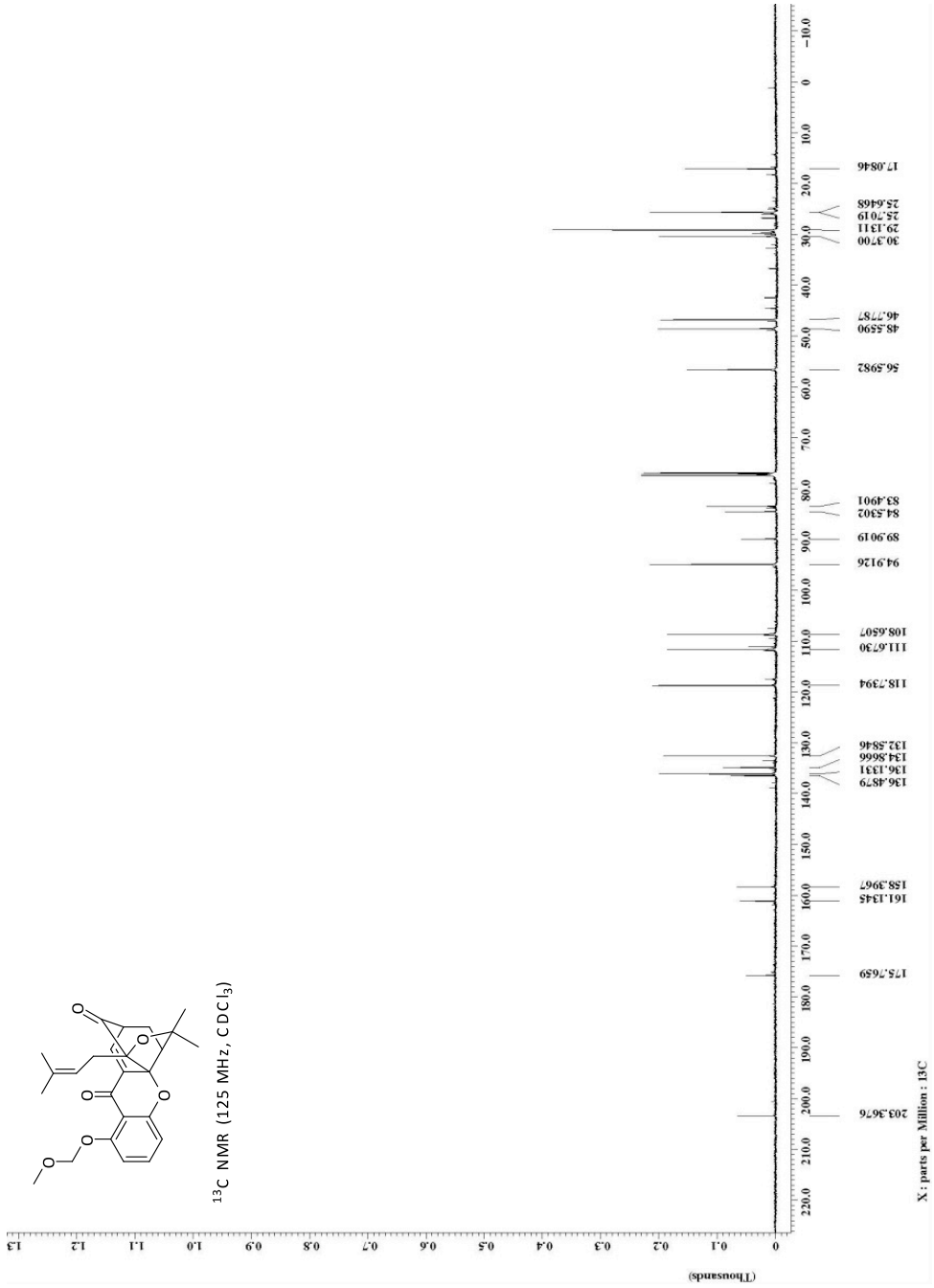

Spectrum 1.20: Compound 15: ^{13}C NMR

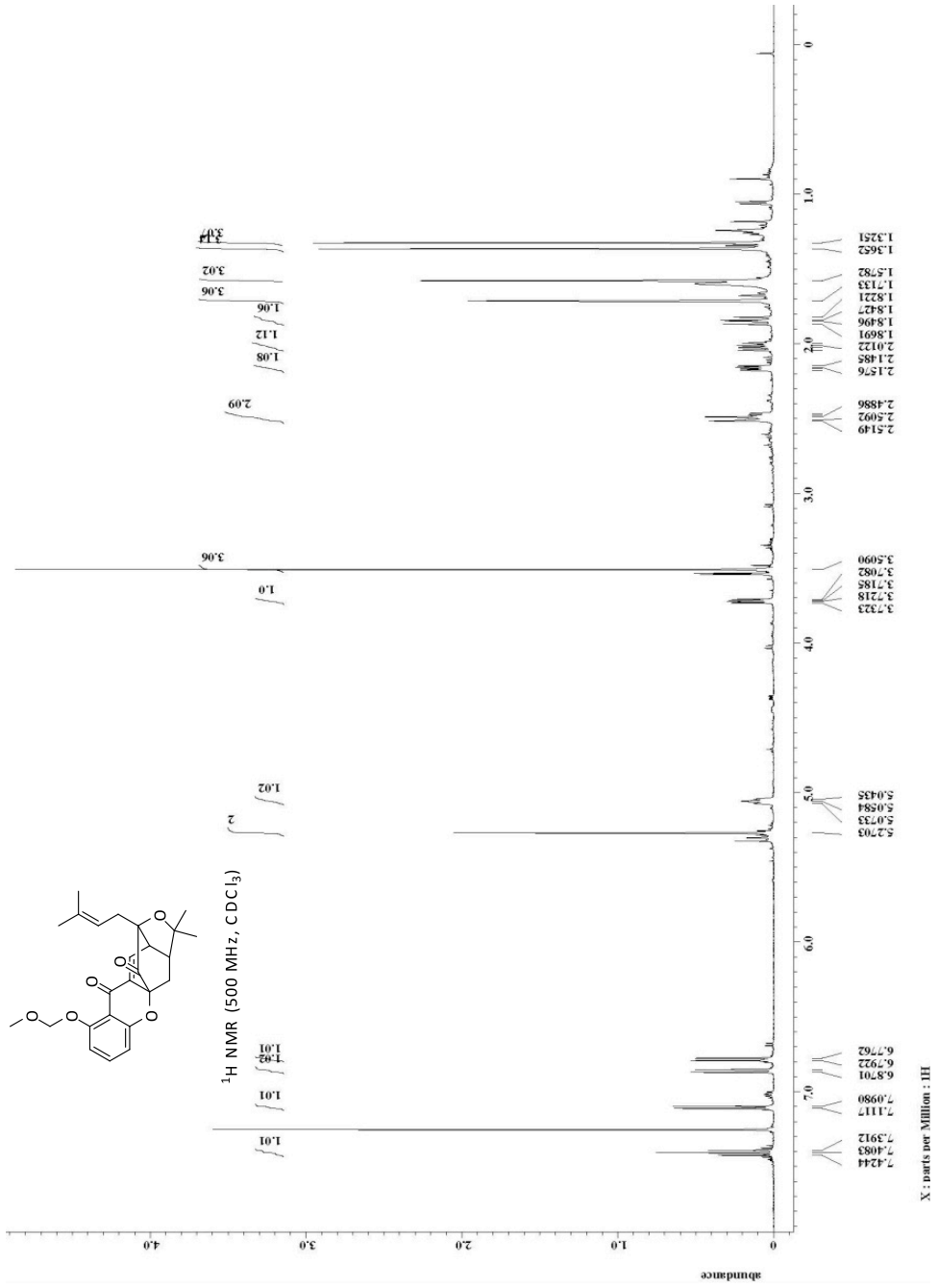

Spectrum 1.21: Compound 16: ^{1}H NMR

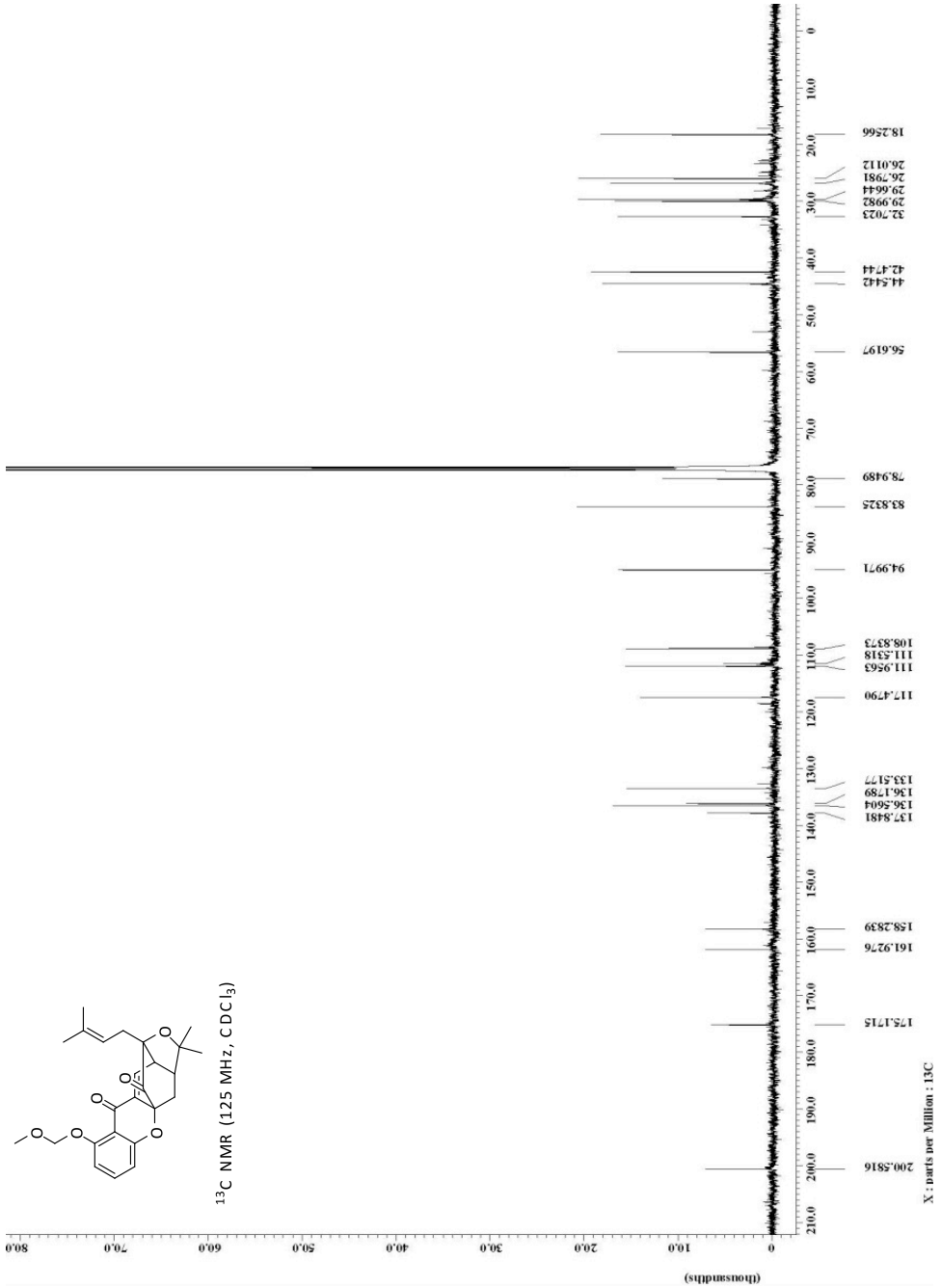

Spectrum 1.22: Compound 16: ^{13}C NMR

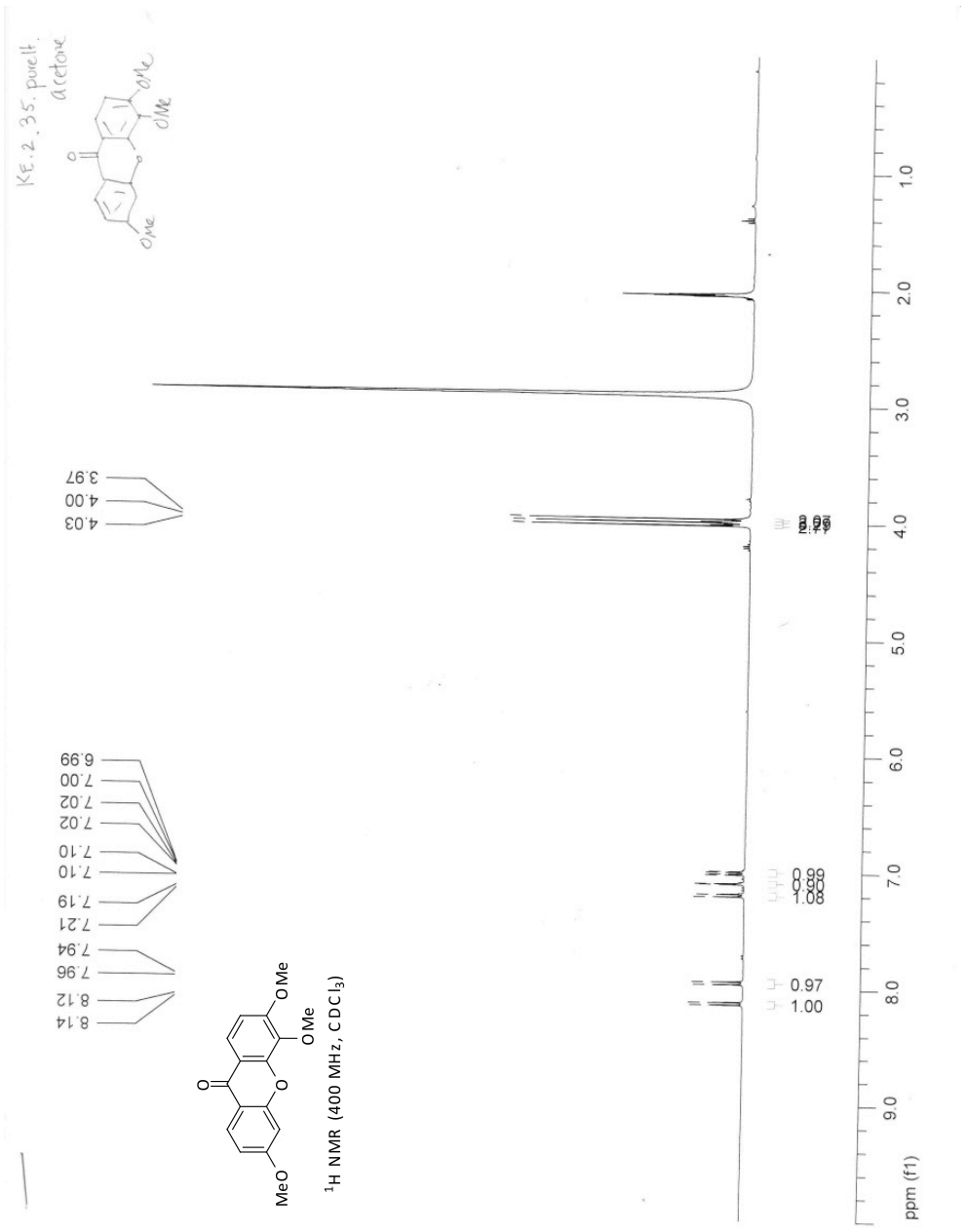

Spectrum 1.23: Compound 9b: ^{1}H NMR

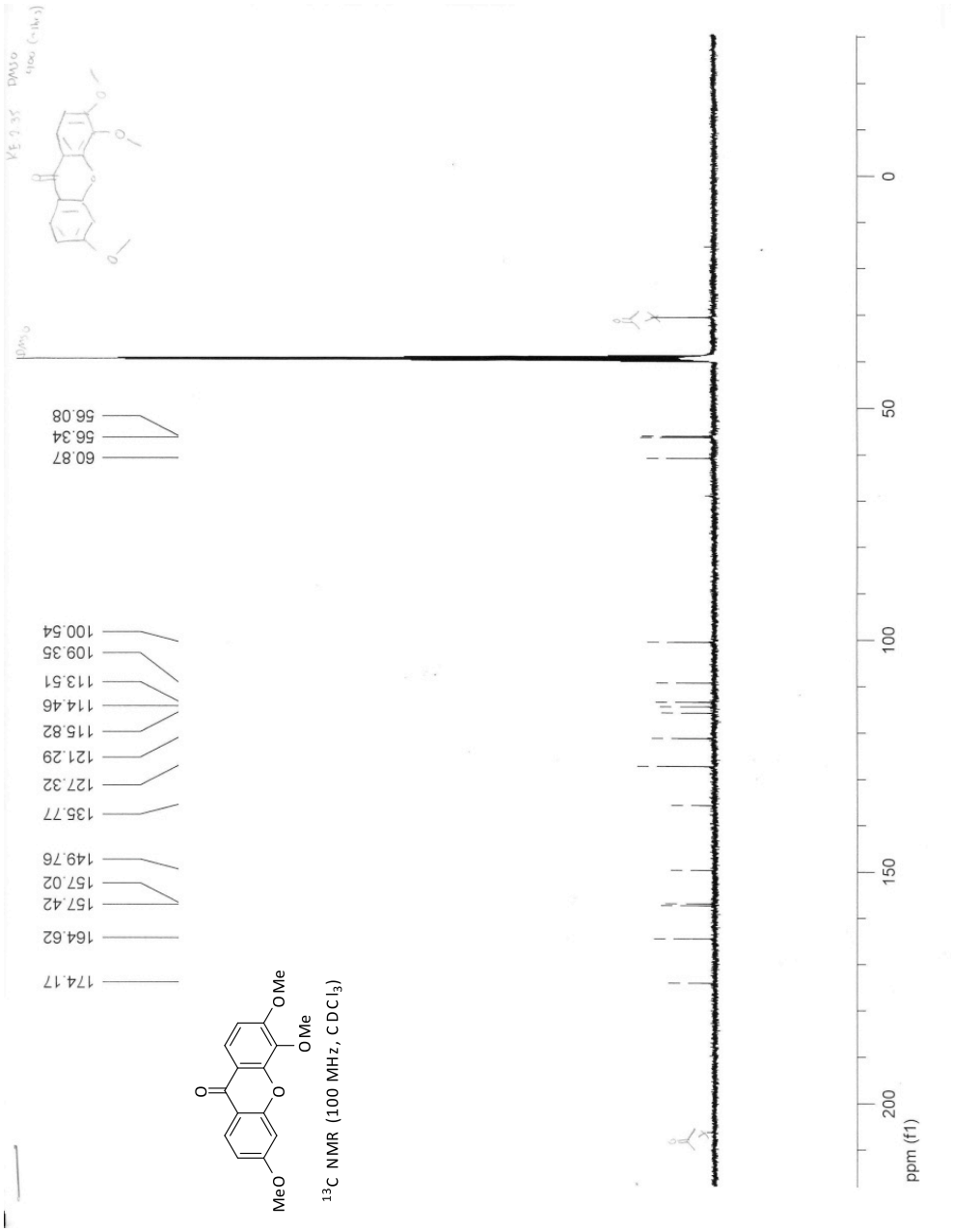

Spectrum 1.24: Compound 9b: ^{13}C NMR

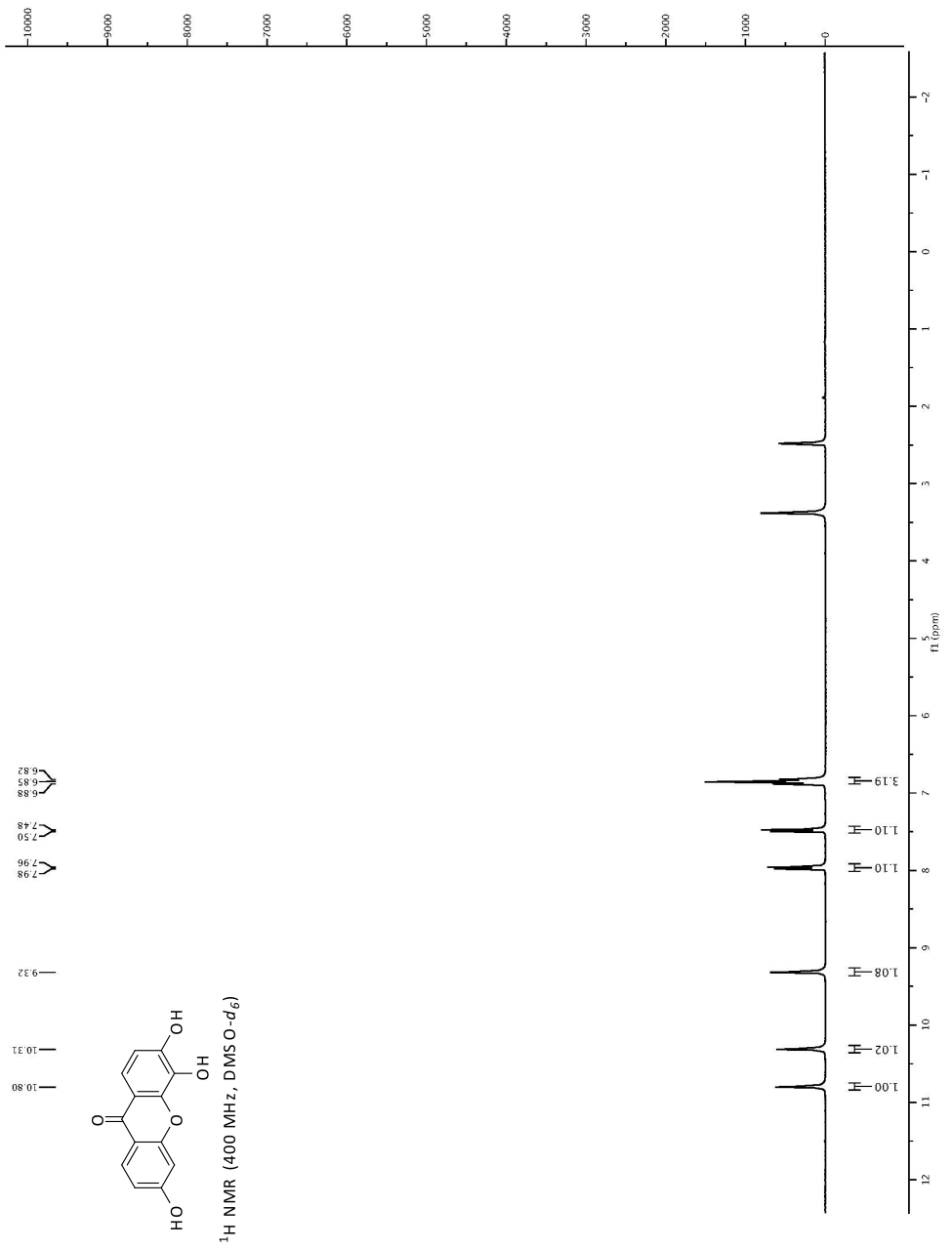

Spectrum 1.25: Compound 10b: ^{1}H NMR

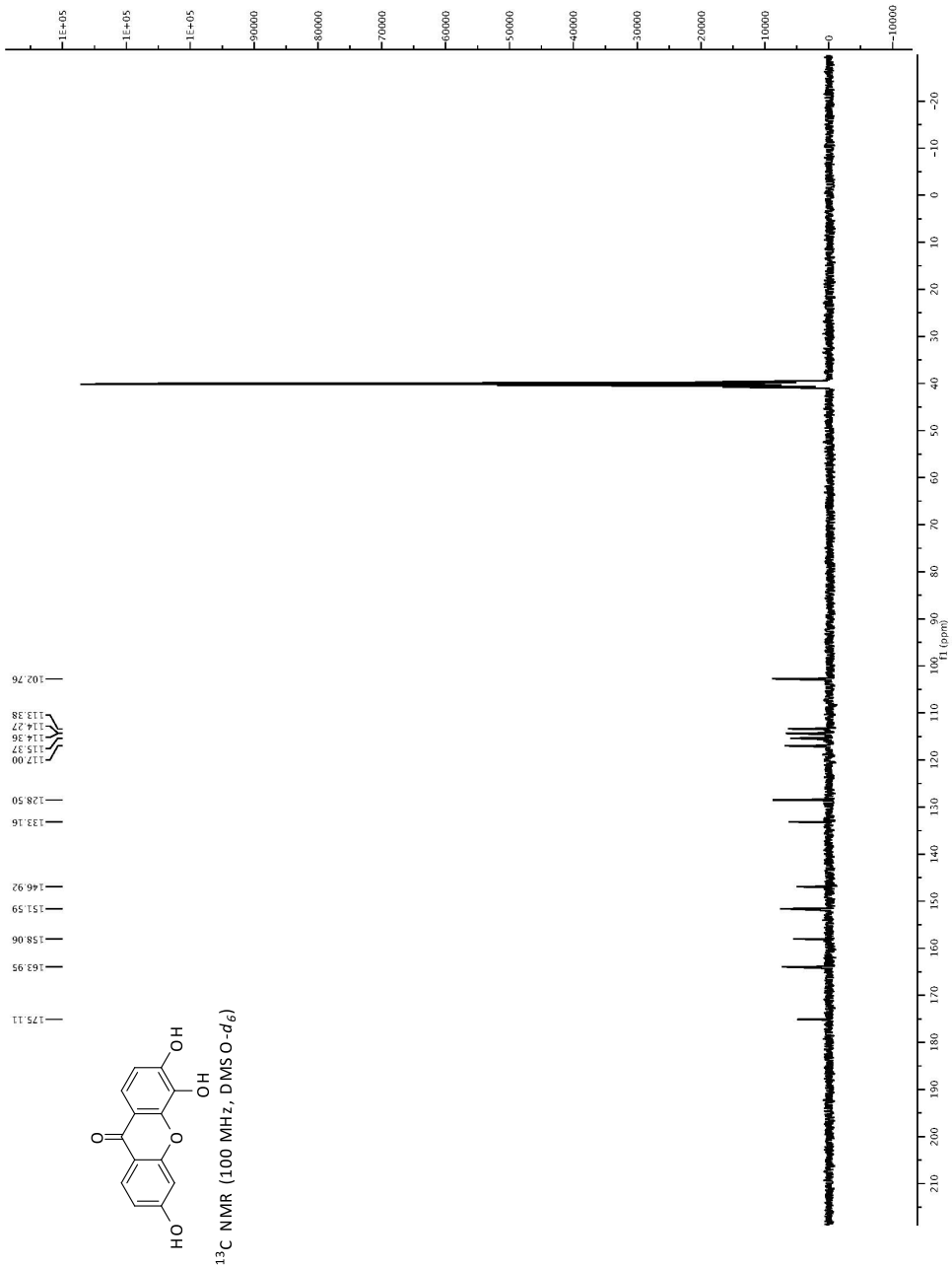

Spectrum 1.26: Compound 10b: ^{13}C NMR

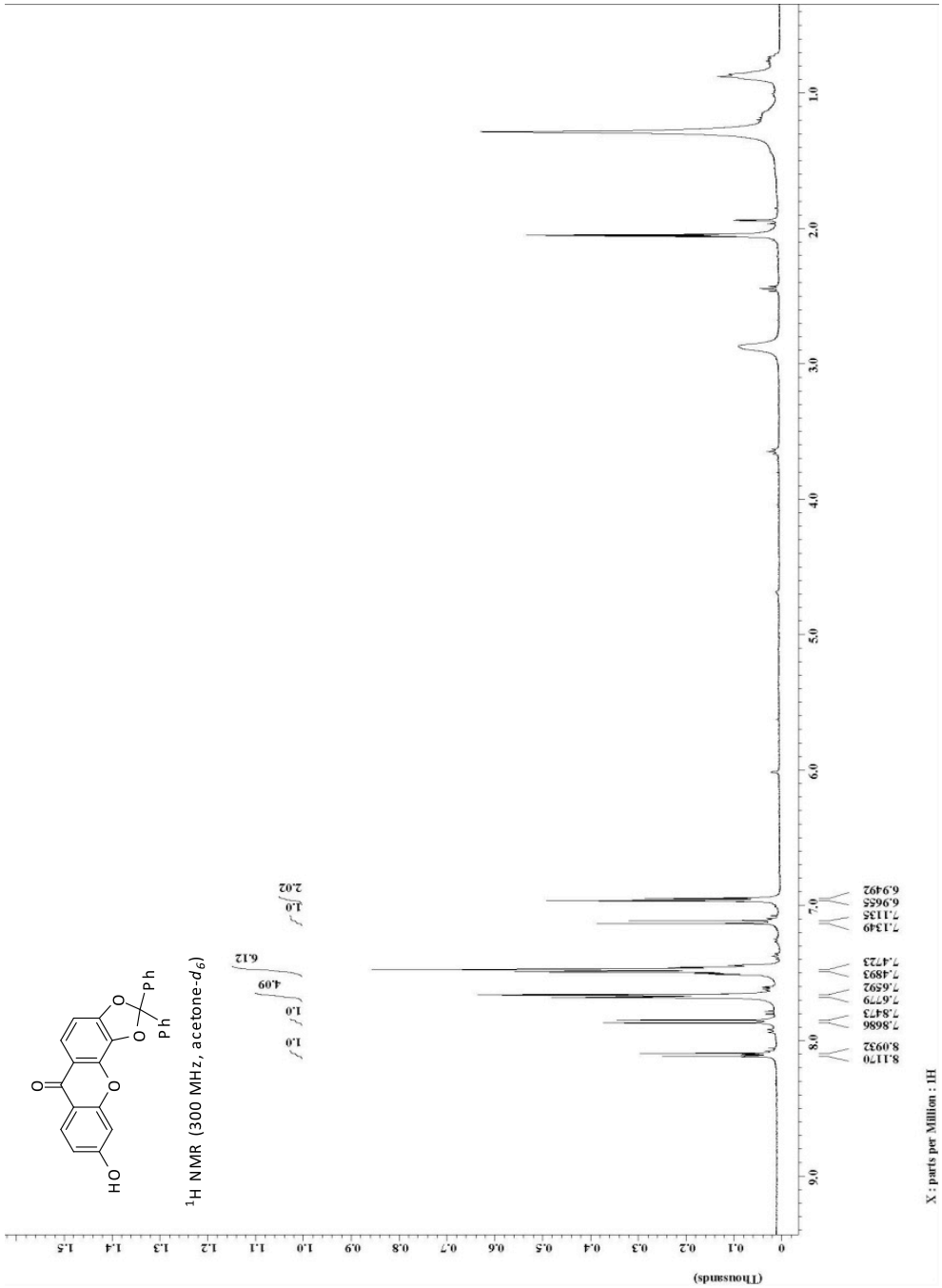

Spectrum 1.27: Compound 1b-i: ^{1}H NMR

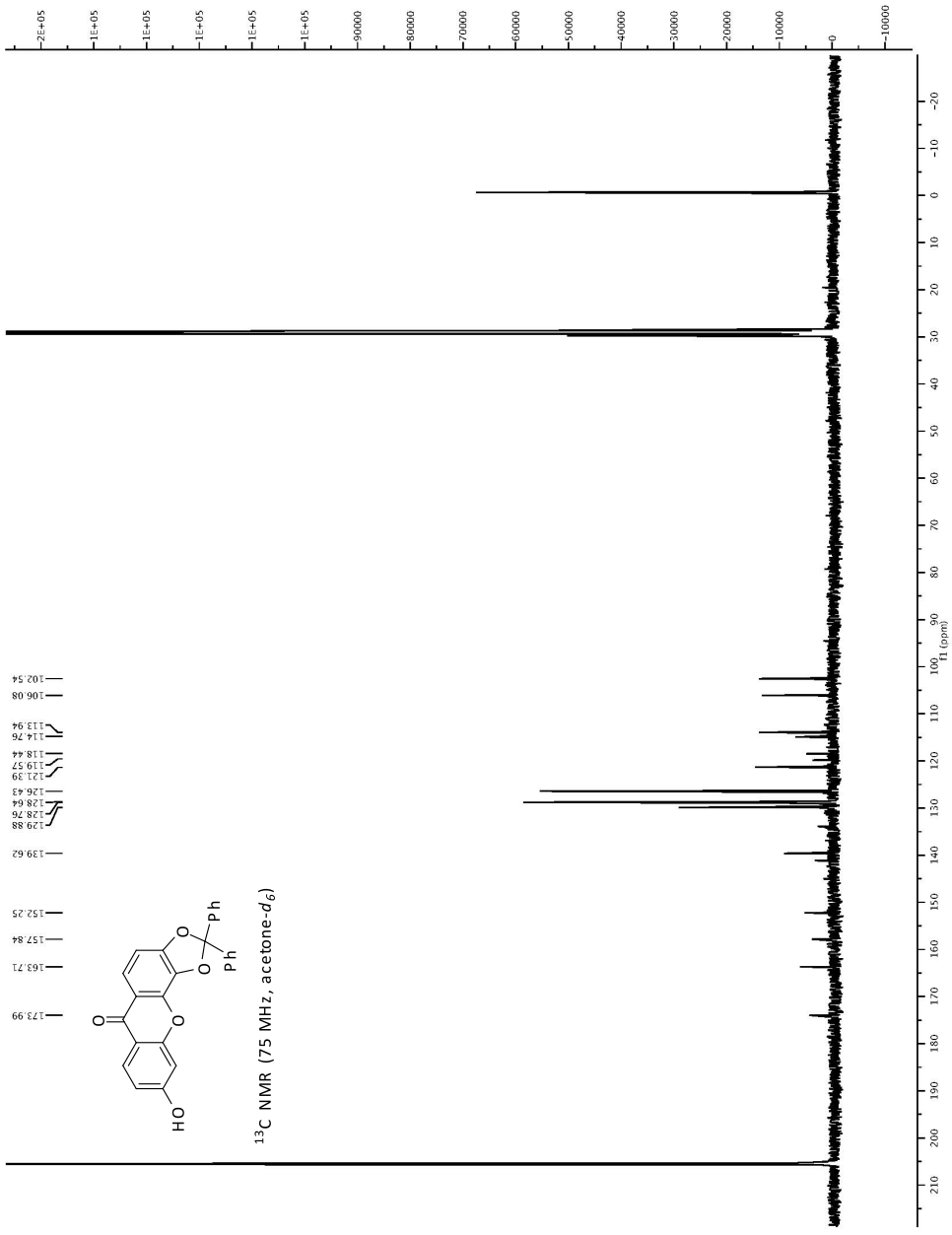

Spectrum 1.28: Compound 10b-i: ^{13}C NMR

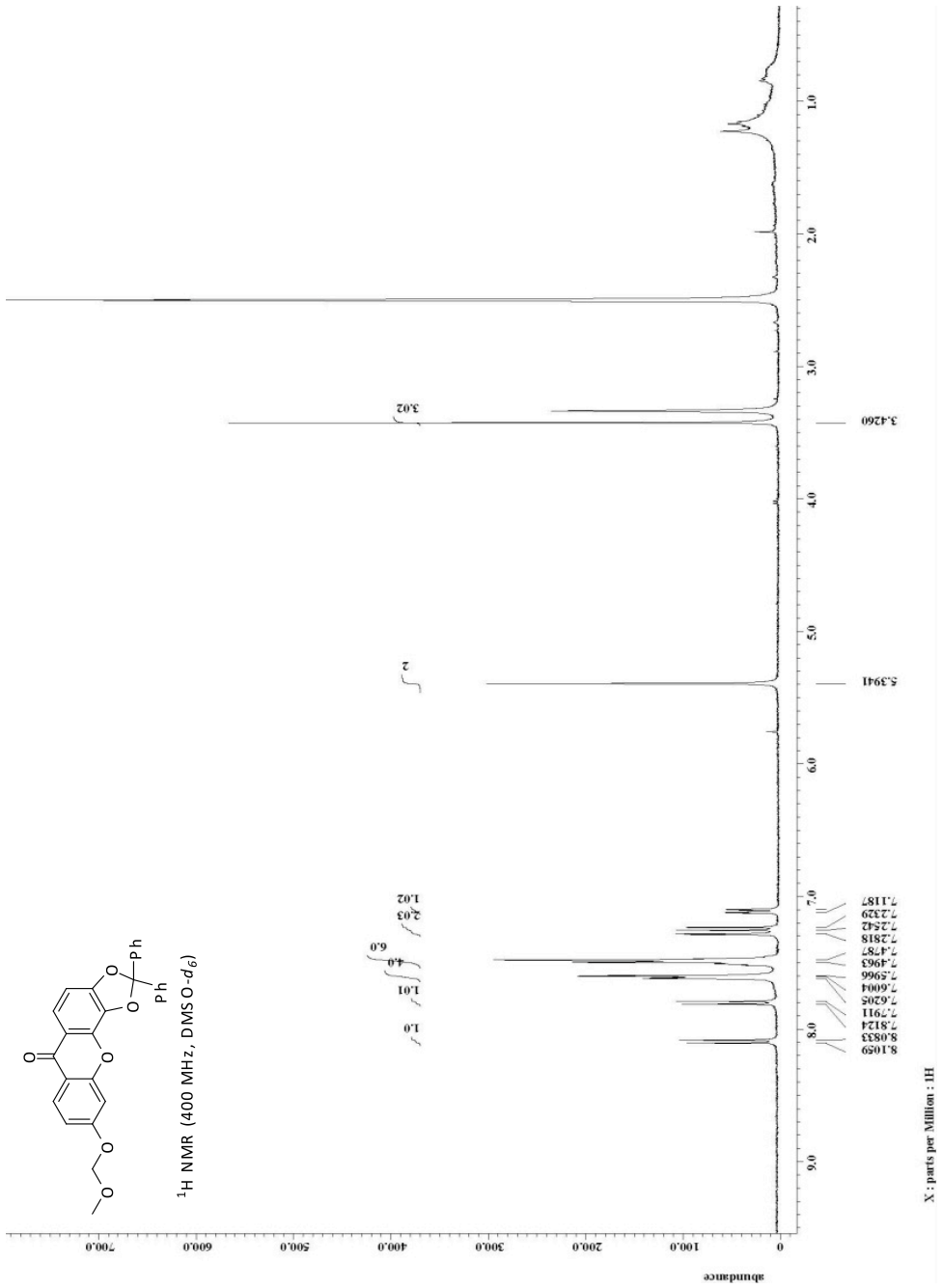

Spectrum 1.29: Compound 10b-ii: ^{1}H NMR

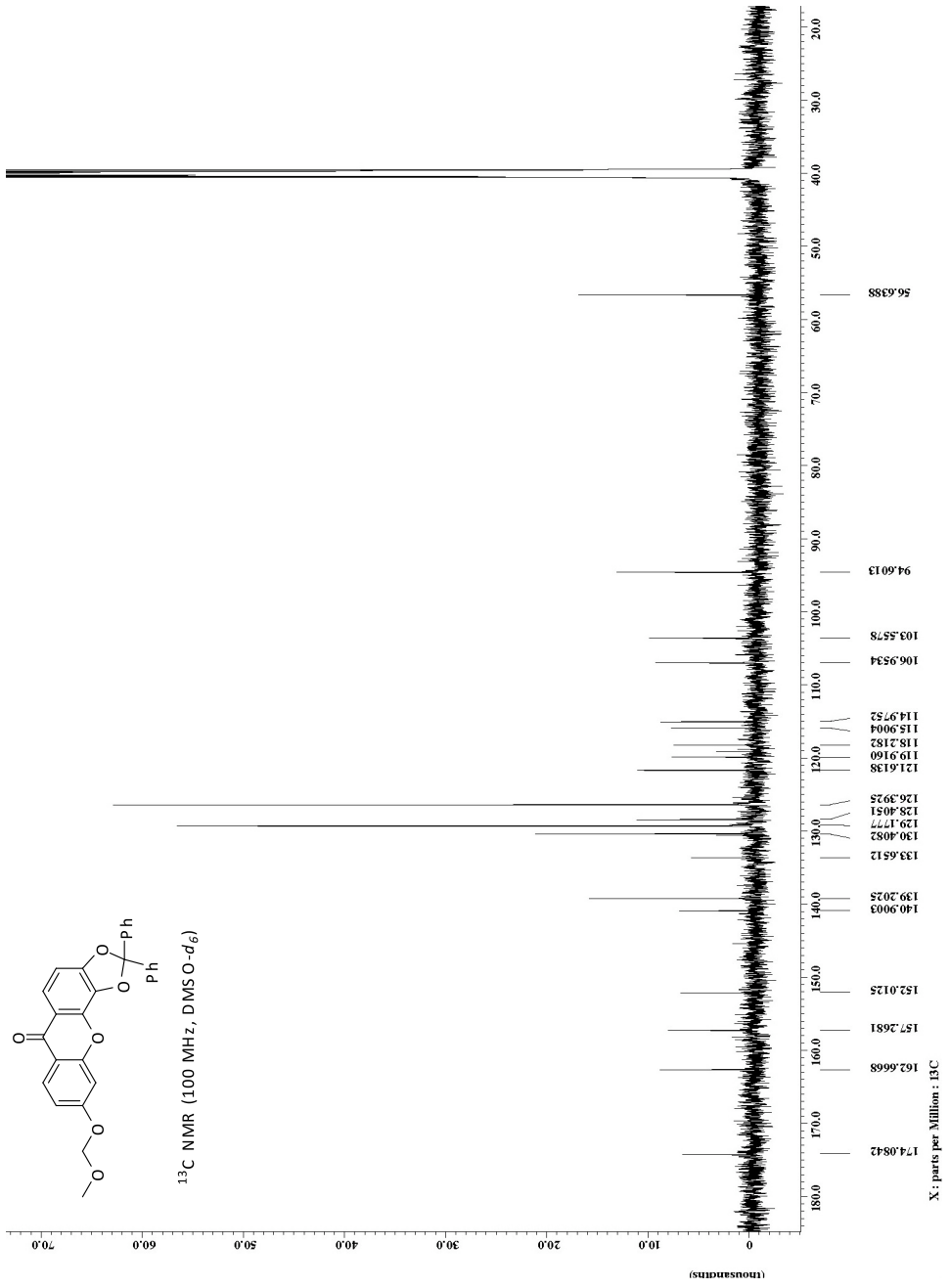

Spectrum 1.30: Compound 10b-ii: ^{13}C NMR

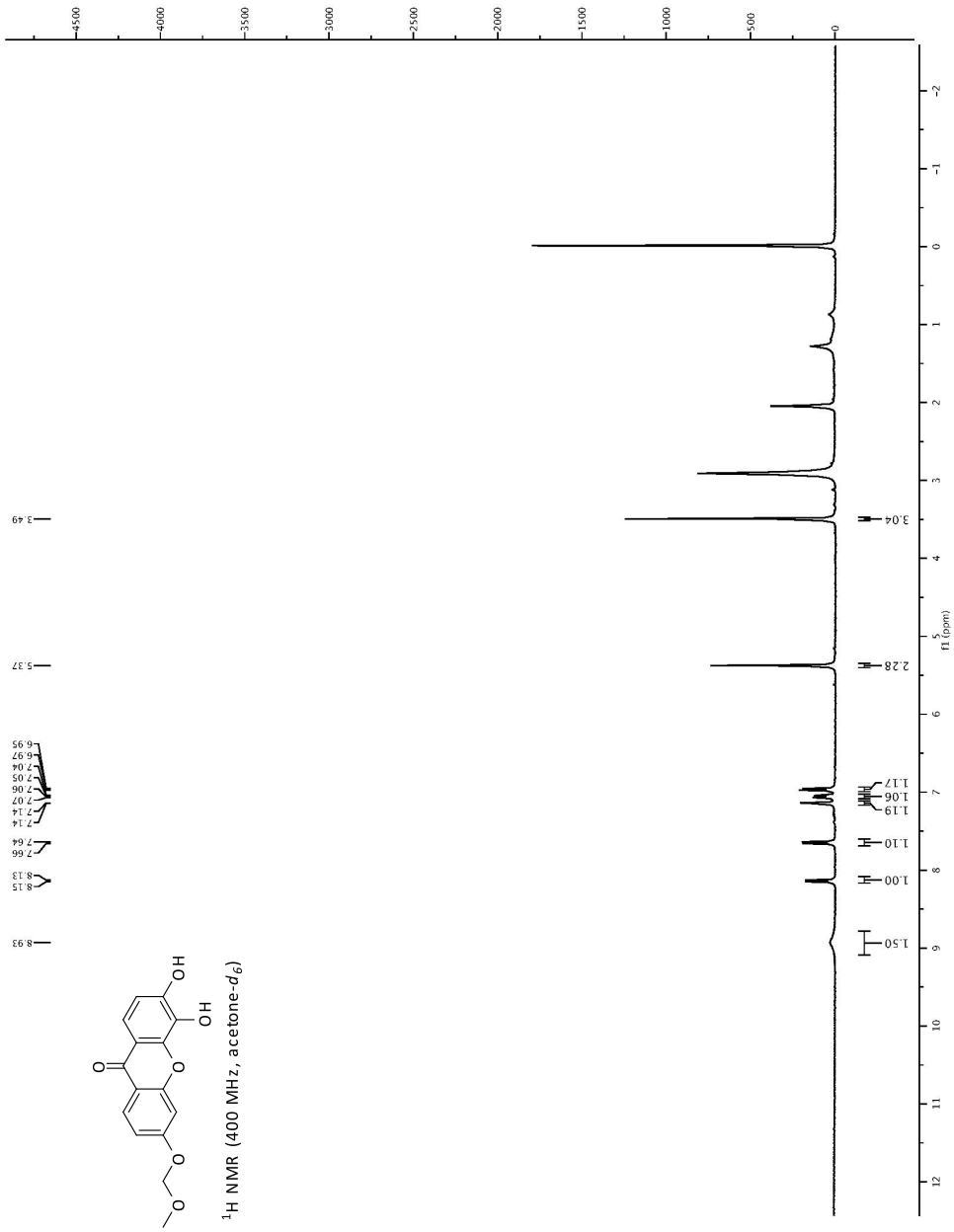

Spectrum 1.31: Compound 11b: ^{1}H NMR

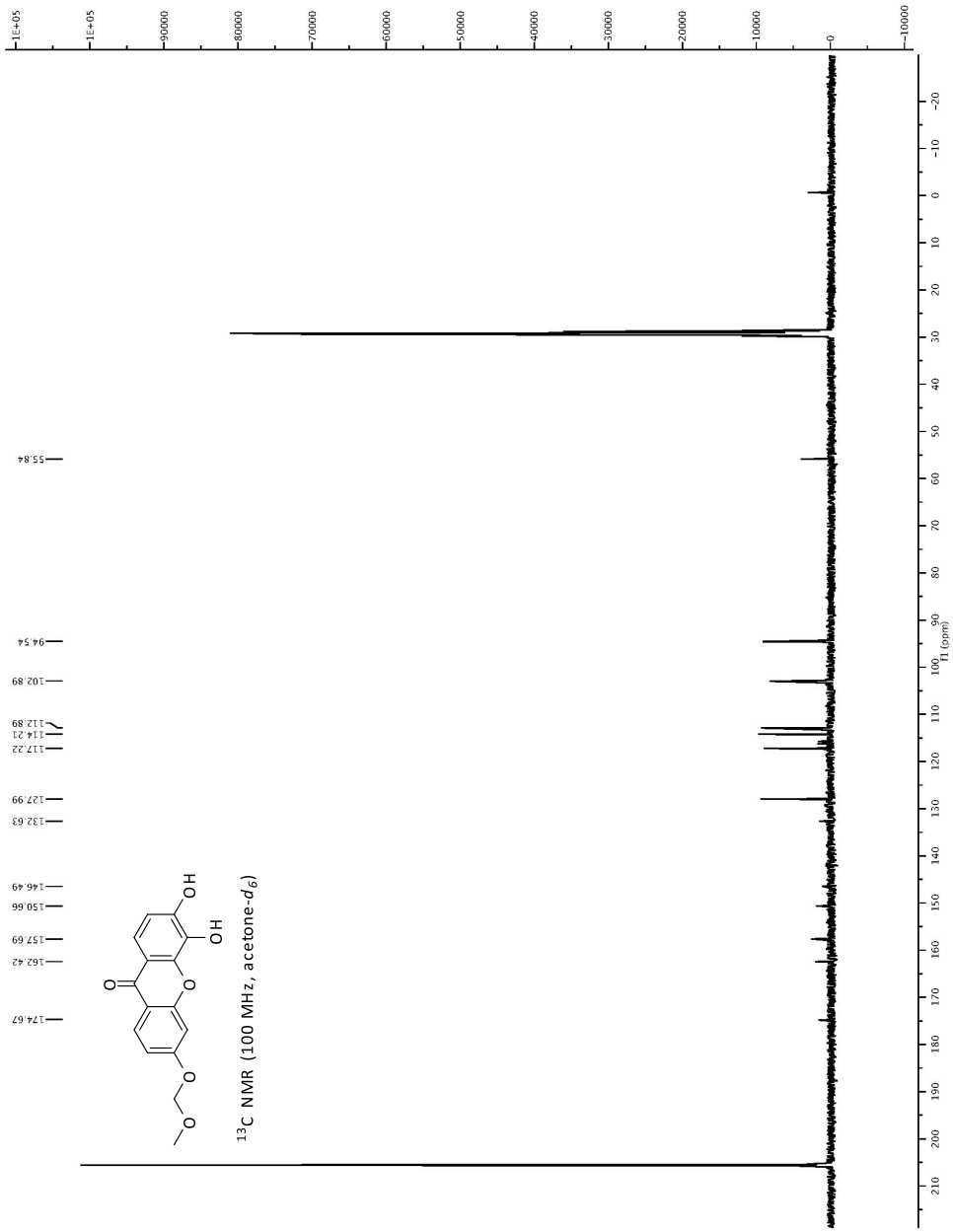

Spectrum 1.32: Compound 11b: ^{13}C NMR

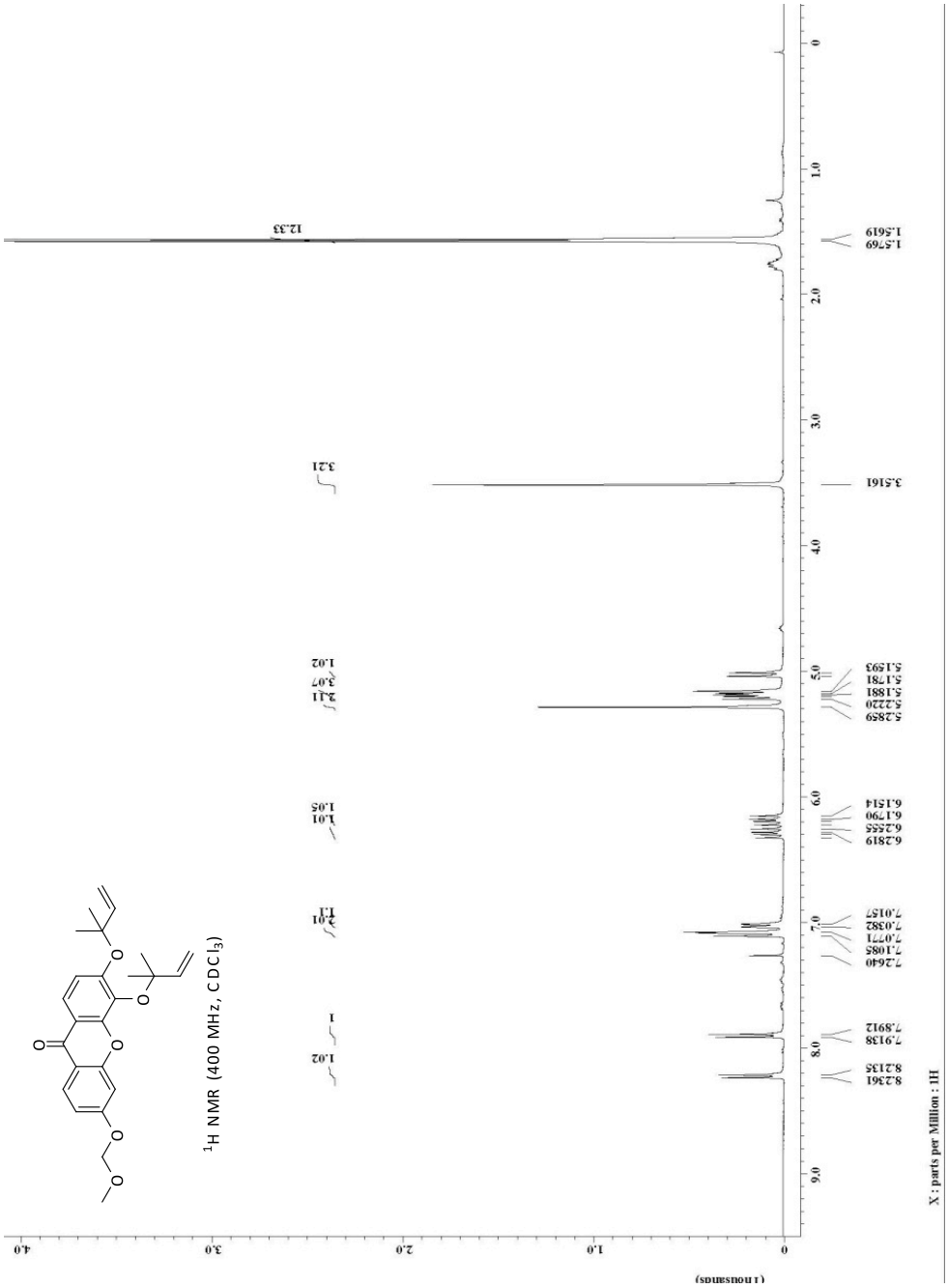

Spectrum 1.33: Compound 13b: ^{1}H NMR

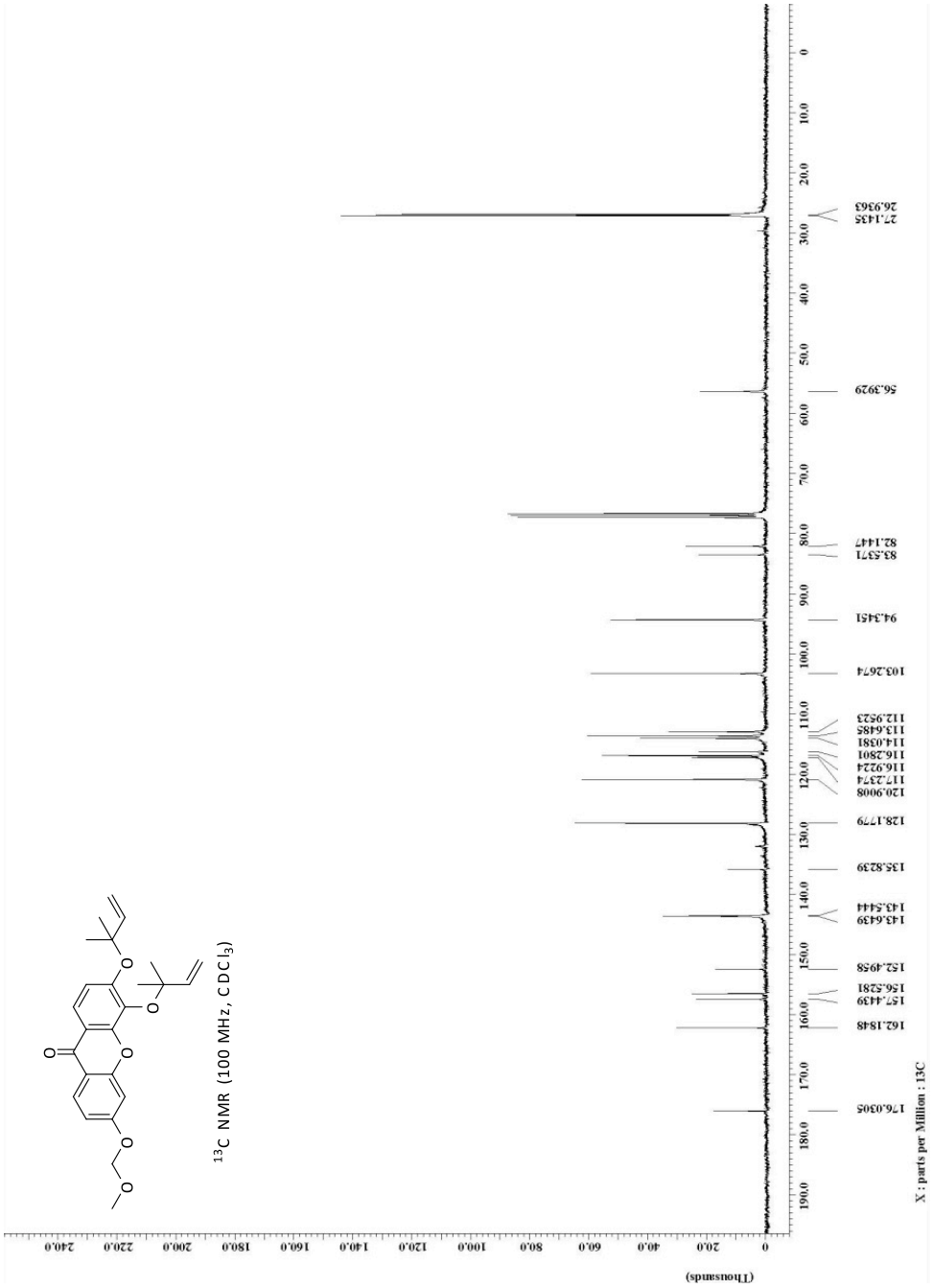

Spectrum 1.34: Compound 13b: ^{13}C NMR

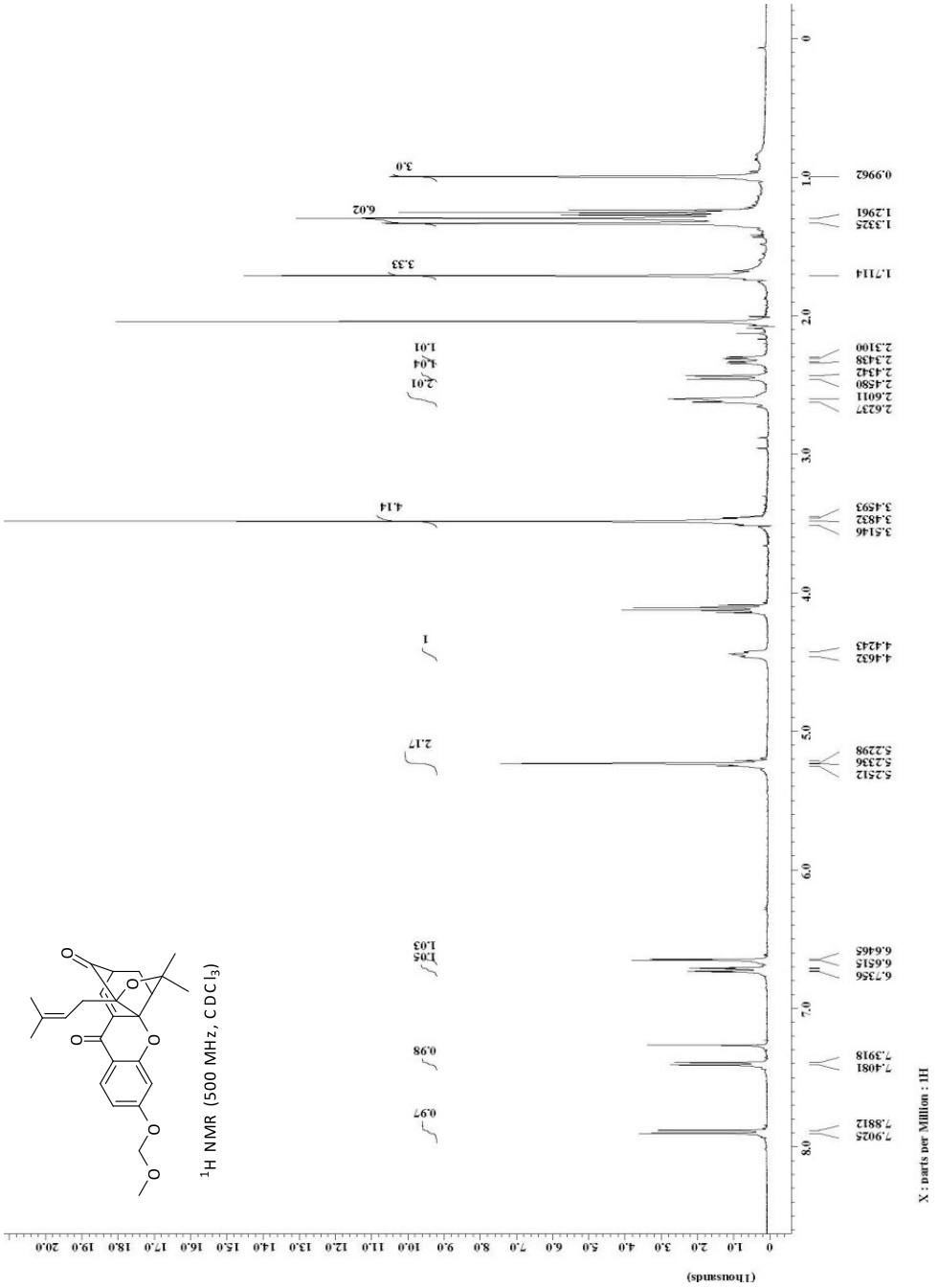

Spectrum 1.35: Compound 19: ^{1}H NMR

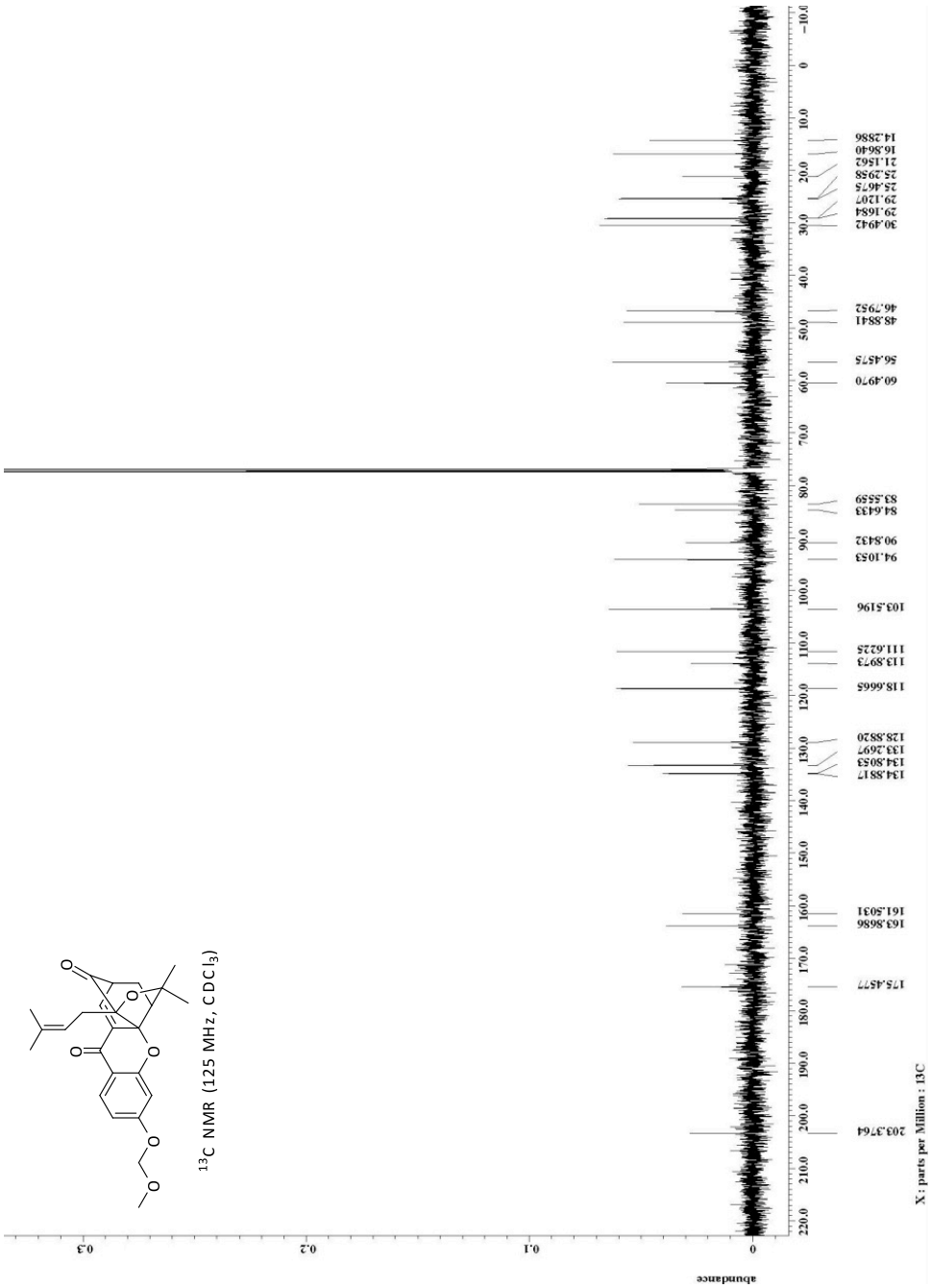

Spectrum 1.36: Compound 19: ^{13}C NMR

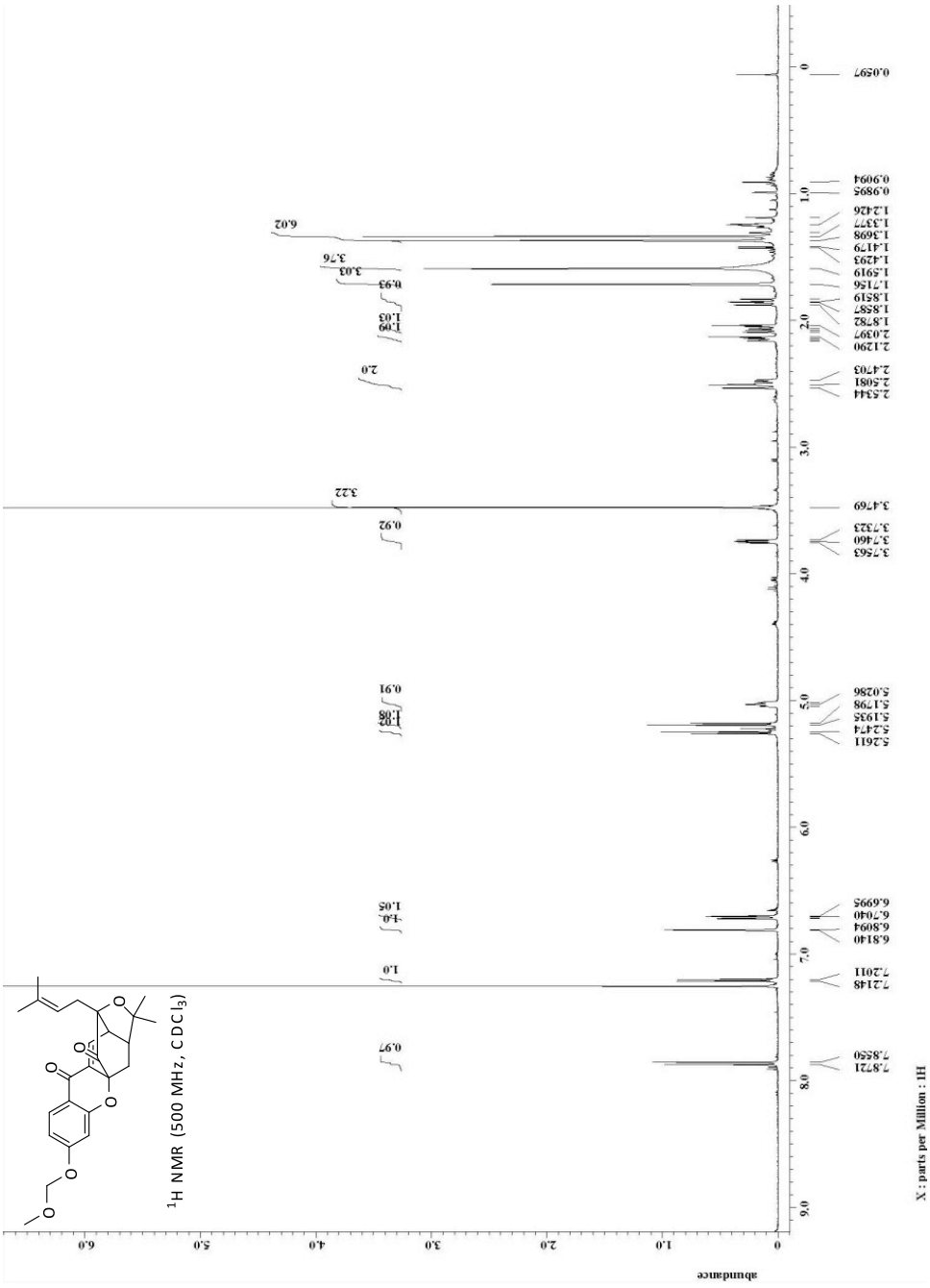

Spectrum 1.37: Compound 20: ^{1}H NMR

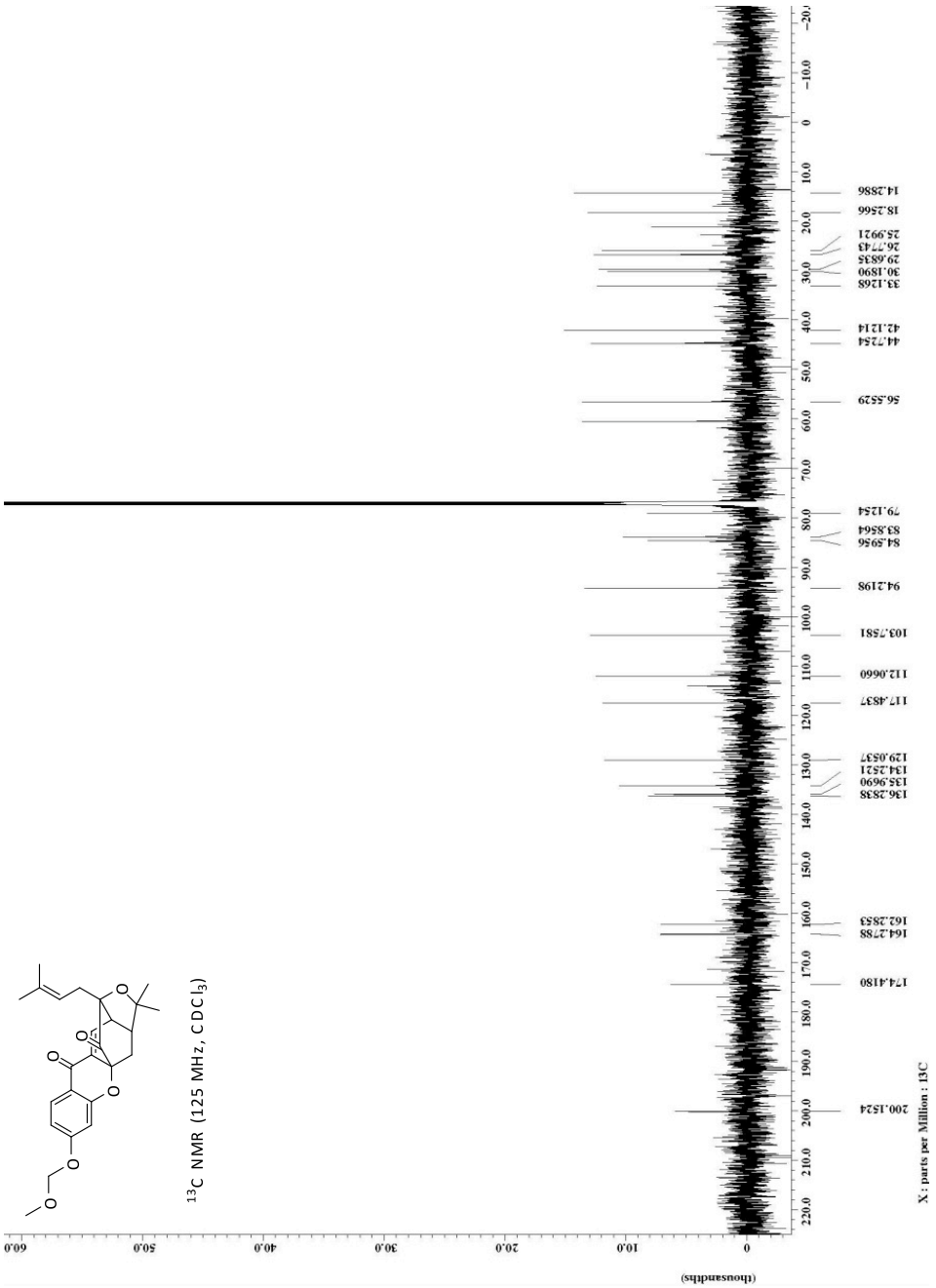

Spectrum 1.38: Compound 20: ^{13}C NMR

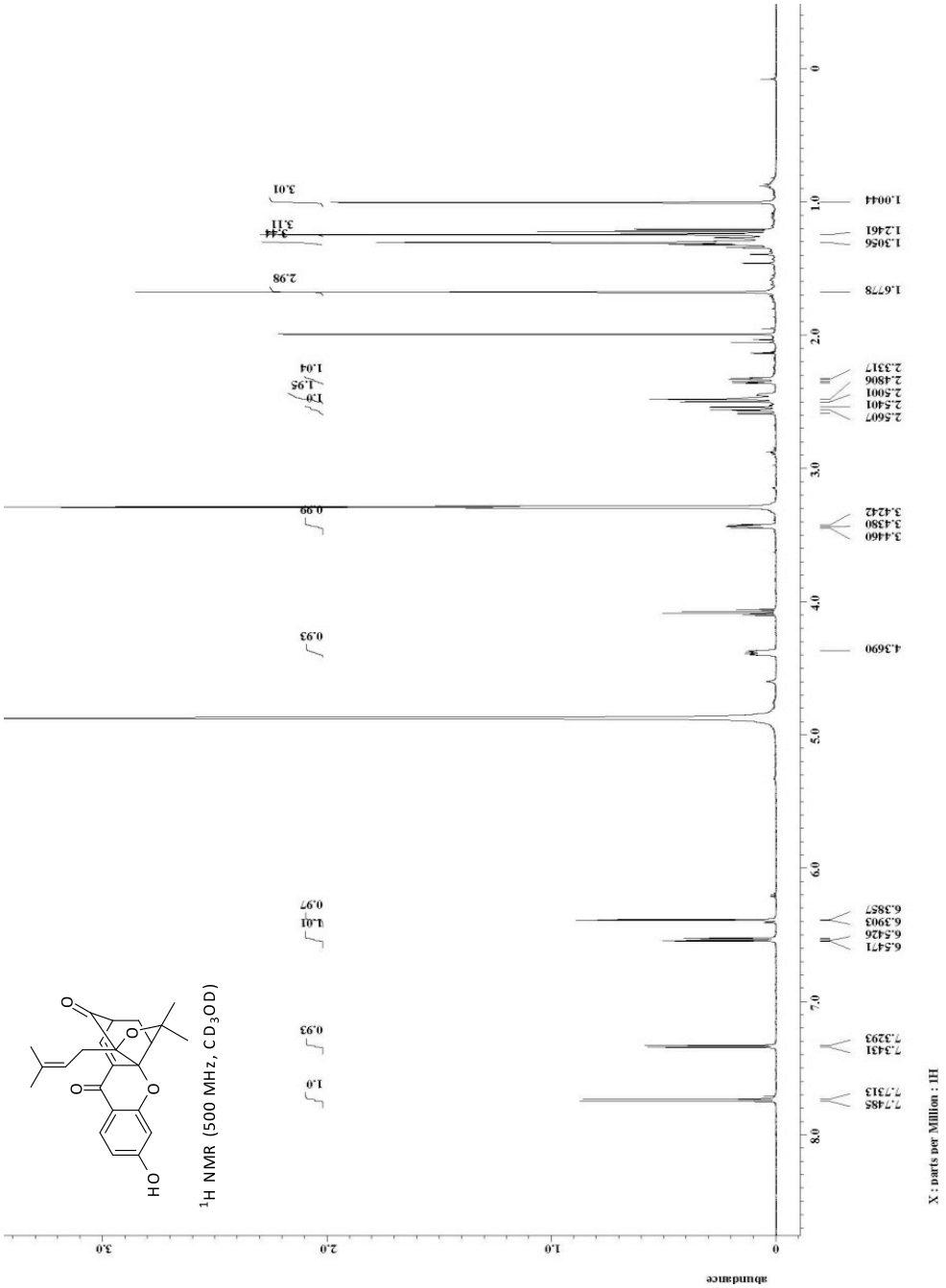

Spectrum 1.39: Compound 4: ^{1}H NMR

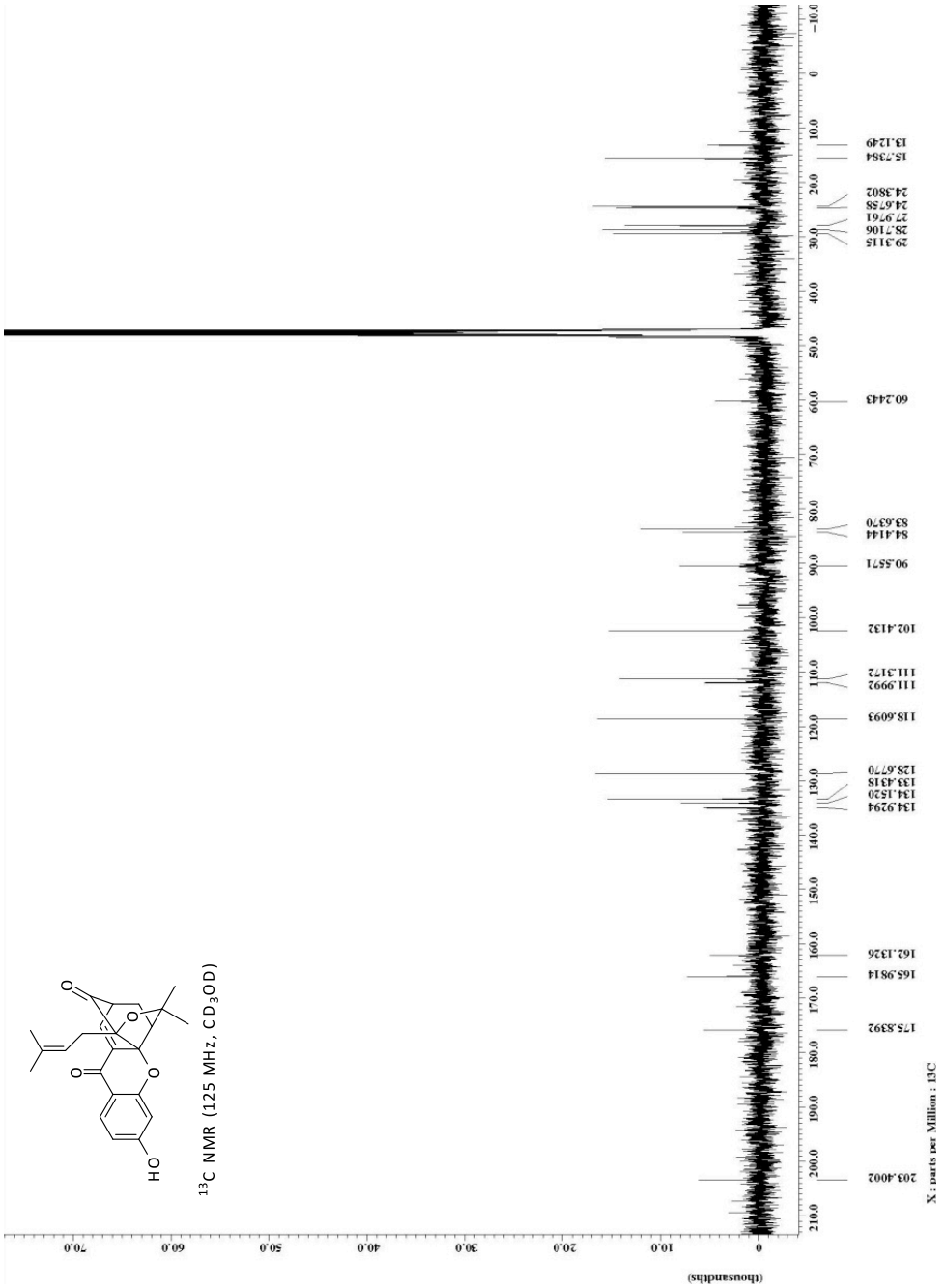

Spectrum 1.40: Compound 4: ^{13}C NMR

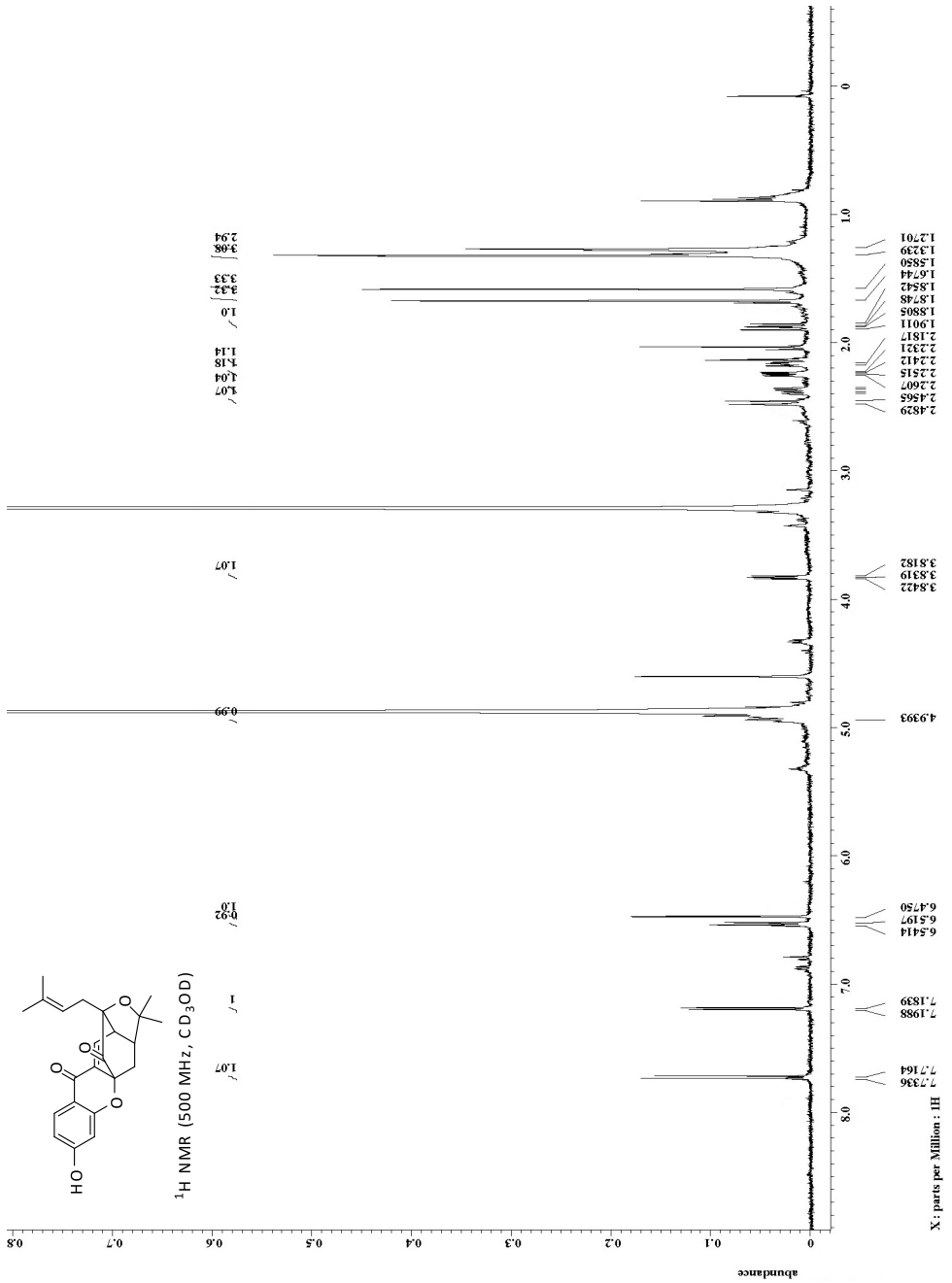

Spectrum 1.41: Compound 21: ^{1}H NMR

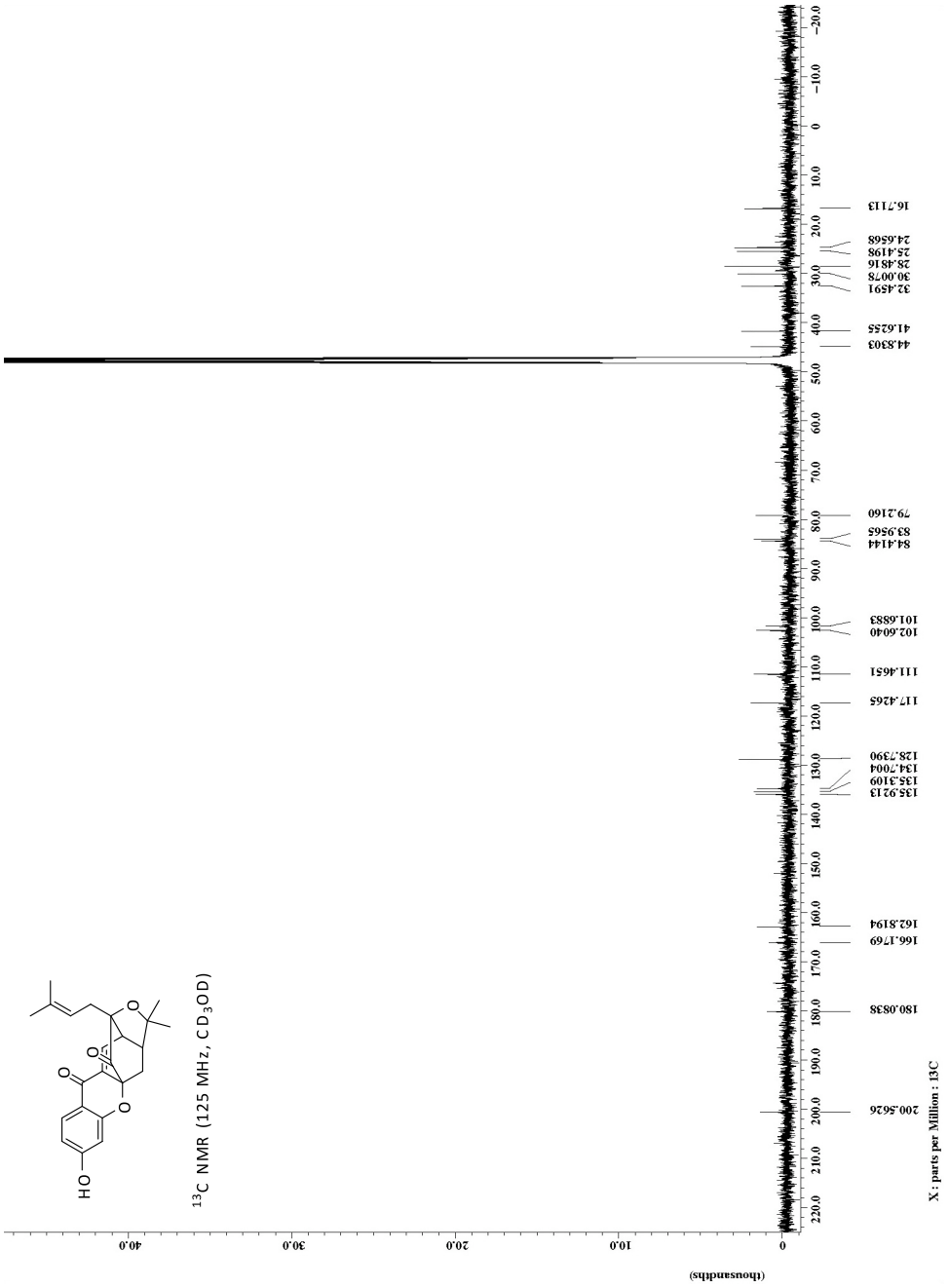

Spectrum 1.42: Compound 21: ^{13}C NMR

1.6 References

1. For selected general references on this topic see: (a) W. D. Ollis, B. T. Redman, I. O. Sutherland and K. Jewers, *J. Chem. Soc. Chem. Commun.* 1969, 879-880. (b) P. Kumar and R. K. Baslas, *Herba Hungarica* **1980**, *19*, 81-91.

2. For selected recent reviews on caged *Garcinia* xanthones see: (a) O. Chantarasriwong, A. Batova, W. Chavasiri and E. A. Theodorakis, *Chem. Eur. J.*, **2010**, *16*, 9944-9962. (b) N. Pouli and P. Marakos, *Anti-Cancer Agents Med. Chem.* **2009**, *9*, 77-98. (c) Q.ĐB. Han and H.-X. Xu, *Curr. Med. Chem.* **2009**, *16*, 3775-3796.

3. (a) P. Yates, S. S. Karmarkar, D. Rosenthal, G. H. Stout and V. F. Stout, *Tetrahedron Lett.* **1963**, *4*, 1623-1629. (b) A. Anthony and G. R. Desiraju, *Supramol. Chem.* **2001**, *13*, 11-23. (c) T. J. R. Weakley, S. X. Cai, H.-Z. Zhang and J. F. W. Keana, *J. Chem. Crystallogr.* **2001**, *31*, 501-505. (d) Y. Ren, C. Yuan, H. Chai, Y. Ding, X.-C. Li, D. Ferreira and A. D. Kinghorn, *J. Nat. Prod.* **2011**, *74*, 460-463.

4. (a) Q. Guo, Q. Qi, Q. You, H. Gu, L. Zhao and Z. Wu, *Basic & Clin. Pharmacol. & Toxicol.* **2001**, *31*, 178-184. (b) X. Wu, S. Cao, S. Goh, A. Hsu and B. K. H. Tan, *Planta Med.* **2002**, *68*, 198-203. (c) Q. Guo, Q. Qi, H. Gu and Z. Wu, *Basic & Clin. Pharmacol. & Toxicol.* **2006**, *99*, 178-184. (d) Y. Yang, L. Yang, Q. -D. You, F. -F. Nie, H. -Y. Gu, L. Zhao, X. -T. Wang and Q. -L. *Guo, Cancer Lett.* **2007**, *256*, 259-266. (e) Z. T. Zhou and J. W. Wang, *Chin. J. New Drugs* **2007**, *16*, 79-82. (f) Q. Qi, Q. You, H. Gu, L. Zhao, W. Liu, N. Lu and Q. Guo, J. *Ethnopharmacol.* **2008**, *117*, 433-438. (g) H. Gu, Q. You, W. Liu, Y. Yang, L. Zhao, Q. Qi, J. Zhao, J. Wang, N. Lu, H. Ling, Q. Guo and X. Wang *Intern. Immunopharmacol.* **2008**, *8*, 1493-1502. (h) L. Qiang, Y. Yang, Q.-D. You, Y.-J. Ma, L. Yang, F.-F. Nie, H.-Y. Gu, L. Zhao, N. Lu, Q. Qi, W. Liu, X.-T. Wang and Q.-L. Guo, *Biochem. Pharmacol.* **2008**, *75*, 1083-1092. (i) L. Zhao, C. Zhen, Z. Wu, R. Hu, C. Zhou, Q. Guo, *Drug & Chem. Toxicol.* **2010**, *33*, 88-96.

5. (a) W. Liu, Q. L. Guo, Q. D. You, L. Zhao, H. Y. Gu and S. T. Yuan, *World J. Gastroenterol.* **2005**, *11*, 3655-3659; (b) D. Zhai, C. Jin, C. ĐW. Shiau, S. Kitada, A. C. Satterthwait and J. C. Reed, *Mol. Cancer Ther.* **2008**, *7*, 1639-1646; c) X. Xu, Y. Liu, L. Wang, J. He, H. Zhang, X. Chen, Y. Li, J. Yang and J. Tao, *Int. J. Dermatol.* **2009**, *48*, 186-192.

6. (a) L. Zhang, Y. Yi, J. Chen, Y. Sun, Q. Guo, Z. Zheng and S. Song, *Biochem. & Biophys. Res. Commun.* **2010**, *403*, 282-287. (b) J. Davenport, J. R. Manjarrez, L. Peterson, B. Krumm, B. S. Blagg and R. L. Matts *J. Nat. Prod.* **2011**, *74*, 1085-1092.

7. For selected reviews on this topic see: (a) A. S. Sreedhar and P. Csermely, *Pharmacol. & Therapeut.* **2004**, *101*, 227-257. (b) M. Taipale, D. F. Jarosz, and S. Lindquist, *Nature Rev. Mol. Cell Biol.* **2010**, *11*, 515-528. (c) F. U. Hartl, A. Bracher, M. Hayer-Hartl, *Nature* **2011**, *475*, 324-332. (d) A. J. McClellan, Y. Xia, A. M. Deutschbauer, R. W. Davis, M. Gerstein and J. Frydman, *Cell* **2007**, *131*, 121-135. (e) V. C. H. Da Silva, and C. H. I. Ramos, *J. Proteomics* **2012**, *75*, 2790-2802. (f) L. Whitesell, S. L. Lindquist,

Nature Rev. Cancer **2005**, *5*, 761-772. (g) L. H. Pearl and C. Prodromou, *Annu. Rev. Biochem.* **2006**, *75*, 271-294.

8. A. Batova, T. Lam, V. Wascholowski, A. L. Yu, A. Giannis and E. A. Theodorakis, *Org. Biomol. Chem.* **2007**, *5*, 494-500.

9. (a) H.-Z. Zhang, S. Kasibhatla, Y. Wang, J. Herich, J. Guastella, B. Tseng, J. Drewe and S.-X. Cai, *Bioorg. Med. Chem.* **2004**, *12*, 309-317. (b) J. Kuemmerle, S. Jiang, B. Tseng, S. Kasibhatla, J. Drewe, S. X. Cai, *Bioorg Med. Chem.* **2008**, *16*, 4233-4241. (c) N. G. Li, Q. D. You, X. F. Huang, J. X. Wang, Q. L. Guo, X. G. Chen, Y. Li, H. Y. Li, *Chin. Chem. Lett.* **2007**, *18*, 659-662. (d) J. Wang, L. Zhao, Y. Hu, Q. Guo, L. Zhang, X. Wang, N. Li, Q. You, *Eur. J. Med. Chem.* **2009**, *44*, 2611-2620.

10. O. Chantarasriwong, W. C. Cho, A. Batova, W. Chavasiri, C. Moore, A. L. Rheingold and E. A. Theodorakis, *Org. Biomol. Chem.* **2009**, *7*, 4886-4894.

11. (a) G. Guizzunti, A. Batova, O. Chantarasriwong, M. Dakanali and E. A. Theodorakis, *ChemBioChem* **2012**, *13*, 1191-1198. (b) G. Guizzunti, E. A. Theodorakis, A. L. Yu, C. Zurzolo and A. Batova, *Invest. New Drugs* **2012**, *30*, 1841-1848.

12. E. J. Tisdale, I. Slobodov and E. A. Theodorakis, *Proc. Natl. Acad. Sci. USA* **2004**, *101*, 12030-12035.

13. (a) E. J. Tisdale, C. Chowdhury, B. G. Vong, H. Li and E. A. Theodorakis, *Org. Lett.* **2002**, *4*, 909-912. (b) E. J. Tisdale, H. Li, B. G. Vong, S. H. Kim and E. A. Theodorakis, *Org. Lett.* **2003**, *5*, 1491-1494. (c) E. J. Tisdale, B. G. Vong, H. Li, S. H. Kim, C. Chowdhury and E. A. Theodorakis, *Tetrahedron* **2003**, *59*, 6873-6887. (d) E. J. Tisdale, I. Slobodov and E. A. Theodorakis, *Org. Biomol. Chem.* **2003**, *1*, 4418-4422.

14. An alternative explanation for the observed site selectivity could be that the Claisen rearrangement is reversible and that the rate of the Diels-Alder reaction controls the product selection. For computational studies in support of this proposal see: A. E. Hayden, H. Xu, K. C. Nicolaou and K. N. Houk, *Org. Lett.* **2006**, *8*, 2989-2992.

15. For related synthetic studies see: (a) K. C. Nicolaou and J. Li, *Angew. Chem. Int. Ed,* **2001**, *40*, 4264-4268. (b) K. C. Nicolaou, P. K. Sasmal, H. Xu, K. Namoto and A. Ritzen, *Angew. Chem. Int. Ed.* **2003**, *42*, 4225-4229. (c) K. C. Nicolaou, P. K. Sasmal, and H. Xu, *J. Am. Chem. Soc.* **2004**, *126*, 5493-5501. (d) K. C. Nicolaou, H. Xu and M. Wartmann, *Angew. Chem. Int. Ed.* **2005**, *44*, 756-761.

16. For a recent review on this topic see: M. L. Wuerstle, M. A. Laussmann and M. Rehm, *Exper. Cell Res.* **2012**, *318*, 1213-1220.

17. For selected reviews on this topic see: (a) A. G. Porter and R. U. Jaenicke, *Cell Death and Different.* **1999**, *6*, 99-104. (b) E. D. Crawford and J. A. Wells, *Annu. Rev. Biochem.* **2011**, *80*, 1055-1087.

18. A. Kamal, L. Thao, J. Sensitaffar, L. Zhang, M. F. Boehm, L. C. Fritz and F. J. Burrows, *Nature* **2003**, *425*, 407-410.

19. (a) K. Jhaveri, T. Taldone, S. Modi and G. Chiosis, *Biochim. Biophys. Acta.* **2012**, *1823*, 742-755. (b) D. B. Solit and G. Chiosis, *Drug Discov. Today* **2008**, *13*, 38-43. (c) J. Travers, S. Sharp and P. Workman, *Drug Discov. Today* **2012**, *17*, 242-252.

20. (a) J. C. Ame, C. Spenlehauer and G. de Murcia, *BioEssays* **2004**, *26*, 882-893. (b) M. J. Schiewer, J. F. Goodwin, S. Han, J. C. Brenner, M. A. Augello, J. L. Dean, F. Liu, J. L. Planck, P. Ravindranathan, A. M. Chinnaiyan, P. McCue, L. G. Gomella, G. V. Raj, A. P. Dicker, J. R. Brody, J. M. Pascal, M. M. Centenera, L. M. Butler, W. D. Tilley, F. Y. Feng and K. E. Knudsen, *Cancer Discov.* **2012**, *2*, 1134-1149.

Chapter 2

Rational Design of Fluorescent Sensors for Amyloid Detection

2.1 Introduction

Alzheimer's disease (AD) is a progressive neurodegenerative disorder currently affecting 5 million Americans.[1] It is the sixth leading cause of death, behind cancer and heart disease, and is projected to affect over 14 million people by 2050.[2] Of the top ten causes of death in the U.S., AD is the only member on the list for which their is no treatment. There currently is no definitive test or therapy for this disease making it quite an desirable medicinal target for researchers. Early symptoms of AD are often mistaken as "age-related" concerns or manifestations of stress and therefore early symptoms are usually overlooked or dismissed. However, as the disease progresses, symptoms can often include mood swings, depression, confusion, trouble with language, and long-term memory loss.[3] Gradually, bodily functions are lost ultimately leading to death. Many patients survive only ten years after diagnosis.

Alzheimer's is pathologically marked by an accumulation of amyloid beta (Aβ) deposits in the brain.[4] These deposits derive from the aggregation of Aβ1-40 and Aβ1-42 peptides, which are cleaved from the amyloid peptide precursor protein through an unknown process. Ten years before a patient shows any symptoms, aggregates form amyloid fibrils which are believed to be the toxic form of the protein. Thus, due to its prevalent role in the brain in the course of the disease, detection of Aβ plaques remains the popular method for screening for Alzheimer's.[5]

2.2 Imaging Agents

To date, the most common method of AD diagnosis in living patients still relies on cognitive recognition such as memory and behavior tests along with patient and family interviews.[6] The most accurate diagnosis method however is post-mortem examination of the brain tissue. In the past few decades there have been advances in the development of small molecular probes for the specific labeling and imaging of Aβ plaques in living patients. These probes rely on techniques such as Magnetic Resonance Imaging (MRI), Positron Emission Tomography (PET) [7], and Single Photon Emission Computed Tomography (SPECT). [8] The earliest generation of probes used to detect the post-mortem presence of plaques was Thioflavin T (**1**) and Congo Red (**2**). These com-

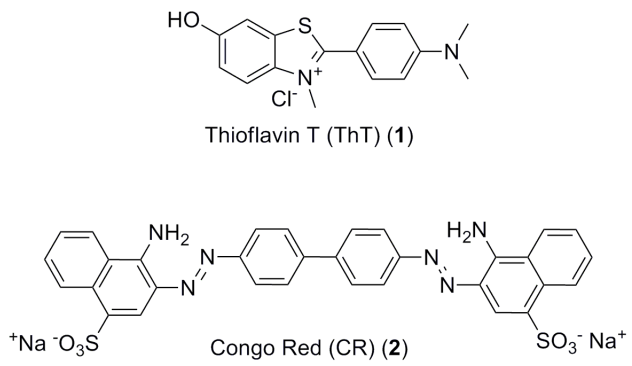

Figure 2.1: Earliest Generation of Amyloid-detecting Probes

pounds, due to their charges, are unsuitable for *in vivo* imaging because of their inability to cross the blood-brain barrier. They are predominately used for plaque detection in brain sections of deceased patients.

In the last decade, researchers have developed molecular probes that rely on a radioactive tracer for use in PET imaging. Both Pittsburgh Compound B (PiB) (**3**) and Florbetapir (^{18}F) (**4**) have been shown to bind to Aβ plaques specifically in living Alzheimer's patients. While PiB (**3**) has been mainly used in the academic area, Florbetapir (**4**) was recently granted FDA approval as a diagnostic tool to be used in a clinical setting. Eli Lilly and Company acquired Avid Radiophramaceuticals, which first created Florbetapir (**4**), and is marketing the new PET scanning probe under the name AMYViD. While both PiB (**3**) and AMYViD (**4**) have been successfully used in humans to detect

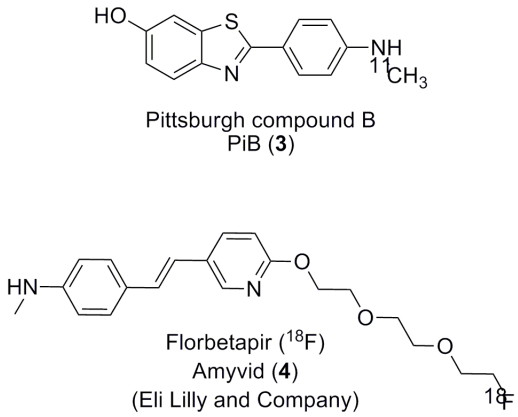

Figure 2.2: Structures of PiB and AMYViD

Aβ plaques, the presence of a radionuclide makes wide spread use difficult. PiB (**3**)

relies on carbon-13, which has a half-life of only 20 minutes, while AMYViD (**4**) contains a radionuclide fluoride-18, half-life of 100 minutes. Due to the short half-lives, both compounds must be synthesized in facilities equipped with a cyclotron and must be administered quickly. This has led to the search for novel fluorescent probes which do not rely on a radiolabel. Such probes are advantageous over PET/SPECT methods since they provide real-time, non-radioactive, and high resolution imagining both *in vivo* and *in vitro*. In general, an appropriate fluorescent probe for amyloid detection should have the following properties: [6,9,10] (a) molecular mass less than 600 Da, (b) emission wavelength greater than 450 nm to minimize background fluorescence from tissue, (c) high quantum yield, (d) appropriate lipophilicity (log P value between 1 and 3), (e) binding specificity to Aβ plaques, (f) sufficient binding affinity to aggregated amyloid peptides, (g) facile synthesis, and (h) upon binding to Aβ deposits, a significant change in fluorescence properties should be observed. [6,11]

2.3 Previous Efforts Towards Designing a Binding Agent

In previous studies, rationally designed molecular rotors were screened for their ability to detect amyloid-beta. A common structural motif, seen in representative structures, is an electron-donor unit in conjugation with an electron acceptor through a π-system.[6,7,8] These compounds produce a fluorescent quantum yield that is dependent on the surrounding environment and exhibit solvatochromic behavior. Solvatochromic behavior is more defined as the ability of a fluorophore to shift its fluorescence emission based on surrounding environment.[12,13] By adjusting the donor and acceptor units, as well as the length of conjugation between them, the fluorescence properties could be tuned. The solubility could also be adjusted by the addition of different water solubilizing groups (WSG), such as triethylene glycol methyl ester of glycerol to facilitate the passage through the blood-brain barrier (BBB).[15] In general, the fluorescent properties of this motif result by the formation of a twisted intra-molecular charge transfer (TICT) complex. This complex, when excited, produces a fluorescent quantum yield that is dependent on the micro-environment surrounding the molecule. Hindrance of the internal molecular rotation of the probe, by increasing the viscosity of the surrounding media

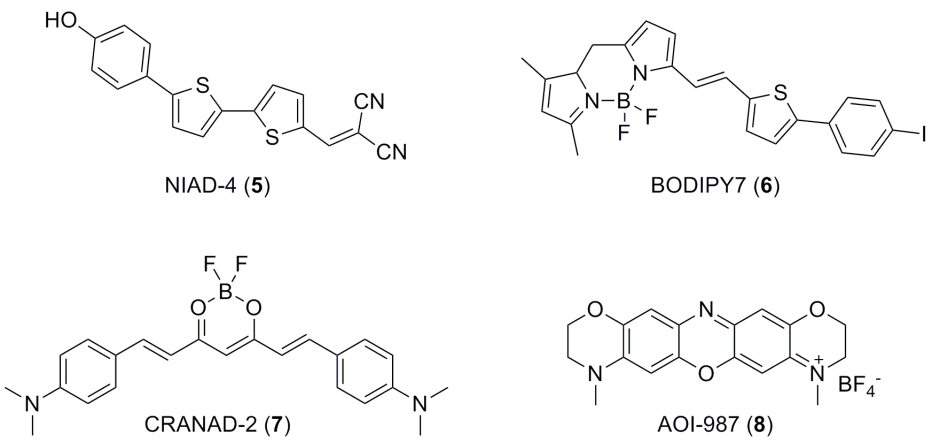

Figure 2.3: Molecular Rotor Motif

or by reducing the free volume needed for relaxation (such as when bound to a protein), leads to a decrease in the probability of non-radiative decay rate therefore increasing the fluorescent emission. Closer evaluation of the screen led to the identification of 6-aminonapthalenyl-2-cyano-acrylate (ANCA) as a motif that possessed potentially useful spectroscopic properties for fluorescent labeling of aggregated Aβ peptides.[10] Specifically, our lab found that compound **9**, referred to as ANCA-11, possessed a long

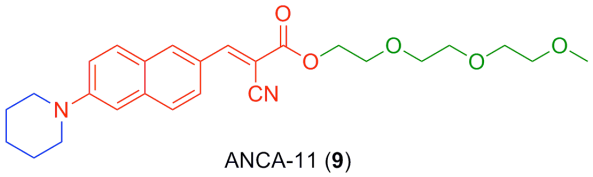

Figure 2.4: Structure of ANCA-11

emission wavelength and large increase in fluorescence intensity upon binding to Aβ fibrils.[14] It was found that small chemical changes to the water-solubilizing group of the ANCA motif did not significantly alter the binding of the probes to Aβ aggregates. However, significant changes to the K_d value were seen when the nitrogen donor moiety was changed. Compounds having piperidine as the electron donor were found to have lower K_d values compared to those possessing piperazine, morpholine, or morphlinoethanamine.[14]

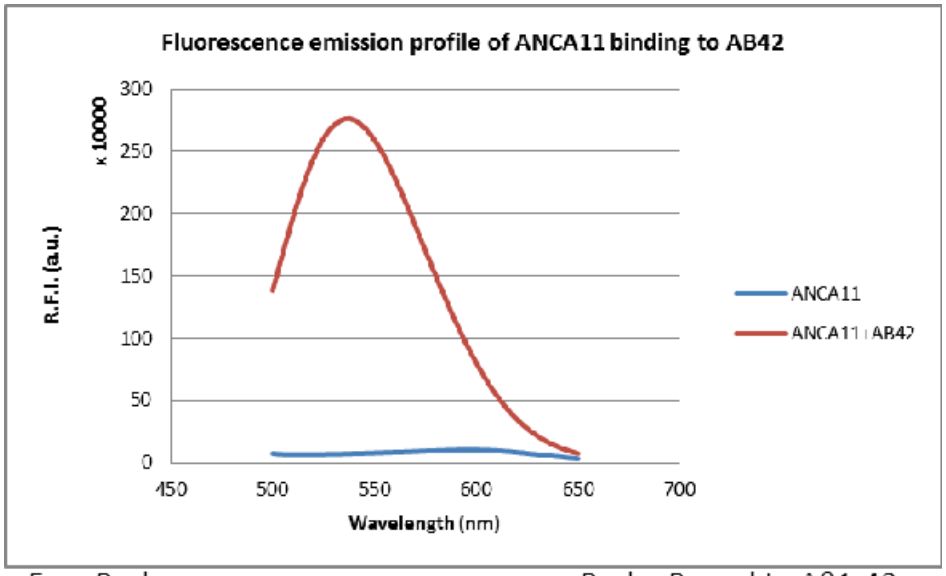

Figure 2.5: Emission Profile of ANCA-11 Free vs Bound

2.4 Current Use of ANCA-11

ANCA-11 (**9**) was shown to have many of the desired features mentioned previously and has been further explored commercially. Given recent findings that amyloid deposition in the brain may be paralleled by deposition in the eye, emerging medical device company Cognoptix has begun exploring using ANCA-11 (**9**), in conjunction with a newly created laser scanning imaging system, to detect Aβ plaque deposits in the eye of human patients.[16,17,18,19,26] Cognoptix suspends ANCA-11 (**9**) in an ointment to be used topically on the lens of the eye. Further studies are needed, however, to accurately correlate the fluorescence intensity seen in the eye to the amount of Aβ plaque deposits in the brain.

2.5 ANCA-11, ANCA-amide, and ANCA-sulfonamide

Ideally the probe could be dissolved in a water-based solution for ease of use either in the eye or intravenously administered to a patient. With this goal in mind, we

first sought to test the water stability of ANCA-11 (**9**). Upon inspection of the structure of ANCA-11 (**9**), the presence of an ester bond was concerning for hydrolytic stability. We therefore synthesized two new molecular probes, ANCA-amide (**10**) and ANCA-sulfonamide (**11**) with the ester bond replaced with a more water-stable motif. These

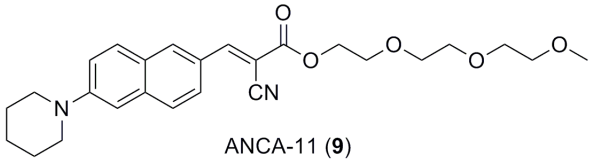

ANCA-11 (**9**)

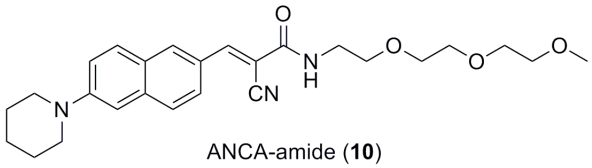

ANCA-amide (**10**)

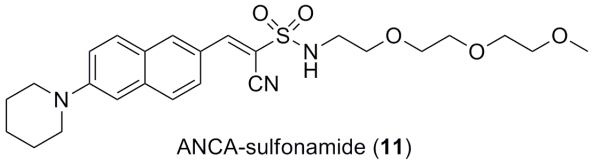

ANCA-sulfonamide (**11**)

Figure 2.6: Structure of ANCA-11, ANCA-amide, and ANCA-sulfonamide

two compounds allowed us to test if changing the electron-accepting group affected the fluorescence profile and if any water-stability was gained by substituting an amide or sulfonamide for the ester bond in ANCA-11 (**9**).

2.5.1 Synthesis of ANCA-amide and ANCA-sulfonamide

Synthesis of ANCA-amide (**10**) began by converting commercially available triethylene glycol (TEG) monomethyl ether (**12**) to the corresponding tosylate (**13**) in 53% yield. Tosylate **13** was then converted to the azide in 60% yield. The resulting azide was then subjected to a Staudinger reduction to give the TEG-amine (**14**). Compound **14** was coupled to cyanoacetic acid (**15**) using 1-Ethyl-3-(3-dimethylaminopropyl)carbodiimide (EDC) in 83% yield to give the cyano-TEG-amide-acrylate (**16**). TEG **16** was then coupled with previously synthesized piperidine-napthalene **19** to give ANCA-amide (**10**) via Knoevenagel condensation in 61% yield.[14] Synthesis of ANCA-sulfonamide (**11**)

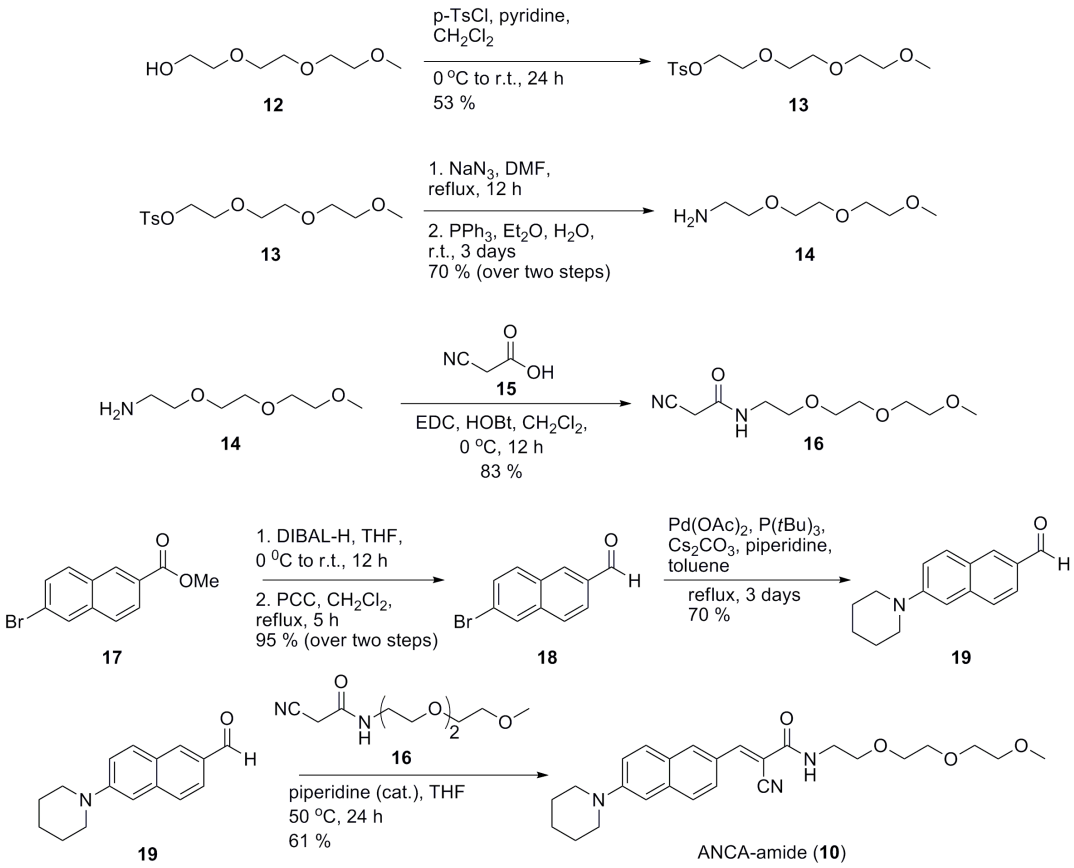

Scheme 2.1: Synthesis of ANCA-amide

began with converting chloroacetonitrile (**20**) to the sulfonic acid and then to the sulfonyl chloride **21** in 13% yield over two steps.[20] Compound **21** was found to be relatively unstable and therefore was quickly reacted with amine-TEG **14** to give sulfonamide-TEG **22** in 86% yield. Sulfonamide-TEG **22** was then condensed with aldehyde **19** to give ANCA-sulfonamide (**11**) in 73% yield.

2.5.2 Hydrolytic Stability Studies

Upon their synthesis, compounds **10**, **11**, and **9** were then all tested for their hydrolytic stability. All three compounds were tested at a concentration of 100 μM in pH 7.4 1X PBS buffer at room temperature in the absence of light. The stability of the compounds was monitored by periodically removing an aliquot (100 μL via microsyringe followed by flash freezing in liquid nitrogen and storage at -20 °C) and performing

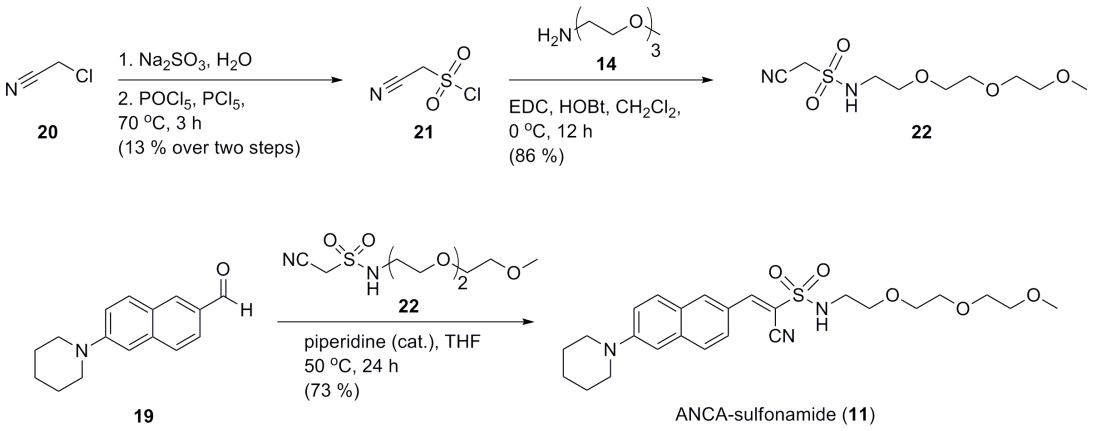

Scheme 2.2: Synthesis of ANCA-sulfonamide

LC-UV analysis with MS analysis on certain fractions. The compounds were monitored for 168-hours and all showed some level of degradation. ANCA-amide (**10**) was the most stable, followed by ANCA-sulfonamide (**11**), and lastly ANCA-11 (**9**). ANCA-11 (**9**) began showing decomposition before 12-hours, with the main degradation product being ANCA-acid (**23**), a result of hydrolysis of the ester bond. At 6-hours, the solution already contained 25% ANCA-acid (**23**) and after 12-hours, the acid had increased to 40%. After 24-hours, a new compound was found by LC-UV-MS and was discovered to be the aldehyde (**19**) precursor to ANCA-11 (**9**), a result of a retro-Knoevenagel reaction.[16,17] This result, however surprising at first, could easily be explained by the equilibrium of the condensation. Removal of water is a driving force of the Knoevenagel reaction and placing the compound in an aqueous environment allowed for a reversal of the condensation to give the aldehyde precursor (**19**). After 58-hours, ANCA-11 (**9**) only comprised 12% of the solution with multiple degradation products seen by LC-UV with the acid (**23**) as the major product. By 168-hours, ANCA-11 (**9**) had almost fully degraded (only 7% remained) and the majority of the solution is comprised of ANCA-aldehyde (**19**). ANCA-amide **10** showed no degradation products after 12-hours in solution and it was only after 12-hours when a new compound is found by LC-UV. This new compound, which was more polar than the starting amide, was found to have the same mass but with different fluorescent properties. It was concluded that this new compound was the *Z* (or *cis*-) isomer (**24**) of ANCA-amide (**10**). The different fluorescent properties were apparent when looking at the LC-UV trace. The samples were

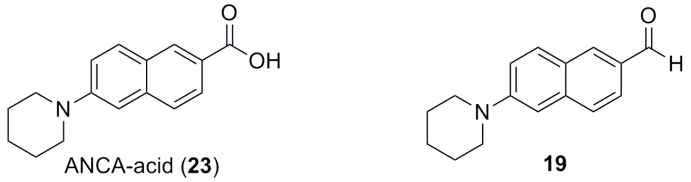

Figure 2.7: Degradation Products

all analyzed at four different wavelengths (215 nm, 254 nm, 280 nm, and 480 nm) and which wavelengths the compounds were seen at indicated their absorption spectra. ANCA-amide (**10**) was seen in all wavelengths while the isomer was not seen in the 480 nm trace, only in the higher energy wavelengths. This strongly suggests that while the two compounds possessed the same mass, they differed in their fluorescence profile. Further research and discussion with collaborators suggested to us that this *Z* isomer might exist in what is called a dark state, where the molecule is no longer aligned correctly to absorb at longer wavelengths.[42] This theory continues to be an area of study in our lab along with collaborators. After 24-hours, the only compounds in the solution are the *Z*- (**24**) and *E*- (**10**) isomers of ANCA-amide (**10**). ANCA-amide (**10**) began to hydrolize to ANCA-acid (**23**) (29%) after 58-hours. After 168-hours, 39% aldehyde (**19**) product is seen but **23** is not, for reasons still being investigated. We found that the ANCA-amide (**10**) is stable up to 24-hours in solution. ANCA-sulfonamide (**11**)

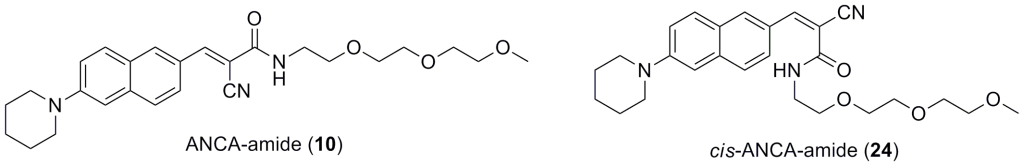

Figure 2.8: *cis*- and *trans*- Isomers of ANCA-amide

was found to be stable for up to 12-hours in solution before degradation began. After 12-hours, 6% of the aldehyde (**19**) is seen along with the parent compound (**11**). By 24-hours, **11** comprised 70% of the solution while the amount of aldehyde (**19**) continued to increase to 22% and the hydrolyzed acid (**23**) product had begun to appear (7%). After 58-hours, ANCA-sulfonamide (**11**) (55%) continued to degrade into the aldehyde (**19**) (39%) while the ANCA-acid (**23**) remained at 6%. After 168-hours, errors stemming from integration values of the LC-UV led to values that did not correlate with the data

from 58-hours, however ANCA-sulfonamide (**11**) continued to degrade.

Unfortunately, issues with LC-UV integration lead to conflicting data at 168-hours. ANCA-sulfonamide (**11**) was present at 63% (higher than 58-hours) and the aldehyde comprised 37% of the solution with no ANCA-acid (**23**) seen.

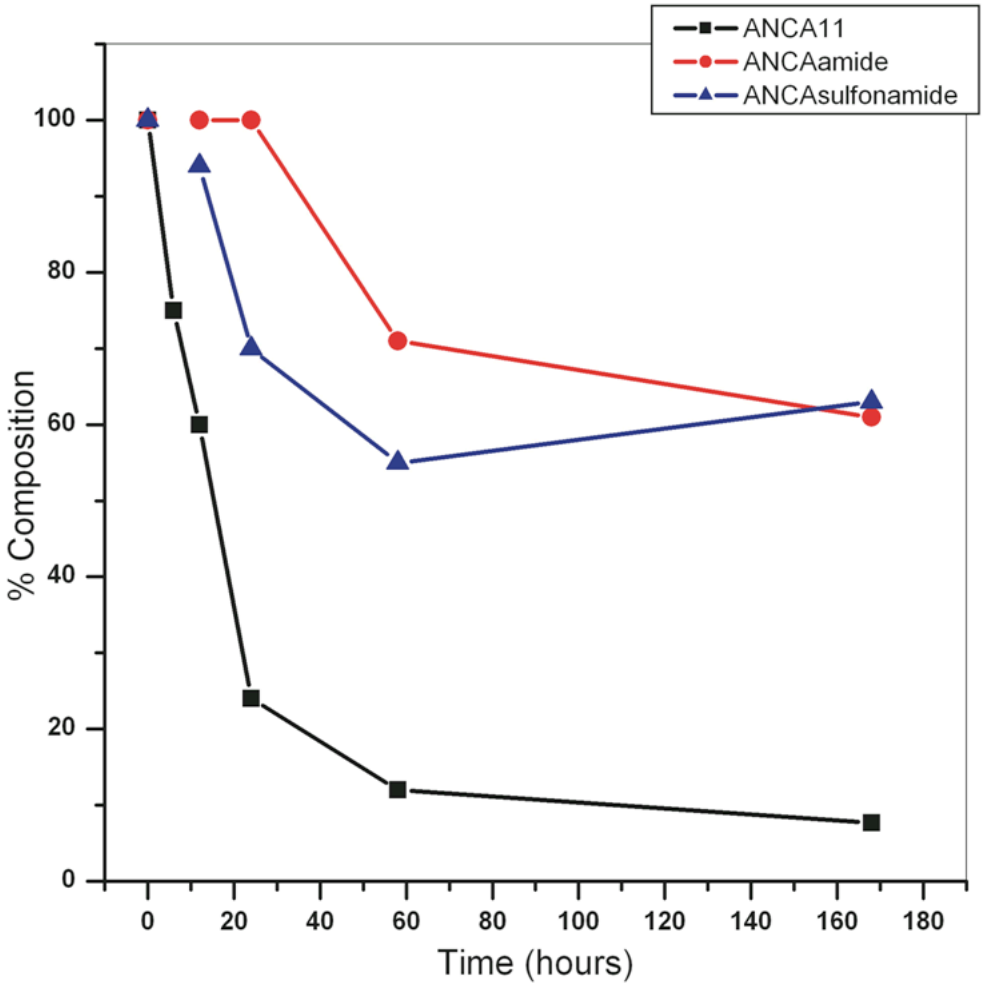

Figure 2.9: Graph of Hydrolytic Stability of ANCA-11, ANCA-amide, and ANCA-sulfonamide

2.5.3 Effect of Change of Acceptor on Fluorescence Profile

We also wanted to test whether the change of the electron-acceptor from an ester to an amide or sulfonamide changed the fluorescence properties of the molecule. All

three compounds (**9**, **10**, **11**) were tested for their absorption and emission values free in solution and bound to Aβ fibrils. Changing the acceptor from an ester to an amide or sulfonamide had little effect on the emission values of the compounds, both free and bound, suggesting that the electron-acceptor is the nitrile group and not the carbonyl.

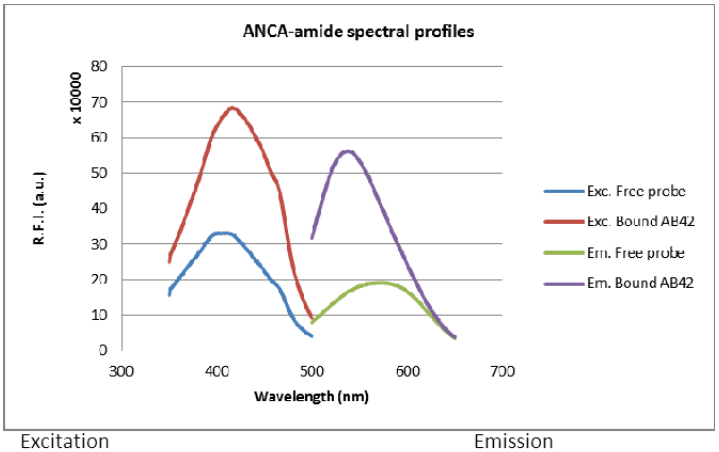

Excitation
Free: 403 +/- 3 nm
Bound: 416 +/- 1 nm

Emission
Free: 396 +/- 1 nm
Bound: 538 +/- 2 nm

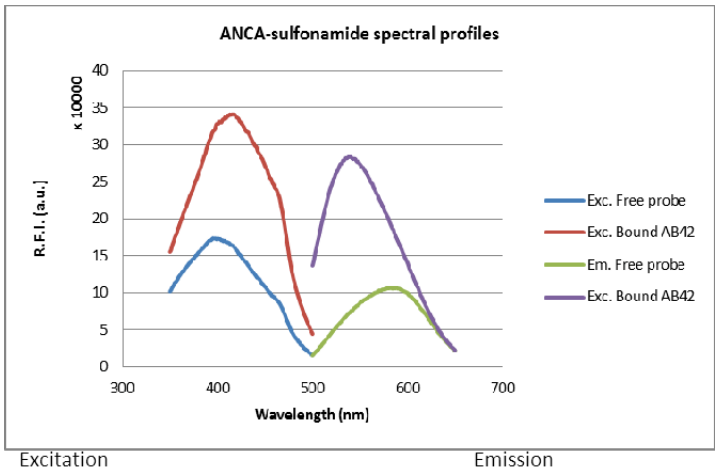

Excitation
Free: 396 +/- 1 nm
Bound: 415 +/- 2 nm

Emission
Free: 584 +/- 2 nm
Bound: 538 +/- 2 nm

Figure 2.10: Emission Profile of ANCA-amide and ANCA-sulfonamide Free and Bound

2.5.4 Conclusion

In order to evaluate and improve the stability of ANCA-11 (**9**), it along with two newly synthesize compounds (**10** and **11**) were tested for their hydrolytic stability. The ultimate goal was to determine if these compounds would be suitable for long-term storage in aqueous media. It was found that the amide (**10**) was the most stable of the three, only beginning to degrade after 24-hours in solution. With only a few easy chemical modifications to the starting water-solubilizing group, a moderate increase in hydrolytic stability could be gained. We also showed that the true acceptor on the molecular rotor is the nitrile group, not the carbonyl, as the fluorescence properties varied only slightly between ANCA-11 (**9**), ANCA-amide (**10**), and ANCA-sulfonamide (**11**). Our lab continues to use the amide-WSG in new molecular rotors due to the hydrolytic stability shown in this study.

2.5.5 Future Directions

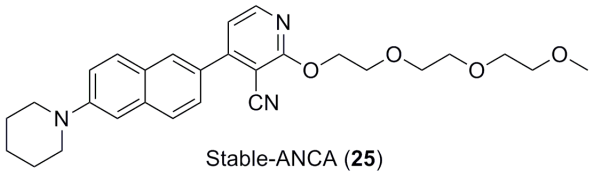

Stable-ANCA (**25**)

Figure 2.11: Structure of Stable-ANCA

While ANCA-11 (**9**) has been used as the parent molecular rotor in our lab, the stability shown by it and the other two compounds (**10** and **11**) leaves something to be desired. The reliance on a final condensation reaction to attach the acceptor and WSG opens the door for the reverse reaction when the compound is stored in water (as discussed previously). A new molecular rotor backbone was designed to maintain the positive characteristics found in ANCA-11 (**9**) while eliminating the need for a water-sensitive functional group. The new structure deemed Stable-ANCA (**25**) retains the piperidine donor and nitrile acceptor, but has introduced a new pyridine ring. It also maintains the distance between the donor and acceptor as found on ANCA-11 (**9**) as well as a WSG. We envisioned this compound stemming from a Suzuki cross-coupling between triflate naphthalene (**26**) and a commercially available pyridine

boronic acid (**27**) containing the nitrile acceptor.[22,23] After the coupling, triethylene glycol monomethyl ether (**12**) would be easy to install utilizing the chloride handle (**28**) under basic conditions.[24] Once this compound is synthesized, its fluorescence properties

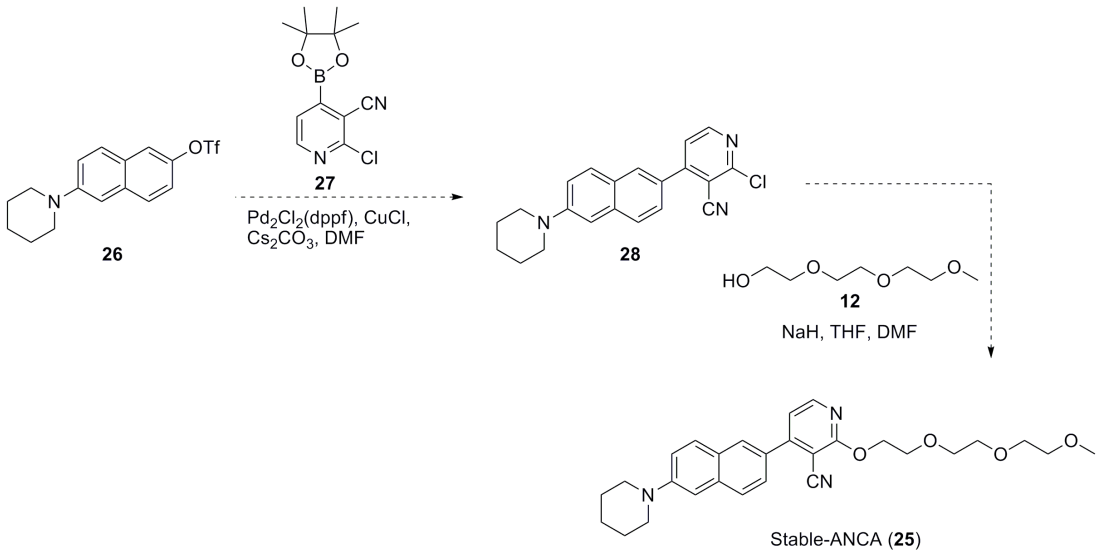

Scheme 2.3: Proposed Synthesis of Stable-ANCA

will be explored as well as its ability to bind selectively to Aβ fibrils. If the fluorescence data is promising, either similar to ANCA-11 (**9**) or better, the hydrolytic stability will be tested. We believe that replacing the Knoevenagel condensation with a Suzuki-coupling will greatly increase the stability of this new compound. This compound could then be further tested to see if it can detect Aβ plaques in the eye and therefore be stored in an aqueous solution to be used as diagnostic eye drops.

2.6 Evaluating the Effect of Dipole and Radius on Fluorescent Properties of Novel Molecular Rotors

We have previously shown that the emission of ANCA-11 (**9**) is dependent on the polarity of the environment that the compound is in.[25] This property, known as solvatochromism, stems from the stabilization of the excited state by polar solvents and allows for the polarity of protein binding pockets to be approximated.[26,27,28,29,30] Cao et. al. found that ANCA-11 (**9**) could fluorescently discriminate Aβ proteins from prion

proteins (PrP^{Sc}) associated with prion disease.[26] The dependence of the environment on the absorbance and fluorescence emission was approximated by the Ooshika-Lippert-Mataga (OLM) equation: where $\Delta\nu$ is the average frequency of the Stokes shift, μ_e and

$$\Delta\upsilon = \frac{2(\mu_e - \mu_g)^2}{hca^3}\left(\frac{\varepsilon - 1}{2\varepsilon + 1} + \frac{n^2 - 1}{2n^2 + 1}\right)$$

Figure 2.12: OLM Equation

μ_g are the dipole moments of the molecules in the excited and ground state, respectively, h is Plank's constant, a is the approximate radius of the molecules assuming a spherical cavity with a rigid dipole at the center, ε_0 is the static relative permittivity (i.e., dielectric constant) of the environment surrounding the molecules, and n is the refractive index of the medium. Using the OLM equation, we could test the effect of changing the length of the molecule (a) as well as the effect of the dipole moment (μ_g and μ_e) on the fluorescence profile.

2.6.1 Effect of Conjugation Length on Fluorescence Profile

We first sought to test the effect of the length of conjugation on the fluorescent profile of our molecular rotors. It is widely known that increasing the conjugation in a molecule increases the stability of the dipole moment in the excited state and therefore the emission wavelength is red shifted.[31] Having a good understanding of ANCA-11 (**9**), we sought to shorten and lengthen the conjugation to effectively either decrease or increase a in the OLM equation. We sought out to synthesize two new molecular rotors possessing conjugation both shorter and longer than ANCA-11 (**9**). The design of the shorter rotor was quite easy in which the naphthalene group on ANCA-11 (**9**) was replaced with a shorter phenyl while retaining the electron donor and acceptor moieties to give ABCA (**29**) (Amino Benzyl Cyano Acrylate). The extended conjugation molecule was not as obvious however. Peter Nilsson has shown that addition of thiophenes to highly conjugated systems lowers the wavelength of emission therefore red-shifting the color of the compound.[32] Using this knowledge, we sought to increase the length of ANCA-11 (**9**) by adding a thiophene after the naphthalene to give ANCA-thiophene

(**30**). These two new compounds (**29** and **30**) along with ANCA-11 (**9**) would show the effect of an increased radius without dramatically altering the rest of the molecular rotor backbone that we had previously established. It is worth to note that while the dipole moments of these three compounds differ, the radius value, being cubed, is believed to have a much more dramatic effect on the average frequency and therefore could still be compared between the three compounds.

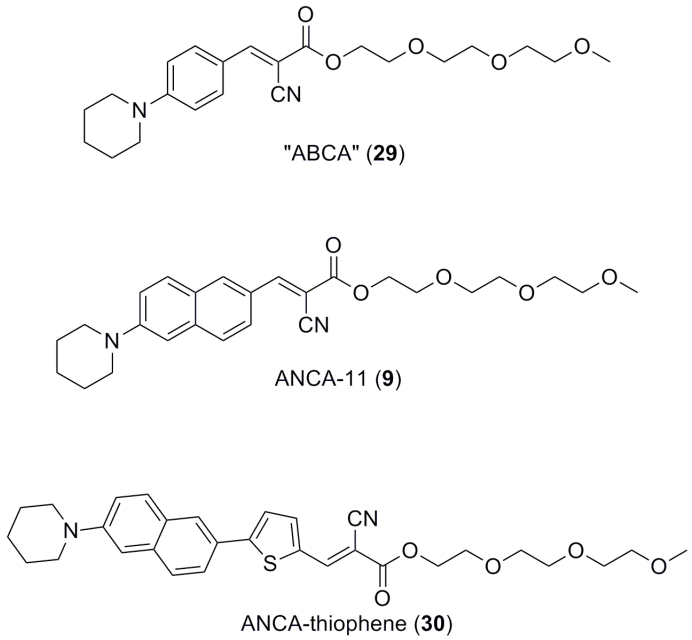

Figure 2.13: Structures of ABCA, ANCA-11, and ANCA-thiophene

2.6.2 Synthesis of ABCA and ANCA-thiophene

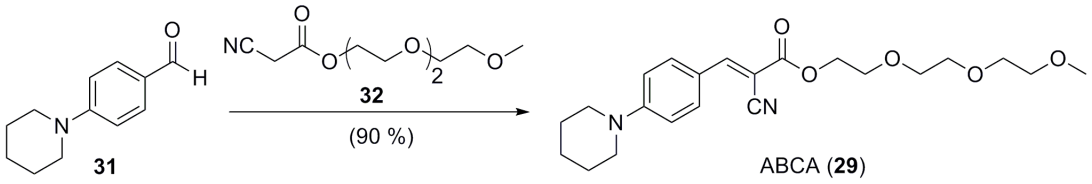

Scheme 2.4: Synthesis of ABCA

Compound **29** was synthesized by previously known Knoevenagel condensation with cyano-TEG (**32**) and commercially available benzyl aldehyde (**31**) to give **29**

in 90% yield.[14] ANCA-thiophene (**30**) was synthesized beginning with commercially available bromo-napthalene-triflate (**33**) to which the piperidine donor was added using Buchwald-Hartwig coupling conditions to give common triflate **26** in 60% yield.[33,34,35] It is interesting to note that the reaction almost solely occurred at the bromine and not at the triflate, although both products could have been used in the reaction sequence. With **26** in hand, it could be derivitized with commercially available thiophene boronic acid (**34**) in a Suzuki coupling in 66% yield.[36] The coupling utilized microwave conditions and was complete within one hour versus conventional heating (> 4 hours). The acceptor-WSG group was added via a Knoevenagel condensation with cyano-TEG **32** to give ANCA-thiophene (**30**) in 71% yield.

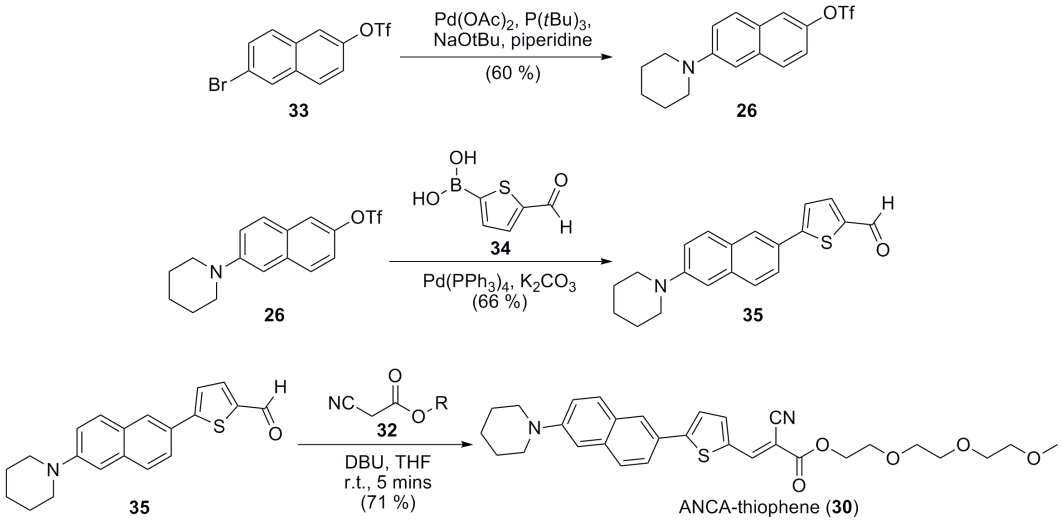

Scheme 2.5: Synthesis of ANCA-thiophene

2.6.3 Effect of Changing Length of Novel Molecular Rotors

The Stokes shift of these compounds in multiple solvents of differing polarities (permittivity) were found and graphed as a plot of solvent permittivity vs. inverse Stokes shift (nm^{-1}). It was hypothesized that if the OLM equation was simplified to give the equation in Figure 2.14 then the smaller the radius (a) would give the largest slope m. Comparing ABCA (**29**) to parent compound ANCA-11 (**9**) the length of **29** is shorter than **9** and therefore the slope should be steeper for **29** than **9**. Using this logic, it was

$$\frac{1}{\lambda_{Emission}} \propto \frac{2(\mu_e - \mu_g)^2}{hca^3}\left(\frac{\varepsilon - 1}{2\varepsilon + 1}\right)$$

Figure 2.14: Simplified OLM equation

believed that **9** should have a larger slope than **30** as compound **30** has a larger a value. Our results strongly support our hypothesis with ABCA (**29**) having the steepest slope of the three while ANCA-thiophene (**30**) has the smallest slope. This correlates that compound **29** is the most fluorescently sensitive to the environment it is in.

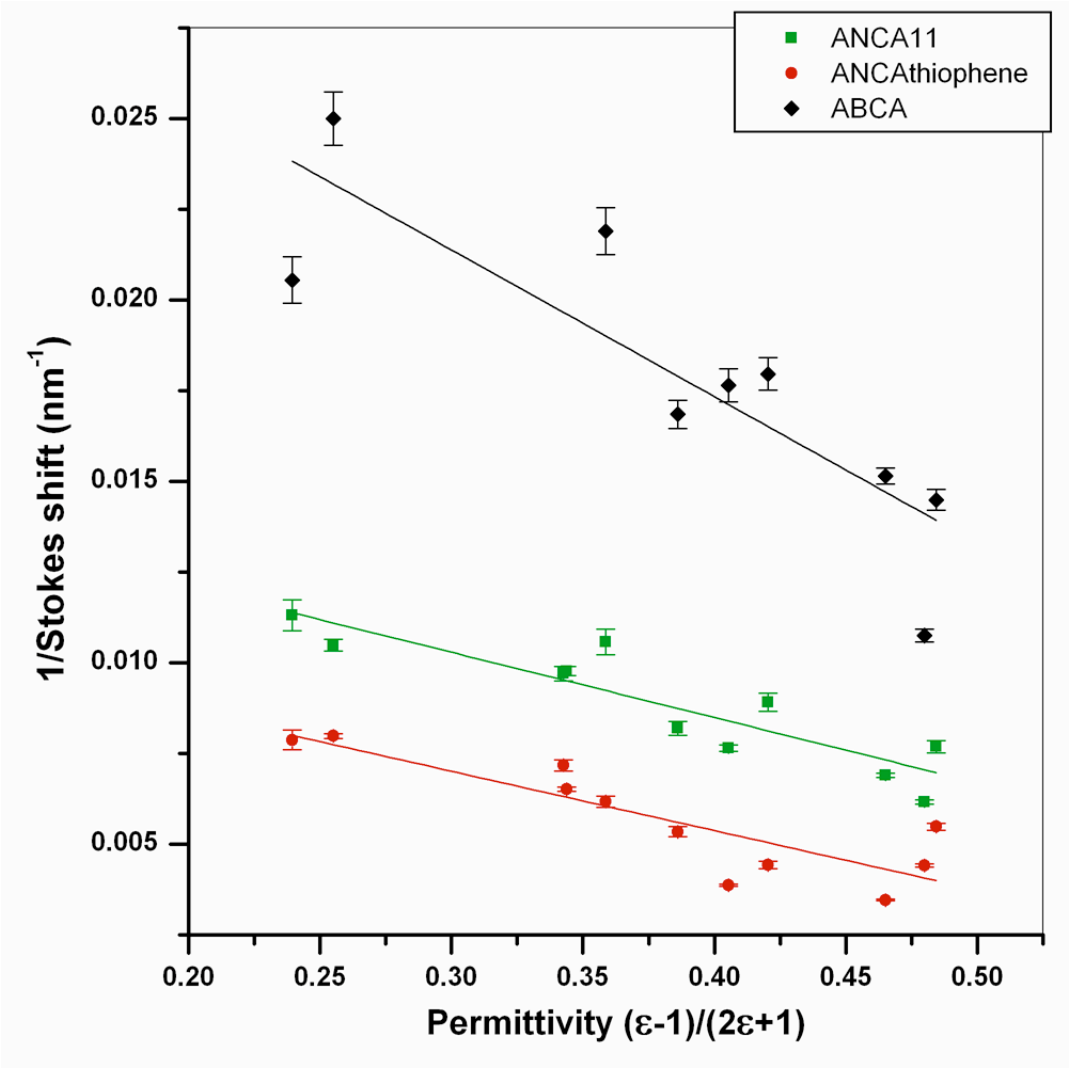

Figure 2.15: Inverse Stokes Shift vs. Solvent Permittivity

2.6.4 Effect of Changing the Dipole Moment

With ANCA-thiophene (**30**) in hand, we could then synthesize similar size compounds with differing dipole moments to test the effect of small dipole changes on the emission wavelength using the OLM equation. In order to keep the radius constant, or as constant as possible, two other heteroaromatic compounds were chosen to extend the ANCA motif with. Along with ANCA-thiophene (**30**), both ANCA-furan (**36**) and ANCA-pyrrole (**37**) were synthesized.

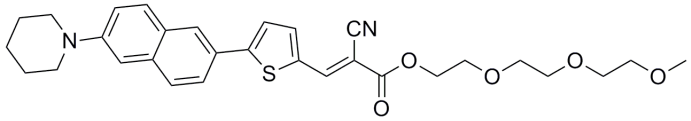

ANCA-thiophene (**30**)

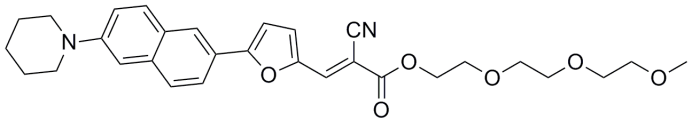

ANCA-furan (**36**)

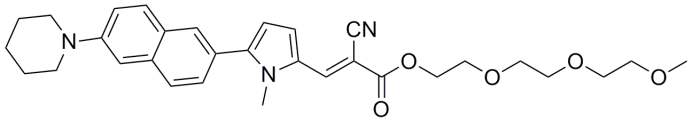

ANCA-pyrrole (**37**)

Figure 2.16: Structures of ANCA-thiophene, ANCA-furan, and ANCA-pyrrole

2.6.5 Synthesis of ANCA-thiophene, ANCA-furan, and ANCA-pyrrole

Compounds **30**, **36**, and **37** were all synthesized from common intermediate **26** discussed previously. Compound **26** could be derivitized with commercially available thiophene (**34**) and furan (**38**) boronic acids in a Suzuki coupling reaction to give the thiophene-aldehyde (**35**) and furan-aldehyde (**39**) in 66% and 91% yield respectively. Both of these Suzuki couplings were achieved using microwave conditions and proceeded very fast (1 hr) versus conventional heating (> 4 hours). The methyl-pyrrole boronic acid was not commercially available and upon attempted synthesis was found

to be unstable so a new route was devised.[37] Commercially available methyl-pyrrole (**42**) was converted to the stannane using trimethyltin chloride and an in-situ protection of the aldehyde to give the necessary methyl-pyrrole coupling partner (**40**).[38] **26** was then subjected to Stille coupling conditions using $PdCl_2(PPh_3)_2$ with **40** to give the methyl-pyrrole-aldehyde (**41**) in 72% yield.

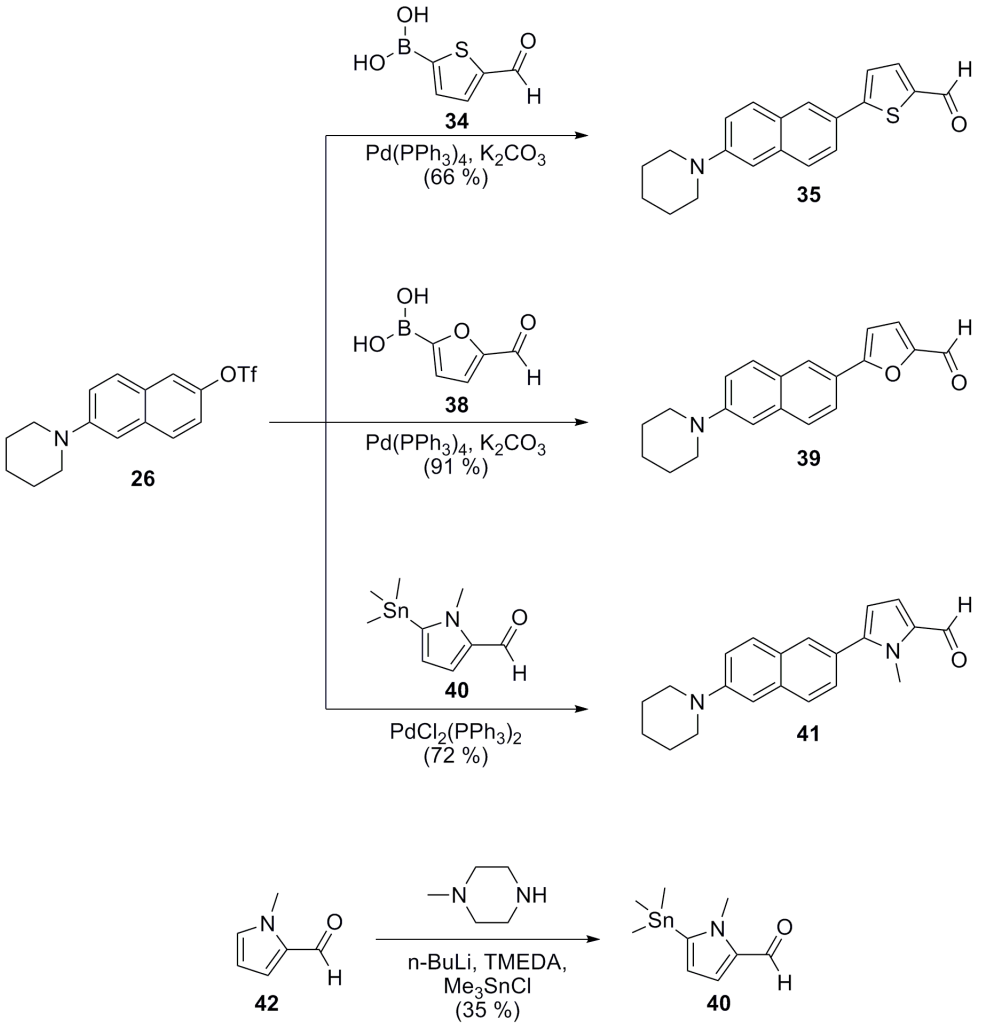

Scheme 2.6: Synthesis of heteroatom aldehydes

With all three aldehydes (**35**, **39**, and **41**) in hand, the acceptor-WSG group was added via previously known Knoevenagel conditions with cyano-TEG **32** to give ANCA-thiophene (**30**), ANCA-furan (**36**), and ANCA-pyrrole (**37**) in 71%, 86%, and 92% respective yields. All three condensations were complete at room temperature within 10 minutes, while the same condensation to give ANCA-11 (**9**) took overnight at 50 °C. These reaction times to give these three extended molecules allowed for easy derivatization and access to large amounts of compound in short order. The names given

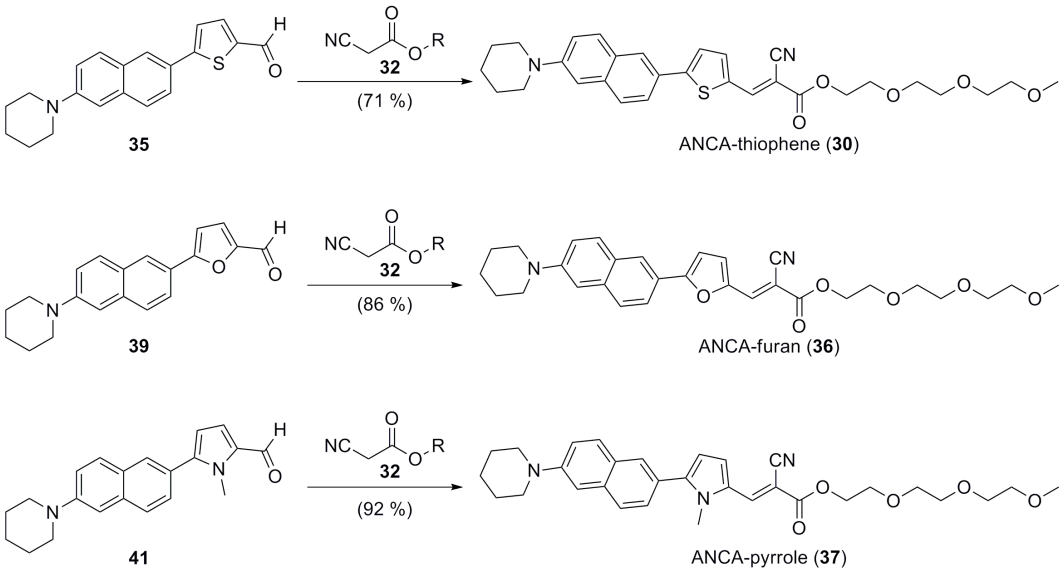

Scheme 2.7: Synthesis of ANCA-thiophene, ANCA-furan, and ANCA-pyrrole

to the compounds reflect the order of conjugation from donor to acceptor. "ANCA" represents the piperidine-napthalene moiety followed by the corresponding heterocycle.

2.6.6 Data and Results

We hypothesized that the greatest difference in the dipole moment from the ground to the excited state would come from the compound containing the least aromatic heterocycle. We believed that the most aromatic 5-membered ring would possess the smallest dipole change as the ring would not be as willing to break aromaticity to achieve the full charge separation seen in the excited state. Therefore, we ranked the compounds from most aromatic (thiophene) to least aromatic (furan) based on many

factors including published computational data.[39] From this hypothesis, we believed that the steepest slope derived from the OLM question would come from ANCA-furan (**36**) which possessed the least aromatic ring of the three and therefore was most likely to break conjugation. These three compounds (**30**, **36**, and **37**) were then tested in a similar manner to the length-based studies discussed previously. The Stokes shift of the three compounds was measured and graphed as a correlation of the permittivity of the solvent vs. the inverse Stokes shift. It was experimentally found that ANCA-pyrrole (**37**) had the steepest slope followed by ANCA-furan (**36**) and lastly ANCA-thiophene (**30**). This trend supported our hypothesis stating that ANCA-thiophene (**30**) would be most aromatic and therefore possess the smallest dipole change between the ground and excited state. The data did not support ANCA-furan (**36**) being the least aromatic (steepest slope) and actually showed that ANCA-pyrrole (**37**) was the least aromatic. Further experiments and data collection are on-going with these three compounds to further understand the trend seen. Our lab is currently working with the Paesani Group at UCSD to calculate the energy of each molecule in the ground and excited state to allow for a better understanding of how these compounds behave and the results gathered from the OLM equation.

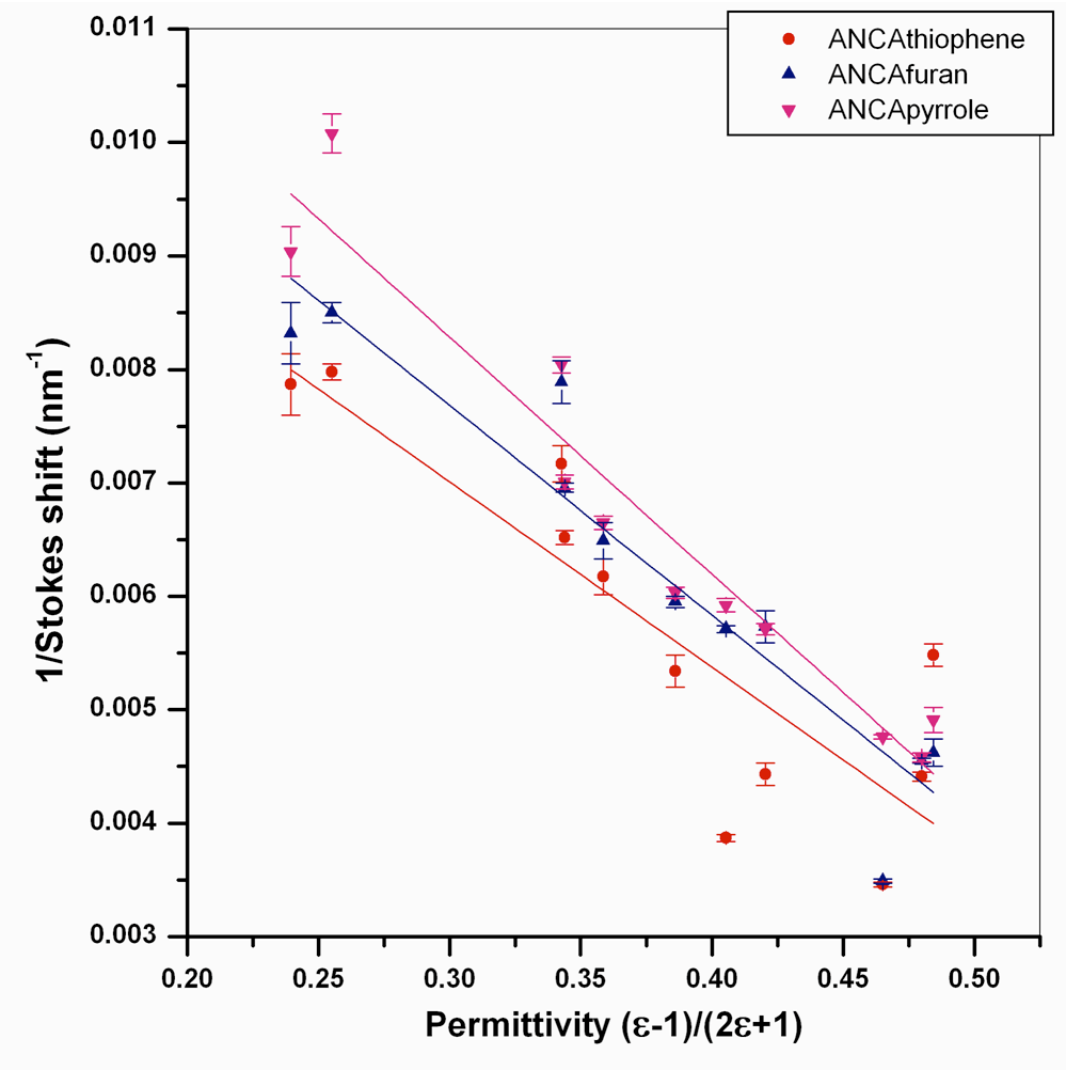

Figure 2.17: Graph of Inverse Stokes Shift vs Solvent Permittivity for ANCA-thiophene, ANCA-furan, and ANCA-pyrrole

2.7 Molecular Rotors Overall Conclusions

We have synthesized a series of fluorogenic small molecules which all show solvatochromic behavior. The compounds also show selectivity towards Aβ, a desired trait.

In order to move forward with *in vivo* applications, the hydrolytic stability of our parent compound ANCA-11 (**9**) as well as derivatives ANCA-amide (**10**) and ANCA-sulfonamide (**11**) was tested and yielded intriguing results. The derivative compounds retained ANCA-11's (**9**) ability to bind to Aβ both in solution and in tissue. They also all showed solvatochromic behavior following a trend modeled by the OLM equation. It was found that changing the WSG had little effect on the fluorescence profile, therefore showing that the nitrile moiety was the true electron-acceptor. We also showed that all three compounds were too unstable, however, to be used as pre-packaged solutions in hospitals, but that some stability was gained by introducing an amide. All compounds underwent a surprising retro-Knoevenagel, making the degradation product not fluorescently useful as the emission wavelength had shifted too close to the autofluorescence of tissue. This lack of long-term hydrolytic stability led to the development of a new compound, Stable-ANCA (**25**). This proposed molecule does not rely on a condensation to synthesize and therefore should theoretically be much more stable in water. Efforts are on-going in our lab to synthesize this compound and explore its fluorescence and binding properties as well as its hydrolytic stability.

We also synthesized four new compounds to test the effect of length and dipole within the conditions set by the OLM equation for altering the emission of the fluorophore. The effect of changing the length of the compound was shown by synthesizing three molecules (ABCA **29**, ANCA-11 **9**, and ANCA-thiophene **30**) which varied the length of the compound while still maintaining the donor-acceptor moiety. These compounds were then tested and graphed using the OLM equation to show that our hypothesis was in fact correct in that the shortest radius would give the steepest slope. This data will be used when designing new molecular rotors when high environment sensitivity, but small emission windows are desired. Testing the effect of the dipole moment led to the synthesis of ANCA-thiophene **30**, ANCA-furan **36**, and ANCA-pyrrole **37**. These compounds differ in their heteroatom. We therefore hypothesized that the less

aromatic the molecule, the more likely it would break aromaticity to achieve a fully charge separated dipole moment in the excited state. The results obtained from this series of compounds is less conclusive than that of the length-based study. The data does not support our hypothesis concerning aromaticity and we believe that much more is involved, including minute changes of the radius as well as the planarity of the compounds. We have begun computational collaborations to help us better understand and interpret our results.

Overall, we have synthesized new molecular rotors and explored their fluorescence and stability profiles. We have made significant contributions to the understanding of how length and dipole affect the fluorescence profile of a compound and how to rationally design a rotor to fit different needs. Continuing work in our lab will focus on improving the hydrolytic stability of our rotors and also increasing the emission wavelength to emit in the near infrared (NIR) or even move into the IR part of the spectrum. We are also pursuing more *in vivo* experiments with these and other compounds to test their ability to cross the BBB and show deposits in living patients. Our ultimate goal is a stable, fully water soluble molecular rotor which can cross the BBB, bind to Aβ deposits in the brain and eye, and emit in the IR region of the spectrum. This compound would hopefully lead to early diagnosis of Alzheimer's disease, even before patients begin showing symptoms. This would then facilitate early treatment to slow down or halt the progress of the disease. With Alzheimer's disease becoming an ever increasing problem in our society, every effort towards early diagnosis and treatment should be made.

2.8 Appendix: Other Projects and Data

Other synthesis not presented in the main text of this thesis is presented here. It includes developing ideas, work not needed for publications, and work with collaborators.

2.8.1 Continuing Studies on Effect of Changing Dipole Moment and Fluorescence

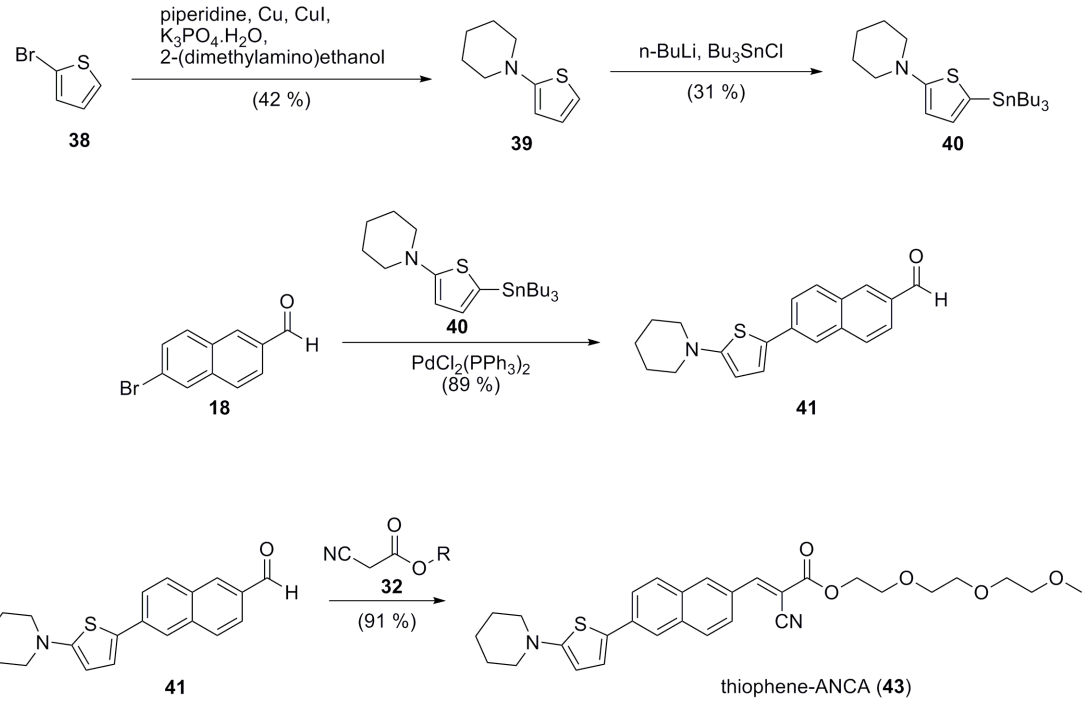

Scheme 2.8: Synthesis of thiophene-ANCA

After synthesizing the three heteroaromatic molecular rotors (**30**, **36**, and **37**), we sought out to discover if the order of conjugation had any effect on the fluorescence properties. We began to synthesize a molecular rotor similar to ANCA-thiophene (**30**) but with the reverse order of conjugation, placing the thiophene between the donor and the naphthalene moiety. Using our naming system, this molecule was titled thiophene-ANCA to denote the reversed order. Beginning with 2-bromothiophene (**38**) and using conditions developed by Twieg,[40] we were able to install the electron donating piperi-

dine through a Cu(I)-mediated amination. We then converted **39** to the stannane (**40**) with moderate success and through a Suzuki coupling, attached **40** to previously used aldehyde **18** to give thio-ANCA-aldehyde **41**. The aldehyde then underwent known condensation with **32** to give thiophene-ANCA (**41**). Compound **41** did not show significant fluorescence activity when tested and also showed very little intensity increase when "bound" to amyloid, an important factor needed in our project. Compound **41** is still undergoing further testing in our lab to see if conjugation order has any effect on fluorescence.

2.8.2 Collaboration with the Brummond Lab at the University of Pittsburg

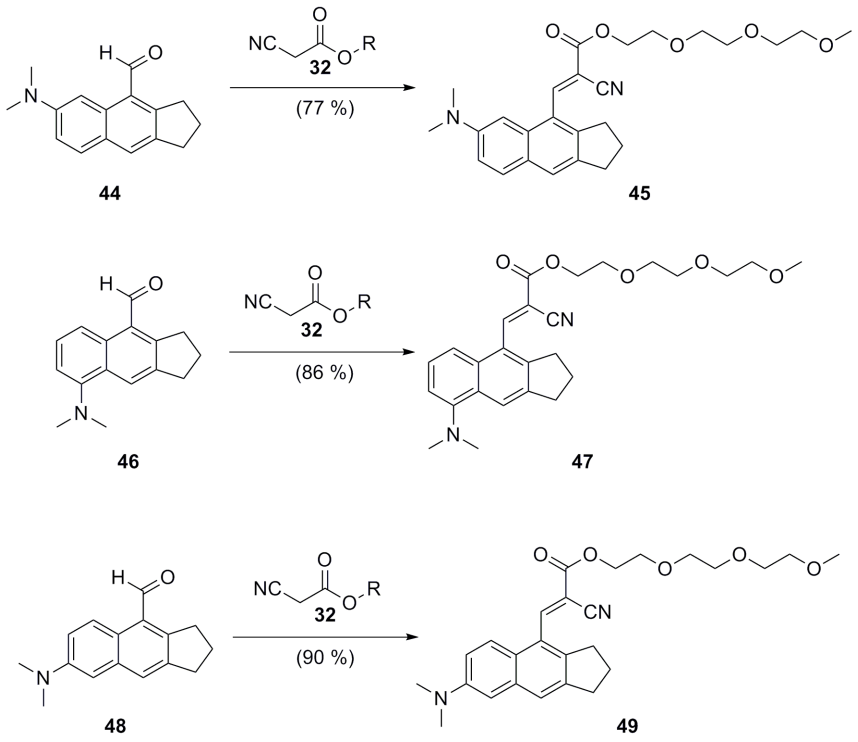

Scheme 2.9: New Possible Molecular Rotors Developed in Collaboration with Kay Brummond

Kay Brummond and her group have developed an intramolecular Diels-Alder reaction to give products which lend themselves well to becoming solvatochromic fluoropho-

res.[41] Our lab was sent compounds **44**, **46**, and **48**, which had been synthesized by the Brummond group and we attached the electron-acceptor WSG used in ANCA-11 and other molecules. The methyl ketone derivatives of **44**, **46**, and **48** showed great solvatochromic activity in the Brummond lab and we collectively hoped that our addition of the WSG would help these compounds become useful for *in vitro* uses. All three aldehydes were condensed with **32** to give **45**, **47**, and **49** which were all tested for fluorescence activity. Surprisingly, none of these compounds were very fluorescent. After many experiments, we determined that these molecules did not exhibit solvatochromic behavior and the fluorescence activity had been almost completely destroyed. This was surprising, as the methyl ketones had shown great promise as molecular rotors and the molecules contained an electron donor conjugated through an electron acceptor as desired. We hypothesize that the cyano group added on to the molecule through the condensation is sterically hindered by the 5-membered ring and is therefore unable to rotate. We suggested to the Brummond group to synthesize an α,β-unsaturated aldehyde precursor to which the WSG could be attached. We believe that this would relieve some of the steric hindrance on the molecule and allow it to behave as a molecular rotor. Work on this project is currently ongoing.

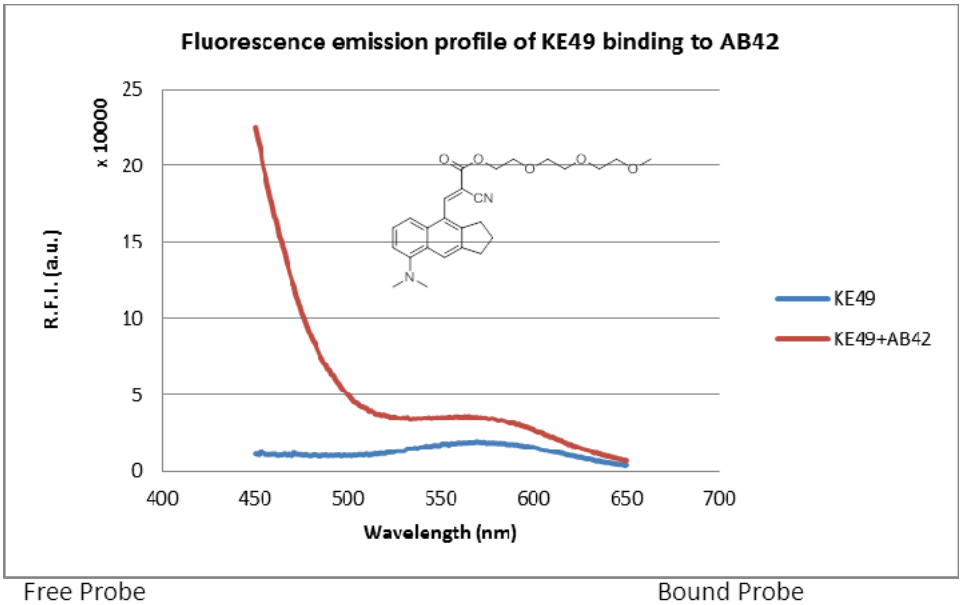

Free Probe
Emission: 569 +/- 1 nm
Excitation: 392 +/- 2 nm

Bound Probe
Emission: 565 +/- 2 nm
Excitation: 390 +/- 1 nm

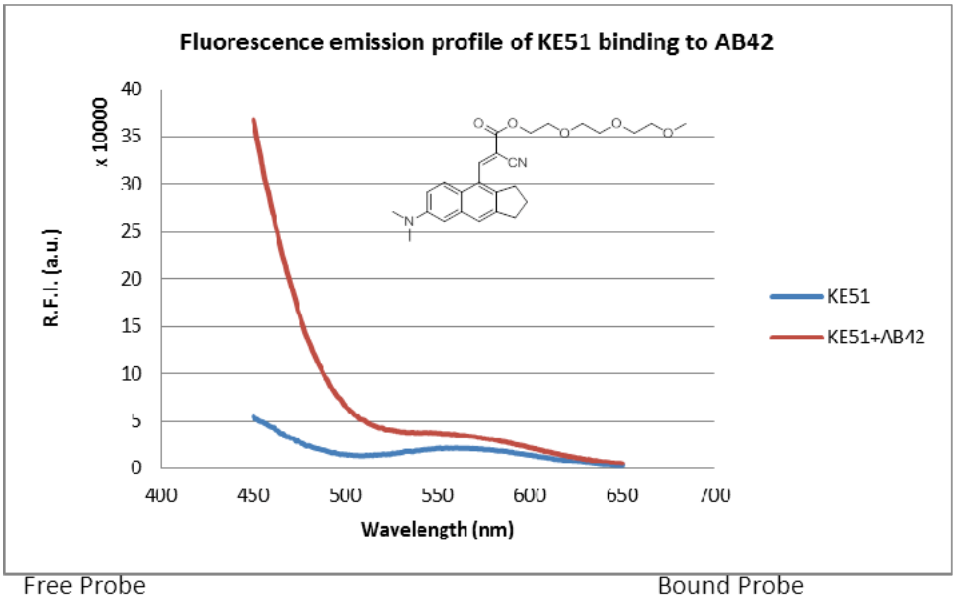

Free Probe
Emission: 561 +/- 7 nm
Excitation: 363 +/- 1 nm

Bound Probe
Emission: N/A
Excitation: 359 +/- 1 nm

Figure 2.18: Emission of Bound and Free selected probes from Kay Brummond

2.8.3 Increasing Hydrolytic Stability of ANCA-11

Before the development of Stable-ANCA (**25**), a minor modification to ANCA-11 was attempted. We believed by making the double bond installed through the condensation more bulky, that we could slow down the attack of water and hopefully improve the hydrolytic stability. The simplest way was to install a methyl group through a series of facile transformations. First, **18** was reacted with a methyl Grignard to give the secondary alcohol **50** which was then oxidized to the methyl ketone **51**. Compound **51** was subjected to known Knoevenagel condensation conditions but showed no reaction, even after one week at raised temperatures. It was determined that the methyl ketone was much less reactive than the aldehyde and might not improve stability as much as we had hoped. The route was therefore abandoned in favor of Stable-ANCA (**25**).

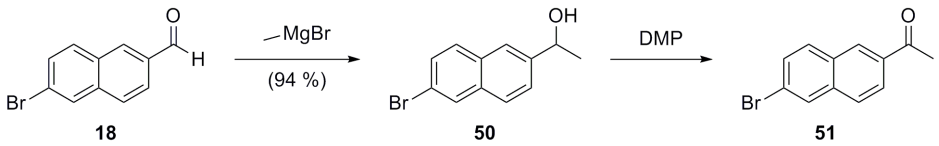

18 **50** **51**

Scheme 2.10: Synthesis of methyl-ketone ANCA-11 precursor

2.9 Experimental

2.9.1 General Techniques

Unless indicated, all commercially available reagents and anhydrous solvents were purchased at the highest commercial quality and were used as received without further purification. All non-aqueous reactions were carried out under argon atmosphere using dry glassware that had been flame-dried under a stream of argon unless otherwise noted. Anhydrous tetrahydrofuran (THF) and dichloromethane (CH_2Cl_2) were obtained by passing commercially available pre-dried, oxygen-free formulations through activated alumina columns. Flash column chromatography was performed on silica gel (Merck Kieselgel 60, 230-400 mesh) using Hexanes-EtOAc or EtOAc-MeOH or toluene-acetone or diethyl ether mixtures of increasing polarity. The progress of all the reactions was monitored by thin-layer chromatography (TLC) using glass plates pre-coated with silica gel-60 F_{254} to a thickness of 0.5 mm (Merck), and compounds were visualized by irradiation with UV light and/or by treatment with a solution of CAM stain or potassium permanganate ($KMnO_4$) in water stain followed by heating. ^{13}C NMR and ^{1}H NMR spectra were recorded on either 400 MHz or 500 MHz Varian instrument or 500 MHz JEOL instrument. $CDCl_3$ was treated with anhydrous K_2CO_3, chemical shifts (δ) are quoted in parts per million (ppm) referenced to the appropriate residual solvent peak reference ($CDCl_3$), with the abbreviations s, br s, d, t, q, m, td, dt and qd denoting singlet, broad singlet, doublet, triplet, quartet, multiplet, quartet of doublets, triplet of doublets, doublet of triplets and quartet of doublets respectively. J = coupling constants given in Hertz (Hz). High-resolution Mass spectra (HRMS) were recorded on a trisector WG AutoSpecQ spectrometer. Compounds **9**, **19**, and **32** were prepared as reported in reference 14.

2.9.2 Experimental Procedures and Data

2-(2-(2-methoxyethoxy)ethoxy)ethyl 4-methylbenzenesulfonate (13): (Methoxyethoxy)ethoxy ethanol (**12**) (20.0 g, 0.122 mol) was added to a solution of dry pyridine (49.0 mL) and CH_2Cl_2 (152 mL). The solution was cooled to 0 °C and p-toluensulfonyl chloride (27.9 g, 0.146 mol) was added in one portion with stirring. The reaction was allowed to come to room temperature and stir for 24 hours. The reaction was then concentrated in vacuo and the solution was filtered to remove solids. Filterate was purified by flash silica column chromatography (0-3% MeOH/EtOAc) to give **13** (20.5 g, 53%) as a clear pale yellow oil. R*f* = 0.85 (9% MeOH/EtOAc); ^{1}H NMR (500 MHz, $CDCl_3$) δ 7.79 (d, *J* = 8.0 Hz, 2H), 7.33 (d, *J* = 8.0 Hz, 2H), 4.15 (m, 2H), 3.52-3.69 (m, 10H), 3.37 (s, 3H), 2.44 (s, 3H); ^{13}C NMR (125 MHz, $CDCl_3$) δ 144.9, 133.0, 129.9, 128.1, 72.0, 72.0, 71.5, 70.9, 7038, 70.7, 70.7, 70.7, 69.4, 68.8, 59.2, 42.9, 21.8; HRMS calcd. for $C_{14}H_{22}O_6SNa$ $[M+Na]^+$ 341.1029, found 341.1030 by ESI.

2-cyano-N-(2-(2-(2-methoxyethoxy)ethoxy)ethyl)acetamide (16): To a solution of **13** (1.0 g, 3.14 mmol) in DMF (125 mL) was added sodium azide (0.51g, 7.85 mmol) and the flask was equipped with a condenser and the reaction was heated to 67 °C for 15 hours. The reaction was then cooled to room temperature, diluted with water (125 mL), and stirred for 30 minutes. The reaction mixture was then poured into ice (150 mL), extracted with diethyl ether (3 x 50 mL), and the combined organic extracts were washed with water (2 x 30 mL) then dried with anhydrous $MgSO_4$. The solvent was then removed in vacuo and the residue was purified via silica gel flash chromatography (10-70% EtOAc/hexanes) to give 1-azido-2-(2-(2-methoxyethoxy)ethoxy)ethane (355 mg, 60%) as a clear colorless oil. R*f* = 0.57 (50 % EtOAc/hexanes); ^{1}H NMR (500 MHz, $CDCl_3$) δ 3.65 (m, 8H), 3.55-3.56 (m, 2H), 3.39-3.40 (m, 2H), 3.38 (s, 3H); ^{13}C NMR (125 MHz, $CDCl_3$) δ 72.0, 70.8, 70.8, 70.2, 59.2, 50.8; HRMS calcd for $C_7H_{15}N_3O_3Na$ $[M+Na]^+$ 212.1006, found 212.1006 by ESI.

1-azido-2-(2-(2-methoxyethoxy)ethoxy)ethane (3.0 g, 15.7 mmol) was dissolved in diethyl ether (628 mL) and cooled to 0 °C. Triphenylphosphine (5.0 g, 18.8 mmol) was added in one portion and the mixture was allowed to stir at 0 °C for 1 hour and then at room temperature for 6 hours. Water (200 mL) was then added and the reaction was allowed to stir for 12 hours. Toluene (150 mL) was then added and the reaction was

allowed to stir for an additional 12 hours. The water layer was then isolated and washed with toluene (1 x 200 mL) and then removed in vacuo to give the amine (**14**) as a clear yellow oil which was carried through to the next reaction.

A solution of amine (**14**) (1.79 g, 10.97 mmol) from previous reaction and HOBt (1.48g, 10.97 mmol) in CH_2Cl_2 (10 mL) was added dropwise via syringe to a cold (0 °C) solution of cyanoacetic acid (**15**) (0.621 g, 7.3 mmol) in CH_2Cl_2 (15 mL) under argon. The reaction mixture was then allowed to stir for 10 minutes at 0 °C. EDC (2.1 g, 10.97 mmol) was then added in one portion and the reaction was allowed to stir overnight at 0 °C. The reaction was then concentrated in vacuo and purified via silica gel flash chromatography (0-2% MeOH/CH_2Cl_2) to give **16** (1.4 g, 83%) as a clear yellow oil. R*f* = 0.36 (10 % MeOH/EtOAc); ^{1}H NMR (500 MHz, $CDCl_3$) δ 7.04 (bs, 1H), 3.63-3.65 (m, 6H), 3.55-3.59 (m, 4H), 3.45-3.48 (m, 2H), 3.39 (s, 2H), 3.37 (s, 3H); ^{13}C NMR (125 MHz, $CDCl_3$) δ 161.5, 114.8, 71.9, 70.6, 70.4, 70.2, 69.3, 59.0, 40.1, 25.9; HRMS calcd. for $C_{10}H_{18}N_2O_4Na$ $[M+Na]^+$ 253.1159, found 253.1161 by ESI.

(E)-2-cyano-N-(2-(2-(2-methoxyethoxy)ethoxy)ethyl)-3-(6-(piperidin-1-yl)naphthalen-2-yl)acrylamide (10): To a solution of **19** (0.15 g, 0.627 mmol) and **16** (0.115 g, 0.501 mmol) in THF (2.5 mL) was added piperidine (0.01254 mmol) and the reaction was heated to 50 °C for 16 hours. The reaction was then concentrated in vacuo, adsorbed on to silica, and purified via silica gel flash chromatography (0-20% acetone/toluene) to give **10** (138 mg, 61%) as an orange viscous oil. R*f* = 0.25 (5 % acetone/toluene); ^{1}H NMR (500 MHz, $CDCl_3$) δ 8.33 (s, 1H), 8.11 (s, 1H), 8.00-8.02 (dd, *J* = 8.5 Hz, 1.5 Hz, 1H), 7.69-7.71 (d, *J* = 9.5 Hz, 1H), 7.60-7.62 (d, *J* = 8.5 Hz, 1H), 7.24-7.26 (m, 1H), 7.01 (bs, 1H), 6.84 (m, 1H), 3.64-3.66 (m, 6H), 3.62-3.63 (m, 4H), 3.54-3.55 (m, 2H), 3.35 (s, 3H), 3.12-3.34 (m, 4H), 1.69 (m, 4H), 1.61-1.62 (m, 2H); ^{13}C NMR (125 MHz, $CDCl_3$) δ 161.2, 152.9, 151.6, 137.2, 133.8, 130.3, 127.2, 126.6, 126.1, 125.7, 119.4, 117.8, 108.6, 100.5, 71.9, 70.6, 70.6, 70.5, 69.4, 59.0, 49.5, 40.2, 25.5, 24.3; HRMS calcd. for $C_{26}H_{32}N_2O_5Na$ $[M+Na]^+$ 474.2363, found 474.2363 by ESI.

1-cyano-N-(2-(2-(2-methoxyethoxy)ethoxy)ethyl)methanesulfonamide (22): To a round bottom flask, chloroacetonile (**20**) (5 g, 41.68 mmol) was added to a suspension of sodium sulfite (5.253 g, 41.68 mmol) in water (25 mL). The mixture was

stirred at room temperature for 1 hour. Removal of water under reduced pressure, and recrystallization from 98% ethanol gave the product in high yield. The crude product contains sodium chloride was suitable for preparation of cyanomethansulfonyl chloride (**21**) without further purification. Crude sodium cyanomethanesulfonate (3.0 g, 20.97 mmol) was suspended in phosphoryl chloride (7.35 mL) and powdered phosphorus pentachloride (4.365 g, 20.97 mmol). The mixture was stirred for 3 hours at 70 °C under argon condition, with exclusion of moisture. Afterward, sodium chloride was removed by filtrate. The phosphoryl chloride was removed under reduced pressure and the residual oil was distilled via a short Vigreux column and the cyanomethansulfonyl chloride (**21**) which was collected as a pale yellow oil (1.2 g, 13% over two steps). Compound **21** was found to be unstable and was therefore used immediately in the next reaction. (b.p. 78-82 °C at 0.15 mmHg) To a solution of **21** (3.44 mmol), 2-(2-(2-methoxyethoxy)ethoxy)ethanamine (**14**) (5.41 mmol) in CH_2Cl_2 (10 mL) and HOBt (5.43 mmol) was added dropwise at 0 °C. Finally, EDC (5.43 mmol) as added and the reaction mixture was stirred at 0 °C for 6 hours. Then the reaction was concentrated under reduced pressure and the residue was purified by silica gel flash chromatography to yield **22** (787.0 mg, 86%) as a clear, colorless oil. R*f* = 0.2 (100% Et2O); ^{1}H NMR (500 MHz, $CDCl_3$) δ 6.13 (s, 1H), 4.22 (s, 2H), 3.63-3.68 (m, 8H), 3.55-3.57 (m, 2H), 3.47-3.49 (m, 2H), 3.38 (s, 3H); ^{13}C NMR (125 MHz, $CDCl_3$) δ 112.1, 71.9, 70.4, 70.3, 70.23, 70.17, 59.0, 44.3, 42.6; HRMS calcd. for $C_9H_{18}O_5N_2Na$ $[M+Na]^+$ 289.0829, found 289.0830 by ESI.

(E)-1-cyano-N-(2-(2-(2-methoxyethoxy)ethoxy)ethyl)-2-(6-(piperidin-1-yl)naphthalen-2-yl)ethenesulfonamide (11): To a solution of **19** (0.0224 g, 0.0939 mmol) and **22** (0.02 g, 0.0751 mmol) in THF (0.38 mL) was added DBU (0.0094 mmol) and the reaction was heated to 50 °C under argon for 5 hours. The reaction was then concentrated in vacuo, adsorbed on to silica, and purified via silica gel flash chromatography (0-20% diethyl ether/hexanes) to give **11** (18.2 mg, 50%) as an orange viscous oil. R*f* = 0.5 (100% diethyl ether); ^{1}H NMR (500 MHz, $CDCl_3$) δ 8.12 (s, 1H), 8.05 (s, 1H), 7.98-8.00 (dd, *J* = 9.0 Hz, 2.0 Hz, 1H), 7.74-7.76 (d, *J* = 9.5 Hz, 1H), 7.64-7.66 (d, *J* = 9.0 Hz, 1H), 7.29-7.31 (dd, *J* = 9.0 Hz, 2.5 Hz, 1H), 7.05 (d, *J* = 2.0 Hz, 1H), 5.48 (bs, 1H), 3.64-3.68 (m, 8H), 3.53-3.57 (m, 3H), 3.39-3.42 (m, 3H), 3.38 (s, 3H), 3.33-3.35

(m, 2H), 1.73 (m, 4H), 1.67 (m, 2H); ^{13}C NMR (125 MHz, $CDCl_3$) δ 161.2, 152.9, 151.6, 137.2, 133.8, 130.3, 127.2, 126.6, 126.1, 125.7, 119.4, 117.8, 108.6, 100.5, 71.9, 70.6, 70.6, 70.5, 69.4, 59.0, 49.5, 40.2, 25.5, 24.3; HRMS calcd. for $C_{25}H_{33}N_3O_5SNa$ $[M+Na]^+$ 510.2033, found 510.2035 by ESI.

(E)-2-(2-(2-methoxyethoxy)ethoxy)ethyl 2-cyano-3-(4-(piperidin-1-yl)phenyl)acrylate (29): Commercially available 4-piperidinyl benzaldehyde (31) (0.05 g, 0.255 mmol) was dissolved in THF (2.0mL) under nitrogen. 2(2-(2-methoxyethoxy)ethoxy)ethyl-2-cyanoacrylate (**32**) (0.216 mmol) and 1,8-Diazabicyclo[5.4.0]undec-7-ene (DBU) (0.02 mmol) were then added and the mixture left stirring at 30 °C. The reaction was monitored by TLC and was completed in 6 hrs. The crude solution was concentrated under reduced pressure and the product purified with flash chromatography (1:1 Hexanes/ethyl acetate) to give a red-orange oil (90%). R*f* =0.70 (1:1 Hexanes/Ethyl acetate); ^{1}H NMR (500 MHz, $CDCl_3$) δ 8.06 (s, 1H), 7.91-7.93 (d, J = 9.0 Hz, 2H), 6.84-6.86 (d, J = 9.5 Hz, 2H), 4.41-4.43 (m, 2H), 3.80-3.82 (m, 2H), 3.72-3.74 (m, 2H), 3.67-3.69 (m, 4H), 3.54-3.56 (m, 2H), 3.45-3.46 (m, 4H), 3.37 (s, 3H), 1.67-1.68 (m, 6H); ^{13}C NMR (125 MHz, $CDCl_3$) δ 164.3, 154.6, 154.2, 134.4, 120.2, 117.4, 113.4, 94.4, 72.1, 71.0, 70.8, 70.7, 69.1, 65.2, 59.2, 48.3, 25.5, 24.5; HRMS calcd. for $C_{14}H_{22}O_6SNa$ $[M+Na]^+$ 341.1029, found 341.1030 by ESI.

6-(piperidin-1-yl)naphthalen-2-yl trifluoromethanesulfonate (26): To a microwave vial containing degassed toluene (6.7 mL), 6-bromonaphthalen-2-yl trifluoromethanesulfonate (**33**) (0.25 g, 0.704 mmol), $Pd(OAc)_2$ (0.008 g, 0.0352 mmol), and NaO*t*Bu (0.088 g, 0.915 mmol) was added and allowed to stir for 5 minutes under argon at room temperature followed by addition of P(*t*-Bu)$_3$ (0.0704 mmol) via syringe and continued stirring for an additional 30 minutes. Piperidine (0.845 mmol) dissolved in toluene (0.845 mL) was added dropwise via syringe and the vial was sealed and heated to 110 °C for 12 hours. The reaction was then allowed to cool to room temperature and diluted with CH_2Cl_2 (5 mL), filtered through a pad of celite, and concentrated. The crude material was then adsorbed on to silica and chromatographed (0-20% EtOAc/hexanes) to give **26** as a white solid (0.152 mg, 60%). R*f* = 0.59 (10 % EtOAc/hexanes); ^{1}H NMR (400 MHz, $CDCl_3$) δ 7.69-7.72 (d, J = 12.0 Hz, 2H), 7.59 (m, 1H), 7.35-7.38 (dd, J = 8.0 Hz, 4.0 Hz, 1H), 7.25-7.27 (m, 1H), 7.11 (bs, 1H), 3.29 (m, 4H), 1.73-1.79

(m, 4H), 1.62-1.67 (m, 2H); ^{13}C NMR (100 MHz, $CDCl_3$) δ 151.0, 145.2, 134.1, 128.7, 127.6, 121.5, 120.5, 119.8, 118.9, 117.4, 109.7, 50.6, 25.8, 24.4; HRMS calcd. for $C_{16}H_{17}F_3NO_3S$ $[M + H]^+$ 360.0876, found 360.0876 by ESI.

5-(6-(piperidin-1-yl)naphthalen-2-yl)thiophene-2-carbaldehyde (35): To a solution of 6-(piperidin-1-yl)naphthalen-2-yl trifluoromethanesulfonate **26** (0.01 g, 0.028 mmol) and (5-formylthiophen-2-yl)boronic acid (**34**) (0.042 mmol) in a mixture of THF (0.06 mL) and water (0.025 mL) was added K_2CO_3 (0.0476 mmol) and $Pd(PPh_3)_4$ (0.0042 mmol). The solution was then degassed with argon and microwaved at 50 °C for 1 hour. The reaction was then filtered through cotton and concentrated. The crude mixture was adsorbed on to silica and chromatographed (0-10% EtOAc/hexanes) to give **35** (5.9 mg, 66%) as a yellow powder. R*f* = 0.44 (20 % EtOAc/hexanes); ^{1}H NMR (500 MHz, $CDCl_3$) δ 9.89 (s, 1H), 8.01 (s, 1H), 7.73-7.76 (m, 2H), 7.66-7.70 (m, 2H), 7.46 (d, *J* = 5.0 Hz, 1H), 7.32 (d, *J* = 10.0 Hz, 1H), 7.09 (bs, 1H), 3.31-3.33 (m, 4H), 1.76 (m, 4H), 1.65-1.67 (m, 2H); ^{13}C NMR (125 MHz, $CDCl_3$) δ 182.8, 155.4, 150.9, 141.7, 137.8, 135.3, 129.3, 127.8, 127.6, 127.5, 125.4, 124.4, 123.5, 120.6, 109.6, 50.4, 29.8, 25.8, 24.4; HRMS calcd. for $C_{20}H_{19}NOS$ $[M+H]^+$ 322.1260, found 322.1257 by ESI.

(E)-2-(2-(2-methoxyethoxy)ethoxy)ethyl-2-cyano-3-(5-(6-(piperidin-1-yl)naphthalen-2-yl)thiophen-2-yl)acrylate (30): Compound **35** (0.05 g, 0.156 mmol) and **32** (0.125 mmol) were dissolved in THF (0.62 mL) under an argon atmosphere DBU (0.0078 mmol) was added and the reaction was allowed to stir at room temperature for 5 minutes during which the reaction developed a dark red color. The reaction was then concentrated, adsorbed on to silica, and chromatographed (0-5% acetone/toluene) to give **30** (48.0 mg, 71%) as a red viscous oil. R*f* = 0.38 (70 % EtOAc/hexanes); ^{1}H NMR (500 MHz, $CDCl_3$) δ 8.31 (s, 1H), 8.05 (bs, 1H), 7.75 (d, *J* = 5.0 Hz, 2H), 7.69 (bs, 2H), 7.47 (d, *J* = 5.0 Hz), 7.33 (bs, 1H), 7.08 (bs, 1H), 4.45-4.47 (m, 2H), 3.82 (m, 2H), 3.72-3.74 (m, 2H), 3.67-3.69 (m, 4H), 3.56 (m, 2H), 3.38 (s, 3H), 3.33 (m, 4H), 1.65-1.76 (m, 6H); ^{13}C NMR (125 MHz, $CDCl_3$) δ 174.1, 163.1, 156.1, 150.8, 146.9, 139.9, 134.2, 129.3, 127.7, 127.5, 127.0, 125.6, 124.2, 123.7, 120.4, 116.2, 109.6, 96.7, 77.1, 72.0, 70.9, 70.7, 70.6, 68.9, 65.4, 59.1, 50.3, 29.8, 25.7, 24.4; HRMS calcd. for $C_{30}H_{34}N_2O_5SNa$ $[M+Na]^+$ 557.2081, found 557.2079 by ESI.

5-(6-(piperidin-1-yl)naphthalen-2-yl)furan-2-carbaldehyde (39): 6-(piperidin-1-yl)naphthalen-2-yl trifluoromethanesulfonate (**26**) (50.0 mg, 0.139 mmol), (5-formylfuran-2-yl)boronic acid (**38**) (44.0 mg, 0.209 mmol), K_2CO_3 (33.0 mg, 0.236 mmol), and $Pd(PPh_3)_4$ (24.0 mg, 0.0209 mmol) was dissolved in a mixture of THF (0.3 mL) and water (0.13 mL) in a microwave vial equipped with a stir bar and capped with a septa. The reaction mixture was degassed with argon, sealed, and microwaved for 1 hour at 50 °C. The reaction mixture was then dried with anhydrous Na_2SO_4, condensed in vacuo, and purified by silica flash chromatography (0-10% EtOAc/hexanes) to give **39** (38.4 mg, 91%) as a yellow solid. R*f* = 0.25 (20 % EtOAc/hexanes); ^{1}H NMR (400 MHz, $CDCl_3$) δ 9.63 (s, 1H), 8.21 (s, 1H), 7.67-7.76 (m, 3H), 7.26-7.34 (m, 2H), 7.08 (d, *J* = 2.0 Hz, 1H), 6.85 (d, *J* = 3.6 Hz, 1H), 3.31 (m, 4H), 1.64-1.77 (m, 6H); ^{13}C NMR (100 MHz, $CDCl_3$) δ 177.0, 160.5, 151.8, 151.0, 135.5, 129.5, 127.6, 127.4, 123.0, 120.4, 109.6, 107.2, 50.4, 25.8, 24.5; HRMS calcd. for $C_{20}H_{20}NO_2$ $[M+H]^+$ 306.1489, found 306.1491 by ESI.

1-methyl-5-(trimethylstannyl)-1H-pyrrole-2-carbaldehyde (40): To a solution of N-methyl piperazine (**42**) (0.535 g, 5.038 mmol) and TMEDA (1.17 g, 10.076 mmol) in hexanes (10 mL) was added n-Buli (3.4 mL, 5.038 mmol) at -40 °C and allowed to stir for 30 minutes. Then 1-methylpyrrole carbaldehyde (0.5g, 4.58 mmol) was added dropwise at -40 °C and reaction continued to stir for an additional 45 minutes. A second portion of n-BuLi (6.3 mL, 10.076 mmol) was added dropwise at -40 °C and the reaction was allowed to stir for 1 hour. Trimethyltin chloride solution (1.0M, 10.076 mmol) was added dropwise and the reaction was allowed to come to room temperature and stir overnight. The reaction was then quenched with water, extracted with diethyl ether (3 x 10 mL), dried with anhydrous $MgSO_4$, and concentrated in vacuo to give **40** (442 mg, 35%) as a clear, pale yellow oil which was used without further purification. R*f* = 0.71 (20 % EtOAc/hexanes); ^{1}H NMR (500 MHz, $CDCl_3$) δ 9.53 (s, 1H), 6.93 (d, *J* = 4.0 Hz, 1H), 6.29 (d, *J* = 4.0 Hz, 1H), 3.99 (s, 3H), 0.38 (s, 9H); ^{13}C NMR (125 MHz, $CDCl_3$) δ 178.5, 148.1, 135.5, 124.4, 119.1, 37.5, -8.8; HRMS calcd. for $C_9H_{16}NOSn$ $[M+H]^+$ 274.0250, found 274.0247 by ESI.

1-methyl-5-(6-(piperidin-1-yl)naphthalen-2-yl)-1H-pyrrole-2-carbaldehyde (41): To a solution of 40 (0.05 g, 0.184 mmol) and 26 (0.0794 g, 0.221 mmol) in

degassed DMF (0.2 mL) under argon was added $PdCl_2(PPh_3)_2$ (0.0092 mmol) and the reaction was heated to 60 °C and allowed to stir for 30 minutes. The reaction was then cooled to room temperature and diluted with water (0.2 mL) and diethyl ether (0.2 mL) and filtered through a pad of celite. The reaction mixture was the extracted with diethyl ether (3 x 1 mL) and combined organic layers were washed with brine (1 x 2 mL), dried with anhydrous MgSO4, and concentrated. The residue was adsorbed on to silica and purified by flash column chromatography (0-5% EtOAc/hexanes) to give **41** (42 mg, 72%) as a light yellow powder. R*f* = 0.46 (20 % EtOAc/hexanes); ^{1}H NMR (400 MHz, $CDCl_3$) δ 9.58 (s, 1H), 7.73-7.75 (m, 3H), 7.41-7.43 (dd, *J* = 8.4 Hz, 2.0 Hz, 1H), 7.32-7.35 (dd, *J* = 9.2 Hz, 2.4 Hz, 1H), 7.14 (d, *J* = 2.0 Hz, 1H), 7.00 (d, *J* = 4.4 Hz, 1H), 3.99 (s, 3H), 3.29-3.32 (m, 4H), 1.74-1.80 (m, 4H), 1.64-1.66 (m, 2H); ^{13}C NMR (100 MHz, $CDCl_3$) δ 179.5, 150.8, 145.1, 134.6, 133.0, 129.0, 128.3, 127.7, 127.0, 126.9, 125.4, 124.8, 120.7, 110.9, 109.8, 50.7, 34.7, 25.9, 24.5; HRMS calcd. for $C_{21}H_{23}N_2O$ $[M+H]^+$ 319.1805, found 319.1809 by ESI.

(E)-2-(2-(2-methoxyethoxy)ethoxy)ethyl 2-cyano-3-(5-(6-(piperidin-1-yl)naphthalen-2-yl)furan-2-yl)acrylate (36): 39 (0.017 g, 0.0557 mmol) and **32** (0.0121 g, 0.0524 mmol) was dissolved in THF (0.25 mL) under argon atmosphere. DBU (0.000557 mmol) was added via syringe and the reaction was allowed to stir at room temperature for 5 minutes. The reaction was then concentrated, adsorbed on to silica, and purified via flash chromatography (10-90% EtOAc/hexanes) to give **36** (23.3 mg, 86%) as a red viscous oil. R*f* = 0.3 (60 % EtOAc/hexanes); ^{1}H NMR (400 MHz, $CDCl_3$) δ 8.24 (s, 1H), 7.97 (s, 1H), 7.93 (m, 2H), 7.69-7.71 (m, 1H), 7.33 (m, 2H), 7.10 (bs, 1H), 6.94 (d, *J* = 4.0 Hz, 1H), 4.46 (m, 2H), 3.82-3.84 (m, 2H), 3.73-3.76 (m, 2H), 3.66-3.69 (m, 4H), 3.55-3.58 (m, 2H), 3.38 (s, 3H), 3.32-3.35 (m, 4H), 1.77 (m, 4H), 1.65 (m, 2H); ^{13}C NMR (100 MHz, $CDCl_3$) δ 1635., 161.2, 151.0, 147.7, 138.2, 135.6, 129.9, 127.6, 125.9, 125.2, 123.0, 120.2, 116.3, 109.6, 108.9, 72.1, 71.0, 70.8, 70.7, 69.0, 65.5, 59.2, 59.2, 50.4, 29.8, 25.7, 24.4; HRMS calcd. for $C_{30}H_{34}N_2O_6Na$ $[M+Na]^+$ 541.2309, found 541.2310 by ESI.

(E)-2-(2-(2-methoxyethoxy)ethoxy)ethyl 2-cyano-3-(1-methyl-5-(6-(piperidin-1-yl)naphthalen-2-yl)-1H-pyrrol-2-yl)acrylate (37): To a solution of **41** (0.02 g, 0.063 mmol) and **32** (0.0116 g, 0.05 mmol) in THF (0.25 mL) under argon was added DBU

(0.001 mmol) and the reaction was allowed to stir at room temperature for 10 minutes. The reaction was then concentrated in vacuo, adsorbed on to silica, and purified by flash chromatography (5-80% EtOAc/hexanes) to give **37** (24.5 mg, 92%) as an orange viscous oil. R*f* = 0.38 (80 % EtOAc/hexanes); ^{1}H NMR (500 MHz, $CDCl_3$) δ 8.16 (s, 1H), 7.87 (d, *J* = 4.0 Hz, 1H), 7.72-7.74 (m, 3H), 7.38-7.40 (dd, *J* = 8.5 Hz, 1.5 Hz, 1H), 7.33-7.35 (dd, *J* = 9.0 Hz, 2.0 Hz, 1H), 7.13 (bs, 1H), 6.55 (d, *J* = 4.5 Hz, 1H), 4.42-4.44 (m, 2H), 3.81-3.83 (m, 2H), 3.78 (s, 3H), 3.73-3.75 (m, 2H), 3.66-3.70 (m, 4H), 3.38 (s, 3H), 3.30-3.33 (m, 4H), 1.74-1.78 (m, 4H), 1.64-1.65 (m, 2H); ^{13}C NMR (125 MHz, $CDCl_3$) δ 164.7, 151.0, 145.2, 139.7, 134.7, 129.0, 128.4, 127.6, 127.2, 126.8, 125.2, 120.7, 120.6, 117.7, 114.0, 109.6, 91.1, 72.1, 71.0, 70.8, 70.7, 69.0, 65.2, 59.2, 50.6, 32.2, 29.8, 25.8, 24.4; HRMS calcd. for $C_{31}H_{37}N_3O_5Na$ $[M+Na]^+$ 554.2625, found 554.2626 by ESI.

2.9.3 Biological and Line-Fit Data

Staining of brain tissue sections Male and female transgenic mice overexpression wild type mouse PrP (Tga20) were inoculated with the mouse-adapted prion strain mCWD and were euthanized upon developing terminal signs of prion disease. Transgenic mice (19959) harboring the Aβ plaques express the mutant human amyloid precursor protein 695 APP^{SweInd}, which bears both the Swedish (K670N/M671L) and the Indiana (V717F) mutations, under the control of the Syrian hamster prion protein promoter. Mice were euthanized between 9 - 13 months of age. Frozen brain sections from transgenic mice producing Aβ and PrP^{Sc} protein were dried for 1 Hr, treated with 100%, 95%, and 70% ethanol for 5 min each, and then rinsed with deionized water. Sections were then buffered with phosphate-buffered saline (1X PBS) for 30 min. ANCA11 was diluted 1:50 in 1X PBS (from stock solutions of 3mM) to a final concentration of 60μM, added to brain sections, incubated for 30 min at room temperature, washed with 1X PBS, and coverslipped using DAKO fluorescent mounting media.

Fluorescence microscopy Brain tissue samples were excited with a 488 nm argon/nitrogen laser on an Olympus FluoView FV1000 spectral deconvolution confocal microscope. The emission spectrum ANCA11 bound to Aβ, PrP^{Sc}, and background fluorescence were collected in 1nm increments from 450-650 nm. A minimum of 10 region of interest (ROI) measurements were collected for plaques bound with ANCA11 and non-plaque regions as a background control. The wavelength corresponding to the maximum relative fluorescence intensity (RFI) was taken as the emission λ_{max}.

Brightfield true-color imaging Brain tissue sections were imaged under an Olympus MVX10 Macroview microscope equipped with a MWB2 (Japan) long-pass filter. Each sample was illuminated with epifluorescence and imaged with an exposure time of 0.2sec.

General procedure for the spectral characterization of ANCA probes bound to amyloids Monomeric amyloid proteins were dissolved in 1xPBS or nanopure water to a final concentration of 100 μM and incubated at 37 °C with and without agitation by stirring. Amyloid fibril formation was monitored by the Thioflavin T assay as previously described. 15 μL of aggregated protein was added to 285 μL of the probe (5% DMSO in nanopure water) to attain a final concentration of 5 μM amyloid and 4 μM of probe. The

solution was mixed and transferred to a 300 μL cuvette and the fluorescence measured.

ANCA11 solvatochromic assay and binding pocket permittivity determination

All solvents used were bought at HPLC grade quality, obtained from a dry still, or distilled over drying agent (calcium hydride) prior to use. ANCA11 was dissolved in the appropriate solvent to a final concentration of 100 μM. 10 μL of the stock solution of probe was then added to 190 μL of the same solvent to attain a final concentration of 5 μM of probe. The solution was transferred to a 300 μL cuvette and the fluorescence measured.

Fitting Data for Graphs Graph with Inverse Stokes:
ANCA11: slope: -0.01799 +/- 0.00290, RSQ: 0.81001
ANCA-thiophene: slope: -0.01635 +/- 0.00320, RSQ: 0.74322
ANCA-furan: slope: -0.01850 +/- 0.00212, RSQ: 0.89413
ANCA-pyrrole: slope: -0.02087 +/- 0.00188, RSQ: 0.93227
ABCA: slope: -0.04043 +/- 0.00905, RSQ: 0.74011
Graph with Inverse Emission:
ANCA11: slope: -0.00110 +/- 0.00013, RSQ: 0.88410
ANCA-thiophene: slope: -0.00100 +/- 0.00016, RSQ: 0.85396
ANCA-furan: slope: slope: -0.00105 +/- 0.00011, RSQ: 0.91485
ANCA-pyrrole: slope: -0.00138 +/- 0.00013, RSQ: 0.92217
ABCA: slope: -0.00065 +/- 0.00008, RSQ: 0.89474

2.9.4 Other Compounds

1-(thiophen-2-yl)piperidine (39): 2-bromothiophene (**38**) (3.0 g, 18.4 mmol), piperidine (2.35 g, 27.6 mmol), Cu metal (60 mg, 0.92 mmol), CuI (175 mg, 0.92 mmol), $K_3PO_4 \cdot H_2O$ (8.47 g, 36.8 mmol) and deanol (19 mL) were added to a flask fitted with a magnetic stirbar, a condenser and sealed with a septum. Air was removed from the reaction system and replaced with argon. The reaction mixture was stirred at 80 °C for 15 hours under argon positive pressure. After the reaction cooled to room temperature,

50 mL of water was added and the mixture was extracted with diethyl ether (3 x 75 mL). The combined organic layers were washed with brine (1 x 100 mL) and dried over anhydrous $MgSO_4$. Solvent was removed in vacuo and the residue was purified by silica gel flash chromatography, eluted with 0-10% EtOAc/hexanes. The product was obtained as a clear yellow oil (1.3 g, 42%) that darkened upon standing. R*f* = 0.76 (20 % EtOAc/hexanes); ^{1}H NMR (400 MHz, $CDCl_3$) δ 6.80-6.82 (dd, *J* = 5.6 Hz, 3.6 Hz, 1H), 6.59-6.61 (dd, *J* = 5.6 Hz, 1.6 Hz, 1H), 6.13-6.14 (dd, *J* = 4.0 Hz, 1.6 Hz, 1H), 3.13-3.16 (t, *J* = 11.2 Hz, 4H), 1.72-1.78 (m, 4H), 1.56-1.62 (m, 2H); ^{13}C NMR (100 MHz, $CDCl_3$) δ 160.4, 126.1, 111.8, 104.9, 53.0, 25.5, 23.9; HRMS calcd. for $C_9H_{14}NS$ [M+H]+ 168.0841, found 168.0844 by ESI.

6-(5-(piperidin-1-yl)thiophen-2-yl)-2-naphthaldehyde (41): To a solution of **18** (0.0125 g, 0.053 mmol) and **40** (1-(5-(tributylstannyl)thiophen-2-yl)piperidine) (0.02 g, 0.044 mmol) in DMF (0.05 mL) under argon was added $PdCl_2(PPh_3)_2$ (0.0022 mmol) and the reaction was heated at 60 °C for 16 hours. The reaction was then cooled to room temperature, diluted with EtOAc (0.1 mL), washed with water (2 x 0.1 mL), dried with anhydrous $MgSO_4$, and concentrated in vacuo. The residue was then adsorbed on to silica and purified by flash column chromatography (0-10% EtOAc/hexanes) to give **41** (12.5 mg, 89%) as a yellow solid. R*f* = 0.44 (20 % EtOAc/hexanes); ^{1}H NMR (400 MHz, $CDCl_3$) δ 10.10 (s, 1H), 8.24 (s, 1H), 7.89-7.92 (m, 2H), 7.82-7.85 (m, 2H), 7.74-7.76 (dd, *J* = 8.4 Hz, 1.6 Hz, 1H), 7.25 (m, 1H), 6.09 (d, *J* = 4.0 Hz, 1H), 3.22-3.25 (m, 4H), 1.74-1.77 (m, 4H), 1.57-1.62 (m, 2H); ^{13}C NMR (100 MHz, $CDCl_3$) δ 192.2, 161.0, 137.3, 136.1, 134.4, 133.3, 131.0, 130.0, 121.4, 105.2, 52.1, 29.9, 25.3, 23.9; HRMS calcd. for $C_{20}H_{20}NOS$ $[M+H]^+$ 322.1260, found 322.1259 by ESI.

(E)-2-(2-(2-methoxyethoxy)ethoxy)ethyl 2-cyano-3-(6-(dimethylamino)-2,3-dihydro-^{1}H-cyclopenta[b]naphthalen-4-yl)acrylate (45): To stirring solution of **44** (0.02 mg, 0.0836 mmol) and **32** (0.015 mg, 0.0669 mmol) in THF (0.33 mL) was added DBU (0.001 mmol) under argon. The reaction was heated at 50 °C for 3 hours then cooled to room temperature and evaporated to dryness. The residue was purified by flash chromatography (0-60% EtOAc/hexanes) to give **45** (0.023 mg, 77 %) as a red oil. R*f* = 0.34 (50 % EtOAc/hexanes); ^{1}H NMR (400 MHz, $CDCl_3$) δ 8.91 (s, 1H), 7.64-7.67 (m, 2H), 7.10-7.13 (dd, *J* = 8.0 Hz, 4.0 Hz, 1H), 6.63 (bs, 1H), 4.50-4.52 (m, 2H), 3.85-3.88

(m, 2H), 3.74 (m, 2H), 3.66-3.70 (m, 4H), 3.54-3.56 (m, 2H), 3.36 (s, 3H), 3.03-3.10 (m, 10H), 2.10-2.17 (m, 2H); ^{13}C NMR (100 MHz, $CDCl_3$) δ 162.5, 156.4, 148.9, 145.9, 139.2, 132.0, 129.4, 126.3, 125.8, 122.7, 115.6, 115.3, 108.0, 103.2, 72.1, 71.0, 70.8, 70.7, 68.8, 65.9, 59.2, 40.87, 33.8, 32.7, 29.8, 26.7; HRMS calcd. for $C_{26}H_{33}N_2O_2$ [M + H]$^+$ 453.2384, found 453.2386 by ESI.

(E)-2-(2-(2-methoxyethoxy)ethoxy)ethyl 2-cyano-3-(8-(dimethylamino)-2,3-dihydro-1H-cyclopenta[b]naphthalen-4-yl)acrylate (47): To stirring solution of **46** (0.02 mg, 0.0836 mmol) and **32** (0.015 mg, 0.0669 mmol) in THF (0.33 mL) was added DBU (0.001 mmol) under argon. The reaction was heated at 50 °C for 2 hours then cooled to room temperature and evaporated to dryness. The residue was purified by flash chromatography (0-20% EtOAc/hexanes) to give **47** (26.0 mg, 86 %) as a orange oil. R*f* = 0.26 (40 % EtOAc/hexanes); ^{1}H NMR (400 MHz, $CDCl_3$) δ 8.96 (s, 1H), 8.23 (s, 1H), 7.39-7.41 (m, 2H), 7.09-7.11 (dd, *J* = 4.0 Hz, 1.2 Hz, 1H), 4.51-4.53 (m, 2H), 3.85-3.87 (m, 2H), 3.74-3.76 (m, 2H), 3.66-3.71 (m, 4H), 3.54-3.56 (m, 2H), 3.36 (s, 3H), 3.09-3.14 (m, 4H), 2.88 (s, 6H), 2.14-2.20 (m, 2H); ^{13}C NMR (100 MHz, $CDCl_3$) δ 162.0, 156.8, 151.5, 144.6, 143.0, 131.7, 128.3, 126.8, 124.8, 122.3, 118.7, 115.0, 114.6, 109.6, 72.0, 71.0, 70.8, 70.7, 68.8, 66.2, 59.0, 45.5, 33.4, 33.3, 29.8, 26.7; HRMS calcd. for $C_{26}H_{33}N_2O_2$ [M+H]$^+$ 453.2384, found 453.2387 by ESI.

(E)-2-(2-(2-methoxyethoxy)ethoxy)ethyl 2-cyano-3-(7-(dimethylamino)-2,3-dihydro-1H-cyclopenta[b]naphthalen-4-yl)acrylate (49): To stirring solution of **48** (0.007 mg, 0.03 mmol) and **32** (0.0054 mg, 0.023 mmol) in THF (0.2 mL) was added DBU (0.001 mmol) under argon. The reaction was heated at 50 °C for 2 hours then cooled to room temperature and evaporated to dryness. The residue was purified by flash chromatography (0-40% EtOAc/hexanes) to give **49** (0.0094 mg, 90 %) as an orange oil. R*f* = 0.24 (40 % EtOAc/hexanes); ^{1}H NMR (400 MHz, $CDCl_3$) δ 8.92 (s, 1H), 7.58-7.61 (m, 2H), 7.13-7.16 (dd, *J* = 12.0 Hz, 4.0 Hz, 1H), 6.89 (d, *J* = 4.0 Hz, 1H), 4.50-4.52 (m, 2 H), 3.85-3.87 (m, 2H), 3.74-3.75 (m, 2H), 3.66-3.71 (m, 5H), 3.54-3.56 (m, 2H), 3.37 (s, 3H), 3.05 (m, 9H), 2.10-2.17 (m, 2H); ^{13}C NMR (100 MHz, $CDCl_3$) δ 162.2, 156.7, 148.6, 143.9, 141.2, 134.5, 125.0, 124.8, 124.3, 123.0, 116.2, 115.0, 109.1, 107.3, 72.1, 71.0, 70.8, 70.7, 69.0, 65.9, 59.2, 40.9, 33.1, 33.0, 29.8, 26.7; HRMS calcd. for $C_{26}H_{33}N_2O_2$ [M + H]$^+$ 453.2384, found 453.2381 by ESI.

1-(6-bromonaphthalen-2-yl)ethanol (50): 6-bromo-2-naphthaldehyde (**18**) (0.2 g, 0.851 mmol) was dissolved in THF (4.3 mL) and cooled to -78 °C under argon atmosphere. Methylmagnesium bromide (0.608 mL, 0.851 mmol) was added dropwise to the stirring solution. The reaction was then allowed to continue stirring at -78 °C for 35 minutes and then quenched with NH_4+Cl- (4.0 mL) and extracted with CH_2Cl_2 (2 x 5 mL). The combined organic layers were washed with brine (1 x 15 mL) and dried over anhydrous $MgSO_4$. Solvent was removed in vacuo and compound **50** was obtained as a white solid (200 mg, 94%). R*f* = 0.24 (20 % EtOAc/hexanes); ^{1}H NMR (400 MHz, $CDCl_3$) δ 7.95 (d, *J* = 1.6 Hz, 1H), 7.63-7.72 (m, 3H), 7.47-7.54 (m, 2H), 4.98-5.03 (q, *J* = 6.4 Hz, 1H), 2.40 (bs, 1H), 1.53-1.55 (d, *J* = 6.4 Hz, 3H); ^{13}C NMR (100 MHz, $CDCl_3$) δ 143.8, 134.0, 131.8, 129.8, 129.7, 129.6, 127.4, 125.0, 123.8, 119.7, 70.34, 25.22.

1-(6-bromonaphthalen-2-yl)ethanone (51): 50 (200mg, 0.796 mmol) and sodium bicarbonate (4.01 g, 4.776 mmol) was added to a flask charged with a magnetic stir bar under argon and dissolved in CH_2Cl_2 (4.0 mL). DMP (439 mg, 1.0348 mmol) was added in one portion and the reaction was allowed to stir at room temperature for 5 minutes. The reaction was then quenched with a 1:1:1 water/Na2S2O3/sodium bicarbonate solution (5.0 mL) and allowed to stir for 20 minutes and then extracted with CH_2Cl_2 (3 x 6 mL). The combined organic layers were washed with brine (1 x 10 mL), dried over anhydrous $MgSO_4$, and the solvent was removed in vacuo to give **51** (153 mg, 77%) as a white powder. R*f* = 0.56 (20 % EtOAc/hexanes); ^{1}H NMR (400 MHz, $CDCl_3$) δ 8.34 (s, 1H), 7.98-8.00 (dd, *J* = 8.8 Hz, 1.6 Hz, 1H), 7.94 (d, *J* = 1.6 Hz, 1H), 7.69-7.75 (m, 2H), 7.53-7.56 (dd, *J* = 8.4 Hz, 1.6 Hz, 1H), 2.67 (s, 3H); ^{13}C NMR (100 MHz, $CDCl_3$) δ 197.6, 136.4, 134.7, 131.0, 130.9, 130.2, 129.9, 129.9, 127.5, 125.0, 122.8, 26.7.

2.9.5 Graphs

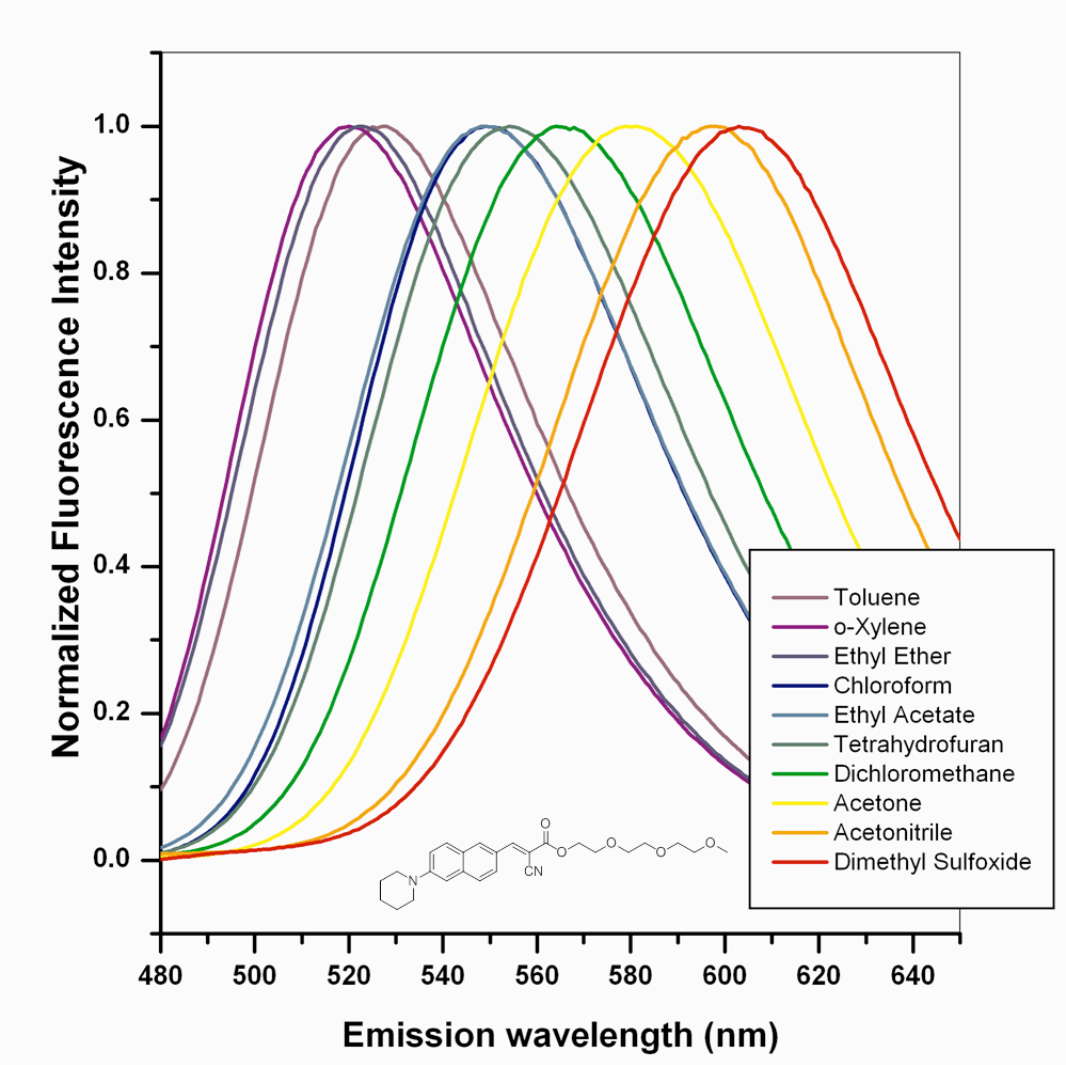

Figure 2.19: ANCA-11 Solvatochromatism: Fluorescence Intensity vs. Emission Wavelength

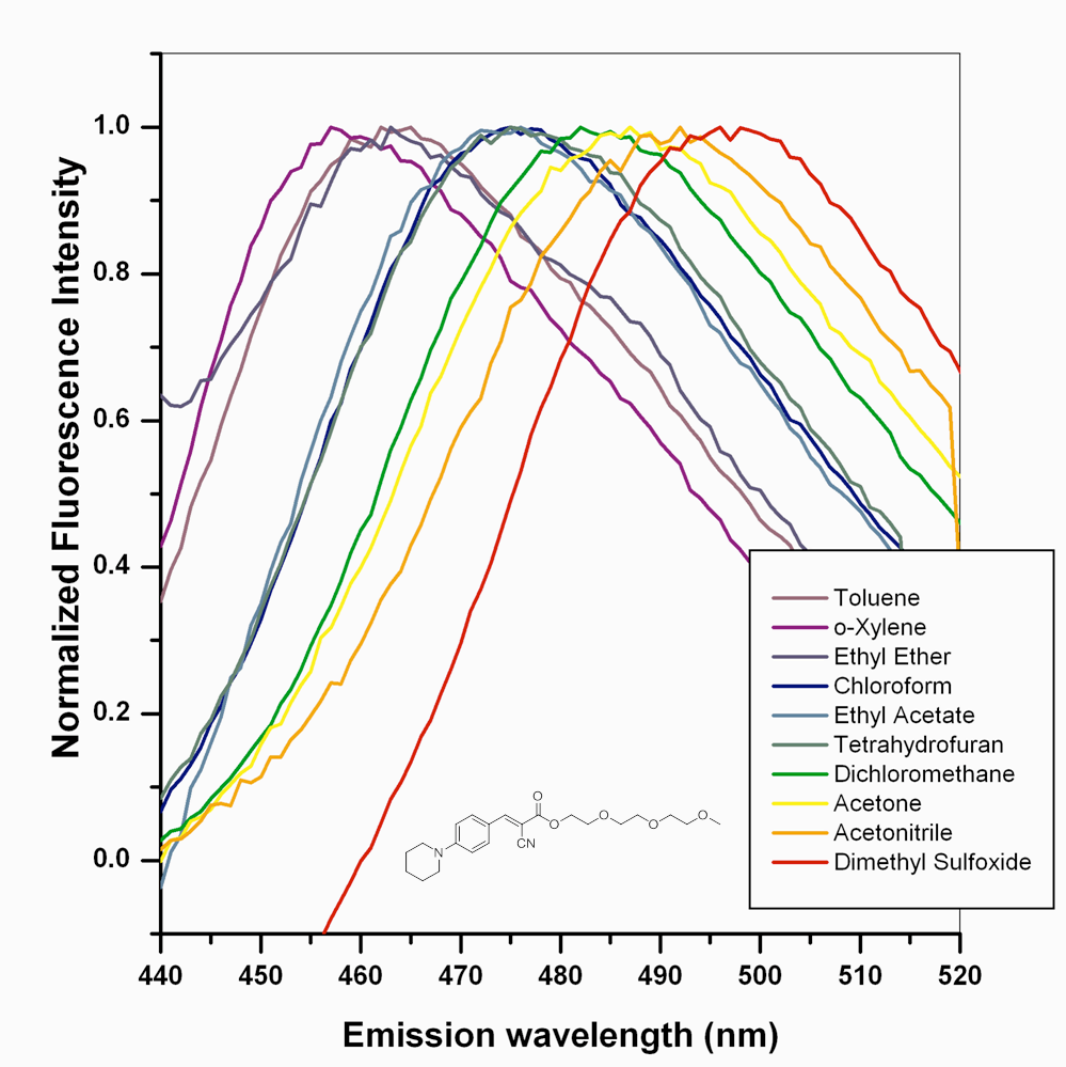

Figure 2.20: ABCA Solvatochromatism: Fluorescence Intensity vs. Emission Wavelength

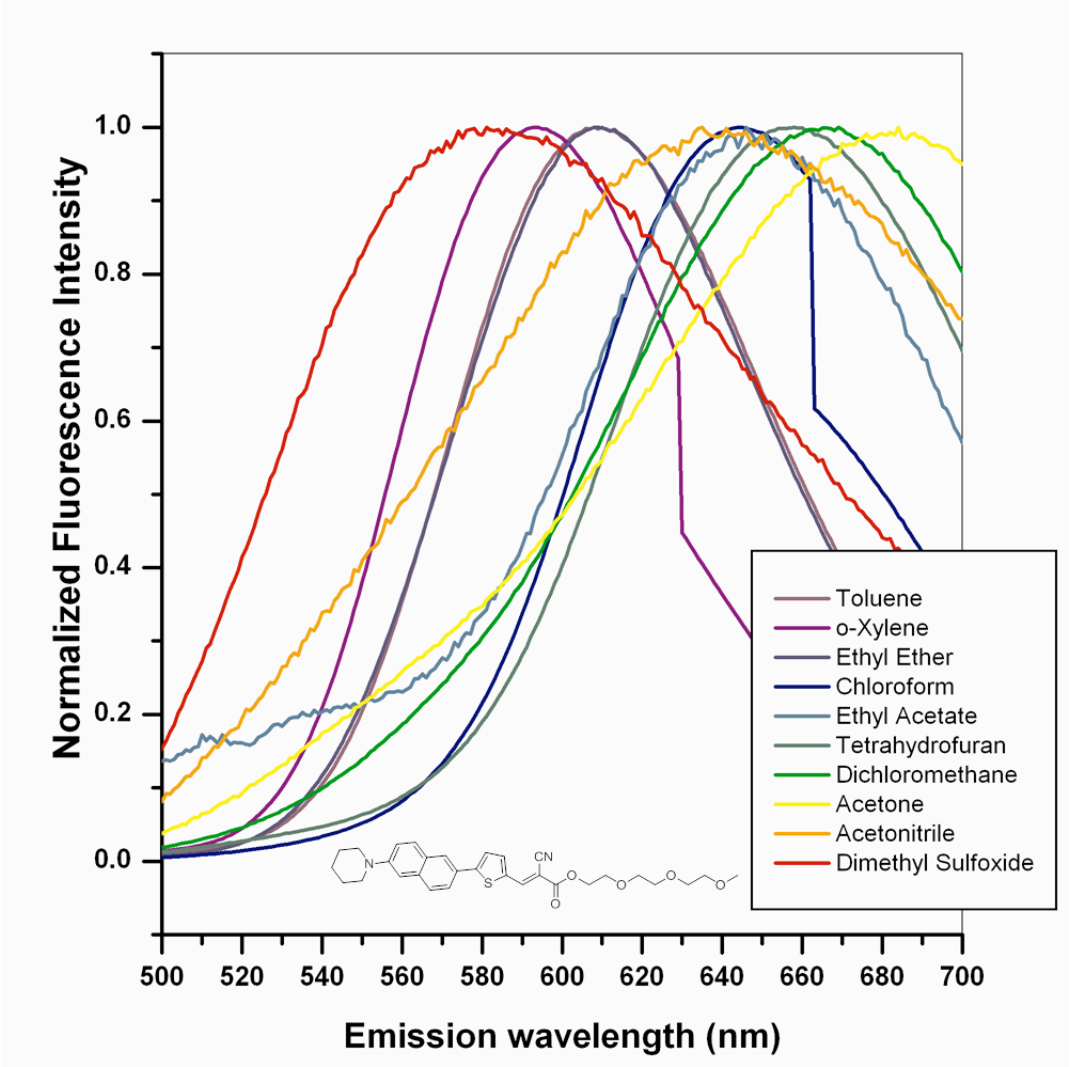

Figure 2.21: ANCA-thiophene Solvatochromatism: Fluorescence Intensity vs. Emission Wavelength

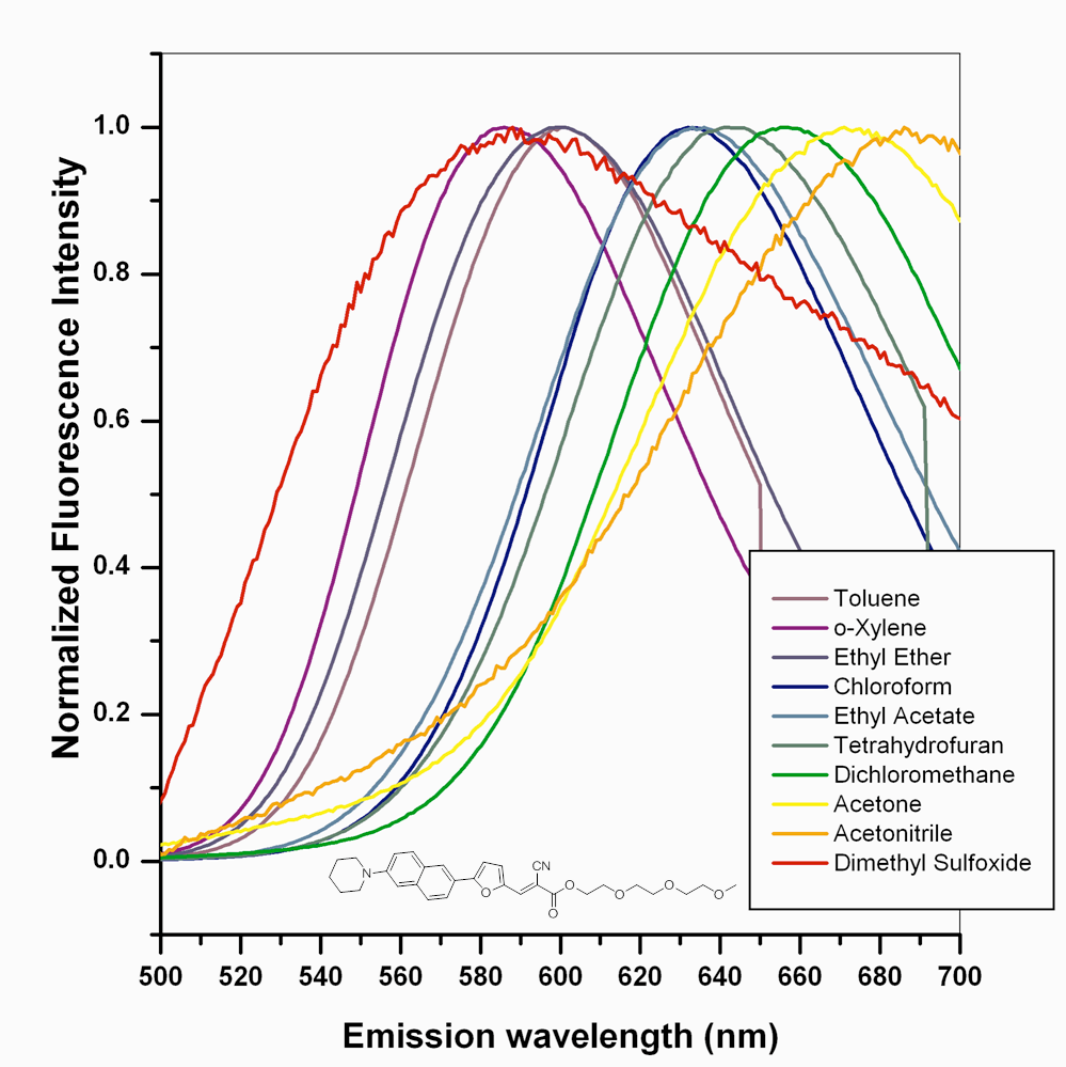

Figure 2.22: ANCA-furan Solvatochromatism: Fluorescence Intensity vs. Emission Wavelength

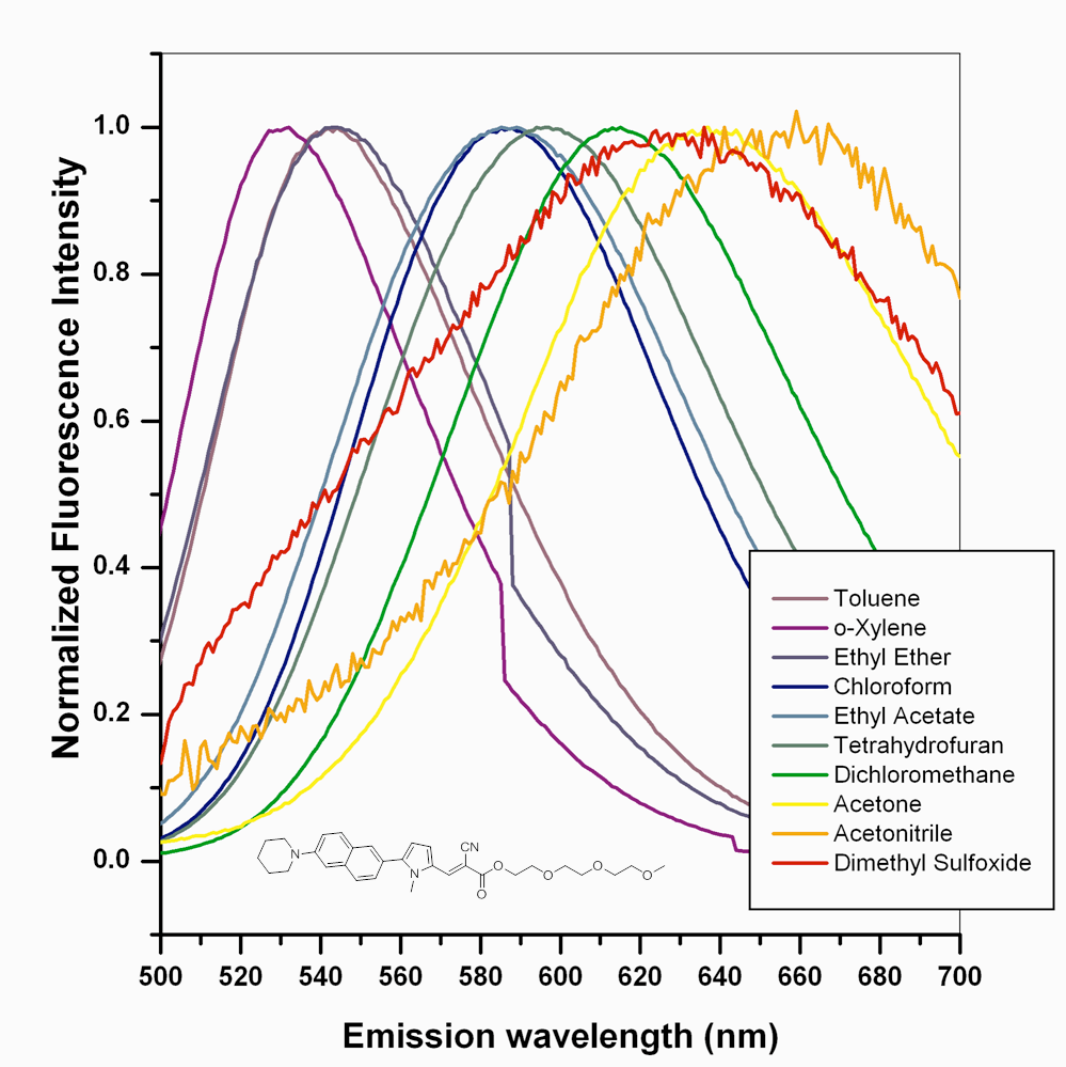

Figure 2.23: ANCA-pyrrole Solvatochromatism: Fluorescence Intensity vs. Emission Wavelength

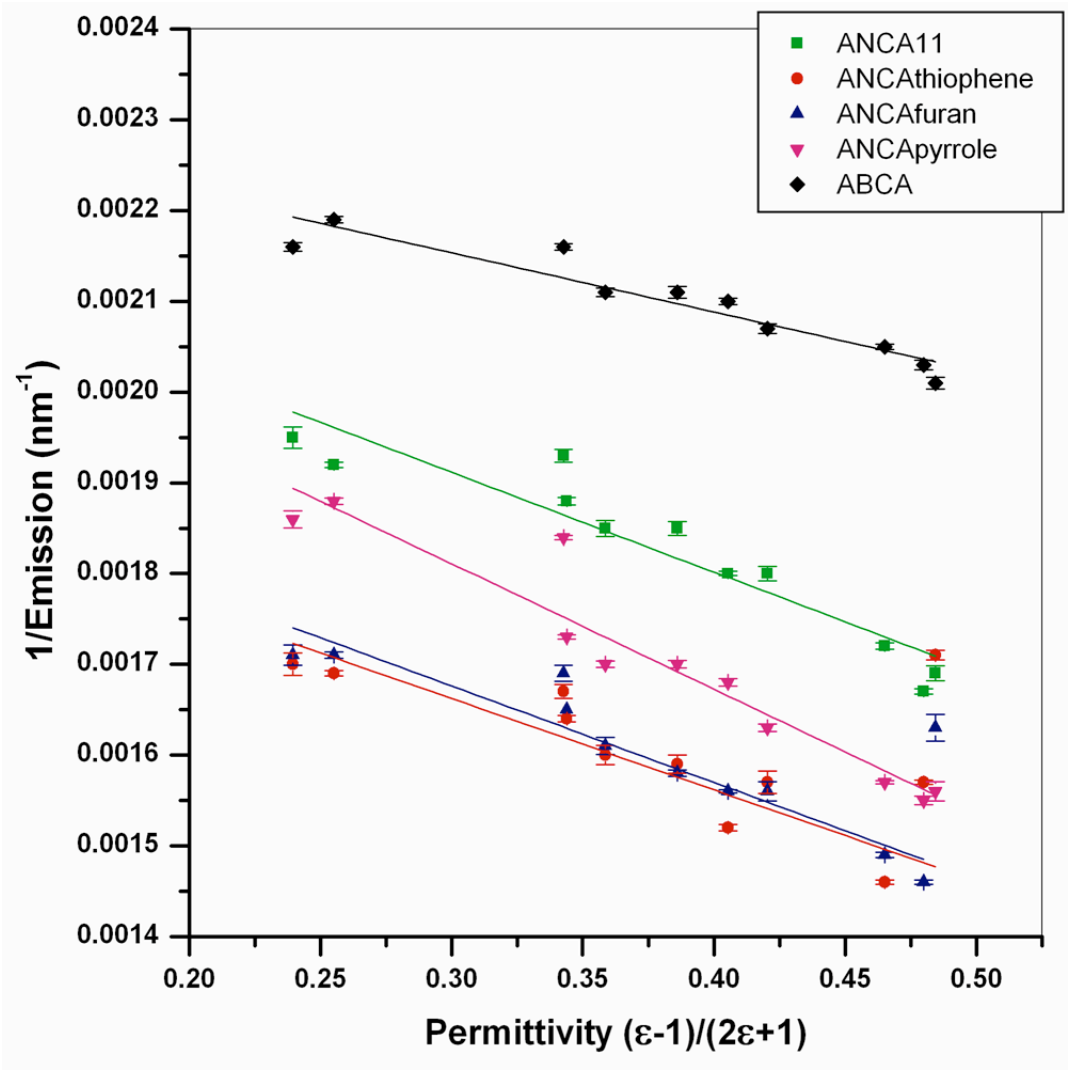

Figure 2.24: Inverse Emission vs. Solvent Permittivity All Compounds

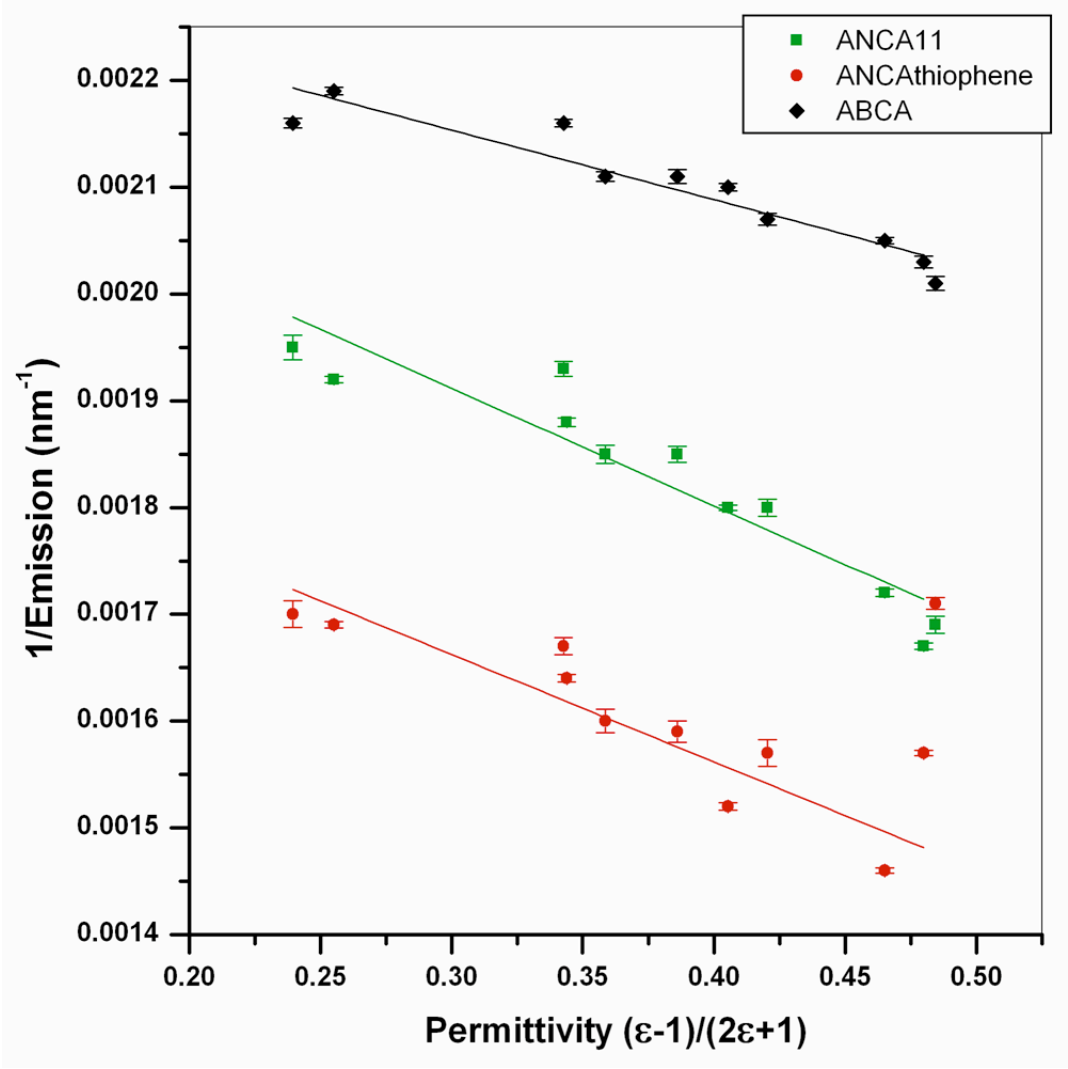

Figure 2.25: Inverse Emission vs. Solvent Permittivity ABCA, ANCA-11, and ANCA-thiophene

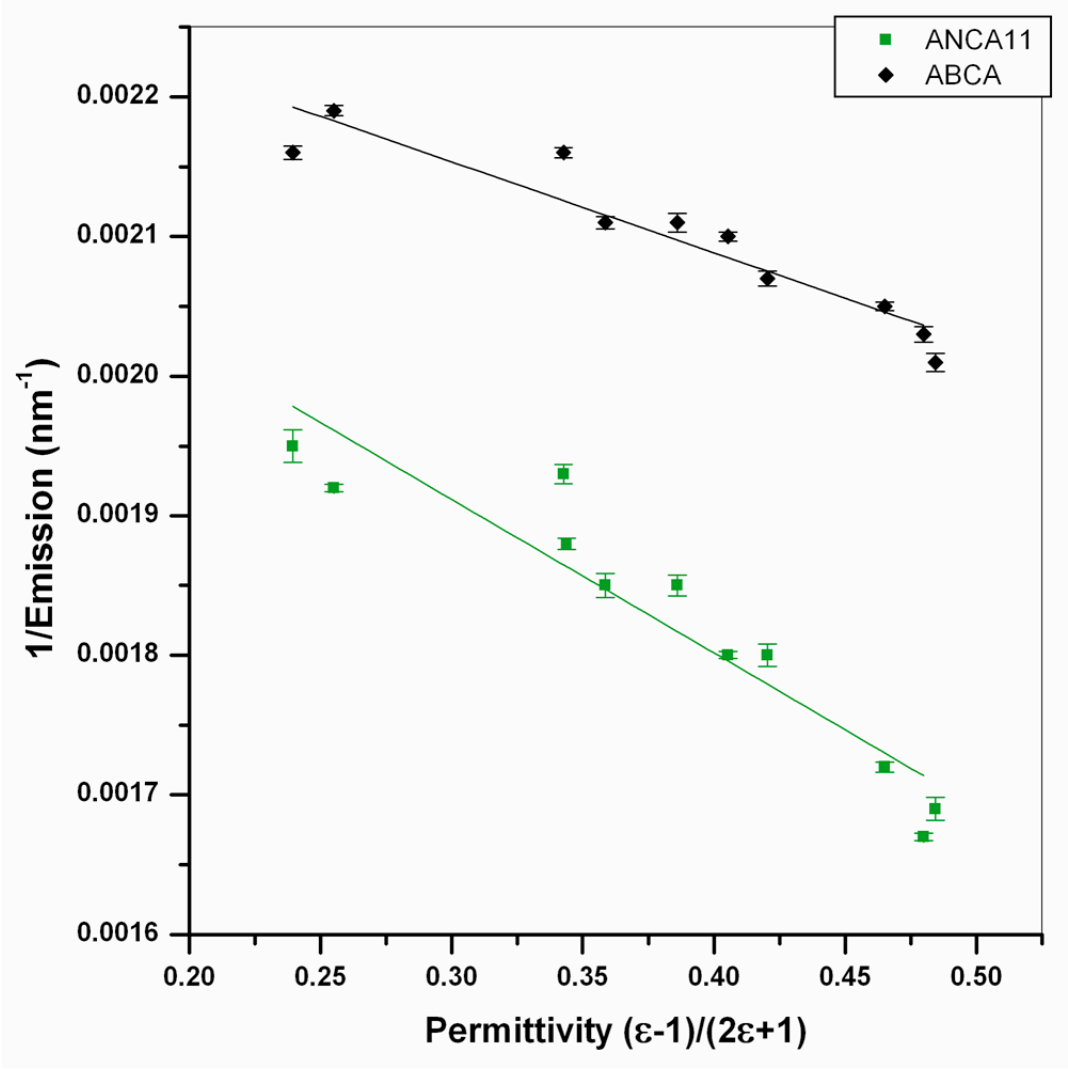

Figure 2.26: Inverse Emission vs. Solvent Permittivity ABCA andANCA-11

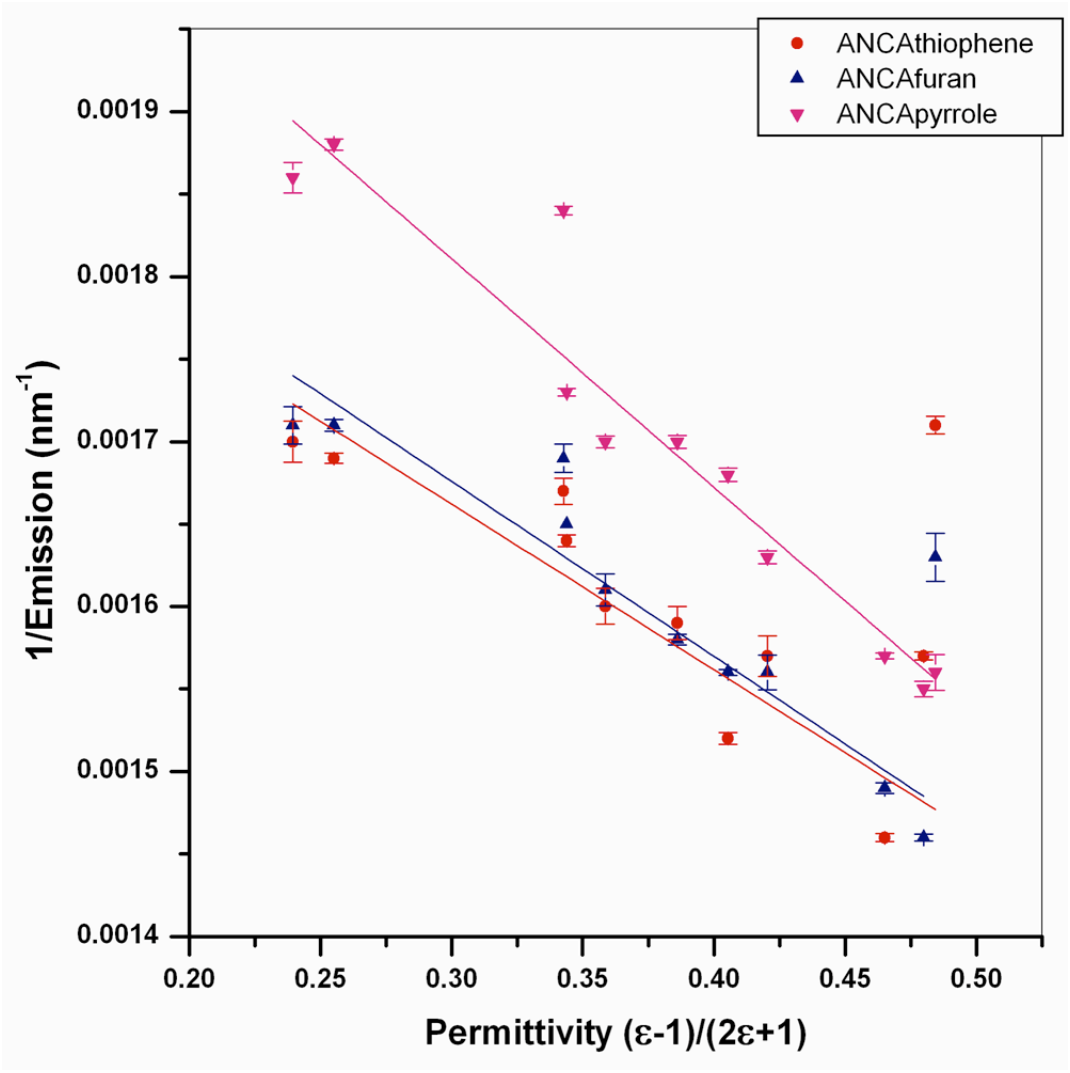

Figure 2.27: Inverse Emission vs. Solvent Permittivity ANCA-thiophene, ANCA-furan, and ANCA-pyrrole

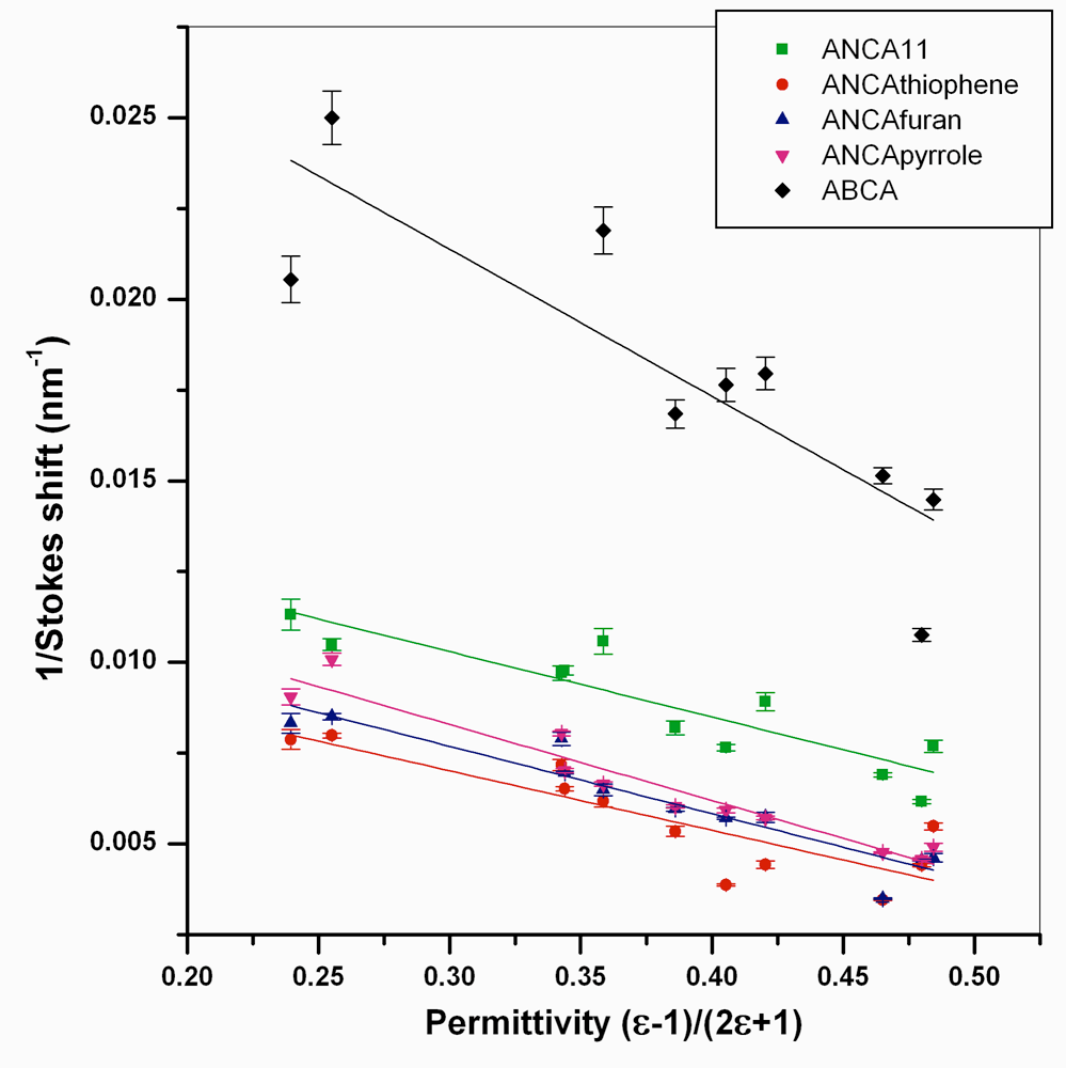

Figure 2.28: Inverse Stokes Shift vs. Solvent Permittivity All Compounds

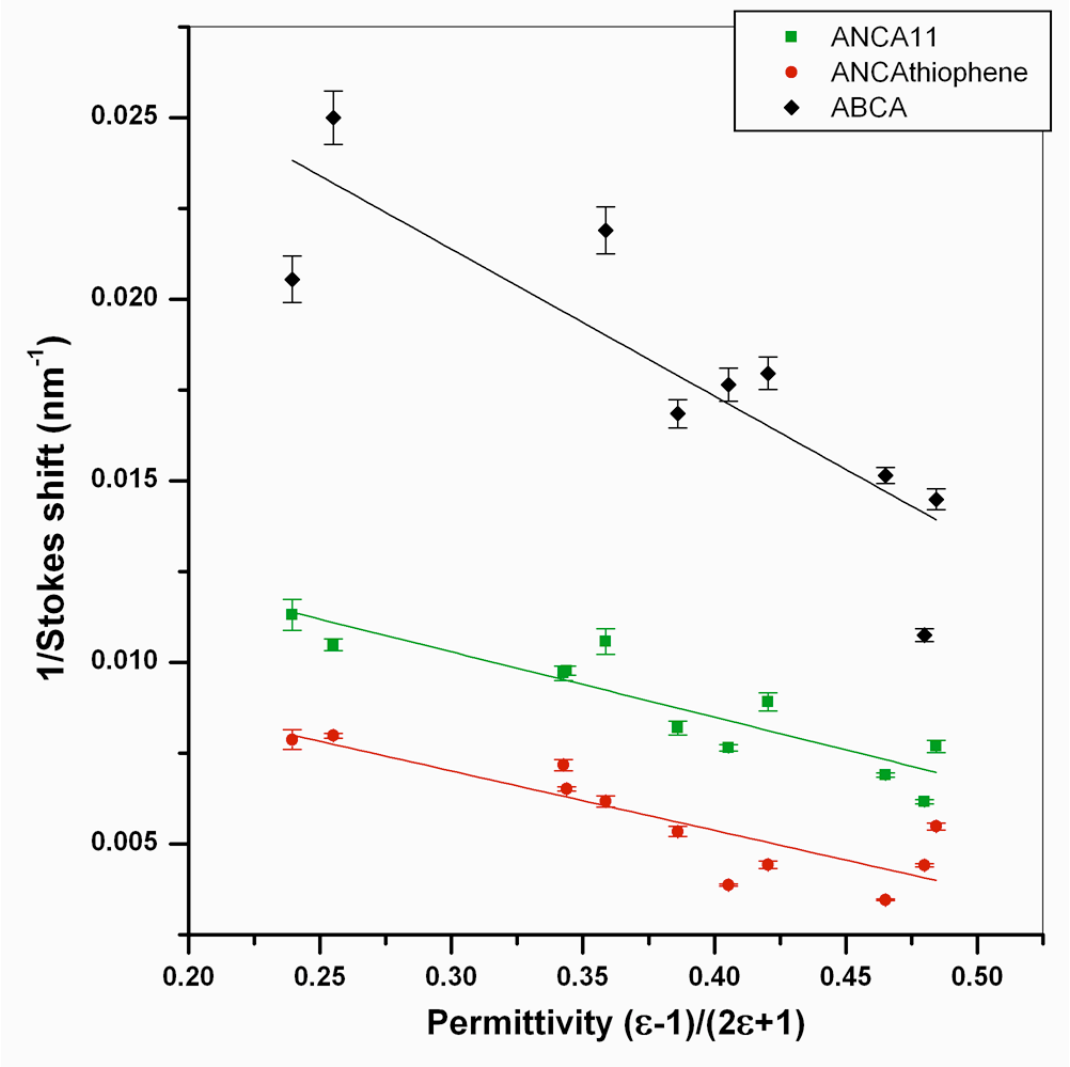

Figure 2.29: Inverse Stokes Shift vs. Solvent Permittivity ABCA, ANCA-11, and ANCA-thiophene

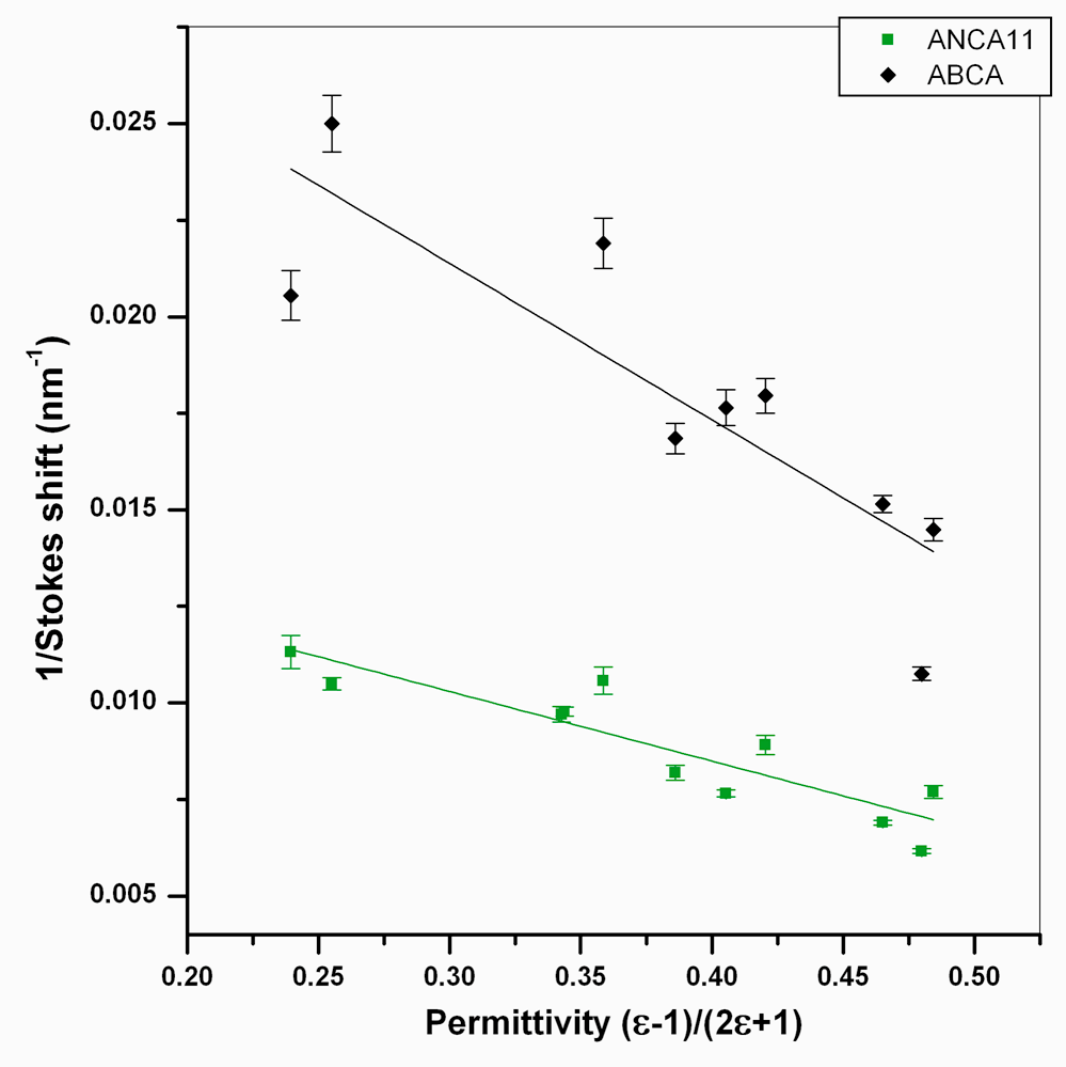

Figure 2.30: Inverse Stokes Shift vs. Solvent Permittivity ABCA and ANCA-11

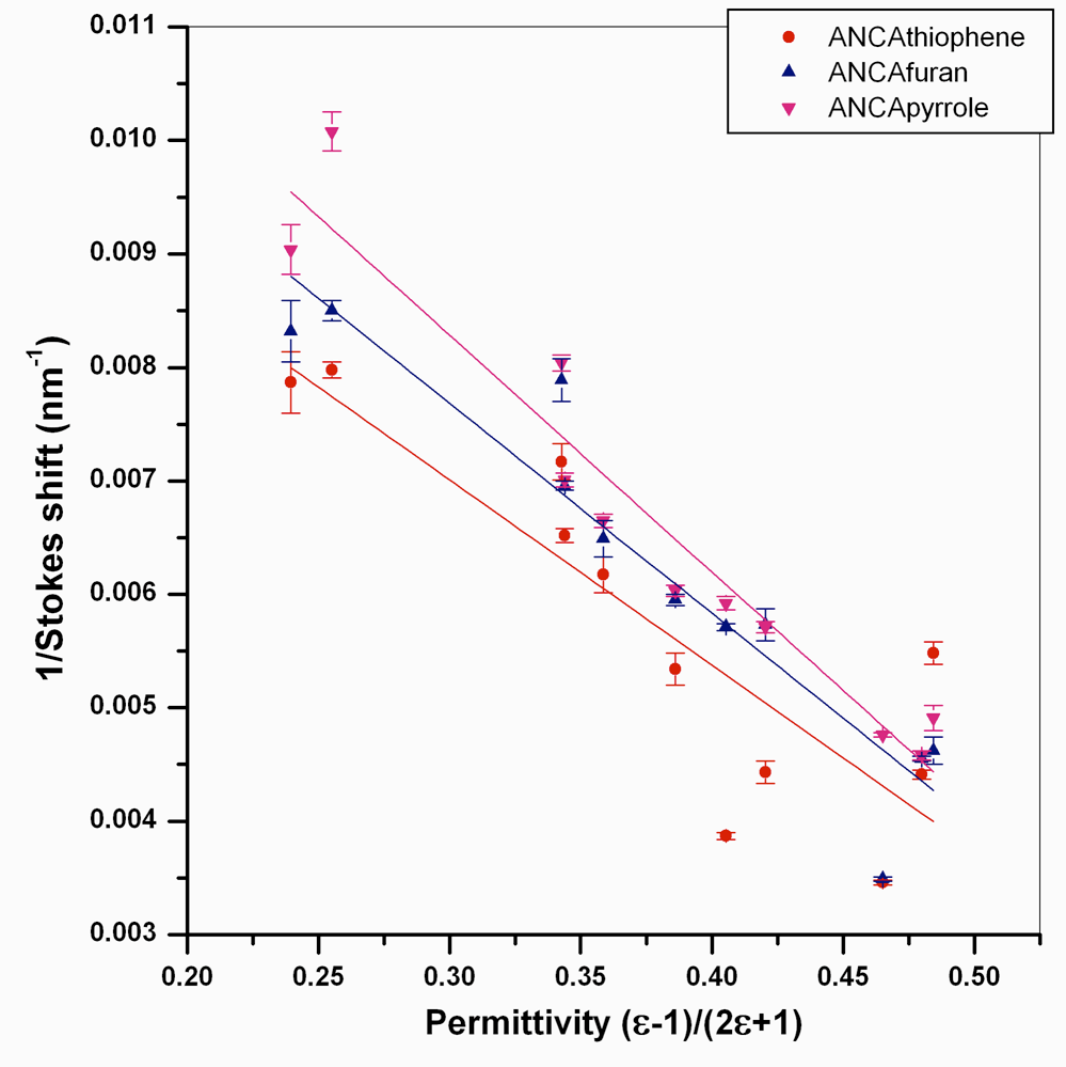

Figure 2.31: Inverse Stokes Shift vs. Solvent Permittivity ANCA-thiophene, ANCA-furan, and ANCA-pyrrole

2.9.6 Tissue Data

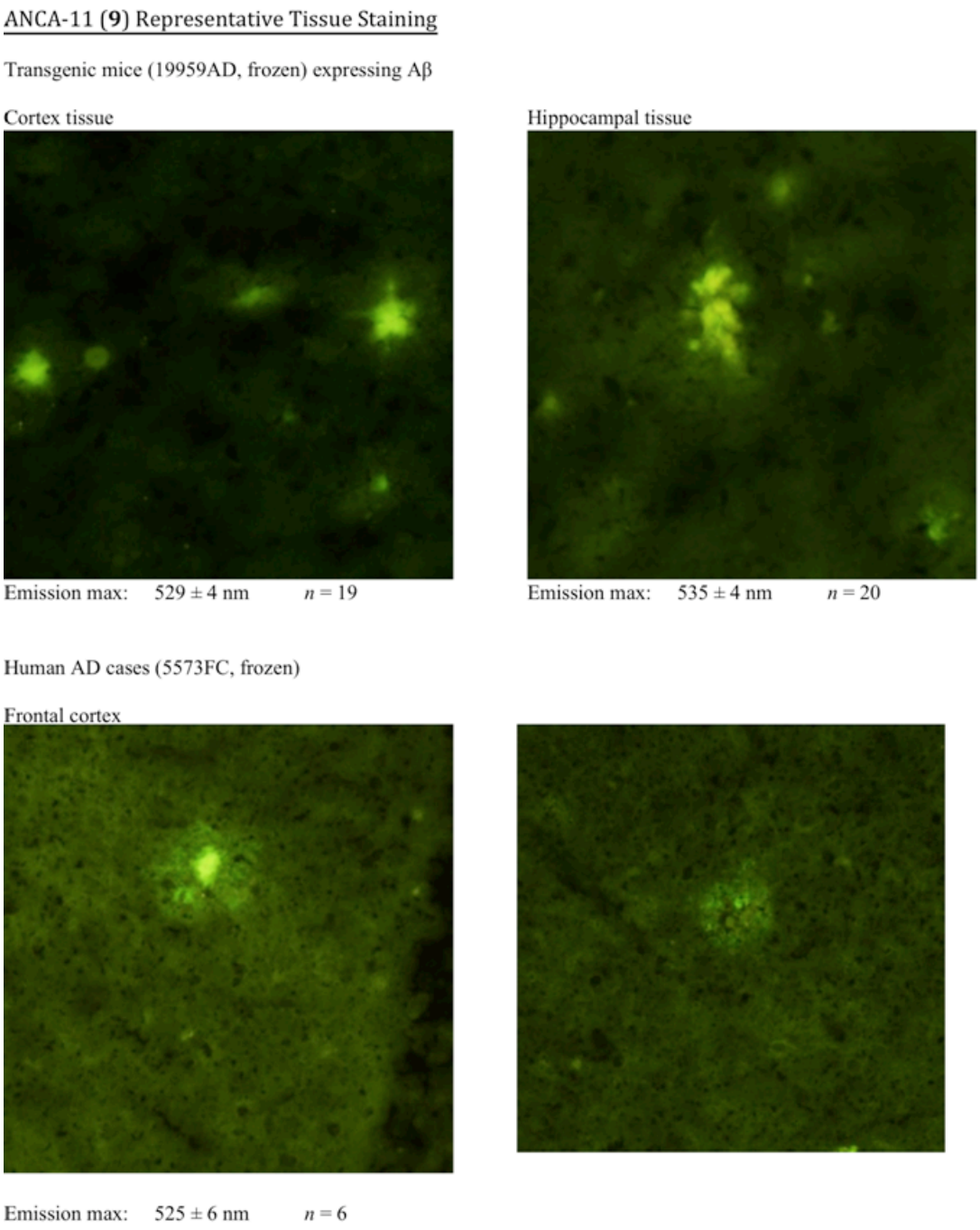

Figure 2.32: ANCA-11 Representative Tissue Staining

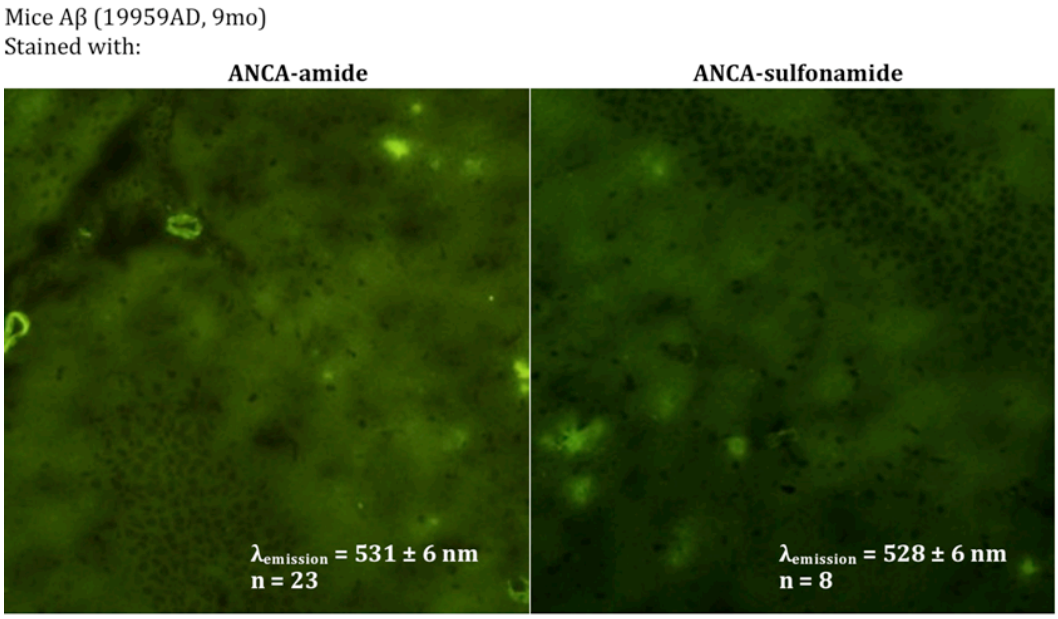

Figure 2.33: ANCA-amide and ANCA-sulfonamide Representative Tissue Staining

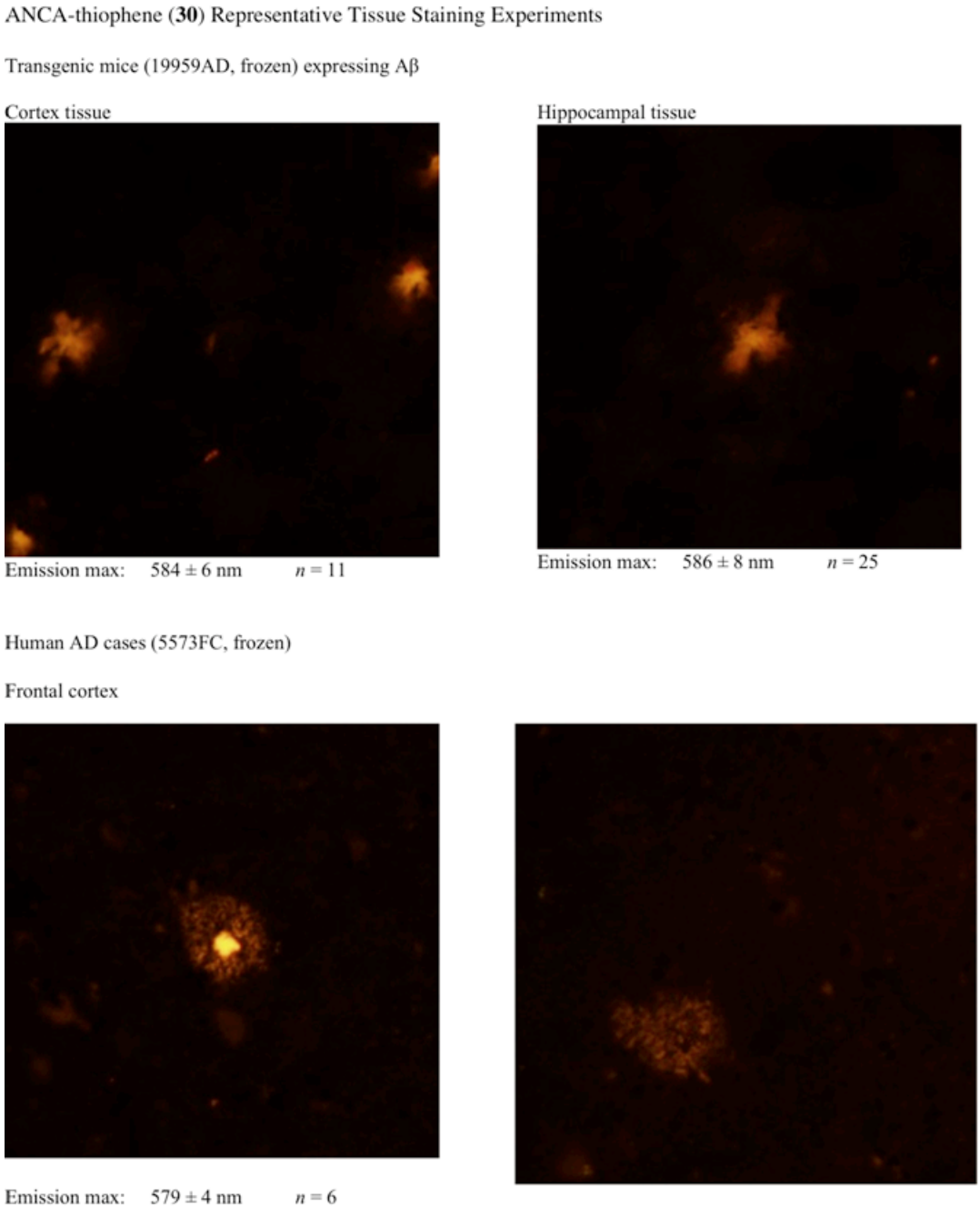

Figure 2.34: ANCA-thiophene Representative Tissue Staining

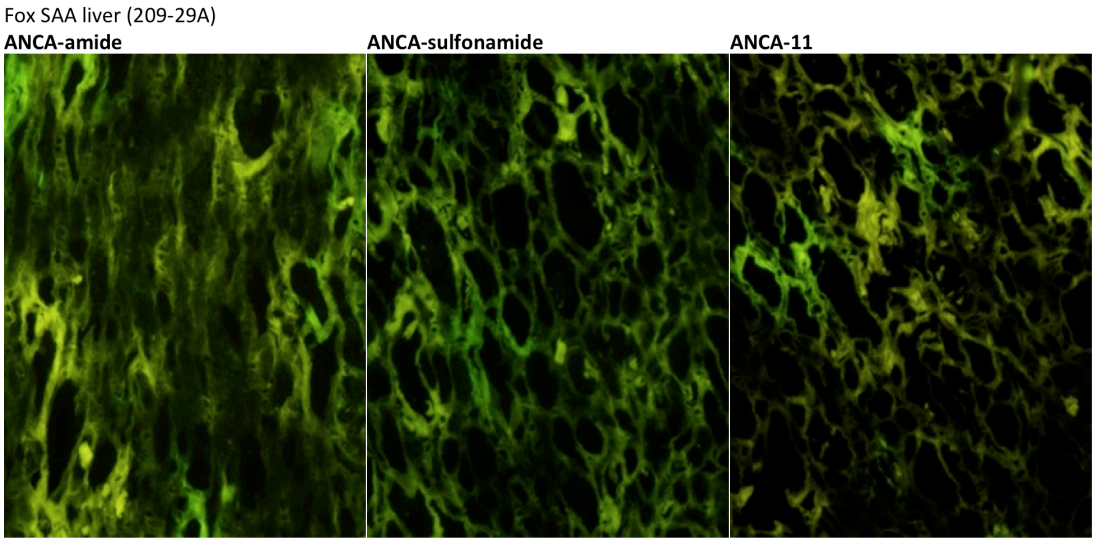

Figure 2.35: ANCA-11, ANCA-amide, and ANCA-sulfonamide Fox SAA liver Tissue Staining

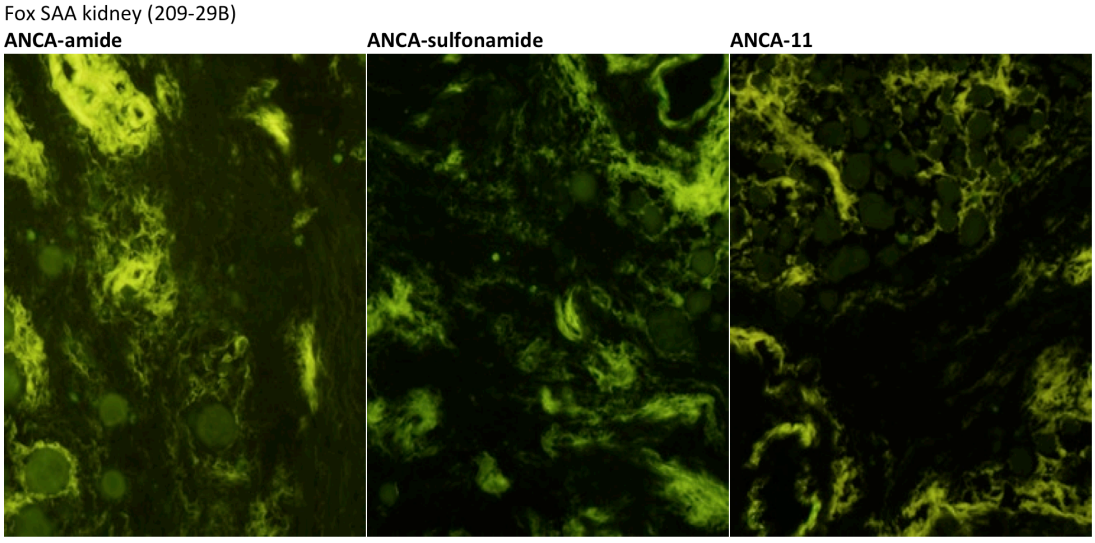

Figure 2.36: ANCA-11, ANCA-amide, and ANCA-sulfonamide Fox SAA kidney Tissue Staining

ANCA11 staining of frozen duck liver containing amyloid (IIN1297)

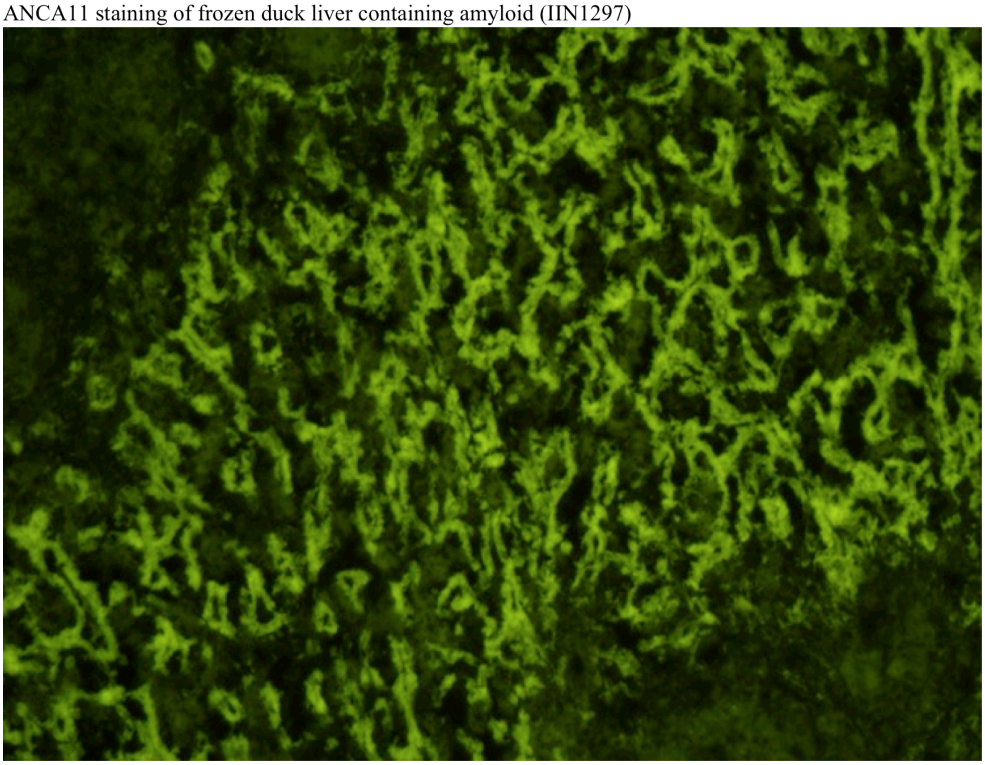

Emission max: 538 ± 3 nm *n* = 17

Figure 2.37: ANCA-11 Duck liver containing amyloid Tissue Staining

ANCA-thio staining of frozen duck liver containing amyloid (IIN1297)

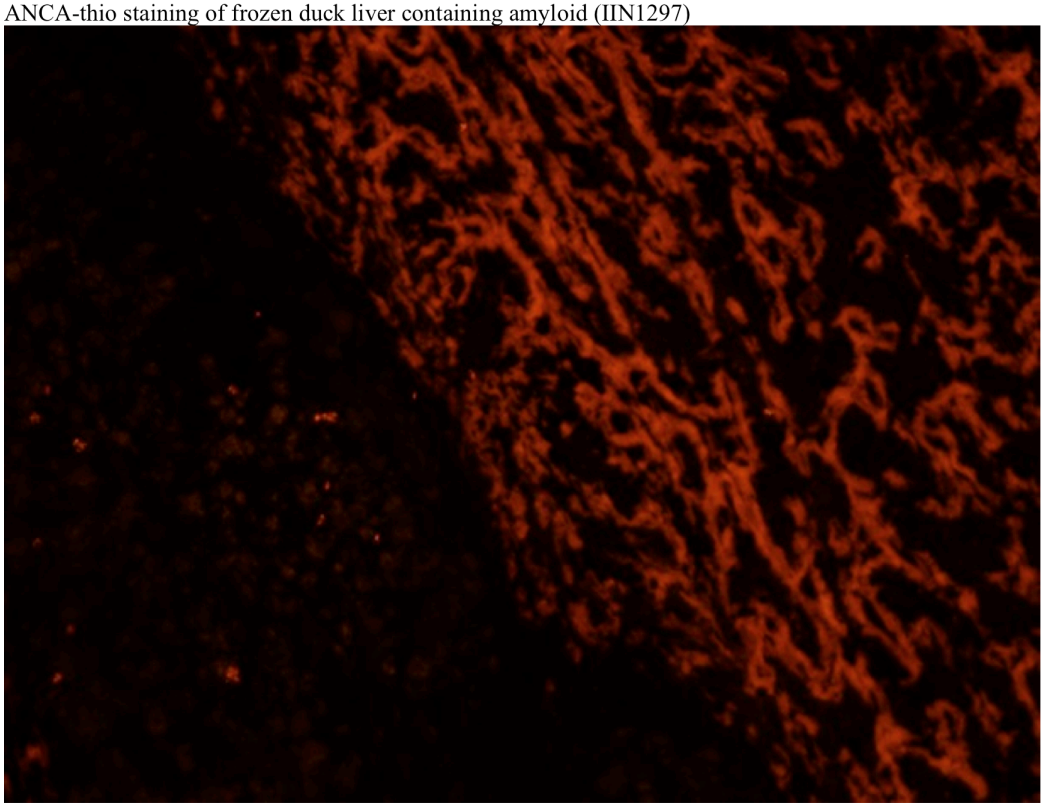

Emission max: 603 ± 2 nm *n* = 12

Figure 2.38: ANCA-thiophene Duck liver containing amyloid Tissue Staining

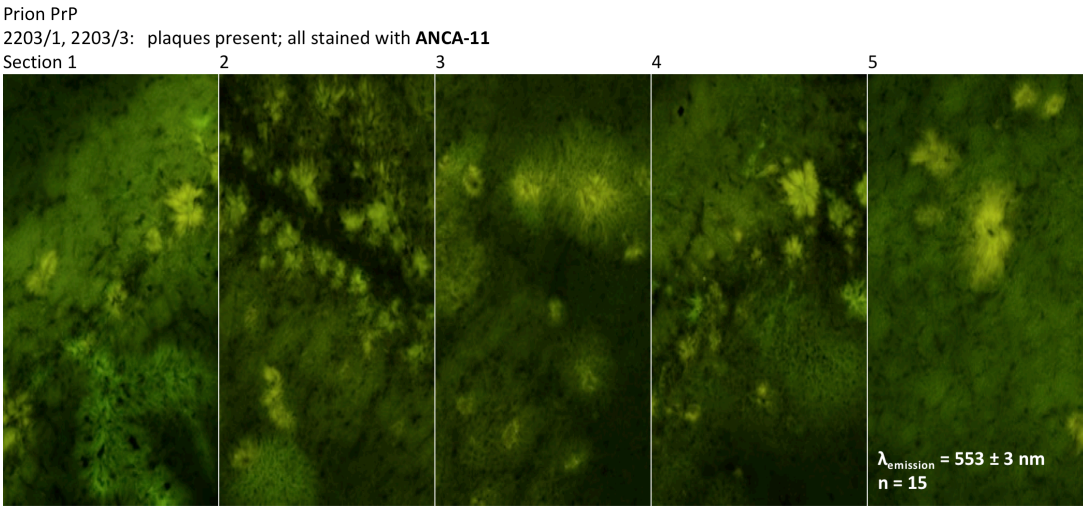

Figure 2.39: ANCA-11 PrP Tissue Staining

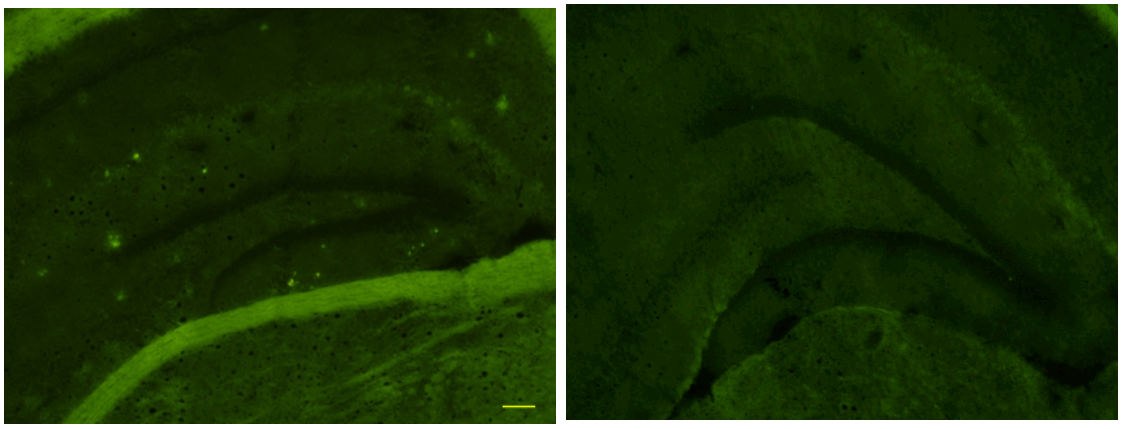

J20 hippocampal stains with ANCA-amide
λ_{max}=535 ± 8nm
n=22 (all hippocampal)

Figure 2.40: ANCA-amide J20 hippocampal Tissue Staining

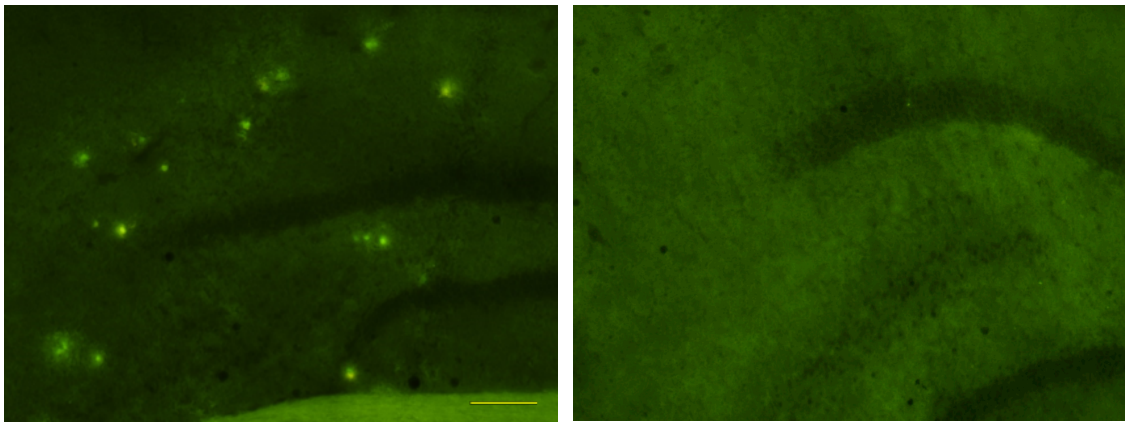

J20 hippocampal stains with ANCA-amide
λ_{max}=535 ± 8nm
n=22 (all hippocampal)

Figure 2.41: ANCA-amide J20 hippocampal Tissue Staining

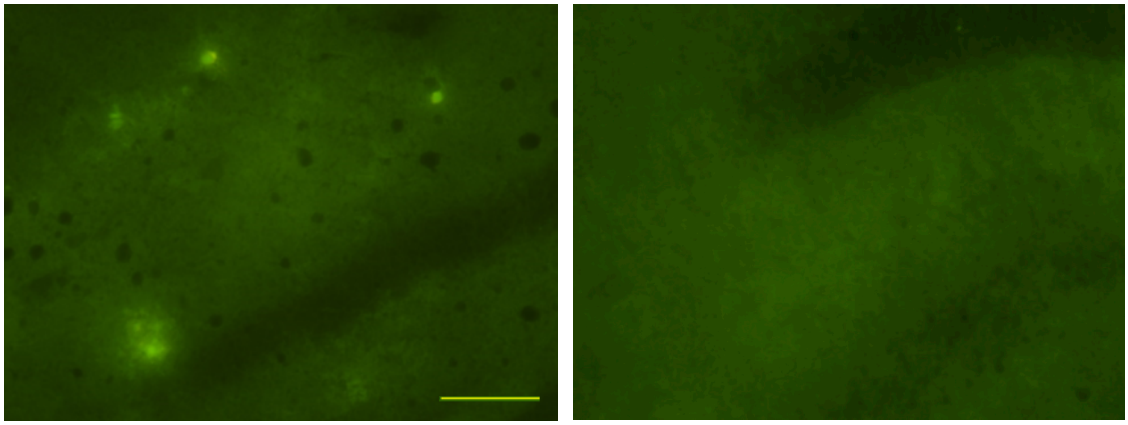

J20 hippocampal stains with ANCA-amide
λ_{max}=535 ± 8nm
n=22 (all hippocampal)

Figure 2.42: ANCA-amide J20 hippocampal Tissue Staining

2.10 ^{1}H and ^{13}C NMR Spectra

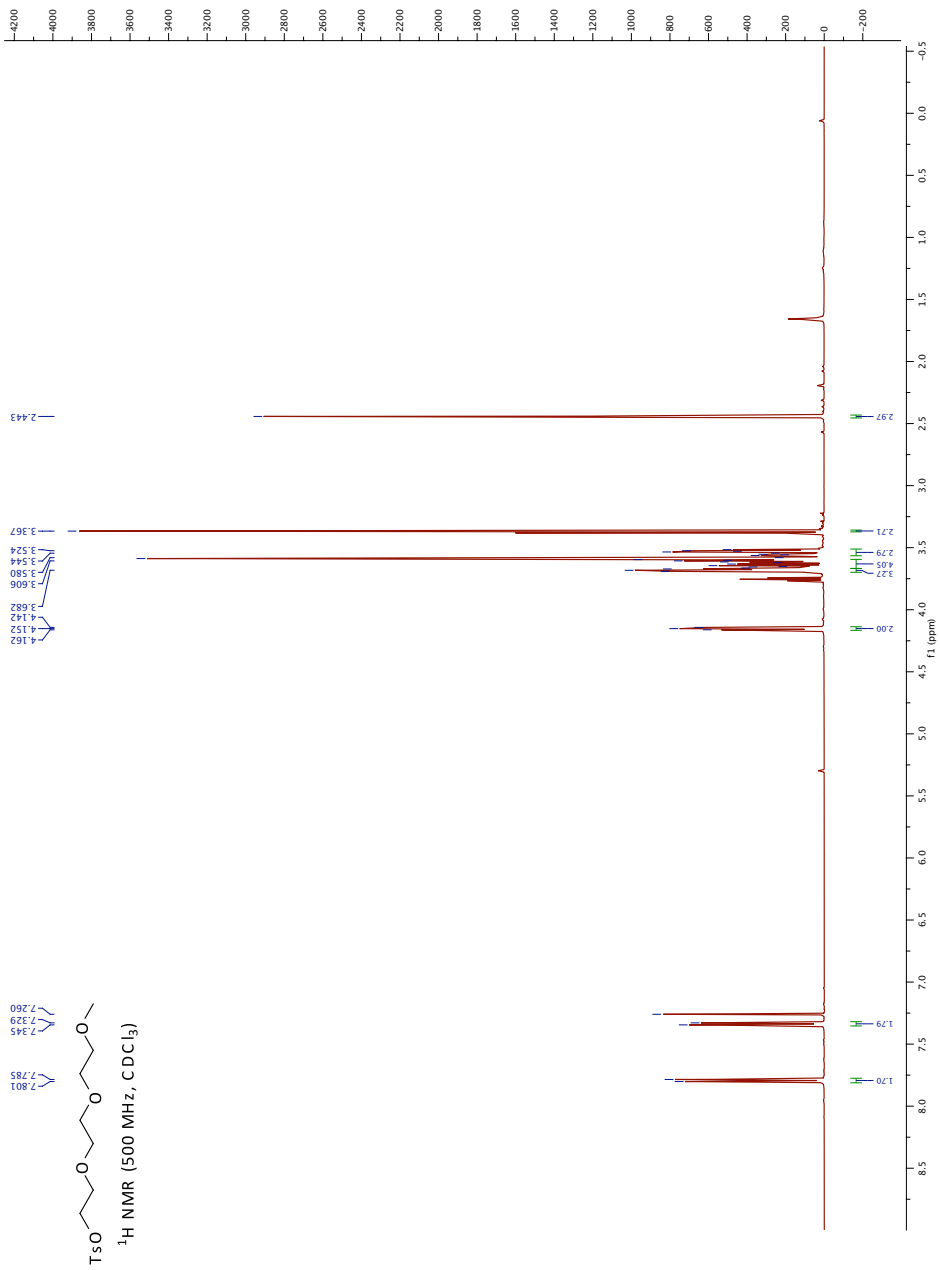

Spectrum 2.1: Compound 13: ^{1}H NMR

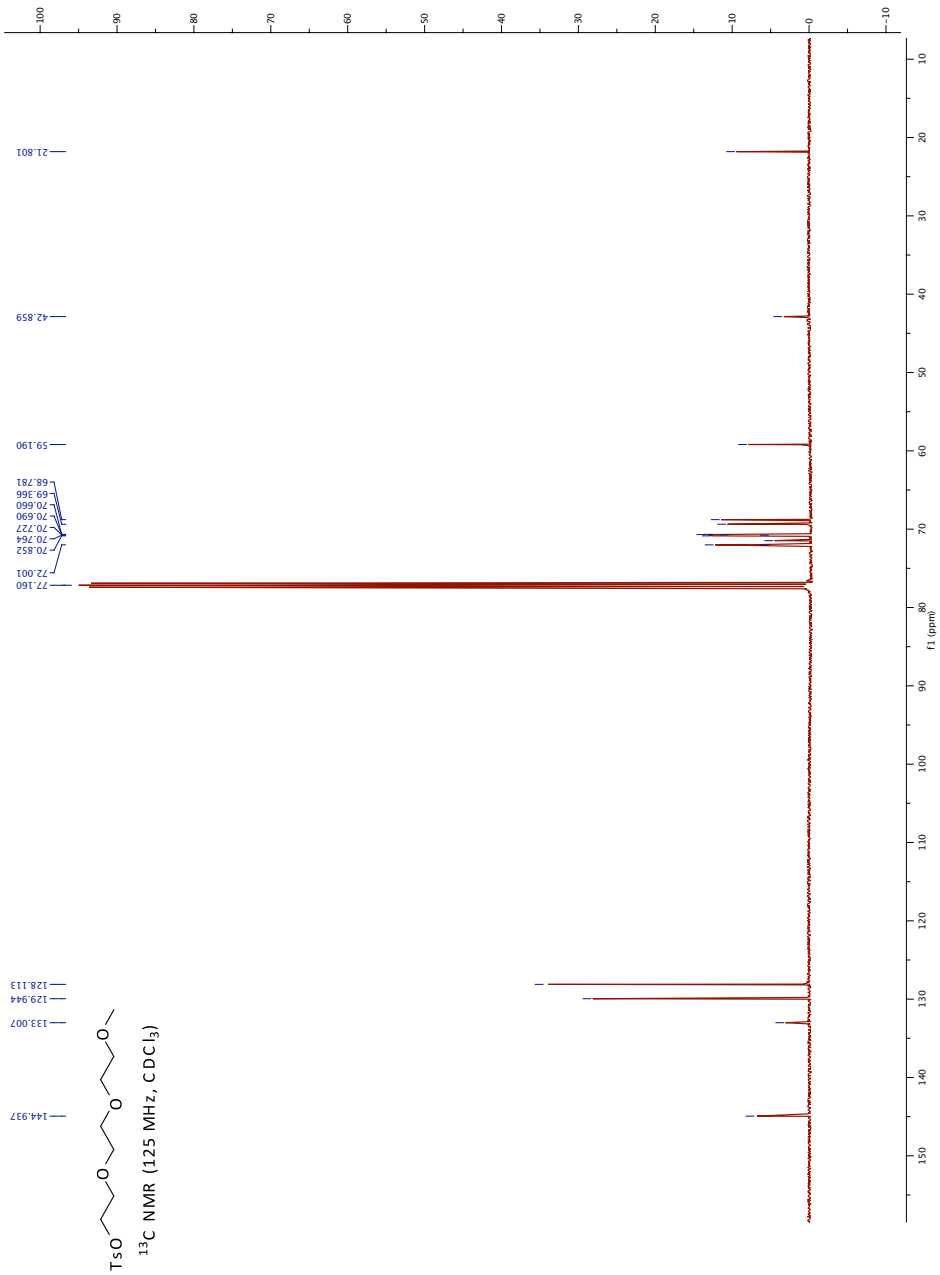

Spectrum 2.2: Compound 13: ^{13}C NMR

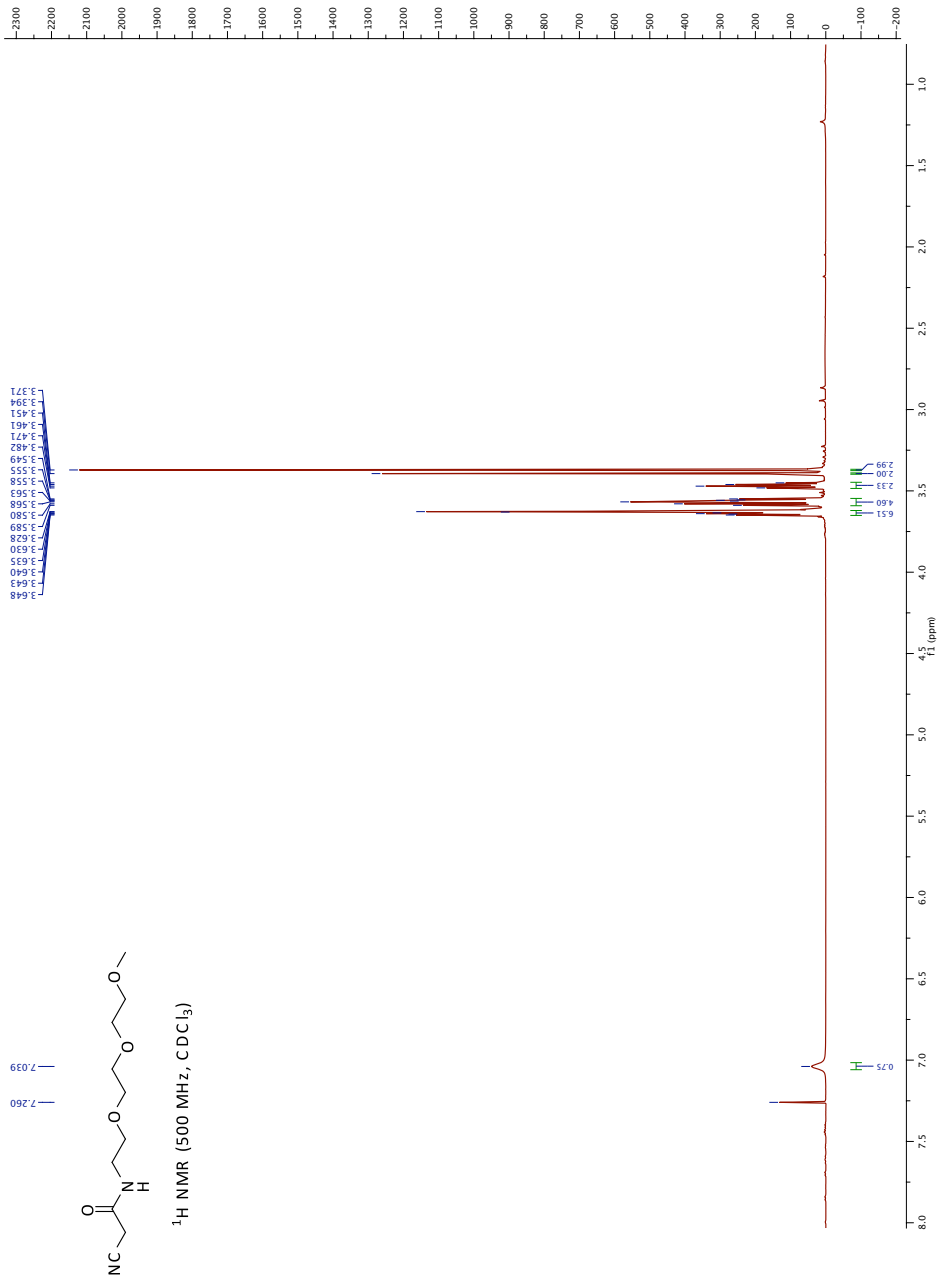

Spectrum 2.3: Compound 16: ^{1}H NMR

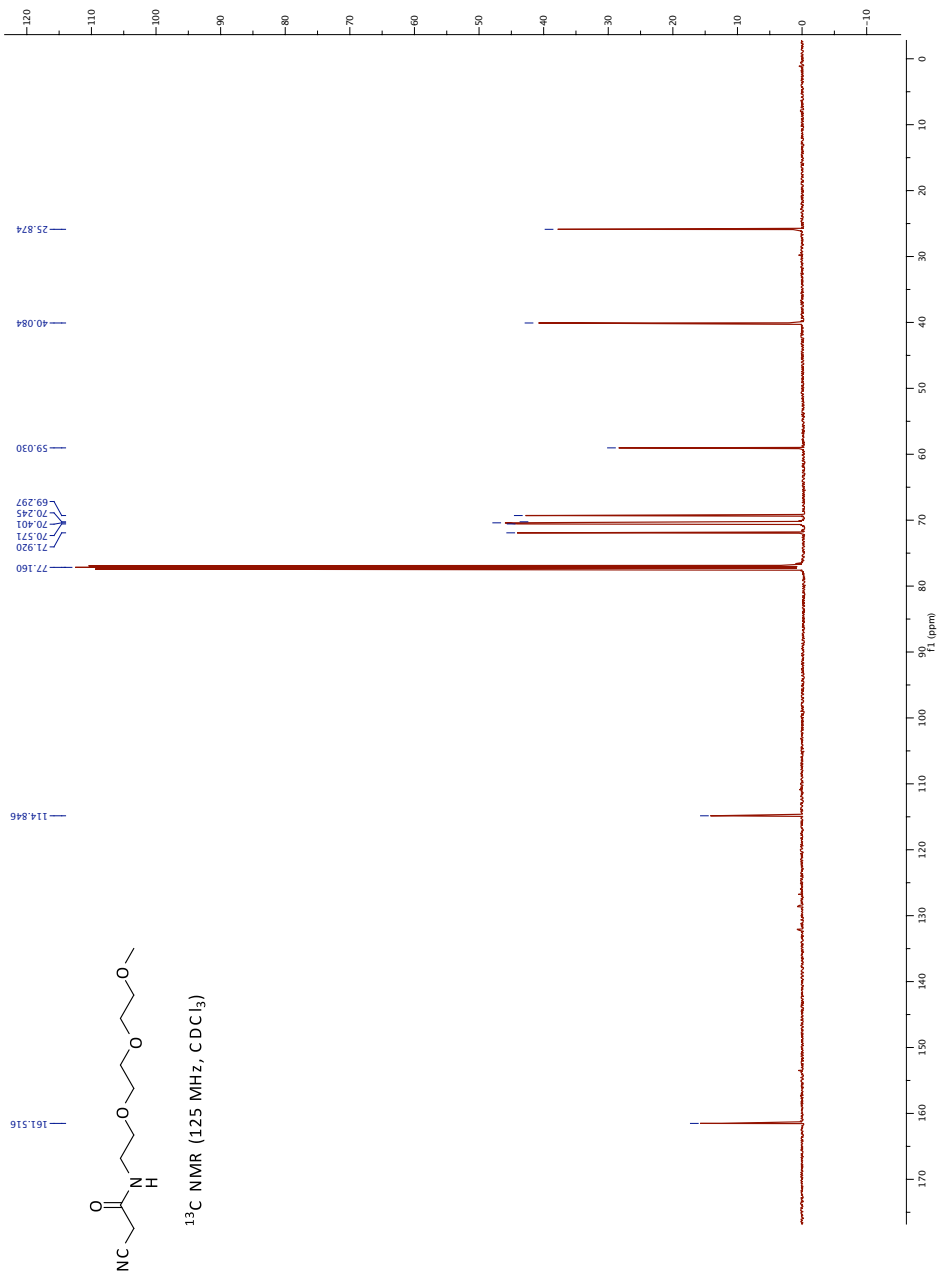

Spectrum 2.4: Compound 16: ^{13}C NMR

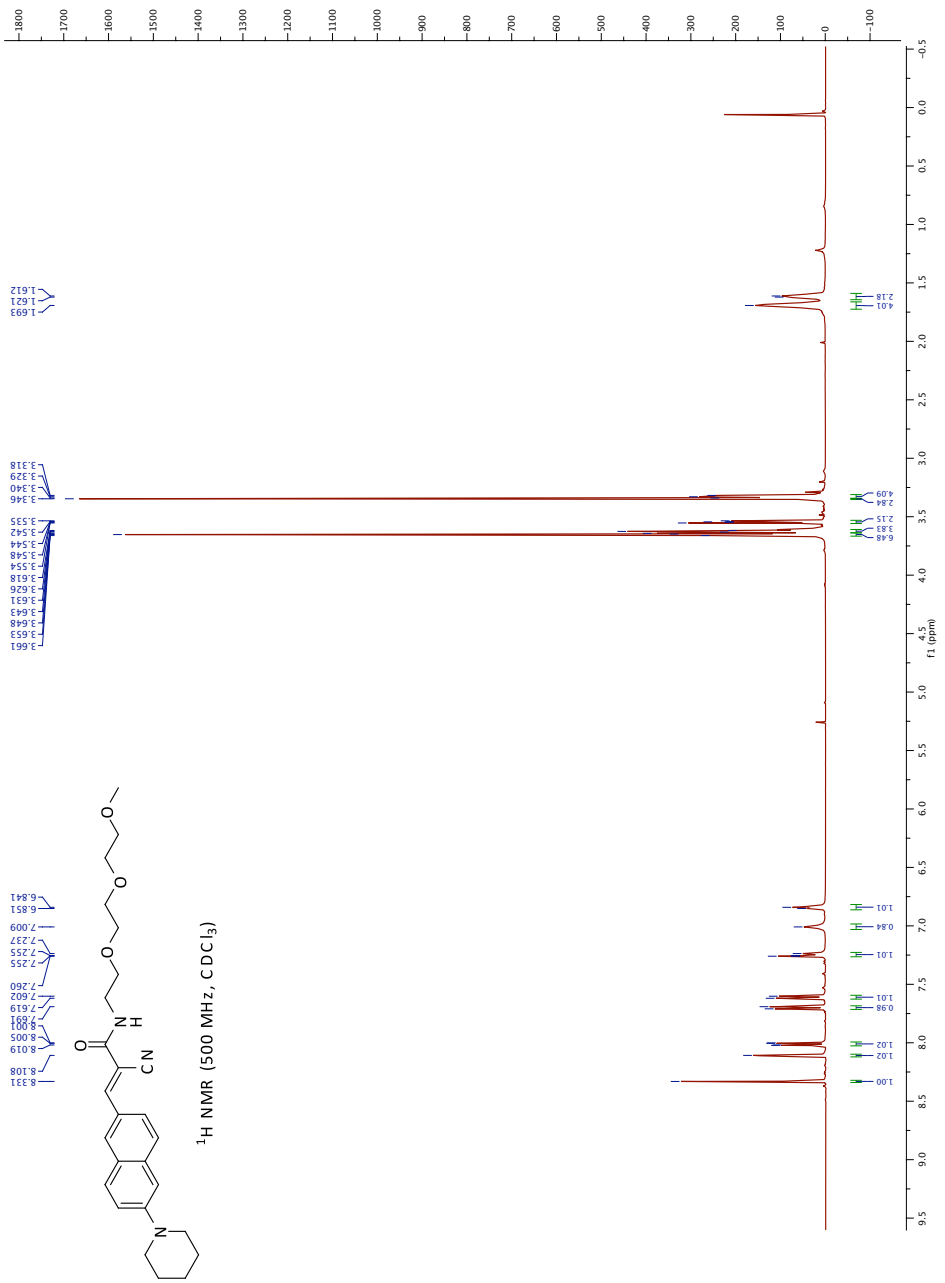

Spectrum 2.5: Compound 10: ^{1}H NMR

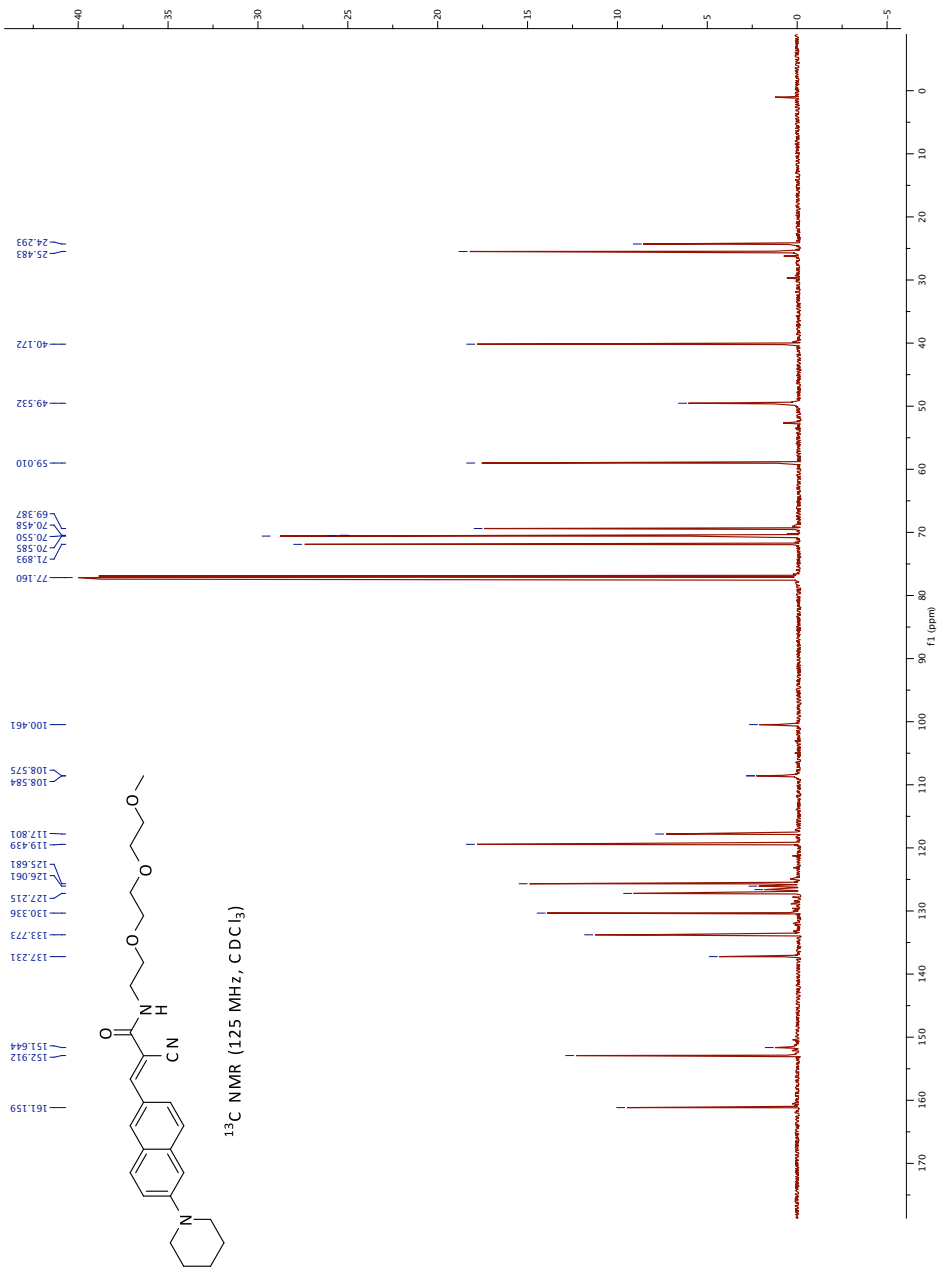

Spectrum 2.6: Compound 10: ^{13}C NMR

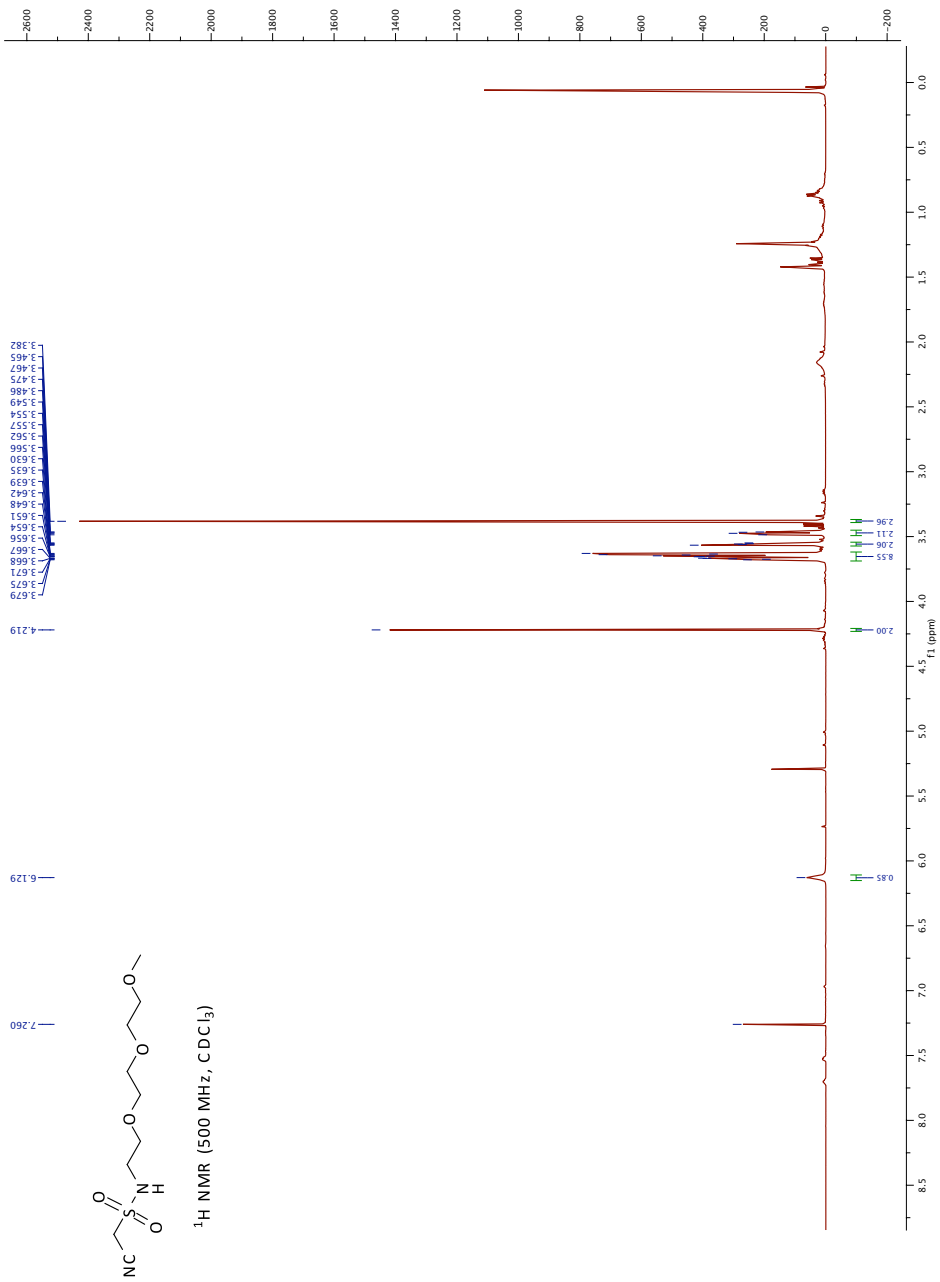

Spectrum 2.7: Compound 22: ^{1}H NMR

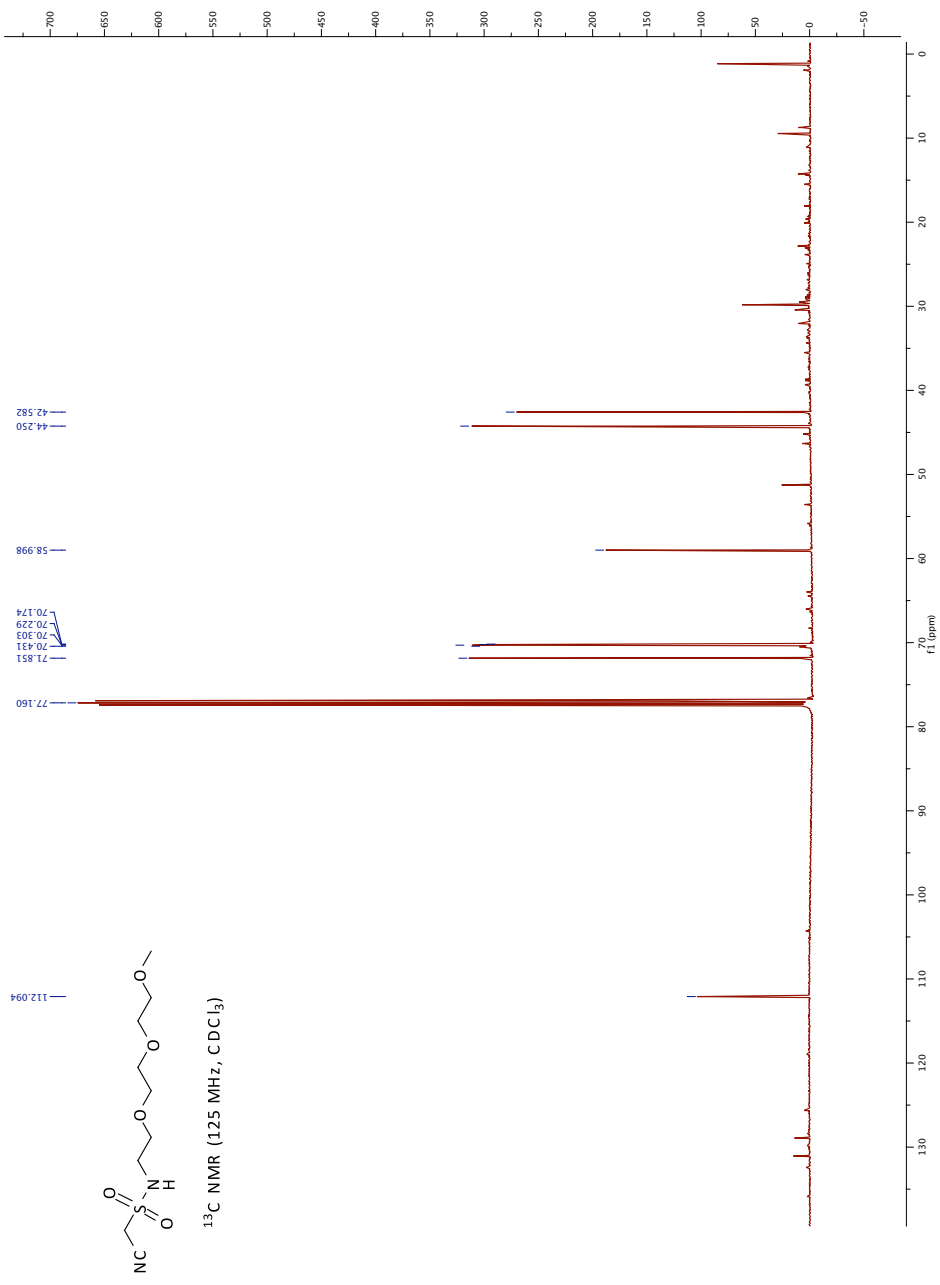

Spectrum 2.8: Compound 22: ^{13}C NMR

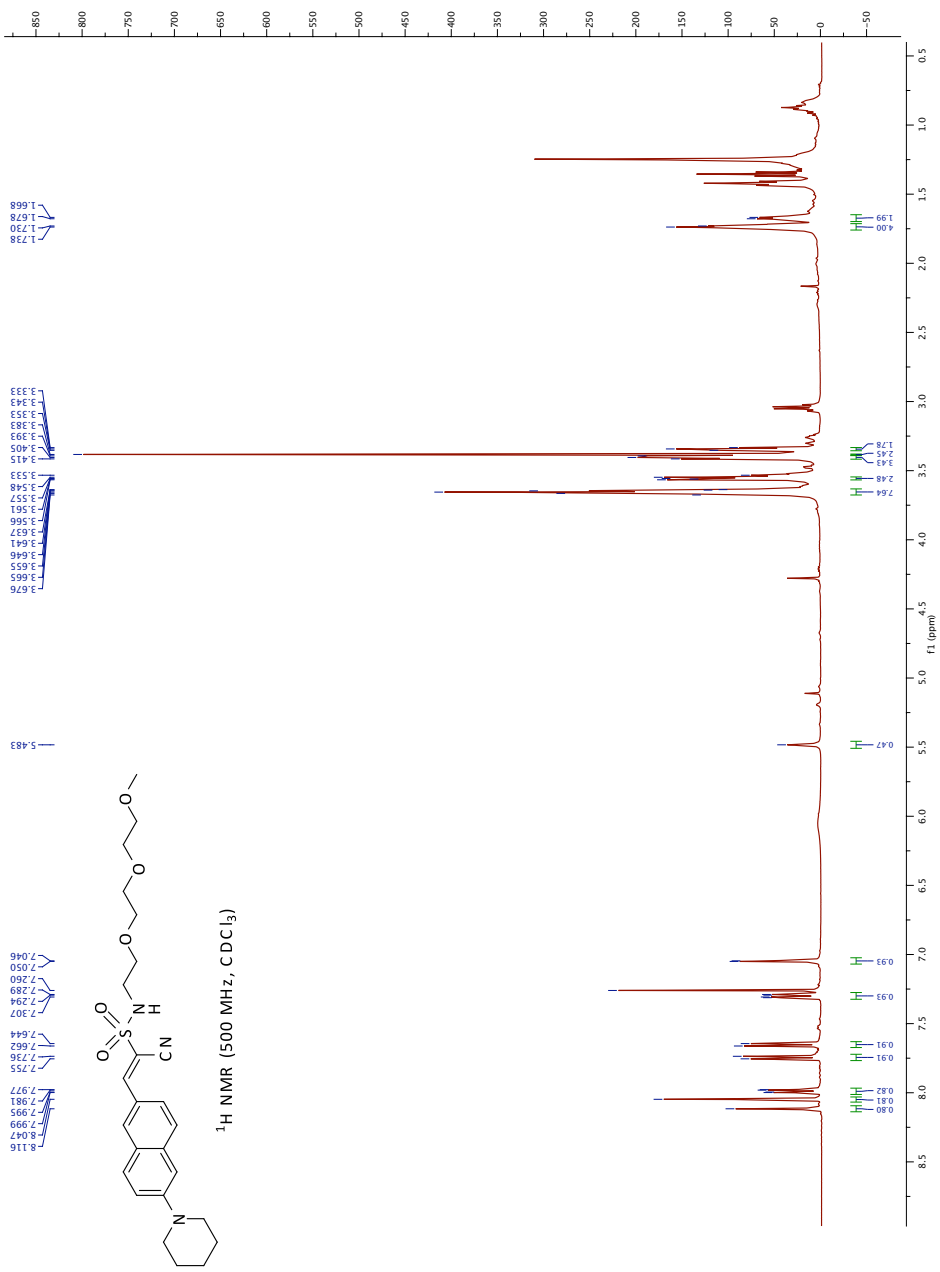

Spectrum 2.9: Compound 11: ^{1}H NMR

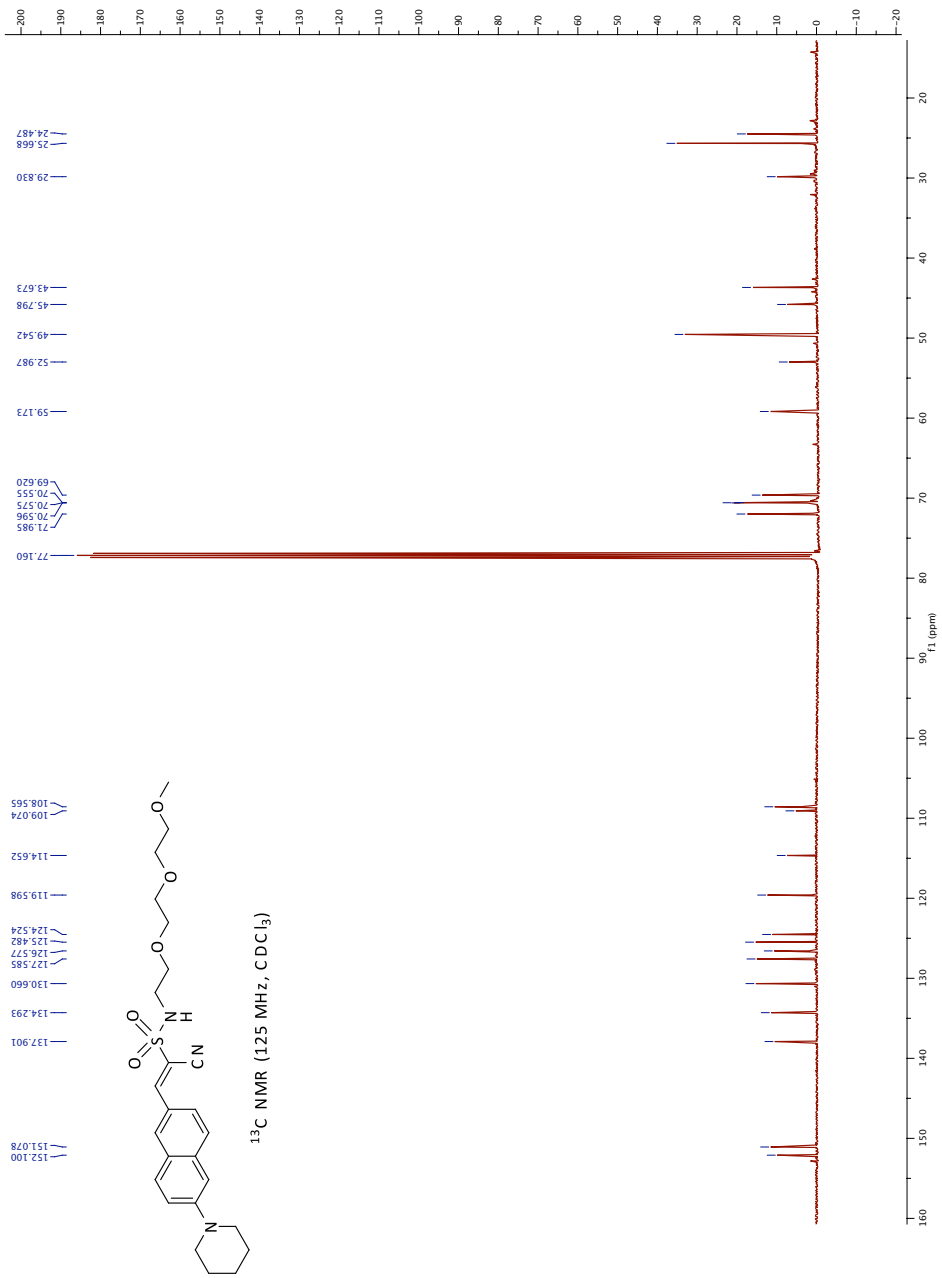

Spectrum 2.10: Compound 11: ^{13}C NMR

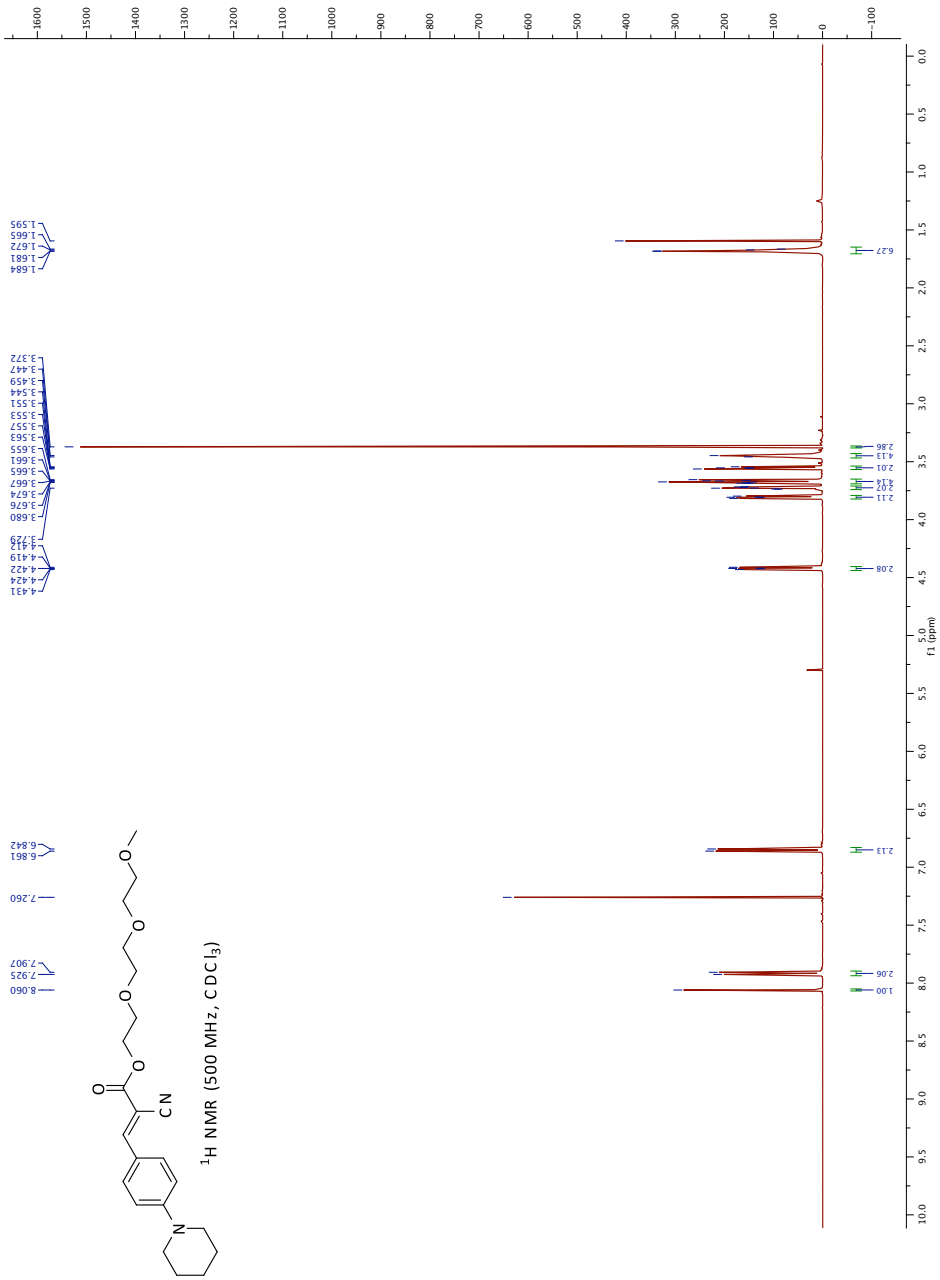

Spectrum 2.11: Compound 29: ^{1}H NMR

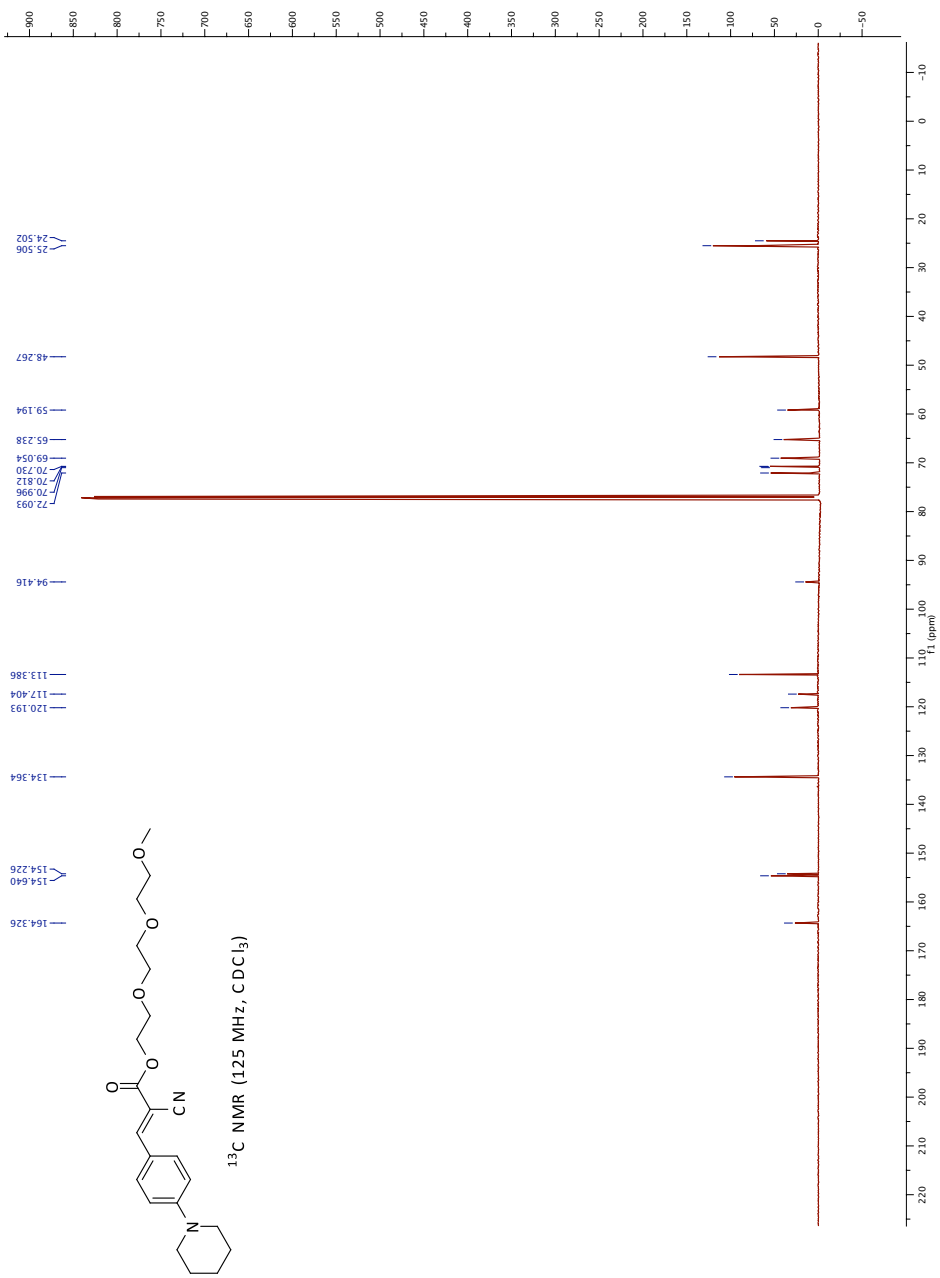

Spectrum 2.12: Compound 29: ^{13}C NMR

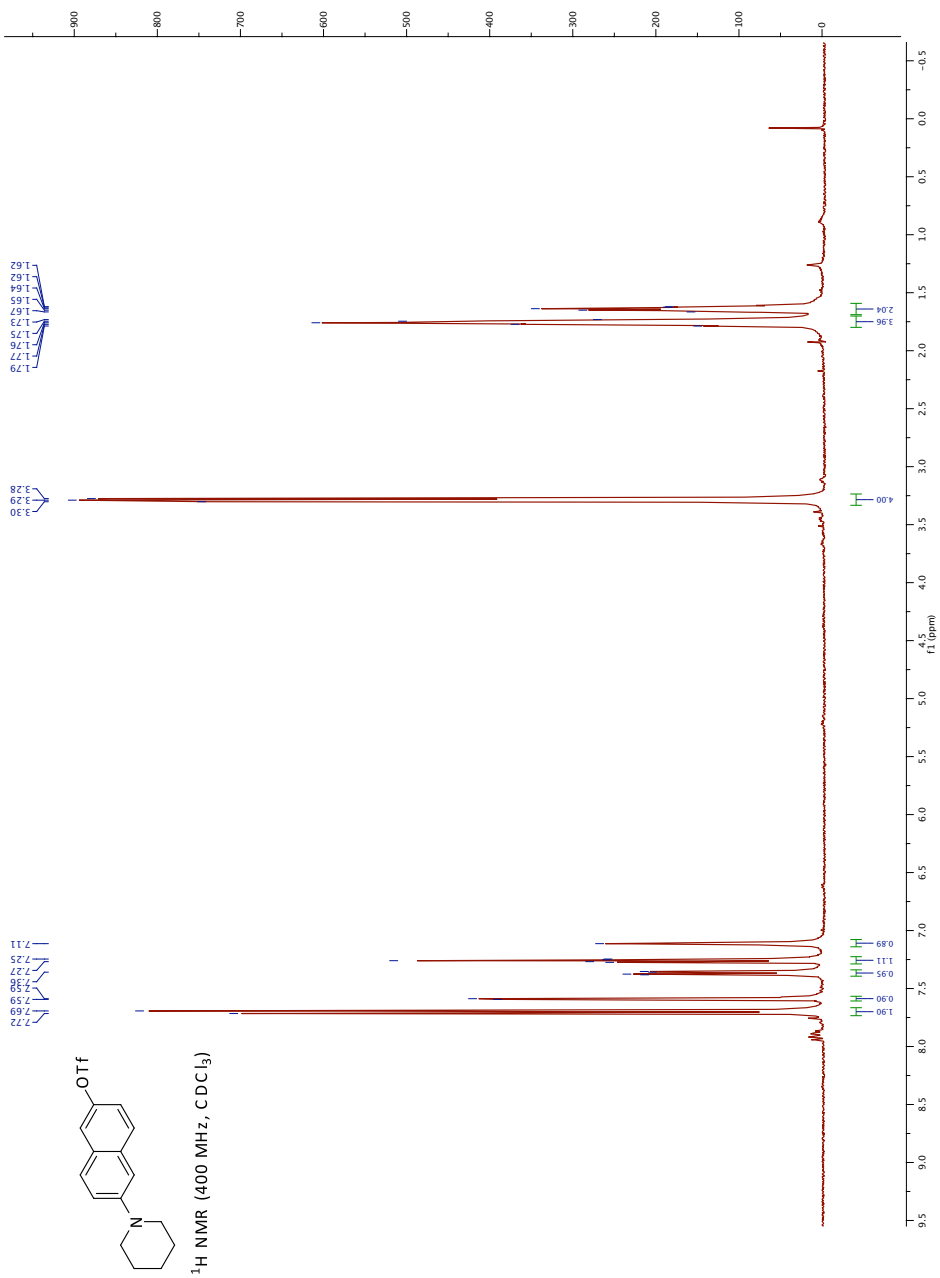

Spectrum 2.13: Compound 26: ^{1}H NMR

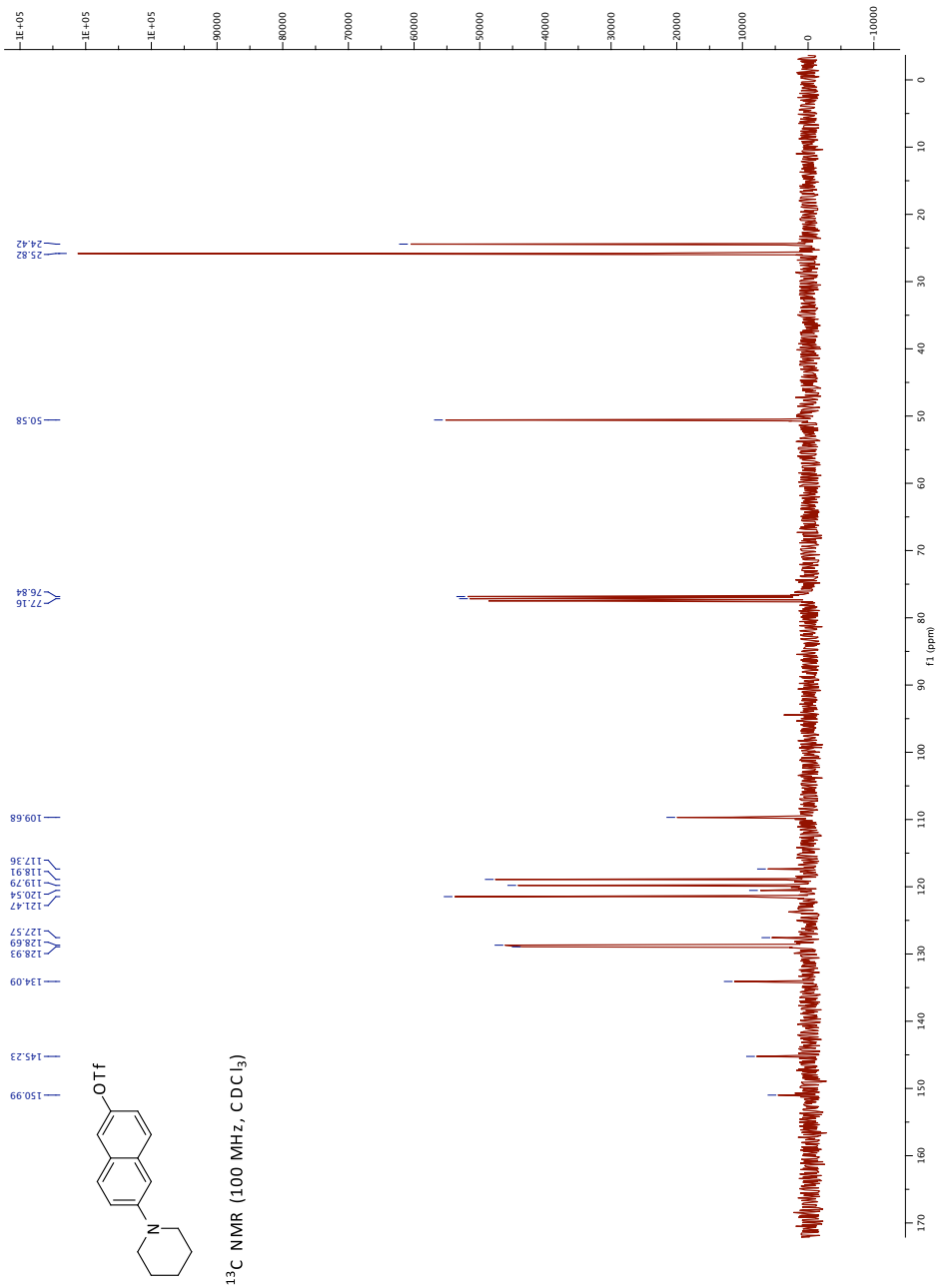

Spectrum 2.14: Compound 26: ^{13}C NMR

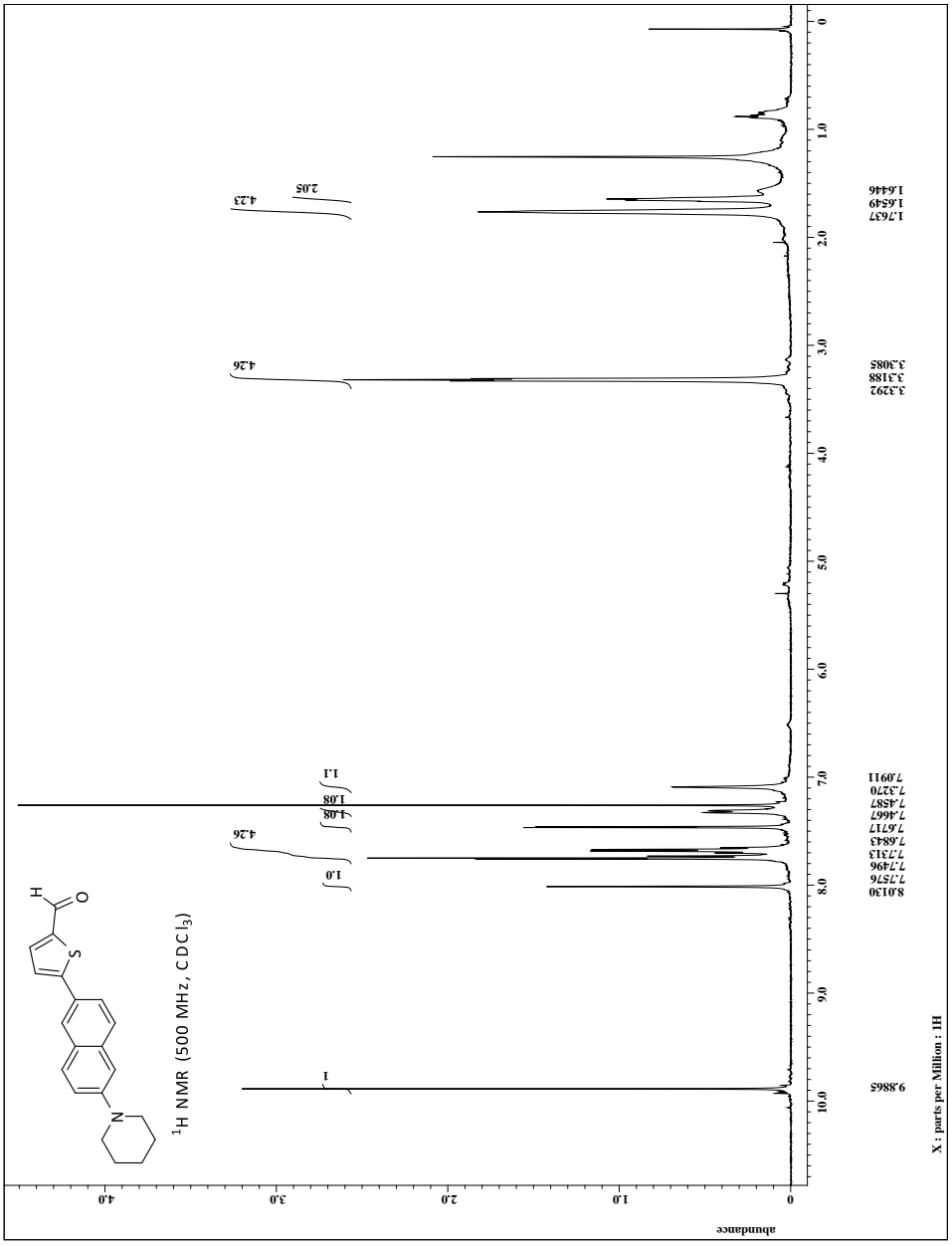

Spectrum 2.15: Compound 35: ^{1}H NMR

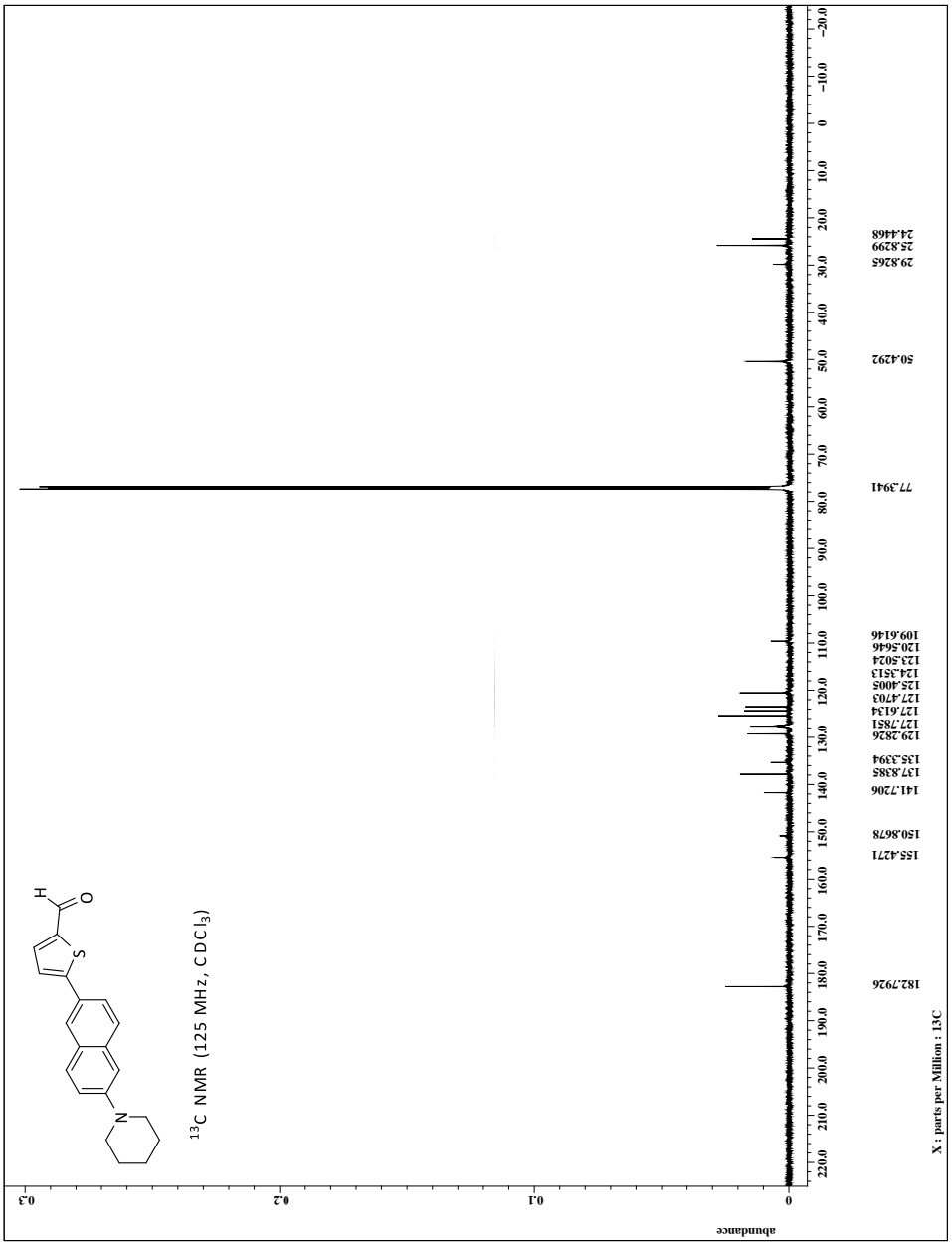

Spectrum 2.16: Compound 35: ^{13}C NMR

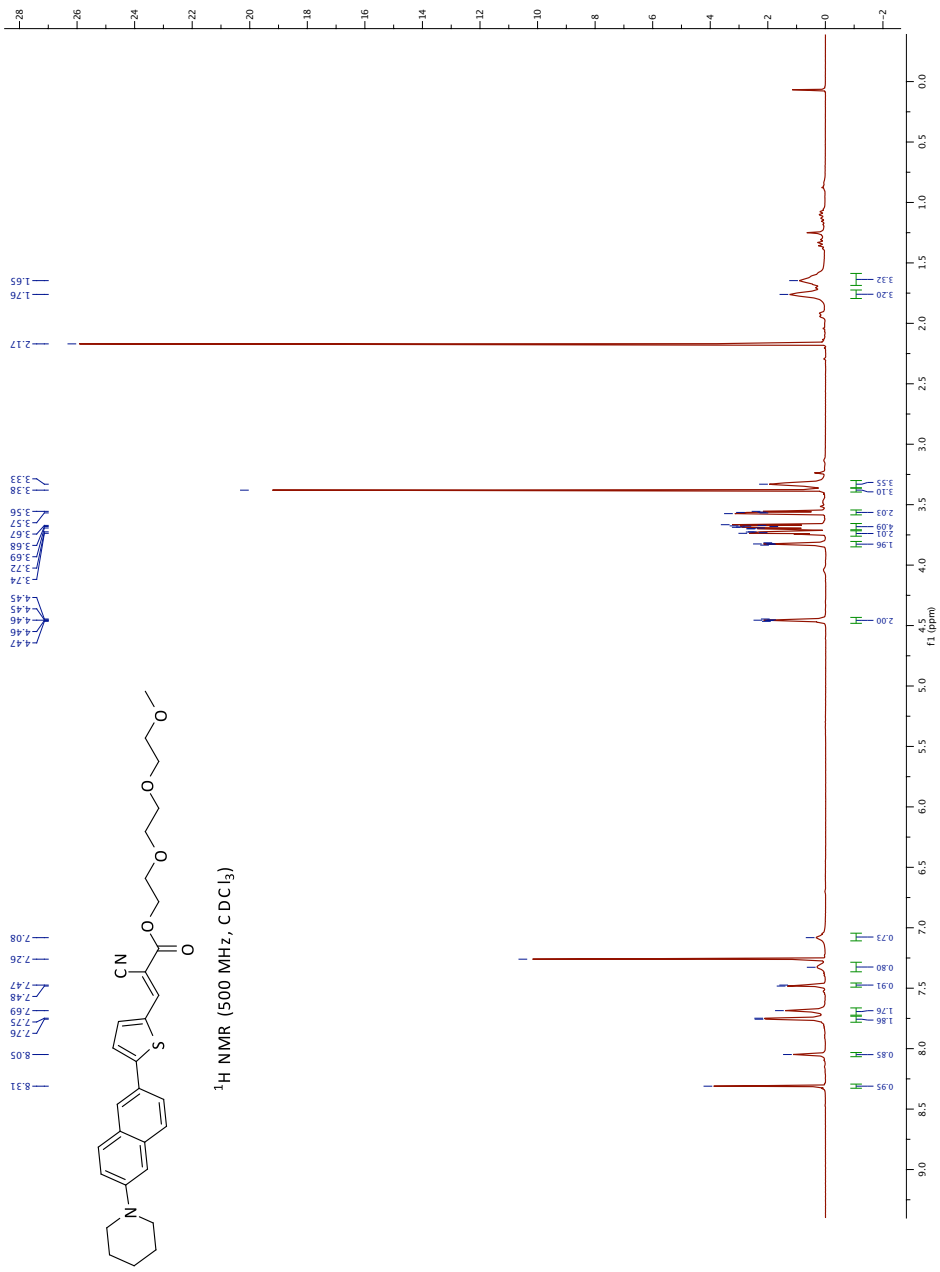

Spectrum 2.17: Compound 30: ^{1}H NMR

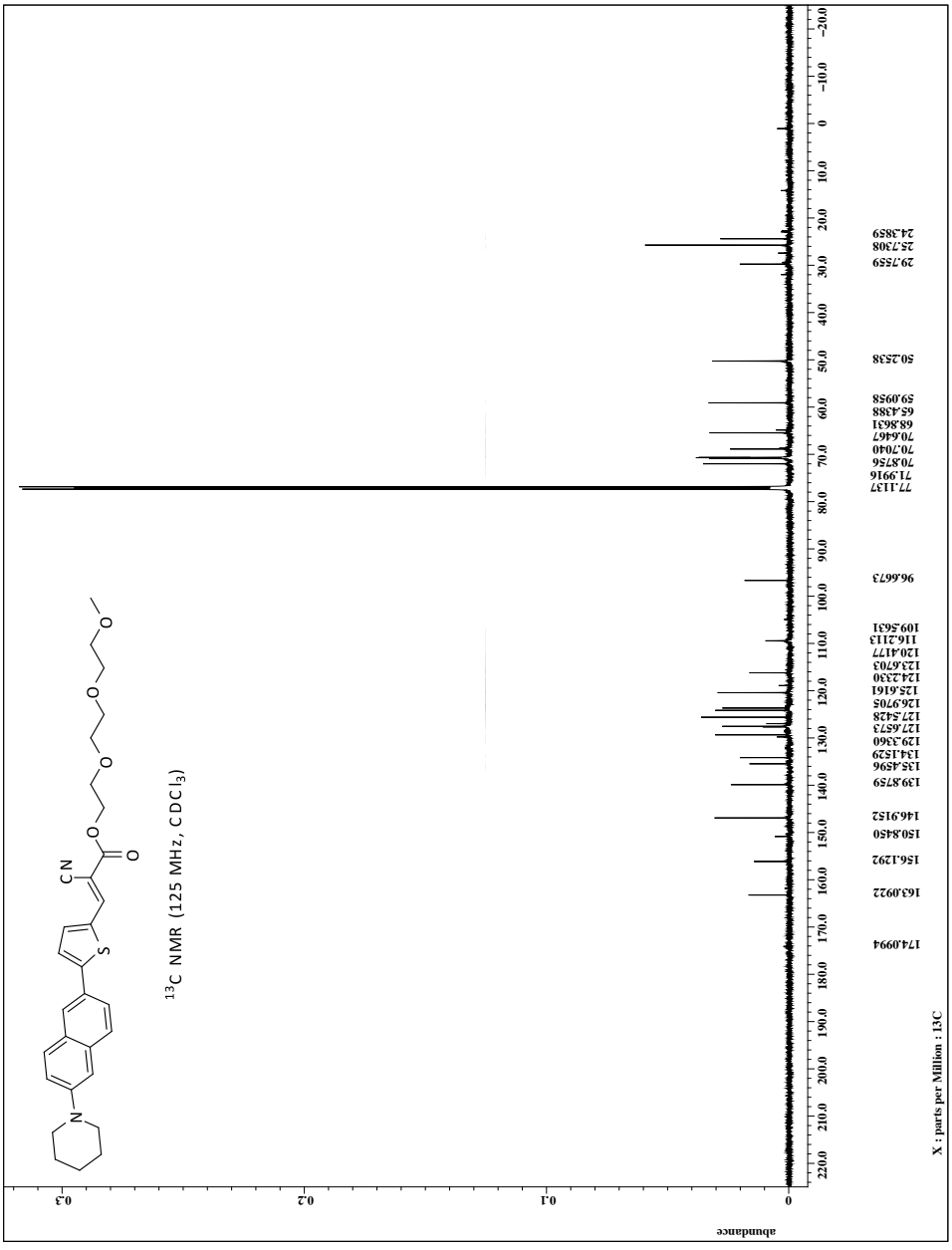

Spectrum 2.18: Compound 30: ^{13}C NMR

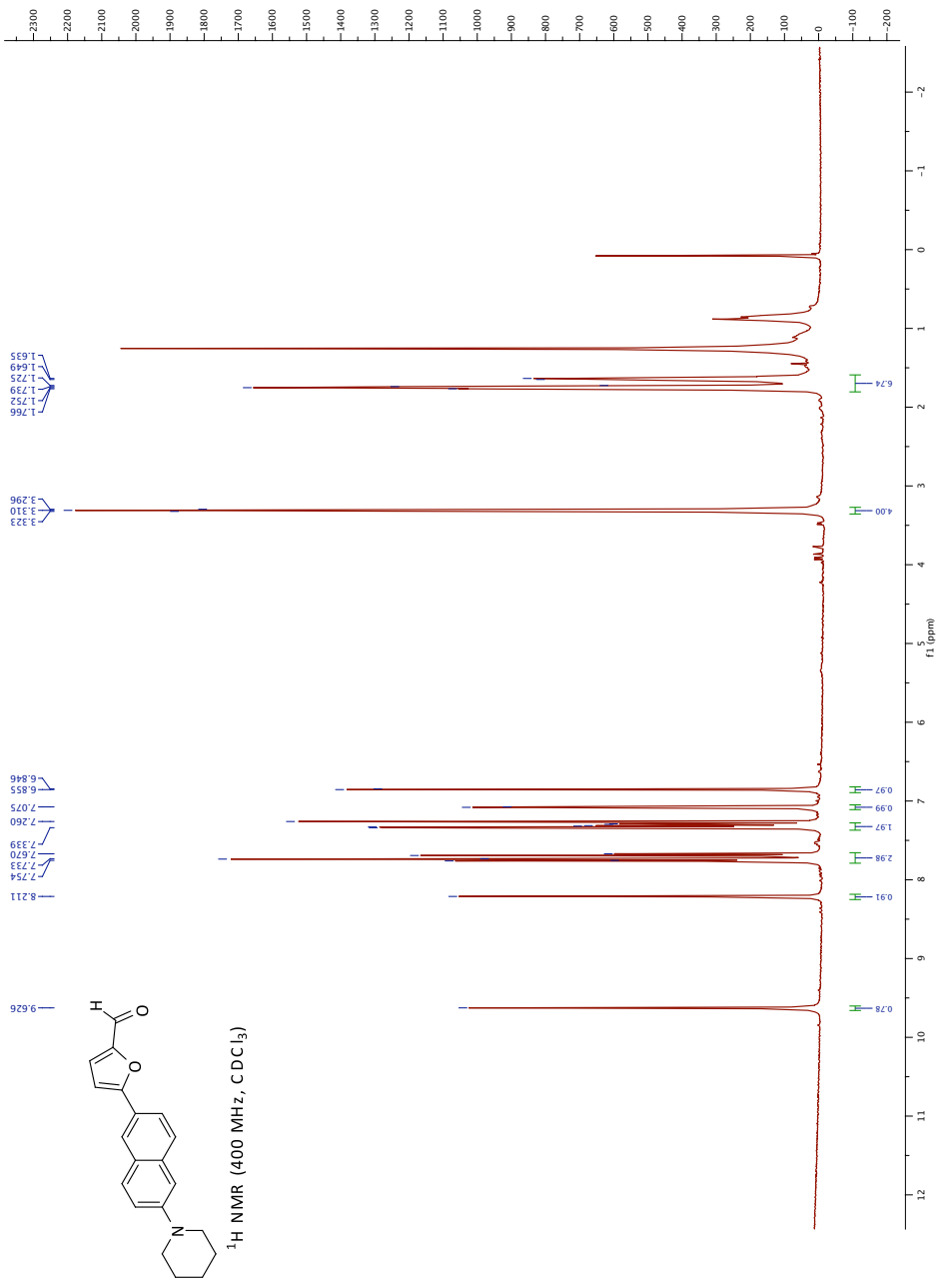

Spectrum 2.19: Compound 39: ^{1}H NMR

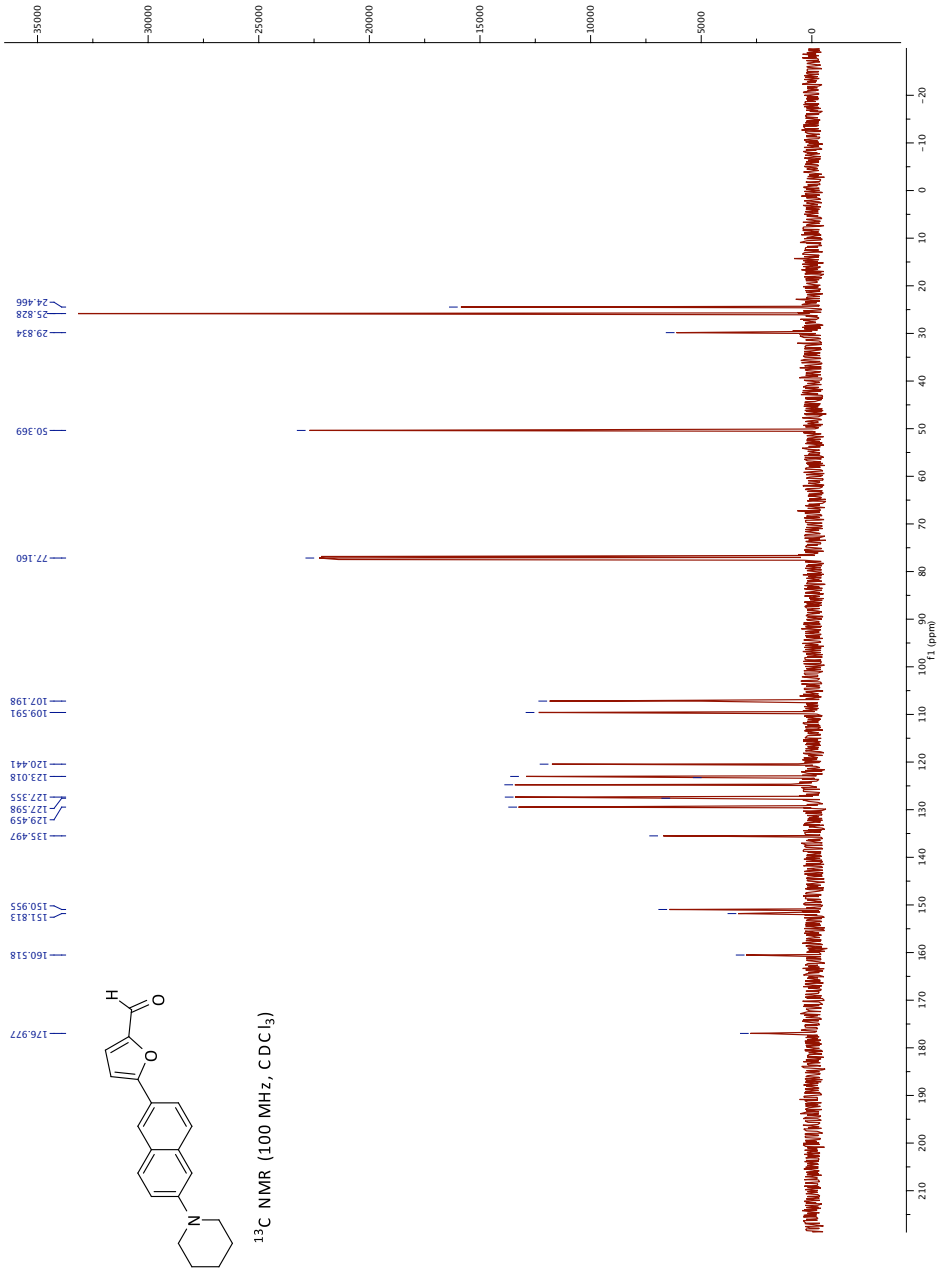

Spectrum 2.20: Compound 39: ^{13}C NMR

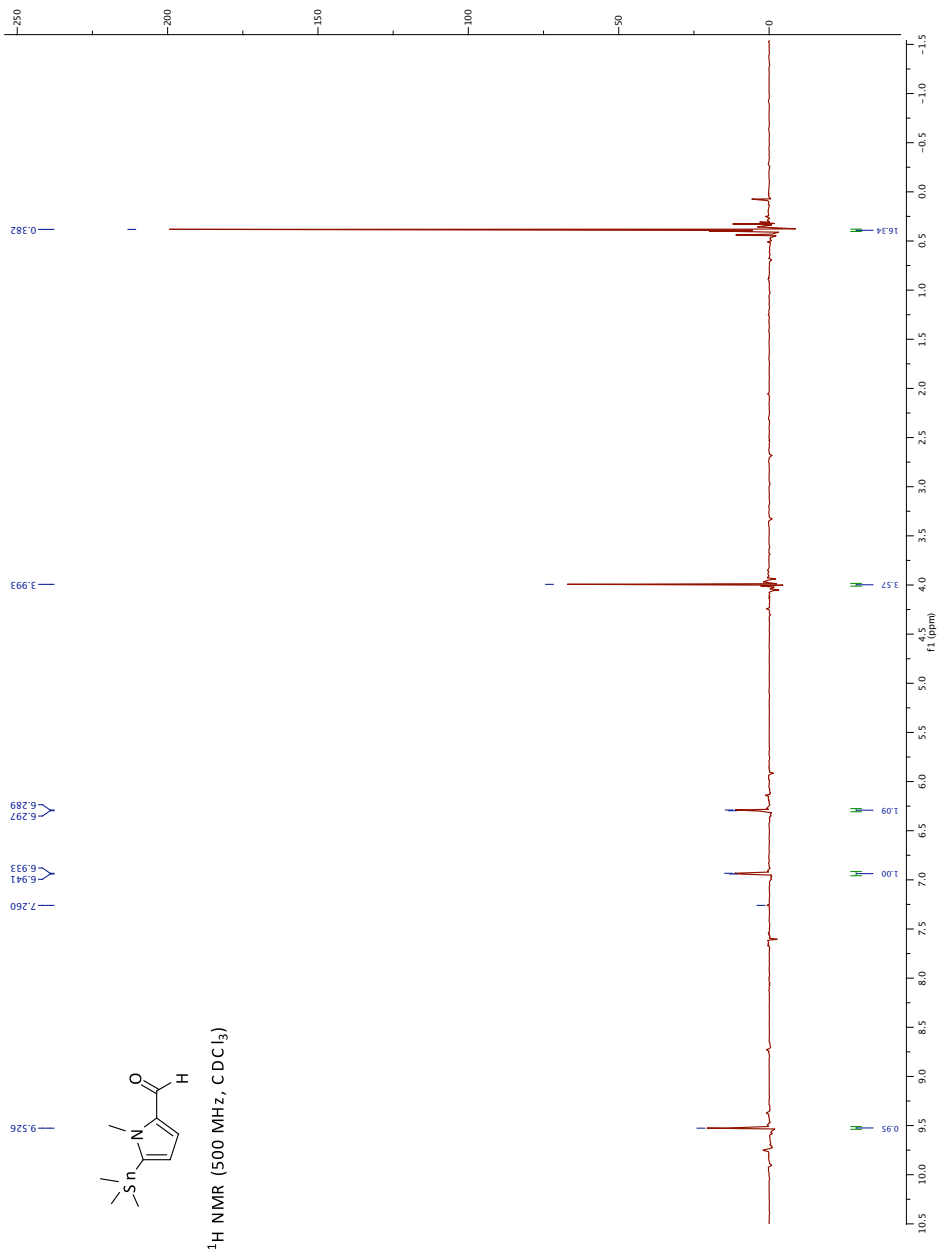

Spectrum 2.21: Compound 40: ^{1}H NMR

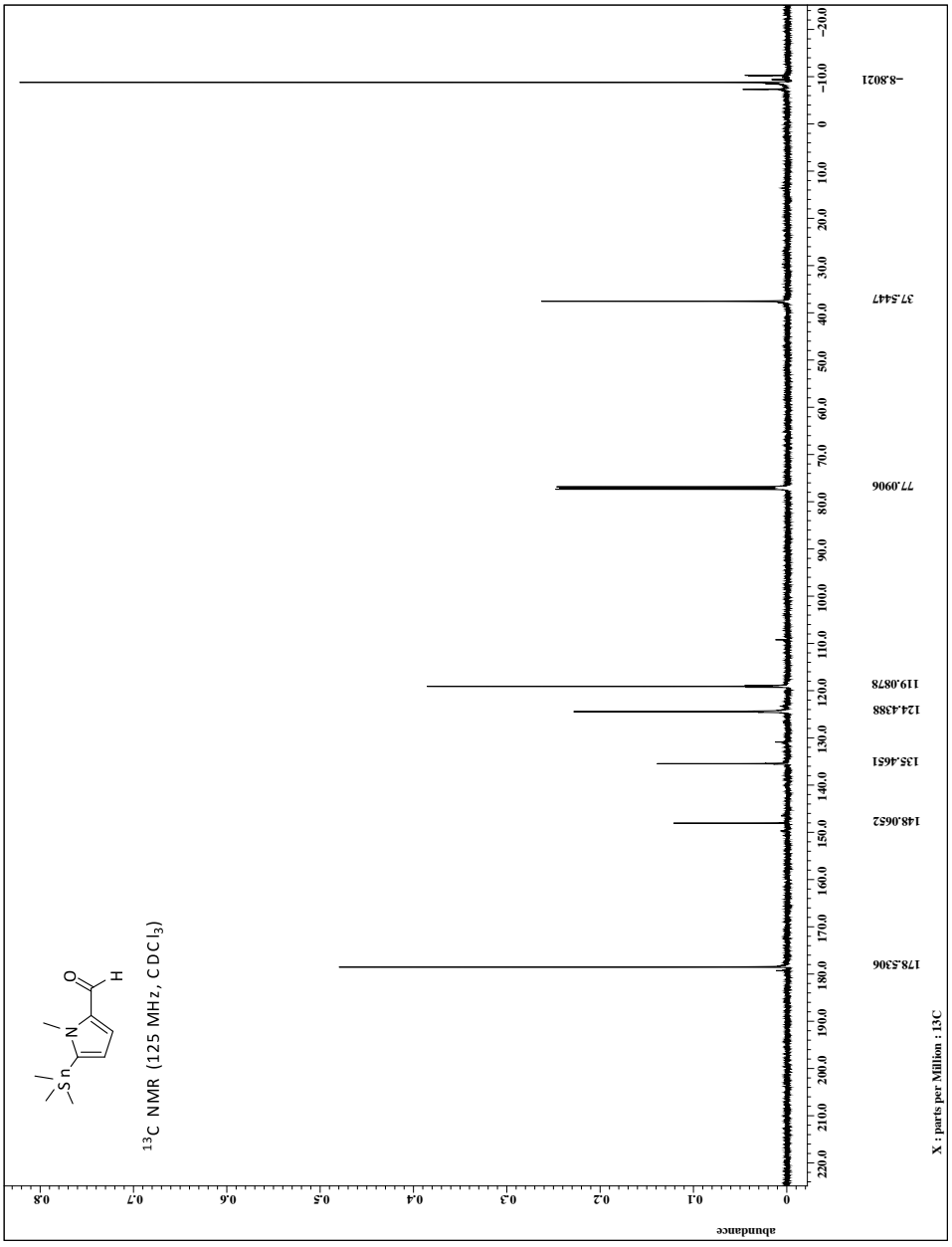

Spectrum 2.22: Compound 40: ^{13}C NMR

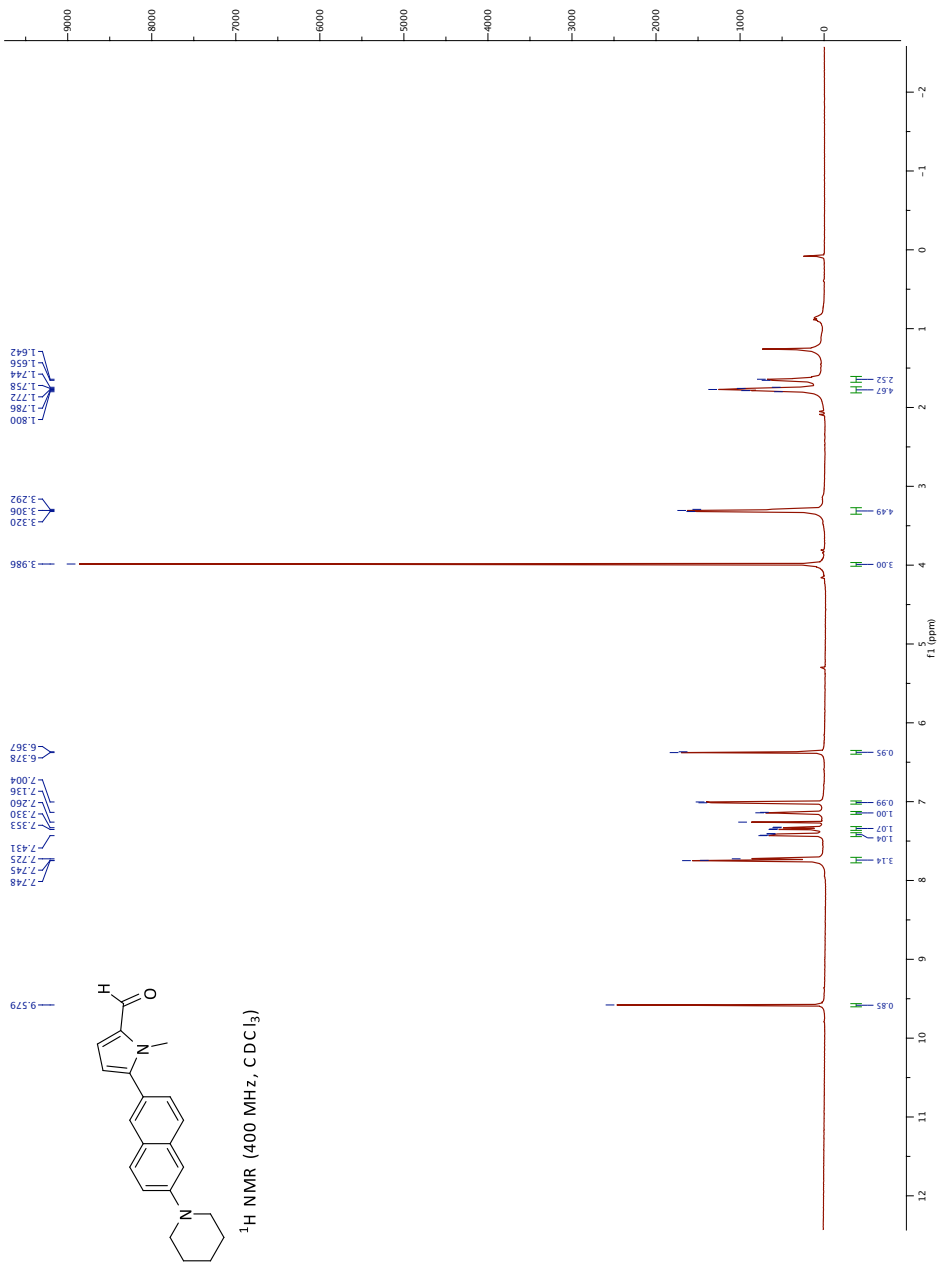

Spectrum 2.23: Compound 41: ^{1}H NMR

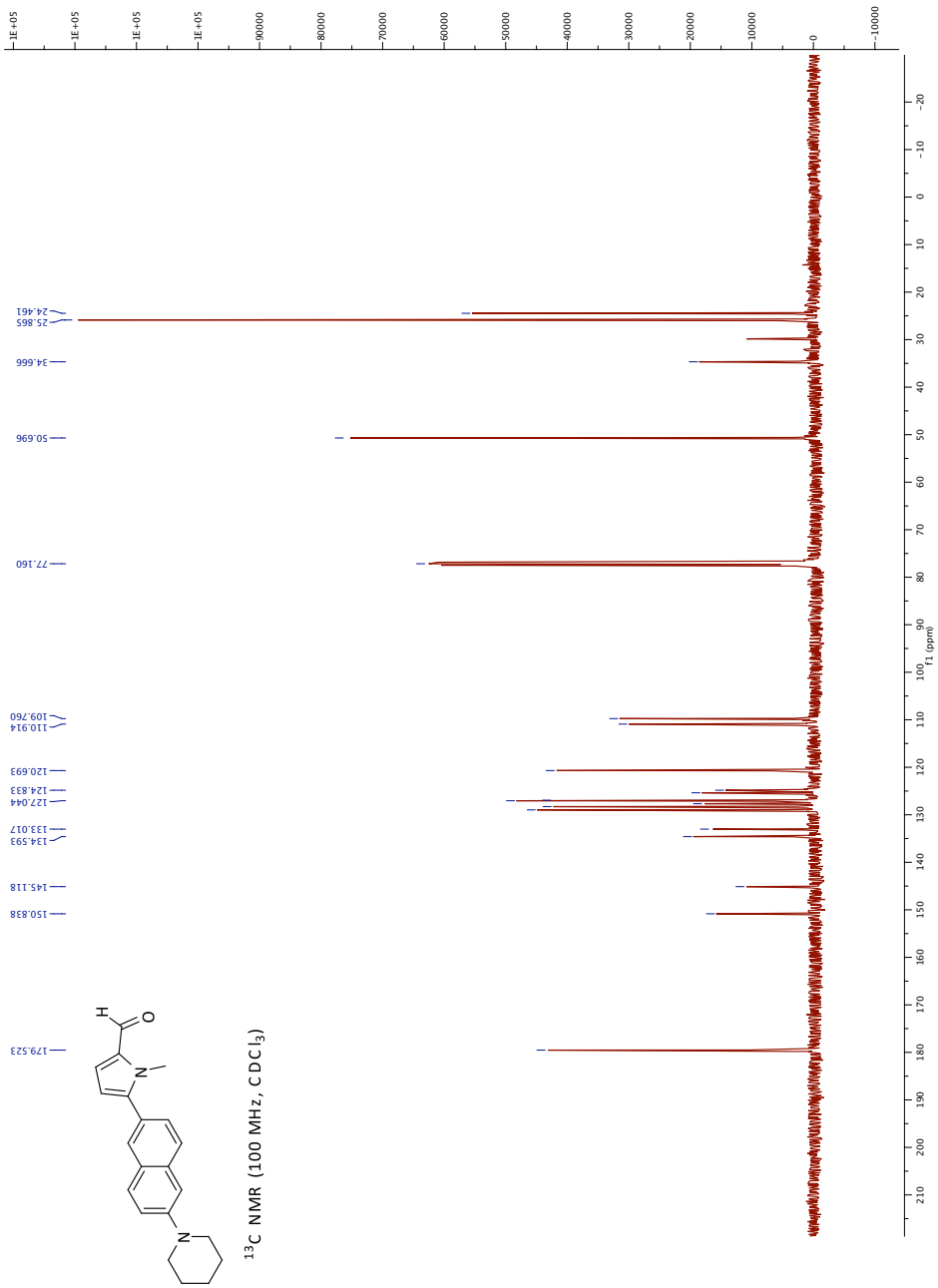

Spectrum 2.24: Compound 41: ^{13}C NMR

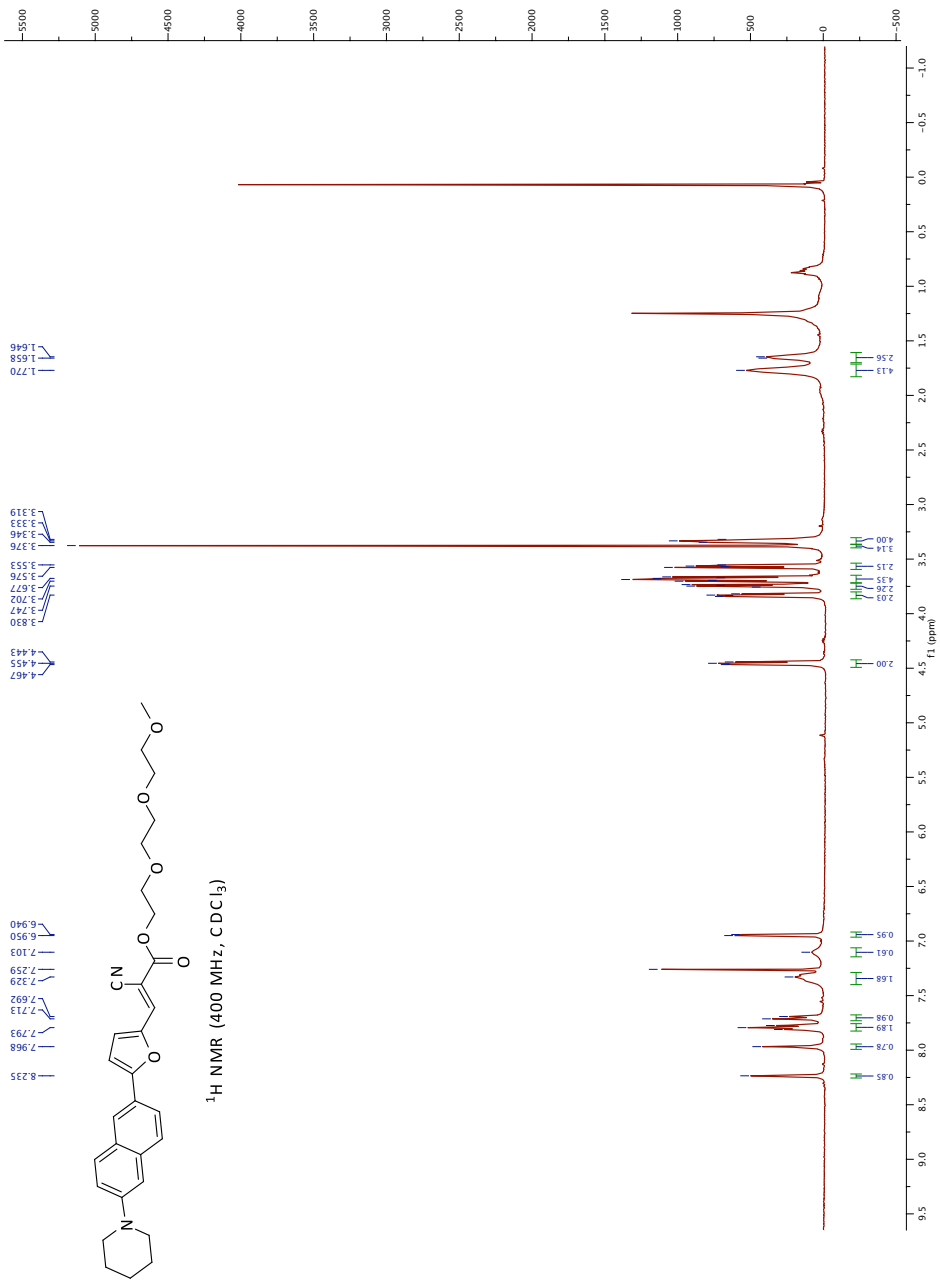

Spectrum 2.25: Compound 36: ^{1}H NMR

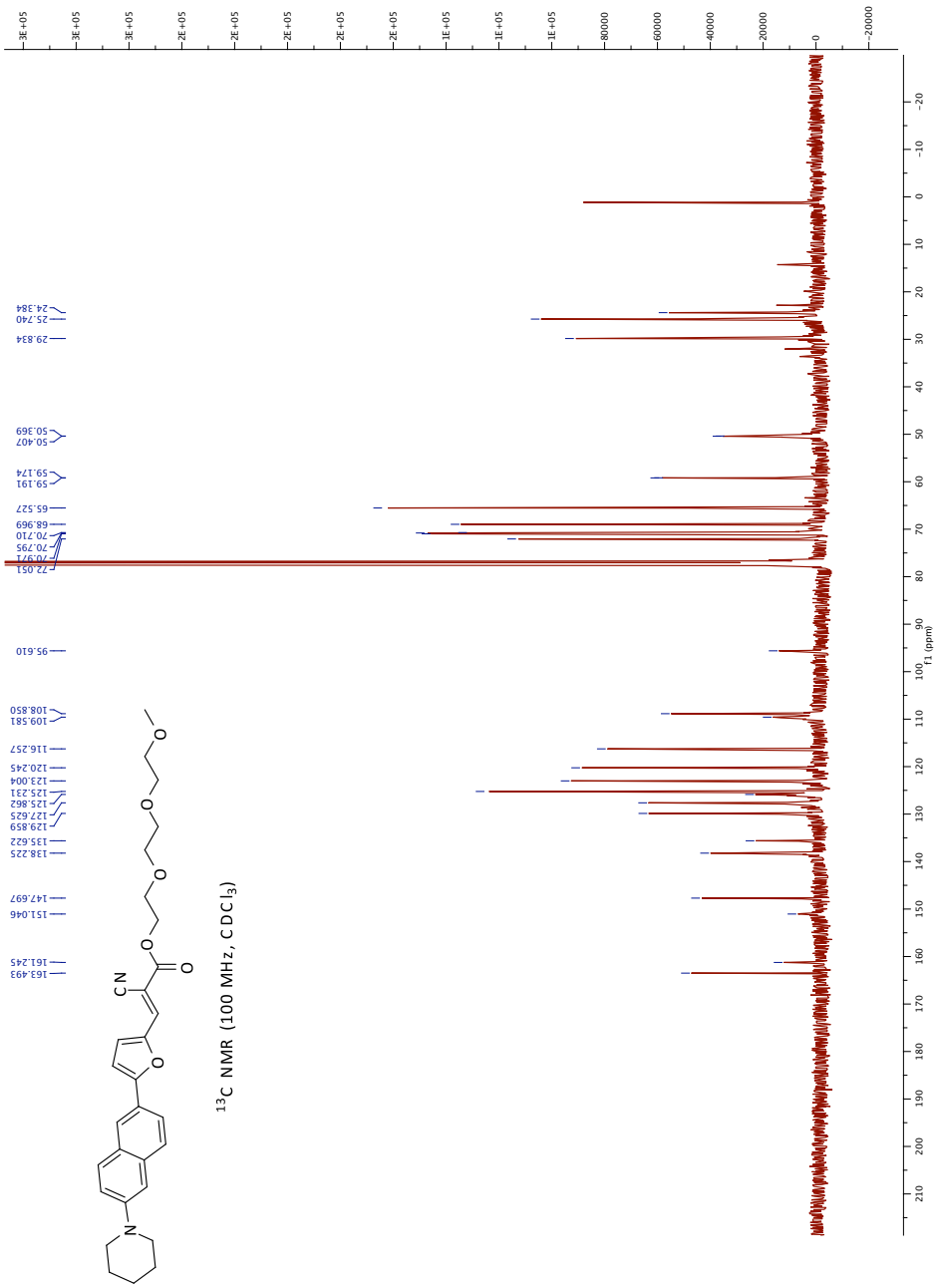

Spectrum 2.26: Compound 36: ^{13}C NMR

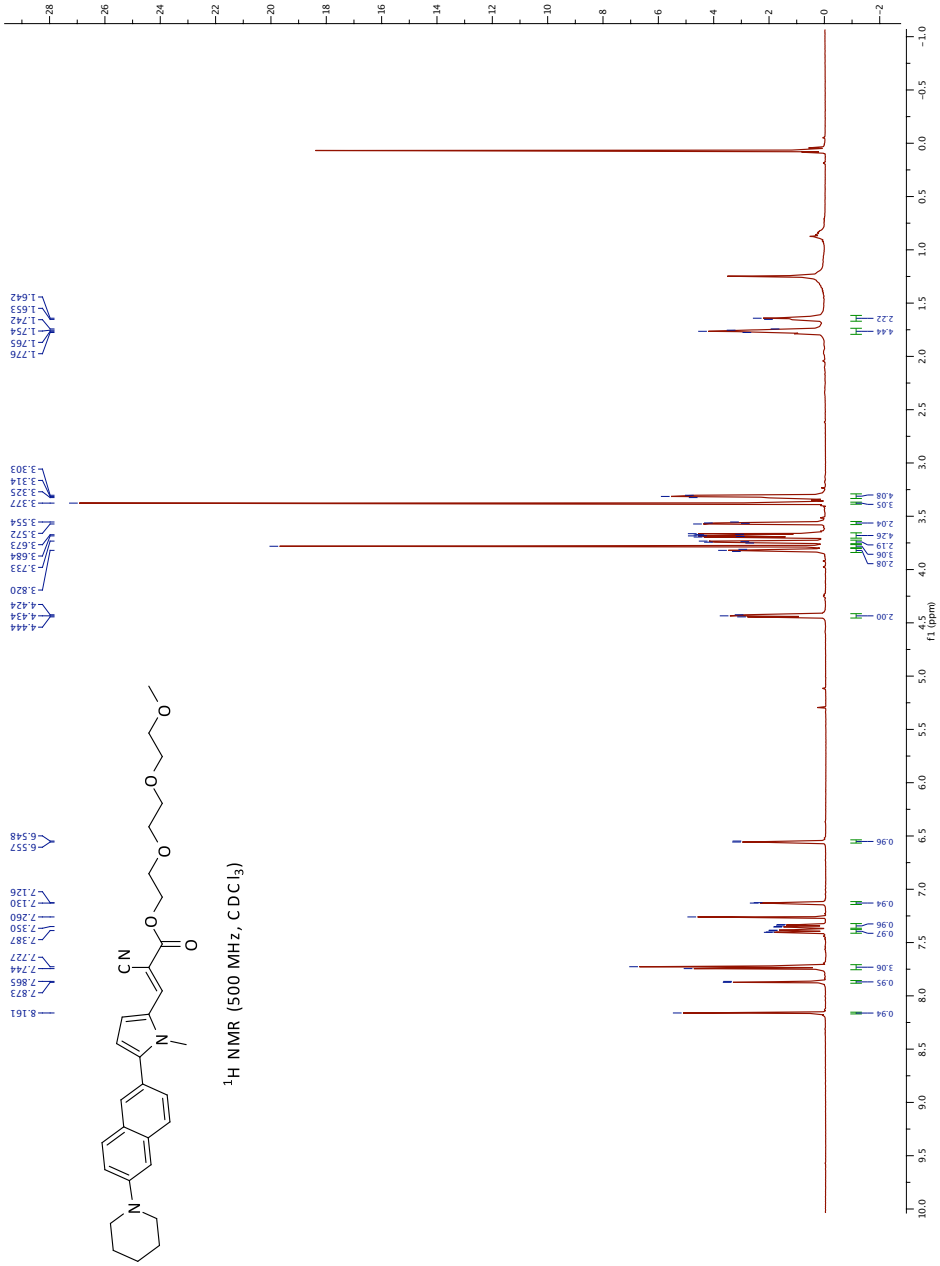

Spectrum 2.27: Compound 37: ^{1}H NMR

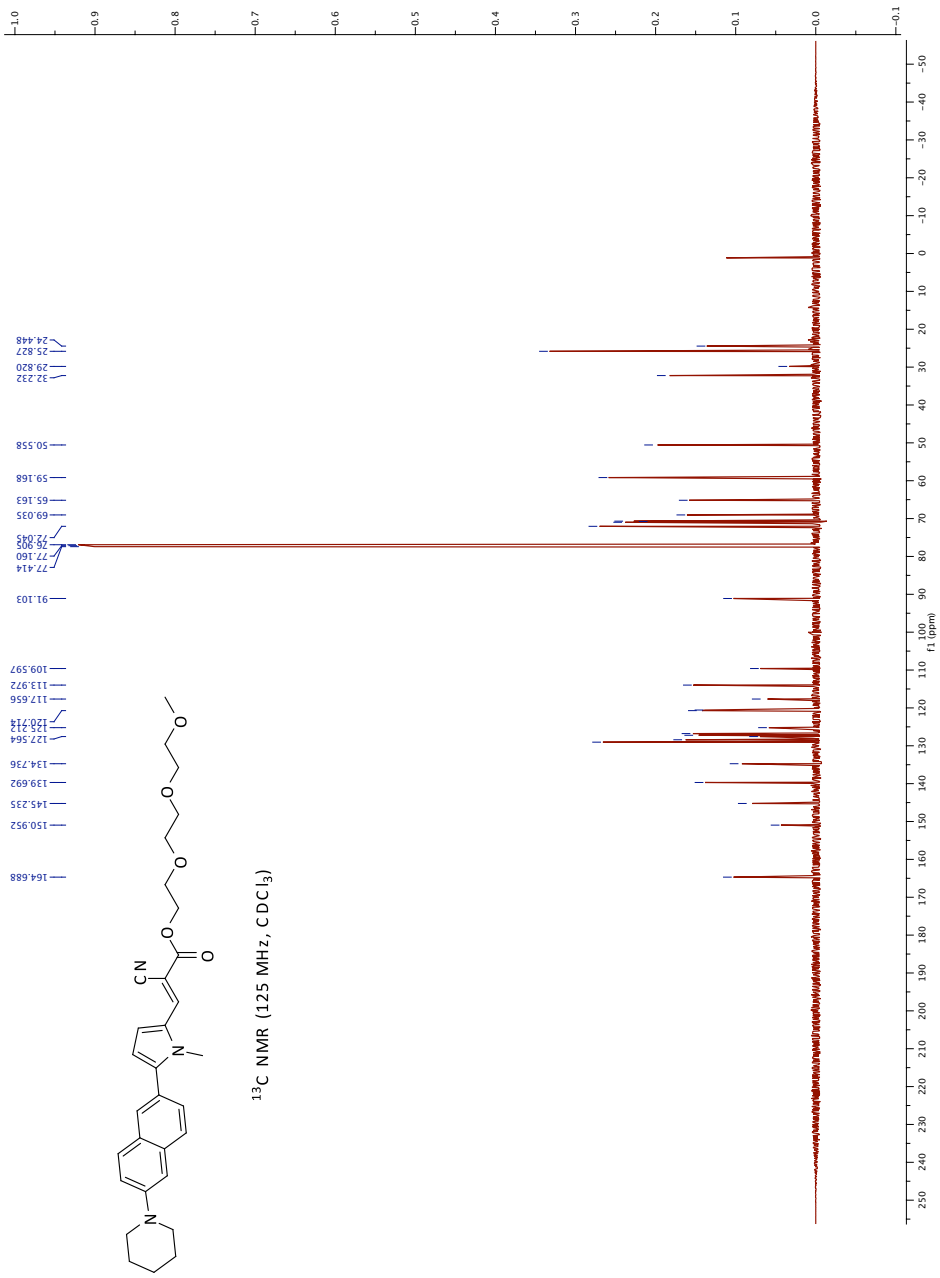

Spectrum 2.28: Compound 37: ^{13}C NMR

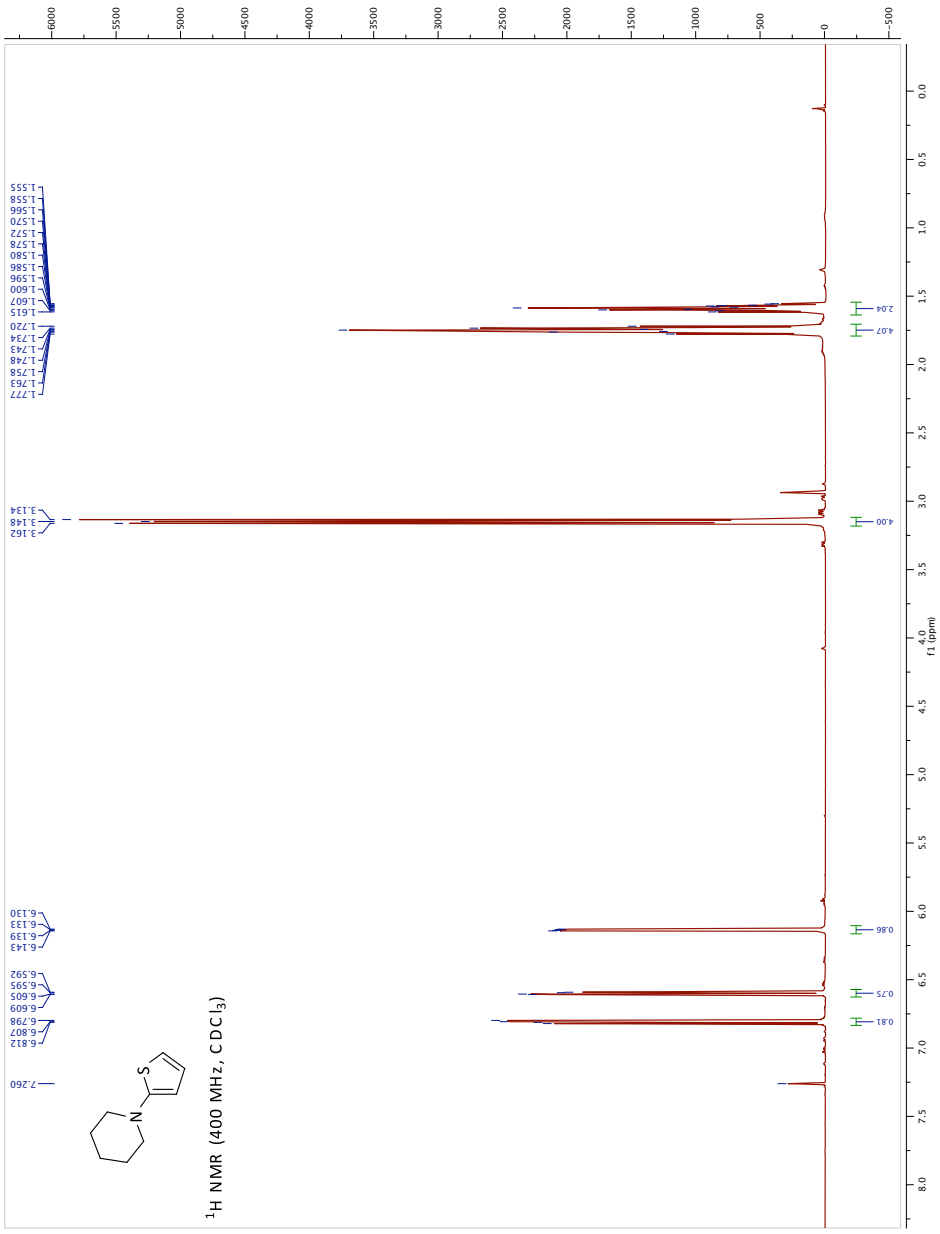

Spectrum 2.29: Compound 39: ^{1}H NMR

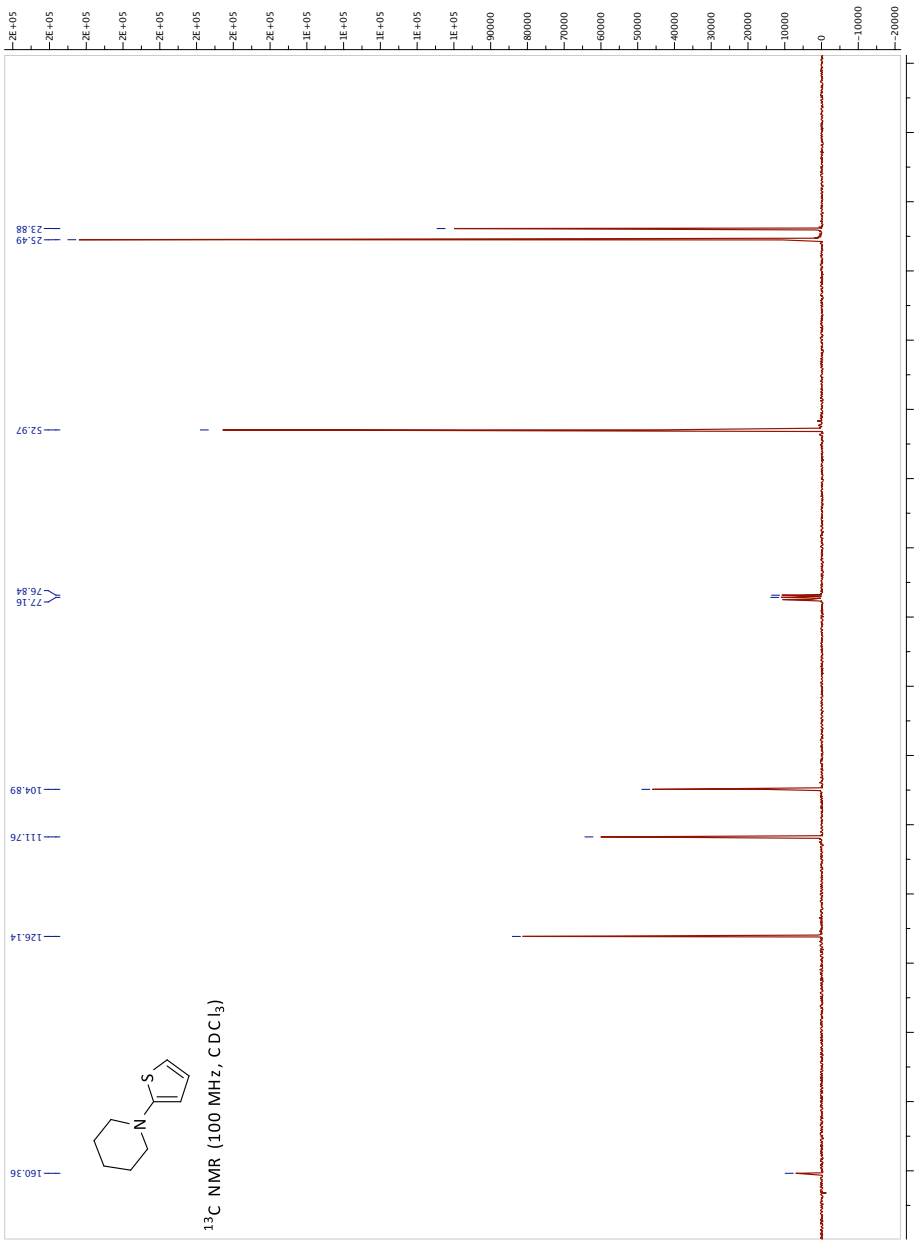

Spectrum 2.30: Compound 39: ^{13}C NMR

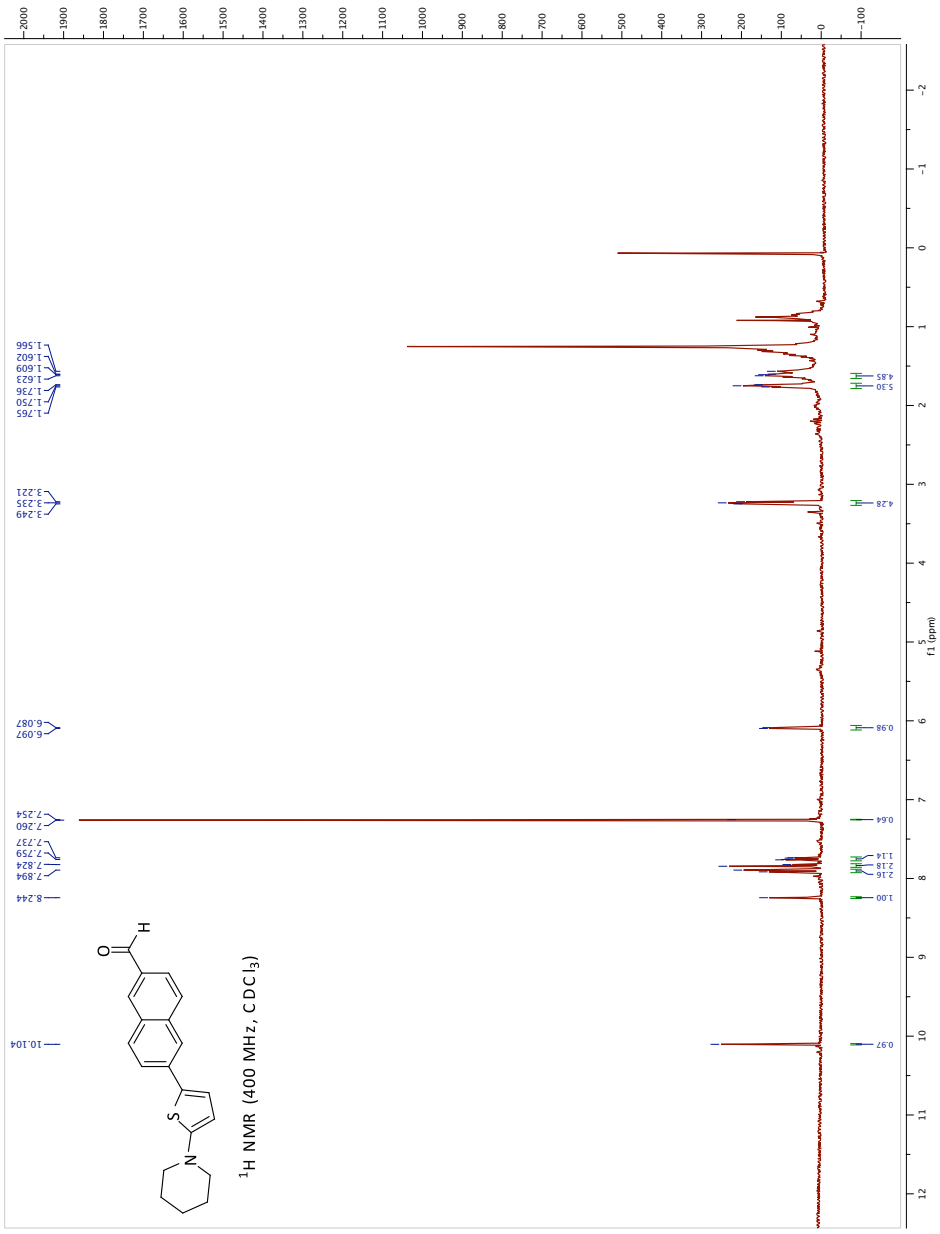

Spectrum 2.31: Compound 41: ^{1}H NMR

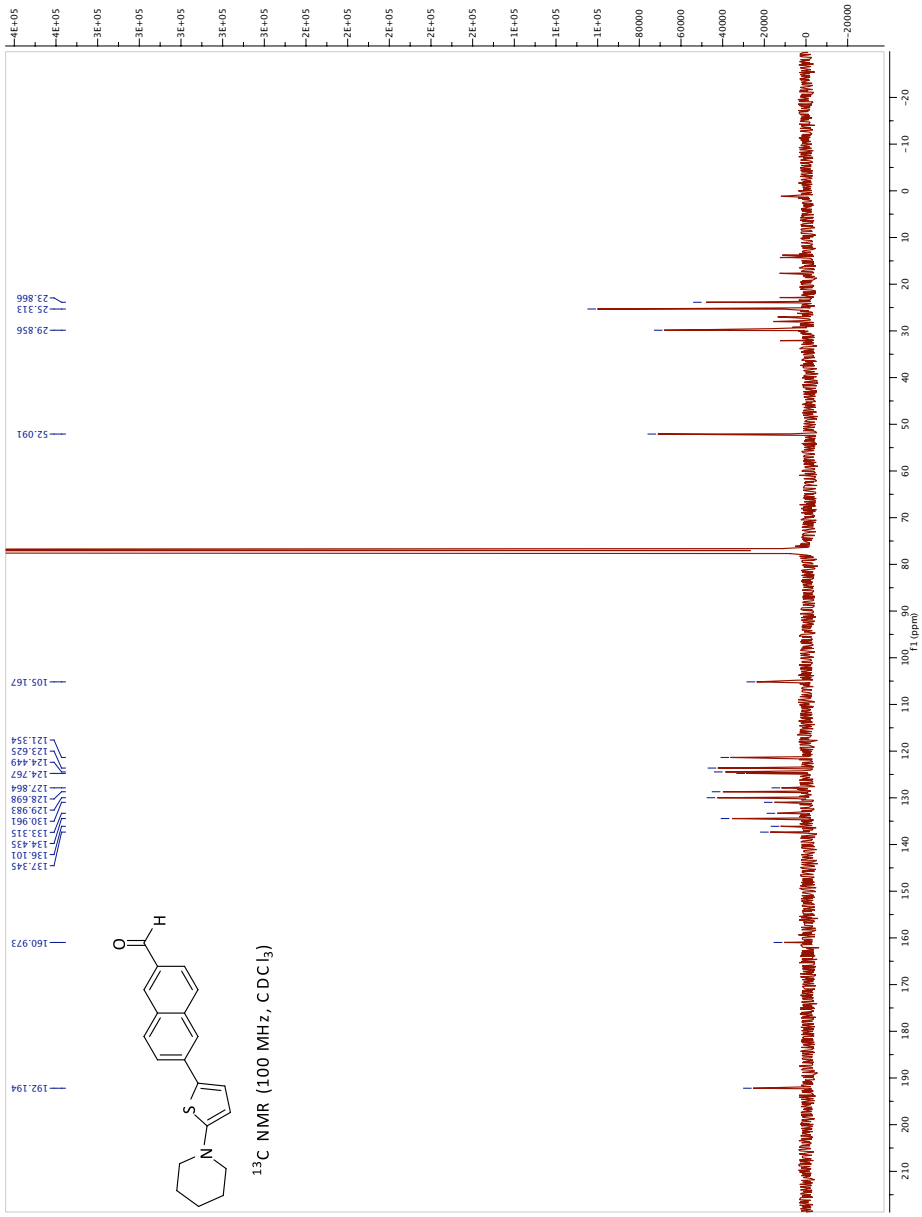

Spectrum 2.32: Compound 41: ^{13}C NMR

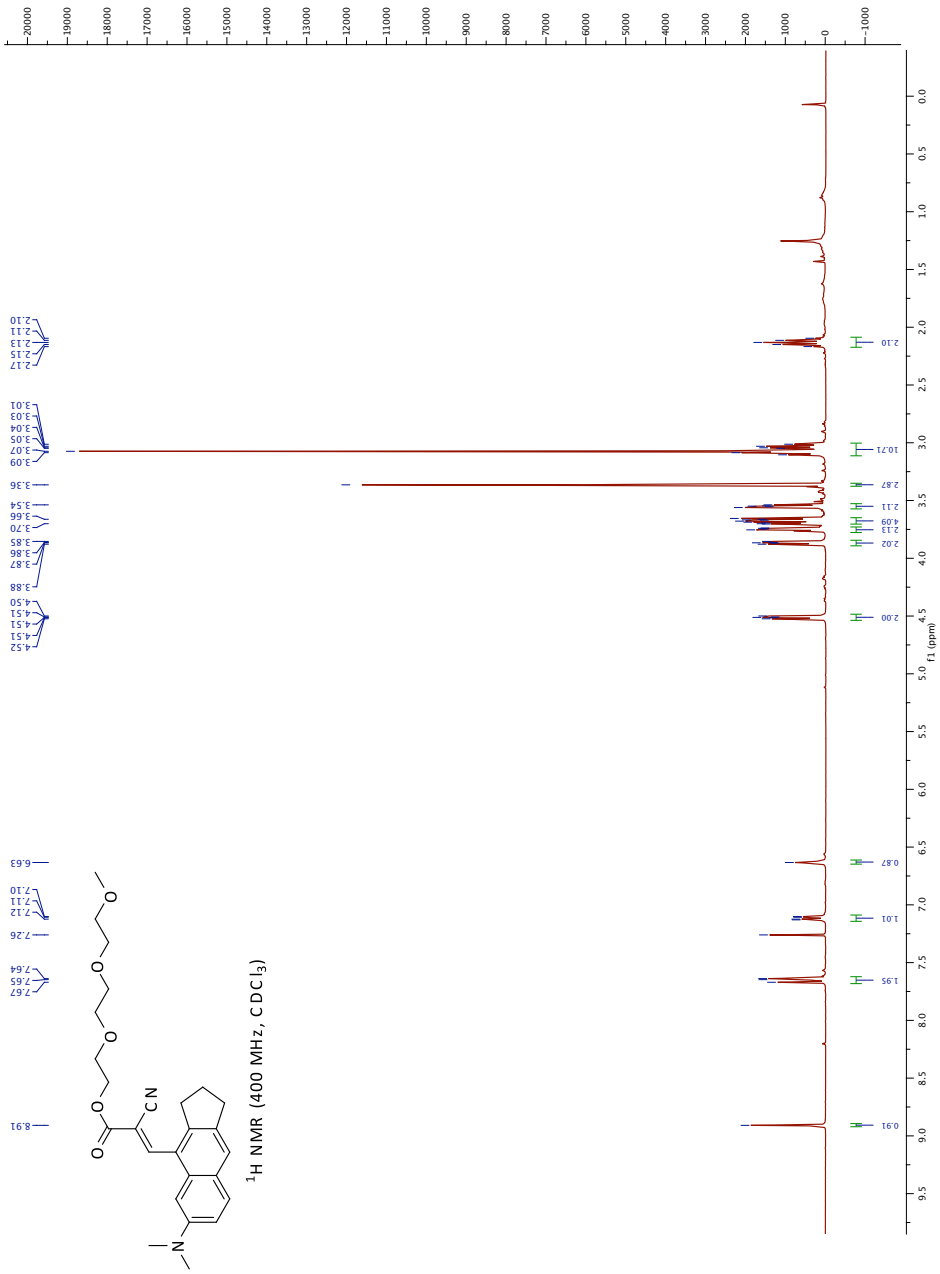

Spectrum 2.33: Compound 45: ^{1}H NMR

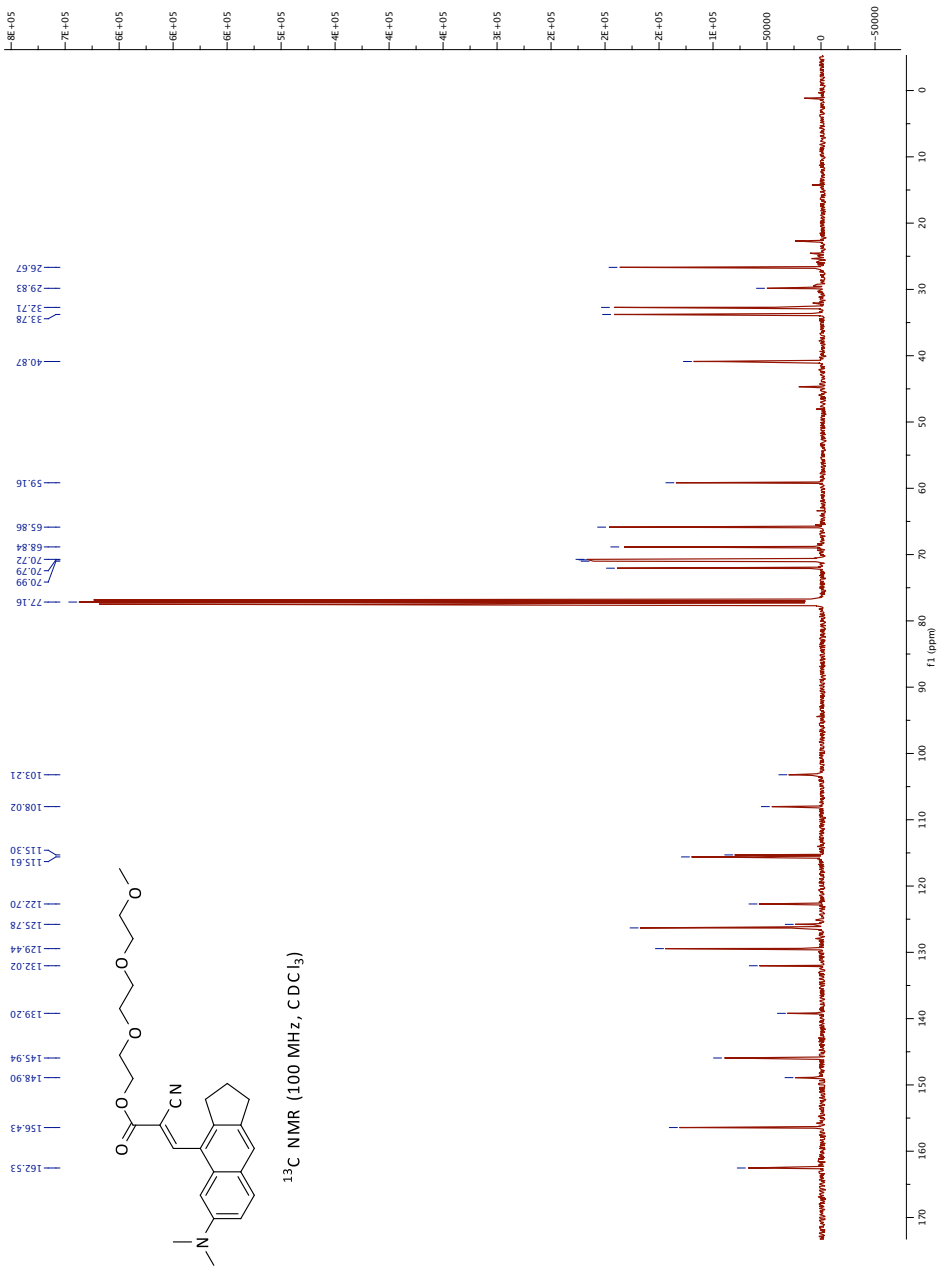

Spectrum 2.34: Compound 45: ^{13}C NMR

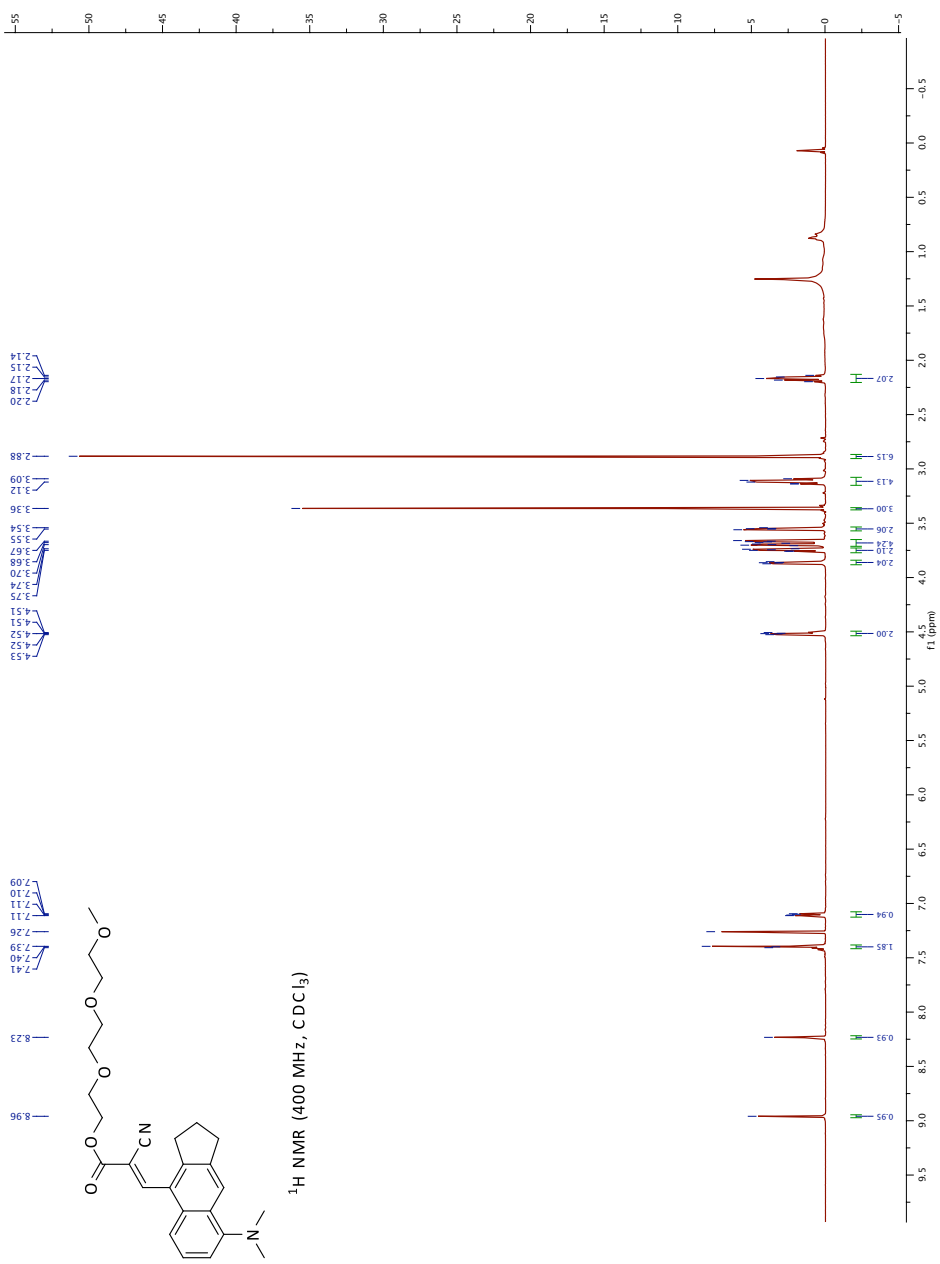

Spectrum 2.35: Compound 47: ^{1}H NMR

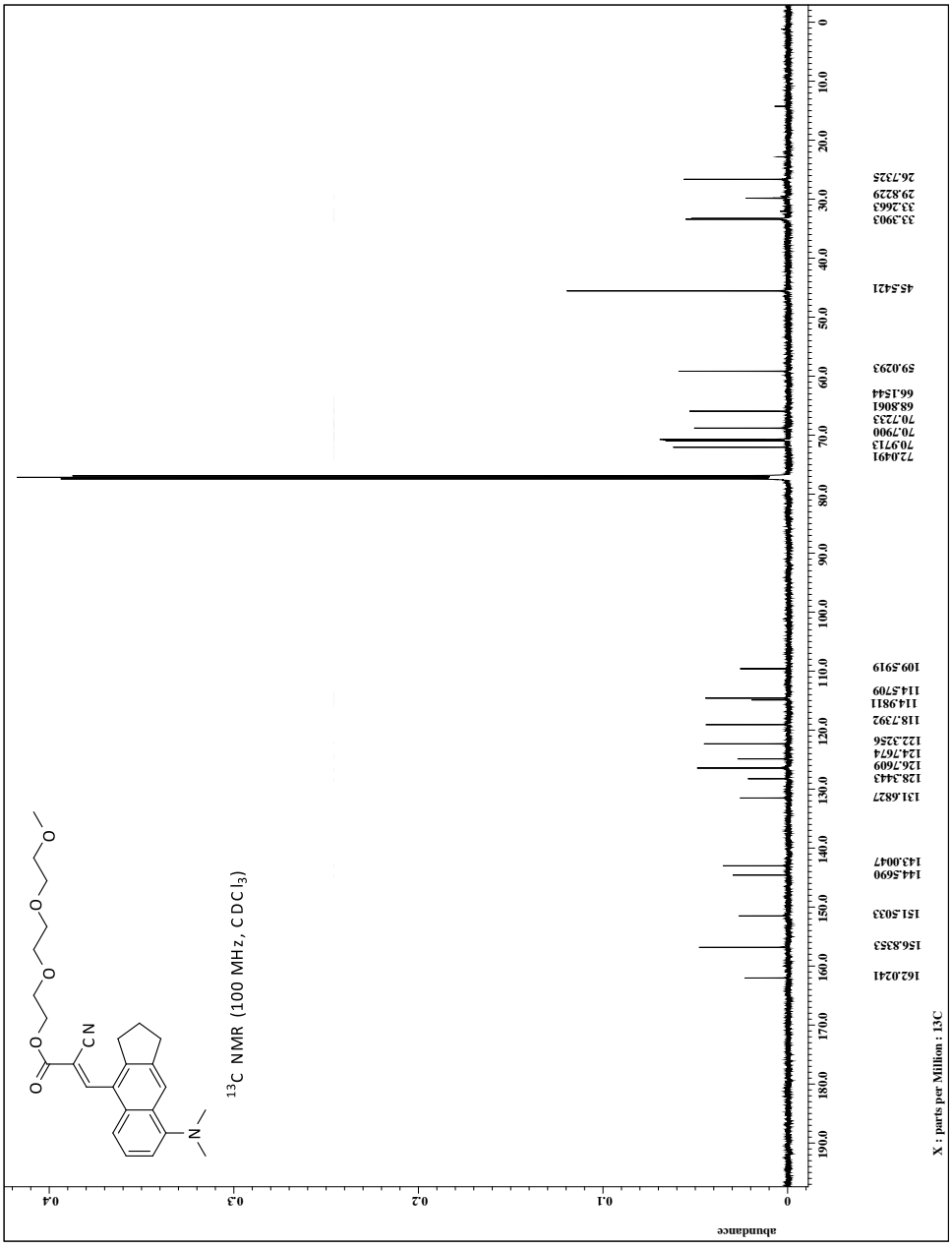

Spectrum 2.36: Compound 47: ^{13}C NMR

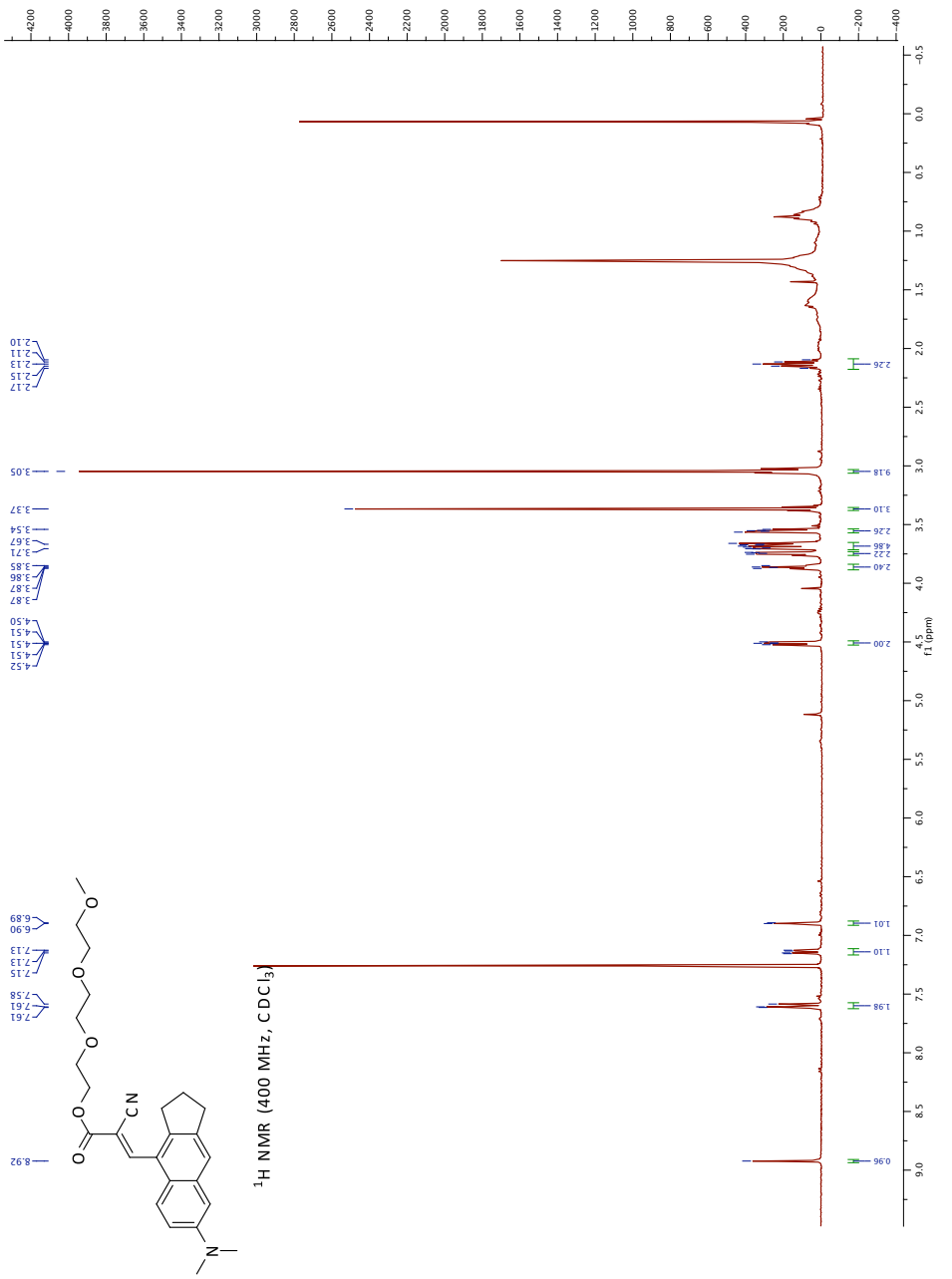

Spectrum 2.37: Compound 49: ^{1}H NMR

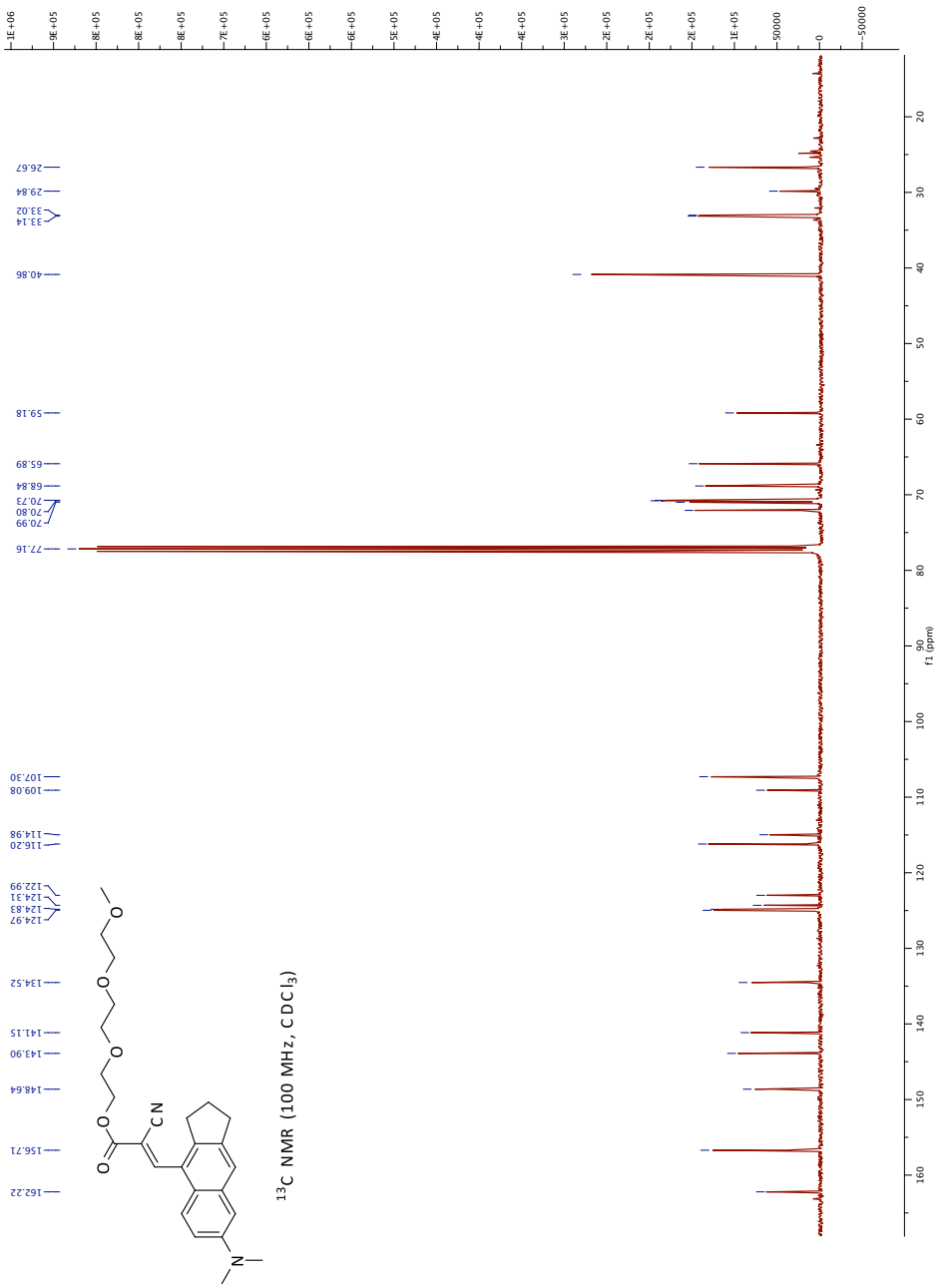

Spectrum 2.38: Compound 49: ^{13}C NMR

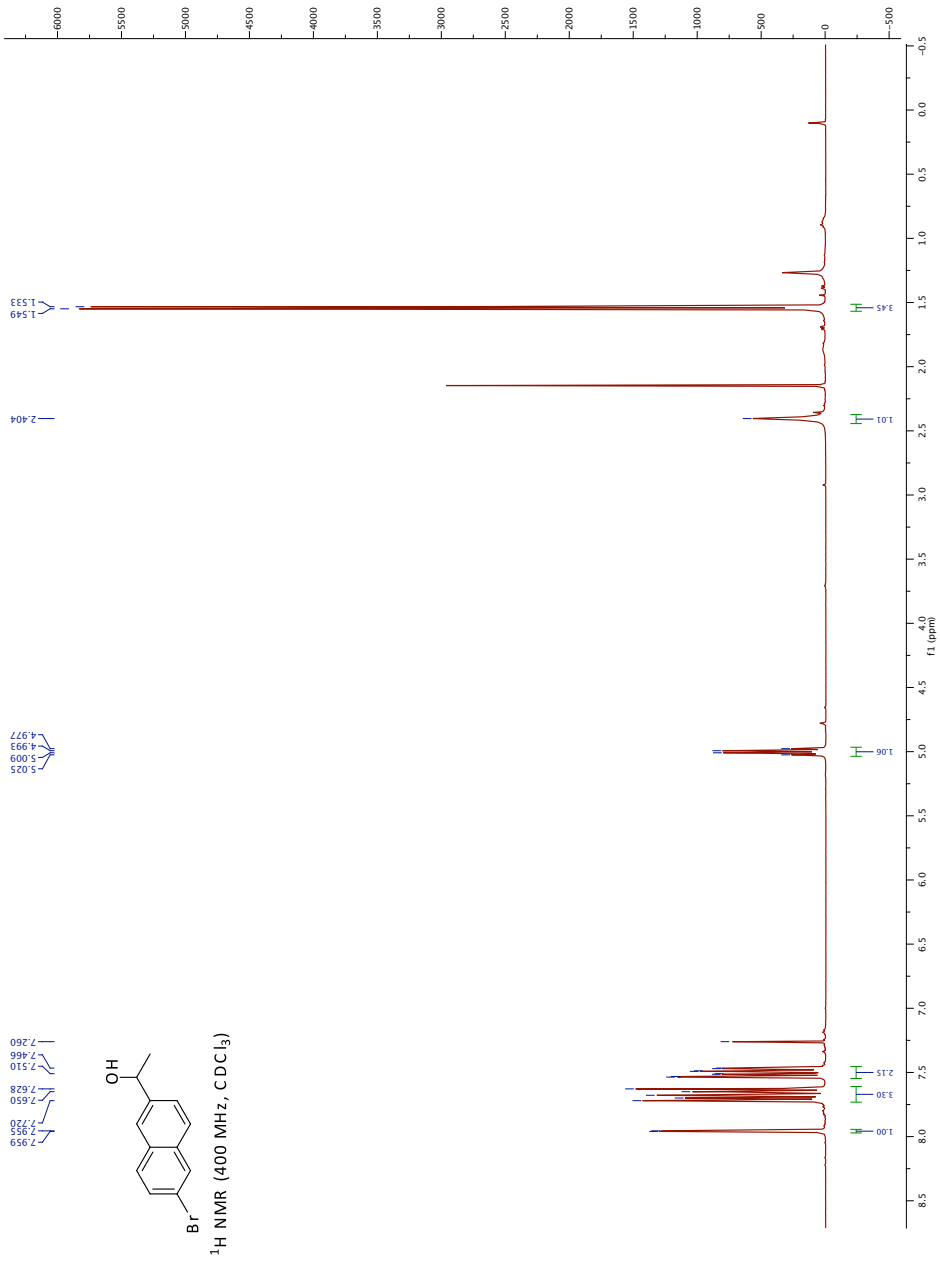

Spectrum 2.39: Compound 50: ^{1}H NMR

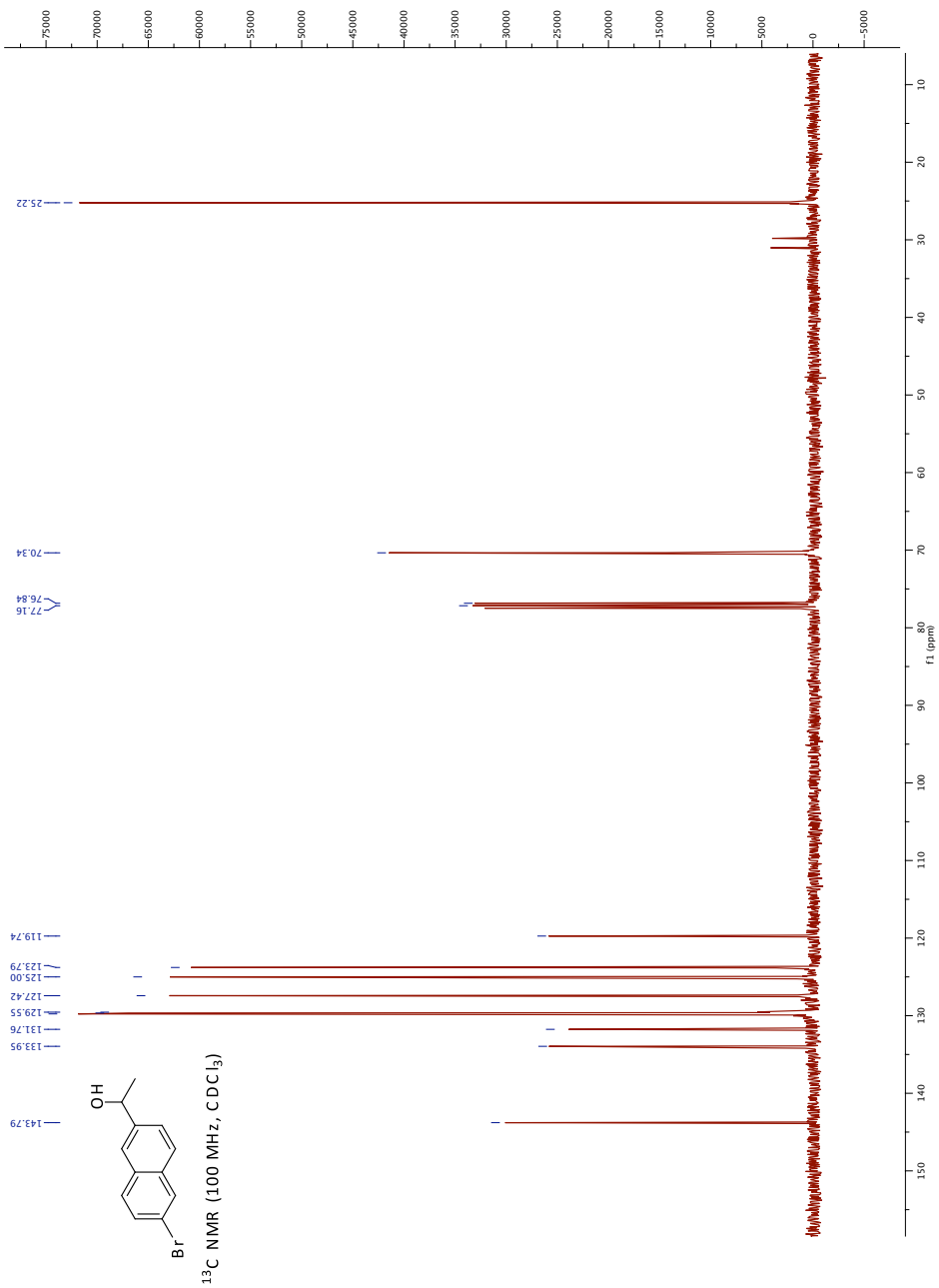

Spectrum 2.40: Compound 50: ^{13}C NMR

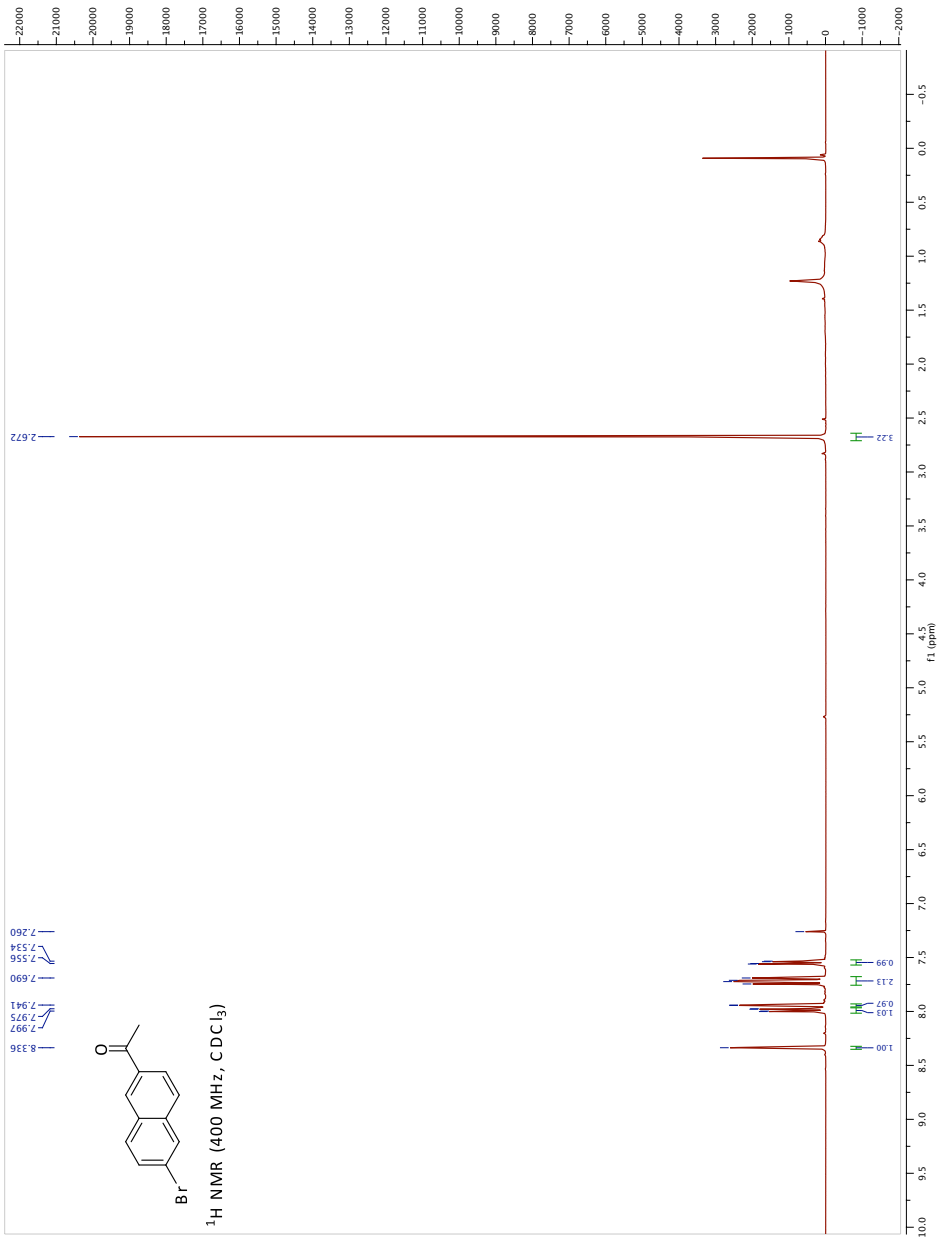

Spectrum 2.41: Compound 51: ^{1}H NMR

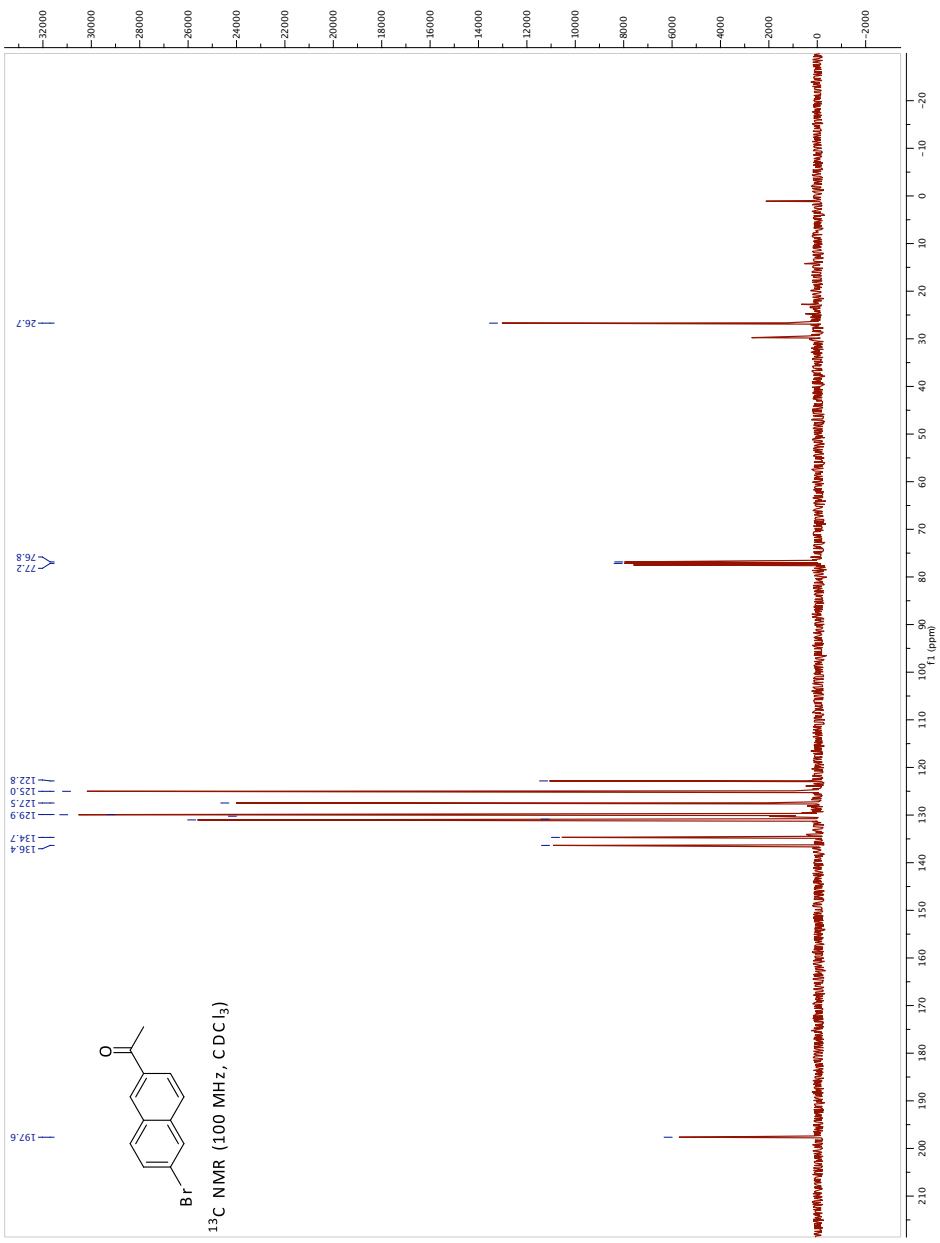

Spectrum 2.42: Compound 51: ^{13}C NMR

2.11 References

1. Brookmeyer, R., Evans, D. A., Hebert, L., Langa, K. M., Heeringa, S. G., Plassman, B. L., et al. *AlzheimersDement.* **2011**, *7*, 61-73.

2. Alzheimer's Association, Alzheimer's disease facts and figures. *Alzheimers Dement.* 2011. *7*, 2.

3. McGuffey EC: Alzheimer's disease: An overview for the pharmacist, *J. Am. Pharm. Assoc.*, **1997**, *3*, 347-352.

4. Ross, C. A., Poirier, M. A. *Nature Med.* **2004**, S10-S17.

5. Abramov, A. Y., Canevari, L., Duchen, M.R. Biochim. *Biophys. Acta* **2004**, *1742*, 81-87.

6. Okamura, N., Furumoto, S., Funaki, Y., Suemoto, T., Kato, M., Ishikawa, Y., Ito, S., Akatsu, H., Yamamoto, T., Sawada, T., Arai, H., Kudo, Y., Yanai, K. *J. Mol. Neuosci.* **2004**, *24*, 247-255.

7. Ran, C., Xu, X., Raymond, S. B., Ferrara, B. J., Neal, K., Bacskai, B. J., Medarova, Z., Moore, A. *J. Am. Chem. Soc.* **2009**, *131*, 15257-15261.

8. Klunk, W. E., Engler, H., Nordberg, A., Wang, Y., Blomqvist, G., Holt, D. P., Bergström, M., Savitcheva, I., Huang, G. F., Estrada, S., Ausén, B., Debnath, M. L., Barletta, J., Price, J. C., Sandell, J., Lopresti, B. J., Wall, A., Koivisto, P., Antoni, G., Mathis, C. A., Långström, B. *Ann. Neurol.* **2004**, *55*, 306-319.

9. Nesterov, E. E., Skoch, J., Hyman, B. T., Klunk, W. E., Bacskai, B. J., Swager, T. M. *Angew. Chem., Int. Ed.* **2005**, *44*, 5452-5456.

10. Poduslo, J. F., Curran, G. L., Peterson, J. A., McCormick, D. J., Fauq, A. H., Khan, M. A., Wengenack, T. M. *Biochemistry*, **2004**, *43*, 6064-6075.

11. Sutharsan, J., Dakanali, M., Capule, C. C., Haidekker, M., Yang, J., Theodorakis, E. A. *ChemMedChem* **2010**, *5*, 56-60.

12. Haidekker, M., Theodorakis, E. A. *Org. Biomol. Chem.* **2007**, *5*, 1669-1678.

13. Lipinski, C. A., Lombardo, F., Dominy, B. W., Feeny, P. J. *Adv. Drug Delivery Rev.* **1997**, *23*, 3-25.

14. Chang, W. M., Dakanali, M., Capule, C. C., Sigurdson, C. J., Yang, J., Theodorakis, E. A. *ACS Chem. Neurosci.* **2011**, *2*, 249-255.

15. Cordeiro, M. F., Guo, L., Coxon, K. M., Duggan, J., Nizari, S., Normando, E. M., Sensi, S. L., Sillito, A. M., Fitzke, F. W., Salt, T. E., Moss, S. E. *Cell Death Dis.* **2010**, *1*, e3.

16. Kerbage, C., Sadowsky, C. H., Jennings, D., Cagle, G. D., Hartung, P. D. *Frontiers in Neurology* **2013**, *4*, article 62, 1-9.

17. Koronyo-Hamaoui, M., Koronyo, Y., Ljubimov, A. V., Miller, C. A., Ko, M. K., Black, K. L., Schwartz, M., Farkas, D. L. *Neuroimage* **2011**, *54*, S204-S217.

18. Moncaster, J. A., Pineda, R., Moir, R. D., Lu, S., Burton, M. A., Ghosh, J. G., Ericsson, M., Soscia, S. J., Mocofanescu, A., Folkerth, R. D., Robb, R. M., Kuszak, J. R., Clark, J. I., Tanzi, R. E., Hunter, D. G., Goldstein, L. E. *PLoS One* **2010**, *5*, e10659.

19. Sammes, M. P., Wylie, C. M., Hoggert, J. G. *J. Chem. Soc. C.* 1971, 2151-2155.

20. Boiadjiev, S. E., Lightner, D. A. *Tetrahedron* **2007**, *63*, 8962-8976.

21. Inoue, M., Bruice, T. *J. Am. Chem. Soc*. **1982**, *104*, 1644-1653.

22. Alessi, M., Larkin, A. L., Ogilvie, K. A., Green, L. A., Lai, S., Lopez, S., Snieckus, V. *J. Org. Chem.* **2007**, *72 (5)*, 1588-1594.

23. Deng, J. Z., Paone, D. V., Ginnetti, A. T., Kurihara, H., Dreher, S. D., Weissman, S. A., Stauffer, S. R., Burgey, C. S. *Org. Lett.* **2009**, *11 (2)*, 345-347.

24. Inokuma, S., Ide, H., Yonekura, T., Funaki, T., Kondo, S., Shiobara, S., Yoshihara, T., Tobita, S., Nishimura, J. *J. Org. Chem.* **2005**, *70 (5)*, 1698-1703.

25. Cao, K., Farahi, M., Dakanali, M., Chang, W. M., Sigurdson, C. J., Theodorakis, E. A., Yang, J. *J. Am. Chem. Soc.* **2012**, *134*, 17338-17341.

26. Mishra, R., Sjölander, D., Hammarström, P. *Mol. BioSyst.* **2011**, *7*, 1232-1240.

27. Brandenburg, E., Berlepsch, H., Koksch, B. *Mol. BioSyst.* **2012**, *8*, 557-564.

28. Benzeid, H., Mothes, E., Essassi, E. M., Faller, P., Pratviel, G., C.R. *Chimie* **2012**, *15*, 79-85.

29. Nilsson, K. P. R., *FEBS Lett*. **2009**, *583*, 2593-2599.

30. Nilsson, K. P. R., Hammarstrom, P., Ahlgren, F., Herland, A., Schnell, E. A., Lindgren, M., Westermark, G. T., Inganas, O. *ChemBioChem* **2006**, *7*, 1096-1104.

31. Lord, S. J., Conley, N. R., Lee, H. D., Nishimura, S. Y., Pomerantz, A. K., Willets, K. A., Lu, Z., Wang, H., Liu, N., Samuel, R., Weber, R., Semyonov, A., He, M., Twieg, R., Moerner, W. E. *ChemPhysChem* **2009**, *10*, 55-65.

32. Klingstedt, T., Ąslund, A., Simon, R. A., Johansson, L. B. G., Mason, J. J., Nyström, S., Hammarström, P., Nilsson, K. P. R. *Org. Biomol. Chem.* **2011**, *9*, 8356-8370.

33. Guram, A. S., Rennels, R. A., Buchwald, S. L. *Angew. Chem., Int. Ed.* **1995**, *34*, 1348-1350.

34. Wolfe, J. P., Buchwald, S. L. *J. Org. Chem.* **2000**, *65*, 1144-1157.

35. Hartwig, J. F. *Acc. Chem. Res.* **2008**, *41*, 1534-1544.

36. Wu, Y., Guo, H., James, T. D., Zhao, J. *J. Org. Chem.* **2011**, *76*, 5685-5695.

37. Denat, F., Gaspard-Iloughmane, H., Dubac, J. *Journal of Organometallic Chemistry* **1992**, *423*, 173-182.

38. Saitman, A., Rulliere, P., Sullivan, S. D. E., Theodorakis, E. A. *Org. Lett.* **2011**, *13*, 5854-5857.

39. Horner, K. E., Karadakov, P. B. *J. Org. Chem.* **2013**, ASAP, DOI: 10.1021/jo401319k.

40. Lu, Z.; Twieg, R. *Tetrahedron* **2005**, *61*, 903 - 918.

41. Benedetti, E., Kocsis, L. S., Brummond, K. M. *J. Am. Chem. Soc.* **2012**, *134 (30)*, 12418-12421.

42. Rumble, C., Rich, K., He, G., Maroncelli, M. *J. Phys. Chem. A.*, **2012**, *116*, 10786-10792.